SELF-HEALING RF SOCS: LOW COST BUILT-IN TEST AND CONTROL DRIVEN SIMULTANEOUS TUNING OF MULTIPLE PERFORMANCE METRICS

A Dissertation
Presented to
The Academic Faculty

by

Vishwanath Natarajan

In Partial Fulfillment
of the Requirements for the Degree
Doctor of Philosophy in the
School of Electrical and Computer Engineering

Georgia Institute of Technology
December, 2010

Copyright 2010 by Vishwanath Natarajan

SELF-HEALING RF SOCS: LOW COST BUILT-IN TEST AND CONTROL DRIVEN SIMULTANEOUS TUNING OF MULTIPLE PERFORMANCE METRICS

Approved by:

Dr. Abhijit Chatterjee, Advisor
School of Electrical and Computer Engineering
Georgia Institute of Technology

Dr. Madhavan Swaminathan
School of Electrical and Computer Engineering
Georgia Institute of Technology

Dr. David Keezer
School of Electrical and Computer Engineering
Georgia Institute of Technology

Dr. Saibal Mukhopadhyay
School of Electrical and Computer Engineering
Georgia Institute of Technology

Dr. Sankar Nair
School of Chemical and Biomolecular Engineering
Georgia Institute of Technology

Date Approved: October 4th, 2010

To my loving family…

ACKNOWLEDGEMENTS

First and foremost I would like to express my heartfelt gratitude to my advisor Prof. Abhijit Chatterjee without whom I will not be here. I thank him for his able guidance in my research. I'm thankful for all the discussions we've had over the years. He was there in every step of my way and I'm fortunate for that. It was by chance that I met Prof. Madhavan Swaminathan in Chennai, India. It was under his advice that I applied for a PhD, not knowing what to assume. By now I'm convinced that my momentary decision was also my best so far. I thank him sincerely for that.

I thank the PhD committee members Prof. Madhavan Swaminathan, Prof. David Keezer, Prof. Saibal Mukhopadhyay, and Prof. Sankar Nair for spending their valuable time in providing me feedback

I'm thankful to the seniors in my research lab Soumendu Bhattacharya, Ganesh Srinivasan, Shalabh Goyal, Donghoon Han, Achintya Halder, Sermet Akbay, Maryam Ashouei, Yuvraj Dhillon and Utku Diril for taking me under their wings when I started my PhD. Their feedbacks both positive and negative have helped me immensely in achieving my goals. I would also like to thank the current crop of students in our research lab; Mudassar Nisar, Shreyas Sen, Shyam Devarakond, Hyun Choi, Aritra Banerjee, Sehun Kook, Jayaram Natarajan, and Joshua Wells for their wonderful company.

I'm thankful for some great friends at Georgia Tech, Amit Bavisi, Souvik Mukherjee, Pratap Muthana, Subramanian Lalgudi, Krishna Bharath and Nevin Altunyurt for befriending me with ease and helping me cope up with the sudden change when I was still a newcomer to this country. I also thank my friends here in Atlanta, Nikhilesh, Urmila, Raj Narisetti, Dharma, Sunil, Antoney, Shaila, Vaibhav, Venkat, Kate, Saurabh and Sylvester whose constant company has kept me afloat all along my journey. Your friendship means a lot to me.

I’m extremely thankful to my mother Suriya Natarajan and my father Natarajan Dorairajan for their countless sacrifices, unconditional love and their unshakable trust. I have always found strength and encouragement in their love and support. I owe everything to them. I also want to thank my brother Srinath Natarajan for his love and support.

TABLE OF CONTENTS

LIST OF TABLES

LIST OF FIGURES

SUMMARY

The advent of deep submicron technology coupled with ever increasing demands from the customer for more functionality on a compact silicon real estate has led to a proliferation of highly complex integrated RF system-on-chip (SoC) and system-on-insulator (SoI) solutions. The use of scaled CMOS technologies for high frequency wireless applications is posing daunting technological challenges both in design and manufacturing test. In [1] the authors describe 54GHz and 100 GHz VCO designs in CMOS 90nm process technologies and show that 100 GHz designs are quite feasible. In the future, higher speed circuits will be possible with scaled devices. However, the resulting circuits will be increasingly susceptible to manufacturing process variations and coupled noise (substrate, power planes) from on-chip digital signal processing circuitry. In the digital area, Intel is already reporting up to 2X variation in performance and up to 20X (worst case) variation in leakage in microprocessor circuitry [2]-[3]. To ensure market success, manufacturers need to ensure the quality of these advanced RF devices by subjecting them to a conventional set of production test routines that are both time consuming and expensive. Typically the devices are tested for parametric specifications such as gain, linearity metrics, quadrature mismatches, phase noise, noise figure (NF) and end-to-end system level specifications such as EVM (error vector magnitude), BER (bit-error-rate) etc. Due to the reduced visibility imposed by high levels of integration, testing for parametric specifications are becoming more and more complex.

To offset the yield loss resulting from process variability effects and reliability issues in RF circuits, the use of self-healing/self-tuning mechanisms will be imperative. Such self-healing is typically implemented as a test/self-test and self-tune procedure and is applied post-manufacture. To enable this, simple test routines that can accurately diagnose complex performance parameters of the RF circuits need to be developed first.

After diagnosing the performance of a complex RF system appropriate compensation techniques need to be developed to increase or restore the system performance. Moreover, the test, diagnosis and compensation approach should be low-cost with minimal hardware and software overhead to ensure that the final product is economically viable for the manufacturer.

As illustrated in Figure 1 the main components of the presented thesis are as follows:

Low-cost specification testing of advanced radio frequency front-ends: Methodologies are developed to address the issue of test cost and test time associated with conventional production testing of advanced RF front-ends. The developed methodologies are amenable for performing self healing of RF SoCs. Test generation algorithms are developed to perform alternate test stimulus generation that includes the artifacts of test signal path such as response capture accuracy, load-board DfT etc. A novel cross loop-back methodology is developed to perform low cost system level specification testing of multi-band RF transceivers. A novel low-cost EVM testing approach is developed for production testing of wireless 802.11 OFDM front-ends. A signal transformation based model extraction technique is developed to compute multiple RF system level specifications of wireless front-ends from a single data capture. The developed techniques are low-cost and facilitate a reduction in the overall contribution of test cost towards the manufacturing cost of advanced wireless products.

Analog tuning methodologies for compensating wireless RF front ends: Methodologies for performing low-cost self tuning of multiple impairments of wireless RF devices are developed. This research considers for the first time, multiple analog tuning parameters of a complete RF transceiver system (transmitter and receiver) for tuning purposes. The developed techniques are demonstrated on hardware components and behavioral models to improve the overall yield of integrated RF SoCs.

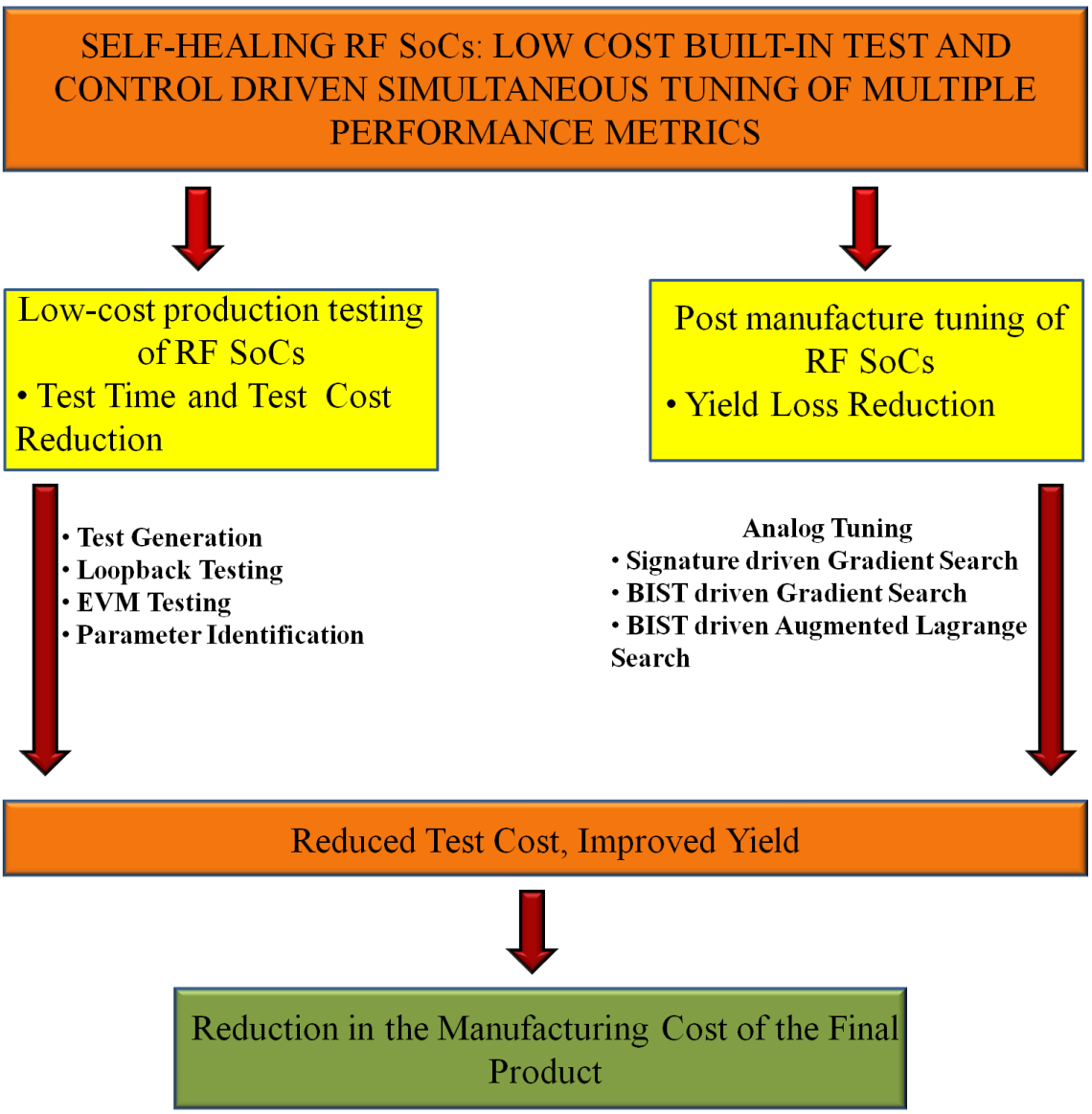

Figure 1: Thesis framework and scope of research

CHAPTER 1

INTRODUCTION

Wireless communications for both mobile and in-office (point-to-point communication) applications is undergoing a revolution due to the proliferation of different communication standards spanning diverse communication bandwidths. The advent of deep sub-micron technologies has rendered these new age devices increasingly susceptible to process variations. The deviations in performances resulting from the above said issues entail careful testing of these devices. The performance metrics for semiconductor devices are usually presented in terms of specifications of the device. The manufacturer needs to carefully test for these specifications to ensure that the effect of these process variations on the specifications are within specified bounds. These tests are conducted over millions of devices requiring automatic test equipment (ATE), and are referred to as production tests. The test cost of modern RF modules and SoC devices is the fastest growing portion of their manufacturing cost and is currently estimated to be around 45% of the total cost. Hence new approaches must be developed to address the test challenges keeping in mind the increasing levels of complexity and more importantly, the need for reduced cost.

1.1 CONVENTIONAL APPROACH FOR PRODUCTION TESTING

Conventional approach for production testing follows a sequential approach to test for each specification of the device as shown in Figure 2. During the characterization phase of the product development cycle, a comprehensive set of specifications along with its guard bands are identified. During production testing phase, test compaction [4]-[5] is performed to identify a set of critical specifications out of the available list of specifications. These specifications are then tested for in a sequential manner. Each test configuration involves the hardware setup, application of the test stimulus, settling time

of the DUT, and the specification measurement time. Thus, the entire process requires switching (using relays) between different setups during the test process, which increases the total test time. With increasing levels of integration and complexity the production test cost can amount to as much as 45% of the manufacturing test cost.

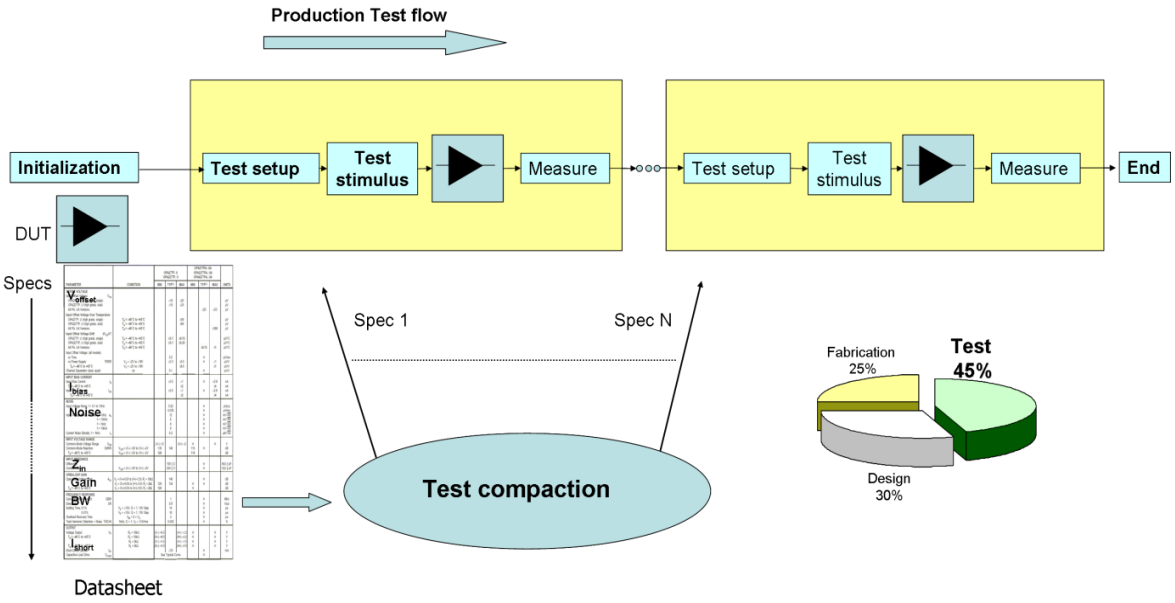

Figure 2: Sequential approach for conventional production testing

Typical specifications that are considered for a RF device include gain, IIP3, adjacent channel power ratio (ACPR), in-phase (I) and quadrature (Q) gain and phase mismatch, phase noise, EVM etc. While other specifications offer module level (such as amplifiers, mixers, VCO etc) information, EVM offers system level information about the performance of a complex RF system (Transmitter, receiver etc). EVM captures the overall effect of all the non-idealities in the transceiver including analog-to-digital converter (ADC) and digital-to-analog converter (DAC) non-linearity, sampling clock jitter, RF front-end non-linearity and gain variations, local oscillator (LO) frequency offset and phase noise etc. Measuring the EVM of a system in lieu of individual RF and baseband circuit specifications is convenient and quantifies the overall transceiver performance. EVM quantifies the difference between the transmitted and received symbols at the baseband. It is computed as follows.

$$EVM = 100 * \frac{\sqrt{\frac{1}{N}\sum_{i=1}^{N}\left|S_{IDEAL,i} - S_{MEAS,i}\right|^2}}{\sqrt{\frac{1}{N}\sum_{i=1}^{N}\left|S_{IDEAL,i}\right|^2}} \quad (1)$$

Where, $S_{MEAS,i}$ is the received complex data symbols, $S_{IDEAL,i}$ is transmitted complex data symbols, N is the number of complex data points used for computation, where *N* is sufficiently large. It computes the root mean square (rms) of the error vector magnitudes of N transmit-receive pairs expressed as percentage of average power of the transmitted data symbols. Typically a large number of symbols need to be transmitted and received to determine the EVM value.

1.2 COST CONSIDERATIONS IN WIRELESS TRANSCEIVER TESTING

Testing complex specifications of highly integrated RF front-ends require high precision RF testers with digital modulation capabilities. In addition, the test time for system-level specifications is large as mentioned in the previous section. Cost of test (CoT) [6] can be expressed as,

$$CoT = \frac{(Fixed\ cost + Recurring\ cost)}{Yield * Throughput} \quad (2)$$

where *Fixed cost* consists of Automated Test Equipment (ATE) cost, probe/handler cost and installation costs, *Recurring cost* consists of ATE maintenance costs and per-device test cost that in total amount to about 10% of the fixed costs, *Yield* is the ratio of the total number of good devices to the total number of tested devices, and *Throughput* is the ratio of the total number of good devices to the test time consumed to test all the devices. The CoT is highly sensitive to the cost of the ATE used to test the devices for a constant processes yield and throughput. RF ATEs are expensive and are projected to cost around two million dollars each. This boils down to around three to five

cents per second of test time. This could be significant for devices that require complex and long tests.

Test cost reduction is critical to reduce the overall manufacturing cost of these devices to ensure market success. One of the objectives of the proposed work is to perform efficient test of wireless devices on low-cost ATE platforms, and thereby, reducing the test cost.

1.3 PRIOR WORK TO REDUCE TEST COST

Testing of RF systems involve testing of the digital baseband units and the RF/analog subsystems separately. Significant research has been done in the field of digital testing to lower the test cost of complex devices. However, research in the area of test cost reduction of RF devices is fairly primitive. A defect-oriented-test (DOT) approach for wireless Bluetooth systems to identify faults present in the system is proposed in [7]-[8]. DOT involves analysis of failure mechanisms through simulation and/or collection of empirical data to build the required fault models. These models are used to predict failures that would normally require lengthy, expensive tests. The fault models themselves are very hard to obtain as a lot of test data analysis across multiple lots of wafers is necessary. While DOT remains common for digital testing [9] it has little application for RF testing due to the lack of knowledge for a comprehensive fault model. Approaches for reduction of test time for system level specifications such as EVM has been explored in the past. The speedup of EVM test measurement for GSM transceivers by avoiding expensive matrix inversions is discussed in [10]. An order of magnitude savings in test time is obtained. The automation of test time savings for QAM devices is discussed in [11] and a built-in test approach that uses the baseband processor for EVM computation is discussed in [12]. In [13], Acar and Ozev develop methods for enhancing EVM test using refined EVM computation in conjunction with measurement of path input-output impedances. In [14], the same authors present methods for computing IQ

mismatch, IIP3 and bit error rate using constellation data obtained from the transmission of OFDM symbols. A statistical model of the distribution of the constellation symbols in the I-Q plane is used to predict bit error rate. Built-in self test (BIST) approaches for RF devices and systems have been explored in the past [12],[15]. In this approach, additional test circuitry is built into the system to enable self-testing with little support from an external tester. While BIST reduces cost significantly for targeted specifications of a system, the additional test circuitry becomes fairly complicated when applied for multiple specifications present in the system. In [16]-[17] low cost test methods for predicting complex specifications of wireless systems such as Gain, IIP3, P1dB, ACPR, Magnitude Error Ratio and Error Vector Magnitude using multi-sine test stimuli are developed. These test techniques are based on the "alternate test" approach proposed by Variyam and Chatterjee in [18] and are applied to *single carrier systems* (as opposed to OFDM which uses multiple orthogonal carriers). In the alternate testing approach, machine learning techniques based on the use of regression splines [19] are used to predict a range of device and system level specifications from the response of the RF device to carefully computed and compact *alternate tests*. Reference [20] discusses new BIST techniques that rely on the use of embedded RF sensors for self-test. These sensors can be embedded in RF circuits for test purposes without impacting overall RF performance. With increasingly complex modulation schemes being used in communication systems, and with the complex radios of the future (cognitive radio, software-defined radio), considerable research is needed towards improved efficient and cost-effective production test techniques. In this thesis, novel test techniques that are amenable for BIST implementation are developed to lower test cost and test time of single-carrier wireless RF systems and wireless RF orthogonal frequency division multiplexing (OFDM) systems. Apart from lowering test cost, and methodologies and algorithms for calibration of RF systems need to be developed to ensure reliable operation of these systems.

1.4 NEED FOR COMPENSATION OF NON-IDEALITIES IN WIRELESS TRANSCEIVER SYSTEMS

A complex multi-band, multi-radio system may integrate FM radio (100 MHz), RFID (13 MHz), Digital TV (800-1600 MHz), GPS (1.5 GHz), Bluetooth (2.4 MHz), Wi-Fi (2.4–5 GHz), 802.11 (2.4-5 GHz), Wi-Max (2.5–3.5 GHz) and UWB (3-10 GHz). In addition, standards for wide area communications such as GSM/GPRS/EDGE (900-1800 MHz), 3GWCDMA (1.8-2.4 GHz) and the proposed 4G (2-8 GHz) may also be integrated into future *software radio* systems [21]-[23] using CMOS RF design technology. This integration problem is made worse by the rapid deployment of scaled RF CMOS technologies in high-frequency RF transceivers. As the authors of [1] point out, individual scaled 90nm CMOS transistors are unconditionally stable above 40 GHz. Hence, matching networks, feedback mechanisms and loading networks must be designed very carefully to prevent oscillations in high frequency circuits. In the future, higher speed circuits will be possible with scaled devices. However, the resulting circuits will be increasingly susceptible to manufacturing process variations and coupled noise from various on-chip sources. The former results in RF circuit non-idealities due to nonlinear behavior and mismatch effects. The latter is manifested as signal integrity problems due to:

- Power and ground bounce effects at the package level,
- On-chip substrate coupling noise between digital & analog functions,
- Noise induced by electromagnetic radiation and,
- Transient errors

Any combination of the above can degrade overall Quality of Service (QoS) and cause spectral content to spill over into adjacent communication channels. It is clear that future advanced scaled-CMOS RF front end modules will need to be carefully tested and calibrated to avoid these problems. In addition, to manage device degradation in the field, self-test and self-calibration capability must be designed into the transceiver itself.

Compensation of the non-idealities of a RF system can be performed both in the DSP domain using digital linearization techniques such as pre-distortion and in the circuit domain (bias tuning, supply voltage tuning, use of reconfigurable passives etc.). Digital compensation technique uses DSP algorithms that run in the baseband processor to correct for or calibrate-out the effects of the various non-idealities before processing the data. Techniques adopted for digital compensation of transceiver systems can in general be classified as adaptive [24]-[29] or non-adaptive [30]. Adaptive compensation is usually performed by continuous online monitoring of the system, and calibration is performed by using search techniques like least squares (LS), least mean squares (LMS) or recursive least squares (RLS). One drawback of such a compensation technique is the time taken to converge for an optimum performance of the system. In non-adaptive compensation, a one-time calibration of the system is done during production test. Each DUT in the production line is tested and calibrated 'on-the-fly' using digital control signals from the ATE. However to ensure optimum compensation such techniques rely on accurate computation of the non-idealities present in a system using expensive RF instrumentation during the production testing phase of these devices. Another drawback of this approach is its inability to track and compensate for variations *in the field* caused by temperature drift and device wear-out etc. Digital compensation techniques in general are limited the dynamic range of operation of the data converters in their ability to compensate for severe non-idealities. While digital compensation techniques by themselves are good enough to compensate for isolated effects such as I/Q mismatch etc, they may not be very effective in a real system that suffers from several such effects simultaneously such as frequency offset, phase noise, non-linearity etc. In analog compensation, the calibration is performed in the analog domain by modifying circuit characteristics such as bias, supply voltage etc [31]-[35]. The authors in [36] develop an adaptive technique to compensate for IQ mismatches observed in typical RF front-ends, by making use of a variable delay gain cell to feed back correction vectors to the system

LO. Compensation for temperature effects using band-gap bias circuits and gain variations using automatic gain control circuits (AGCs) are widely used. Such techniques incur additional hardware requirements thereby increasing the complexity of the proposed solution and are specific to certain test measurements. The authors in [37] develop an oscillation test based self-healing approach, where the DUT is made to oscillate with the help of additional circuitry. The oscillation frequency of the DUT is used to obtain information about system performance and appropriate compensation is performed by adjusting the tuning knobs (bias, capacitances etc) designed into the system. Compensation techniques in general published in the literature involve development of methodologies to compensate for limited effects of non-idealities in isolation. Since no scheme other than the alternate testing technique [38] is able to determine all (or many) spec values with a single test, existing techniques target specific system-level RF performance metrics without regard to the impact that tuning might have on other system-level RF specs.

In the proposed *self-healing* approach, regression based diagnostic tests (Chapter 3) that allow estimation of multiple specifications and methodologies for compensating non-idealities of the system are developed. The key advantage of the proposed technique is the ability to tune for multiple specifications simultaneously. Various optimization techniques are developed (Chapter 4) to identify the best way to tune the analog parameters in a short amount of time. This has direct implications in reducing the overall manufacturing cost by increasing the overall yield of the advanced wireless systems.

CHAPTER 2

ALTERNATE TEST FRAMEWORK

Conventional test strategies for mixed-signal, analog and RF circuits are based upon specification based testing techniques where the DUT specifications are measured and compared against pre-defined specification bounds to make pass/fail decisions for each specification. This requires a different test set-up for each specification resulting in an increase in test time and test cost. Alternate test [16]-[17] & [38], (as shown in Figure 3) on the other hand makes use of a single test configuration and predicts *all of the specifications of interest with a single input stimulus*, thereby, reducing the overall test time and test cost.

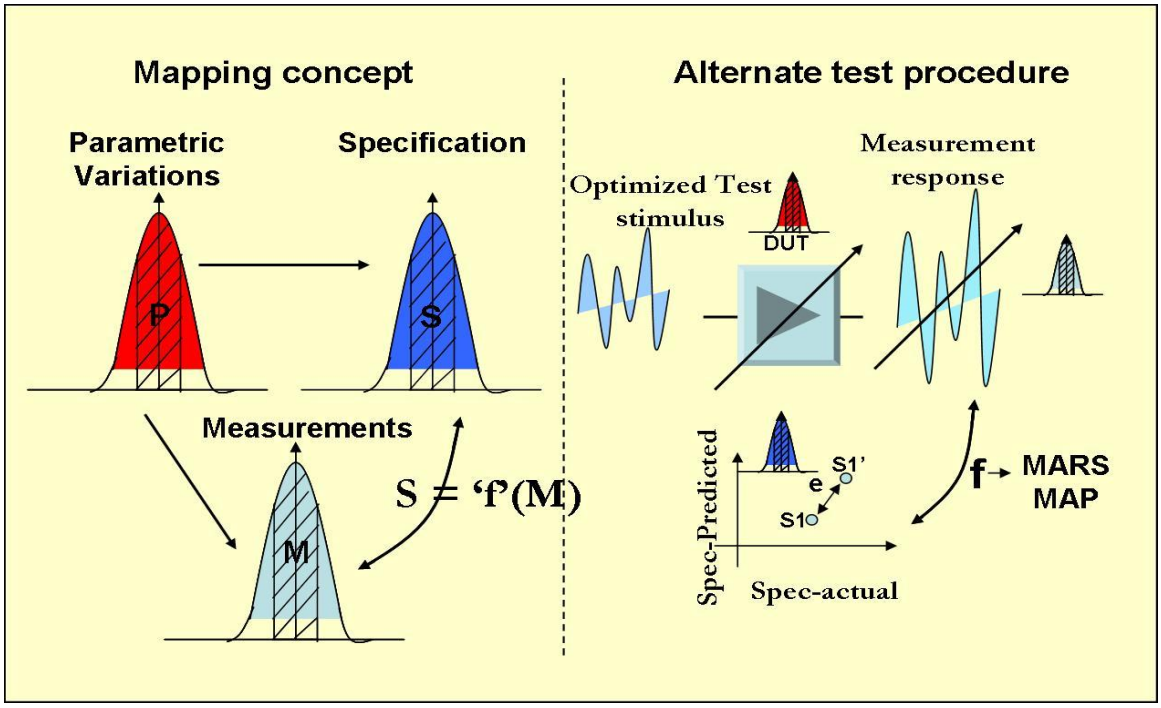

Figure 3: Alternate test framework

The fundamentals of alternate test framework are briefly described in this chapter. Consider variations in the process parameter space **P** of Figure 3 that affect the specifications of the DUT. For low cost diagnosis, an *alternate set of measurements* is determined such that the *test measurements are strongly correlated with variations in the test specification values* of the device under test (DUT) under process variations. This set of measurements defines the *measurement space* **M** of Figure 3. For RF devices, the set of **M** measurements is made on the output of a sensor (e.g. envelope detector) connected to the RF device. Any deviation in the observed measurements from the expected implies a corresponding deviation of the measured RF specifications of the DUT from the expected in the *specification space* **S,** due to perturbations in the process space **P** (see perturbations indicated in Figure 3). A nonlinear regression mapping model using MARS (*M*ulti-Variate *A*daptive *R*egression *S*plines) [19] is then developed using measurements on a "training set" of devices.

The MARS algorithm mainly depends on the selection of a set of basis functions and a set of coefficient values corresponding to each basis function to construct the nonlinear regression model over a predefined training set. The MARS model can also be visualized as a weighted sum of basis functions that span all values of each of the independent variables. MARS uses two-sided truncated functions of the form $(t-x)+$ and $(x-t)+$ as basis functions for linear and non-linear relationships between the dependent and independent variables, t being the knot positions. The basis function has the form:

$$(x-t) = \begin{Bmatrix} x-t & x>t \\ 0 & otherwise \end{Bmatrix} \tag{3}$$

The basis functions together with the model parameters are combined to generate the predicted values from the values of the independent variables. The MARS model for a dependent variable y and M independent terms can be summarized as:

$$y = f(x) = \beta_0 + \sum_{m=1}^{M} \beta_m H_{km}(x_{v(k,m)}) \quad (4)$$

Where, the summation is over the *M* independent variables, and β_0 and β_m are parameters of the model (along with the knots *t* for each basis function, which are also estimated from the data). The function H can be expressed as:

$$H_{km}(x_{v(k,m)}) = \prod_{k=1}^{K} h_{km} \quad (5)$$

Where, $x_{V(k,m)}$ is the k^{th} independent variable of the m^{th} product. During the forward stepwise placement, basis functions are constantly added to the model. After this implementation, a backward procedure is applied, when the basis functions associated with the smallest increase in the least squares fits are removed, producing the final model. At the same time, the *Generalized Cross Validation Error* (GCVE), which is a measure of goodness of fit, is computed to take into account the residual error and the model complexity. The above equation can be further decomposed into sum of linear, square products, cubic products and so forth. Introducing larger or smaller number of basis functions can also change the accuracy.

The relationship between the specifications 'S', mars regression model Ψ and the measurement vector 'p' is of the form:

$$(\overline{s}) = \Psi(p) \cdot (p) \tag{6}$$

Where, *s* represents system performance like Gain, IIP3 etc., *Ψ(p)* represents the non-linear regression function and *p* represents the a vector containing the measurement responses modeled by **'M'**. This model is then used to predict the RF test specifications **S** of the DUT from the observed alternate test measurements **M** as shown in Figure 3. The process of applying the alternate test and predicting the DUT specifications S from the alternate test measurements is performed by algorithms running on the baseband DSP.

The failure coverage of the alternate testing technique depends on the choice of the input test stimulus. The input test stimulus is carefully optimized to result in an output response that is *highly correlated with the specification values of interest*. The optimization of the test stimulus depends on the type of DUT being tested and the performance parameters being evaluated. For a given DUT there are several test generation algorithms [39] available for optimizing the input test stimulus. The optimized test stimulus is applied to each of these DUTs and their resulting responses are sampled and stored. Simultaneously, the output specifications of these devices are measured using the conventional specification test set-ups. The sampled transient measurements are mapped onto the specifications of the device using non-linear regression functions.

During production test, this non-linear regression function is used to predict the specifications of a DUT from its response to the same optimized test stimulus. The production test implementation of alternate test technology is shown in Figure 4.

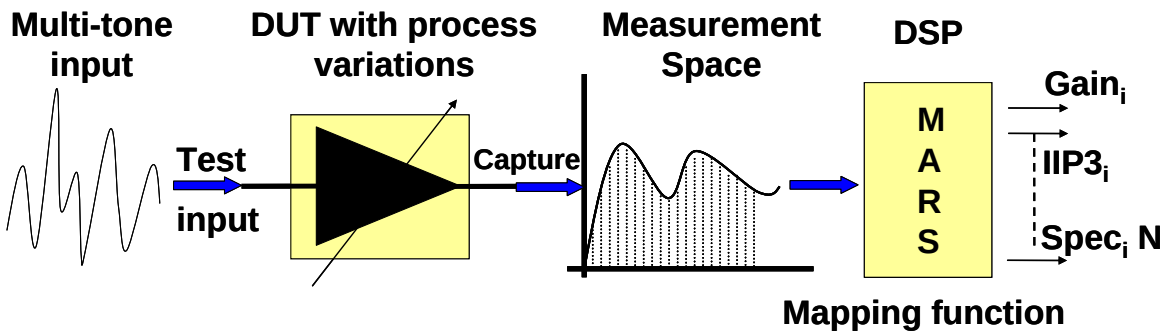

Figure 4: Production test implementation of alternate tests

CHAPTER 3

LOW-COST SPECIFICATION TESTING OF ADVANCED RADIO FREQUENCY FRONT-ENDS

The advent of deep submicron technology along with the high levels of device integration has led to a greater variability in the production yield. Semiconductors in general and RF ICs in particular suffer from severe process variations for technologies approaching 45 nanometer (nm) regimes. The production cycle of RF systems begins with simulations that study the design concepts of a RF system. Upon satisfaction, few prototypes are fabricated and are tested to verify the conformity to design requirements. The findings of the test procedures are fed back to the design cycle for re-evaluation. This is repeated until the design is finalized [40]. Upon finalization, prototypes are fabricated and are characterized heavily to understand the impact of manufacturing process variations. The characterization routines are designed to be extensive and involve high precision bench top equipments to perform testing. A select set of known good devices are identified in this phase. Once a desirable yield is achieved, the devices fabricated go into the production line where the devices are tested for their goodness using a set of carefully chosen parametric and system level tests. The key drawbacks of conventional production testing routines are as follows

- Production test routines are time consuming and often involve switching between multiple test setups.
- The production test infrastructure for testing RF systems is prohibitively expensive due to the requirement of high precision RF sources and sinkers along with high precision digital modulation/de-modulation capability.

In this chapter, several low-cost test solutions that address the issue of test-time and test-cost are discussed. The key objective of these techniques is to accurately

compute multiple RF specifications of advanced RF front-ends in a significantly reduced test time using low-cost test infrastructure environment amenable for production floor deployment.

3.1 ALTERNATE TEST STIMULUS GENERATION: CO-OPTIMIZATION OF TEST INPUT, TEST SIGNAL PATH ARTIFACTS AND EMBEDDED SENSORS FOR SPECIFICATION TESTING OF RF SYSTEMS

It is clear that in the future, advanced scaled-CMOS RF front end modules will need to be carefully tested and calibrated. Built-in-test (BIT) and built-off-test (BOT) solutions offer significant alternatives to conventional production testing to lower the overall manufacturing cost. In the past, there has been significant work in the area of built-in self test using embedded sensors [41]-[43]. The concept of *alternate test* is used to drive the test procedures. However, there exists no formal methodology for determining the *best stimulus to app*ly (which can be generated using the transceiver DSP), the *best embedded sensors to use* (prior work focused only on one specific sensor type for an application), the *nodes at which to place the sensors* and the *accuracy of the data converters* specific to the RF transceiver being tested. The test engineer works with a variety of on-chip physical test circuits and creates a custom test solution for each production part. Significant effort is spent in optimizing and debugging the test approach (derived from bench test procedures) with no systematic tools available to optimally trade off all the built-in test parameters.

A key shortcoming of existing BIT techniques is that separate test procedures and on-chip test hardware is needed for measuring different RF test specifications. In the proposed approach, *all* the RF DUT specs are inferred from a *single* data acquisition resulting in a considerable test time reduction. The proposed methodology determines the *best stimulus to app*ly (generated by software running on the transceiver DSP) and the *best embedded sensors to use* (from a library of sensors) for high quality parametric test

and diagnosis. The *impact of the data converters* specific to the RF transceiver being tested is considered in this methodology. The best sensors to use are those that have the *least* impact on RF DUT performance while generating the *maximum* amount of test information. The volume of data generated by each sensor and the resulting test time is also considered carefully.

3.1.1 GOALS AND OBJECTIVES

The key objectives of the methodology are:

- The applied tests must be generated by an algorithm that *co-optimizes* the test stimulus, the on-chip test stimulus generation and response capture hardware (test access points, test response sensors) in such a way that the non-idealities of the hardware (linearity, noise) are taken into consideration while searching for the "best" built-in test solution (combination of test stimulus, test access points and sensors employed for built-in test).

- The methodology should be able to select the best possible DfT solution for a given DUT. While doing this selection the methodology should take into account the test quality, the dynamic range and the bandwidth of the sensors, the amount of degradation in performance of a DUT due to the insertion of these sensors and the area overhead

- The methodology should significantly reduce the test time and test cost associated with conventional production tests and should be amenable for production floor deployment using a low-cost infrastructure

In the following sections, key components of the proposed methodology are described to address the goals and objectives of this approach.

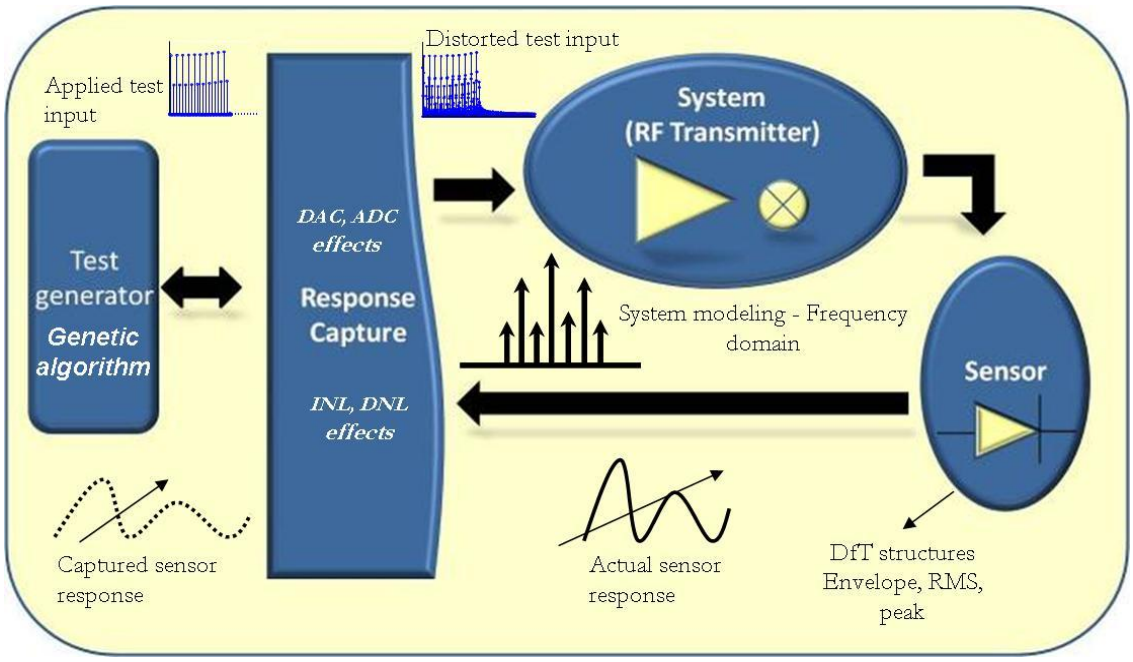

Figure 5: Test Generation Framework

3.1.2 PROPOSED METHODOLOGY

In this work, a formal built-in test development methodology for RF systems is discussed. The test framework uses special embedded RF sensors for test response data acquisition from different points of the RF signal path. The impact of data converters on the quality of test input and the measurement response is modeled into the optimization routines to develop an accurate BIST technique. The methodology is demonstrated on a behavioral model of a 1.5 GHz RF transmitter. The proposed framework is shown in Figure 5.

3.1.2.1 RF Transmitter Modeling

Although, the transistor-level simulation of all the sub-modules yields high accuracy of simulation, long simulation times make this impractical. The primary objective of test generation is to determine the optimal set of test stimuli [44]-[45], rather than to verify the functionality of the design. As long as the behavioral modeling approximations preserve the relative "goodness" of one possible test stimulus versus another, it can be used for fast test generation with little loss in test accuracy as shown in

[44] and [45]. The underlying assumption is that the variations in specification data and measurement data follow the same statistical trend under behavioral parameter perturbations as they would for transistor level parameter perturbations. Figure 6 shows the modeling approach (similar that that proposed in [44], [45]) employed for the RF system-under-test. The behavioral model of each sub-block was constructed as follows

The transfer function of the band-pass filters of the RF subsystem are realized as linear transfer functions with specified magnitude and phase characteristics. The amplifiers of the RF sub-system (e.g. LNA) are realized by implementing a non-linear transfer function of the type

$$y(t) = \alpha_0 + \alpha_1.x(t) + \alpha_2.x^2(t) + \alpha_3.x^3(t) \quad (7)$$

Where, α_0 = DC offset, α_1 = small signal gain, α_2, α_3 = non-linearity coefficients.

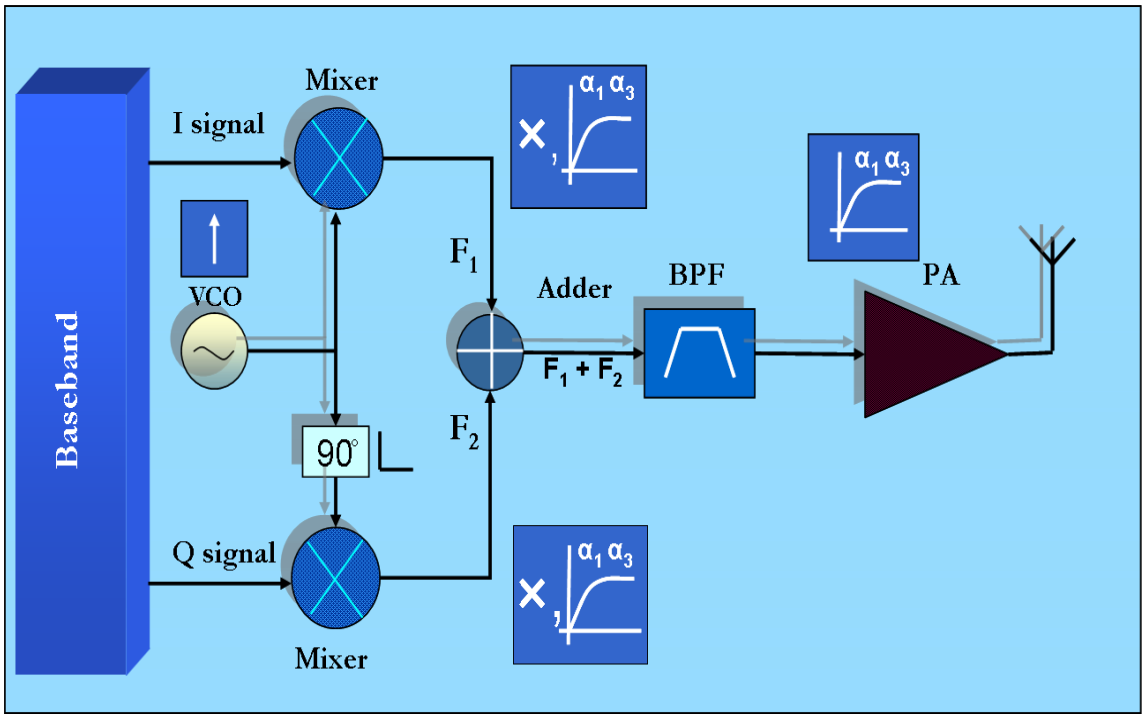

Figure 6: Behavioral modeling of the transmitter

The coefficients are "fitted" to the specified linear (gain) and non-linear (harmonics and inter-modulation terms) effects of the amplifiers concerned. Using the time domain input vs. output characteristic as given by (7), the corresponding output frequency spectrum (both magnitude and phase) is computed. In general, the computation complexity is $O(N^3)$, where N is the number of test tones used for test generation/simulation.

Mixers are modeled as non-linear transfer functions followed by an ideal multiplier. The non-linear transfer function is realized in the same manner as discussed earlier for amplifiers. The frequency mixing operation is realized by the multiplication operation

$$y(t) = C.x_1(t).x_2(t) \tag{8}$$

Where, $\boldsymbol{C}$ represents the conversion gain of the mixer.

The peak amplitude value corresponds to the local oscillator frequency; the amplitudes adjacent to the frequencies fall off according to the phase-noise characteristics of the local oscillator.

The coefficients α_0, α_1, etc. are used to define the linearity of amplifiers and are extracted from the input-output (P_{in}-P_0) relationship of the amplifier as determined by transistor level simulation via least squares polynomial fitting. Alternatively, they can also be extracted from the 1dB compression point and IIP3 specifications of the amplifiers. The coefficients can be determined from P1dB as follows

$$\alpha_3 = \frac{P_0}{\frac{P_{1dB}^2.P_{IN}}{0.145} + \frac{3.P_{IN}}{4}} \tag{9}$$

$$\alpha_1 = \frac{\alpha_3.P_{1dB}^2}{0.145} \tag{10}$$

3.1.2.2 Data Converter Modeling

Modeling the response capture characteristics is a key requirement to ensure the quality of the developed test schemes. The capture characteristics of the ADCs/DACs present in the system (or in testers in production test environment) significantly affects the signal quality of both the applied test stimulus and the observed test response. Hence it becomes imperative to model these characteristics to develop reliable test schemes. In this work the capture characteristics are modeled based on nonlinear characteristics of the PCI6115 data acquisition card (DAQ). PCI6115 is used as a low cost replacement to an ATE to transfer the test data to the baseband processor (PC). The integrated non-linearity (INL) and the differential non-linearity (DNL) characteristics obtained from the datasheets of the PCI6115 DAQ card are used to characterize the sourcing and digitizing properties of the data acquisition system. The frequency domain inputs and outputs of the developed digitizer model are shown in Figure 7.

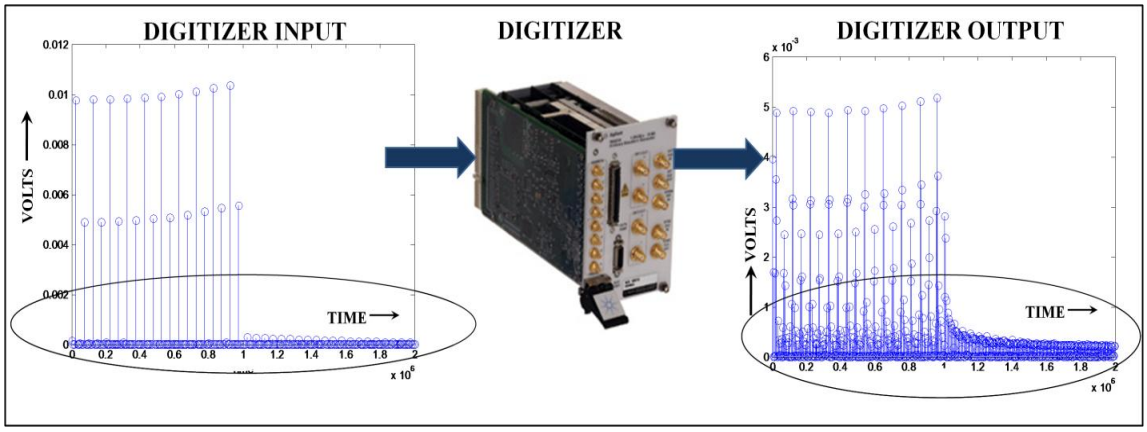

Figure 7: Test response before and after the digitizer module

It can be observed from Figure 7 that the signal quality of the test response is affected significantly by the nonlinearities of the data converter modules.

3.1.2.3 Embedded Sensor Modeling

In this section the modeling of three different types of test response sensors has been discussed.

The envelope detector (shown in Figure 8a) and its uses as a test response sensor were first proposed by Han and Chatterjee in [41]. This is a common circuit for AM demodulation, composed of a diode, a resistor, and a capacitor. Through proper adjustment of the RC constant value, the requisite envelope detection can be performed. The value of the *RC* time constant should be such that: $fo << 1/RC << fc$. This allows the circuit to track the low frequency envelope of the RF signal. Considering that the above two frequencies have large separation, the *RC* time constant can be picked to make the decoded envelope immune to process variations. A key consideration is the loading of the Circuit under Test (CUT) by the envelope detector. The input impedance of the envelope detector depends mainly on the bias resistors and the capacitance of the diode.

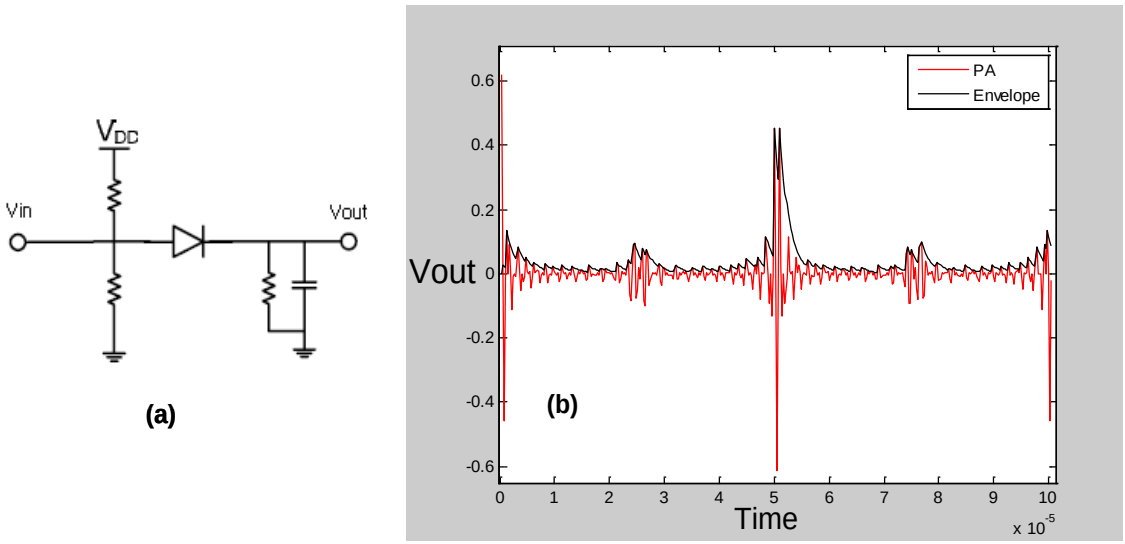

Figure 8: (a) Envelope detector schematic (b) Envelope detector output

The bias resistors are relatively large compared to the typical 50 ohm RF matching impedance. During the normal operating mode, the power for the envelope

detector can be turned off using a transistor switch [46] in which case, the diode behaves like an open switch. In general, the capacitance of a diode is several tens of farads. Therefore, the impedance (loading) of the envelope detector has negligible effect on the RF DUT performance. Figure 8b shows the transient output of the envelope detector showing tracking the input RF envelope. The observed output is a transient waveform and hence it has much more information compared to the output of RMS or peak detectors. However this added information comes at the cost of having to process much more data than just single DC RMS or peak values.

The schematic of the RMS sensor [47] is shown in Figure 9a. Elements L1 and C1 form the matching network, providing a 50 Ohm match at 1.5 GHz. The low value of S11 for this detector (<-45dB) results in minimal loading of the RF system. R2 is chosen so that the circuit provides the "true" RMS value of the input signal at the output of the detector. The output of the detector for a multi-tone input stimulus has been plotted in Figure 9b for four different specified combinations of input power levels. It can be observed that both the DC value as well as ripple voltage increases with increase in input power level.

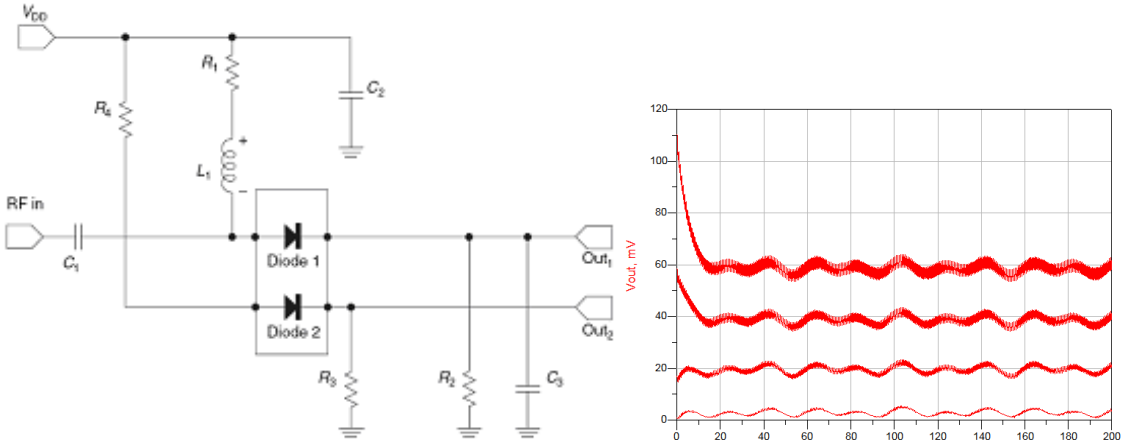

(a) **(b)**

Figure 9 : (a) RMS detector schematic (b): RMS detector output

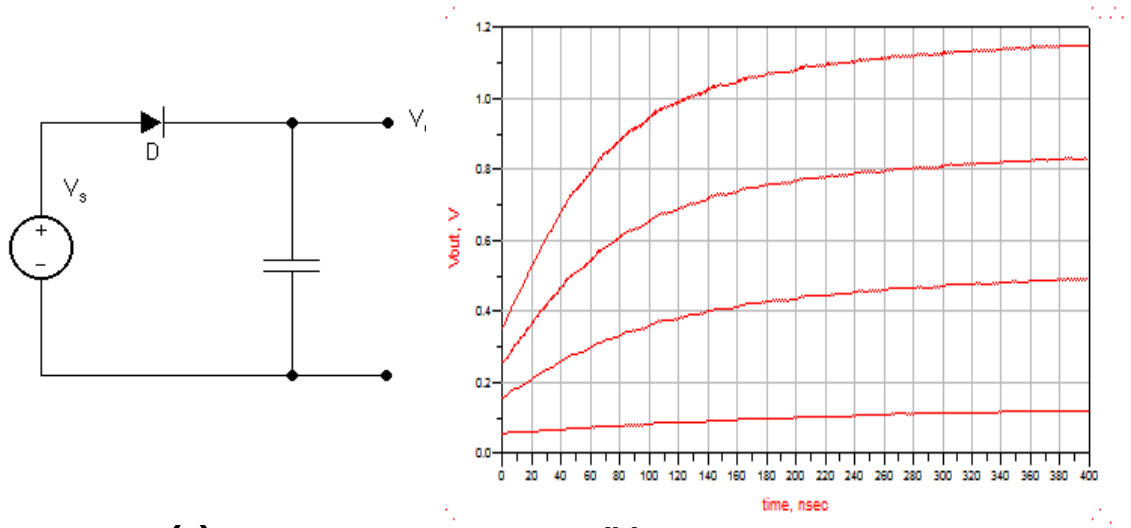

Figure 10: (a) Peak detector schematic (b) Peak detector output

The conceptual diagram of a standard peak detector is shown in Figure 10a. The biasing and matching circuits have not been shown for simplicity. The output is a DC voltage indicating the peak of the applied voltage. As shown in Figure 10b the output voltage takes some time to reach its final value. This transient response is ignored and the final steady state value is considered as the peak value. Figure 10b shows the transient output voltage for different power levels of a multi-tone input signal. The voltage attains a certain steady state level after a certain amount of time depending on the input power level. This information is used to model the peak detector.

3.1.2.4 Test Generation

In this approach, regression functions such as those generated by MARS are used to build a mapping function between the test response and the DUT specifications using a set of devices with random process variations denoted as the *training set.* During the actual test, trained MARS models are used to predict the specifications of the DUT from the observed test response. It should be noted here that a *defect filter* is used to screen out devices with catastrophic faults, and only the devices that "pass" the defect filter are

considered for this study. This defect filter consists of simple algorithms that analyze the test response of the DUT to determine whether it has characteristics that are significantly different from the "training set" of devices used to build the MARS regression model described earlier. The test quality of alternate tests is highly correlated to the sensitivity of the observed measurement response to the changes in the process parameters. For a given DUT there are several test generation algorithms available for optimizing the input test stimulus. In this work a genetic algorithm based test generation (as shown in Figure 11) for the proposed framework (shown in Figure 5) is used due to the nonlinear nature of the search space to avoid local convergence.

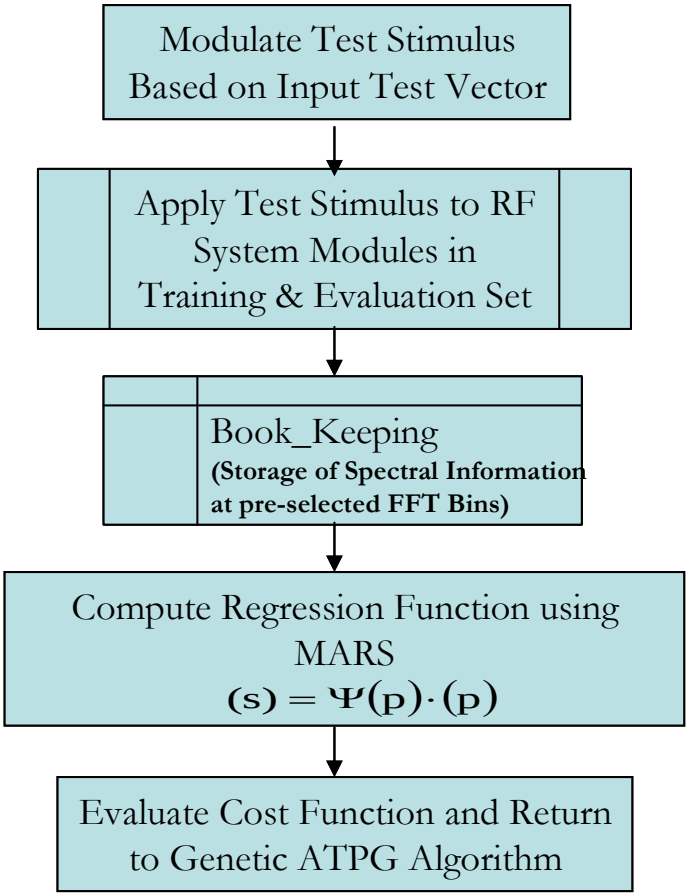

Figure 11: GA based optimization routine.

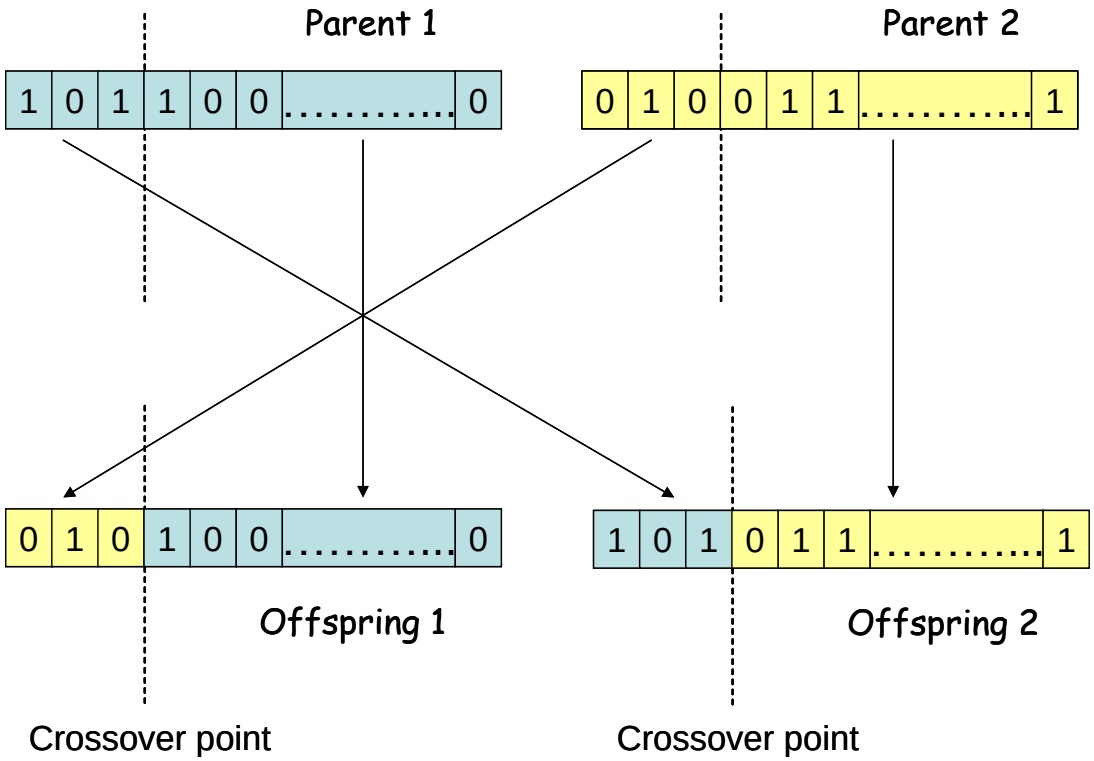

Figure 12: Single-point crossover operation for reproduction in the GA.

C*rossover* and *mutation* are the two mechanisms by which a new generation is created [48]. Figure 12 shows an example case of crossover. In crossover, two parent genes are crossed over in an arbitrary fashion defined by the crossover probability to result in a completely new child. In mutation a single bit of the gene sequence is randomly mutated as defined by a mutation probability to result in a new child. These two mechanisms are responsible for the creation of new chromosomes which in-turn are assessed for their fitness. There is one another mechanism known as elitism in which genes with a particular fitness values are classified as *elite* and are passed on from one generation to another without any crossover or mutation. This ensures that a "minimum" fitness is passed on from one generation to another. Further insights into the algorithms can be found in [48].

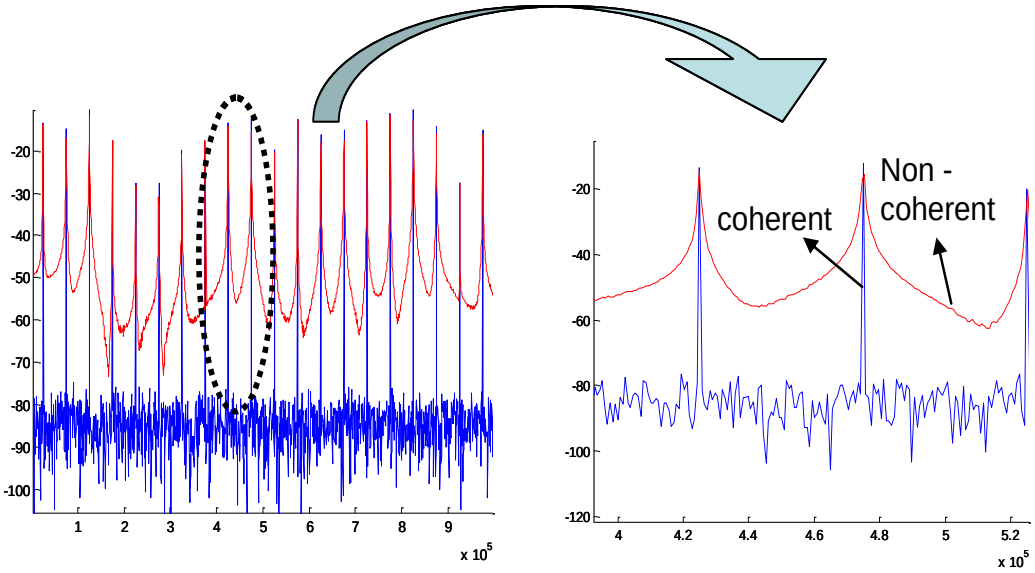

Figure 13: Coherently and non-coherently sampled response

A multi-tone test input is used as the test stimulus of choice. A set of 20 tones are uniformly deployed across a bandwidth of 1MHz. The amplitudes of the tones are detrmined by the optimization algorithm. The amplitude levels are allowed to have 32 (2^5) levels of variation ranging from -70 to 10 dBm. Thus each tone can be coded into a 5 bit gene sequence to result in a 100 bit gene individual thereby defining the search space of the optimization algorithm. Figure 13 shows the frequency domain representation of two multi-tone signals with 20 component tones with coherent and non-coherent sampling. The wide-skirts observed in Figure 13 are the outcome of non-coherent sampling of the time domain wave-form. Coherency is mathematically represented as follows

$$\frac{f_{IN}}{f_S} = \frac{n_{WINDOW}}{n_{RECORD}} \tag{11}$$

Where f_{IN} is the input frequency of the multi-tone signal, f_S is the sampling frequency, n_{WINDOW} is the number of cycles of the signal that fits in a sampling window

and n_{RECORD} is the number of data points in the FFT of the signal. The presence of unwanted tones in the test input degrades the test quality significantly. Hence it is very critical that the multi-tone is coherently sampled. The coherently sampled, genetically optimized multi-tone waveform is then used to obtain the appropriate test response, based on which the RF system level specifications are computed by using nonlinear regression mapping techniques such as MARS.

3.1.3 VALIDATION RESULTS

The proposed test simulator as described above is used to evaluate different BIT alternatives. Three BIT candidates with envelope, peak and RMS sensors at the output of the power amplifier of a wireless OFDM transmitter are selected for evaluation. The test generation algorithm produces an optimized test stimulus for each BIT candidate. The BIT candidates are then ranked in order of the accuracy with which the test specifications of the RF DUT can be predicted from the observed test response. Since the hardware cost of each BIT solution is also known, the test designer can then pick the best solution from a cost vs. accuracy perspective as desired by the test customer.

3.1.3.1 Test Generation Results

The genetic algorithm based test generation is run for each BIT candidate, to obtain the best possible test input. For a multi-tone test input defined by a single individual, the regression functions that define the MARS model are computed by training for a set of 200 devices. The Model is then evaluated for RMS error in prediction. The RMS prediction error of the developed MARS model is used as the fitness function of the proposed genetic algorithm. Gain, IIP3 and EVM and I/Q phase mismatches are considered as the specification of interest for the evaluated BIT technique. The frequency domain representation of the optimized coherently sampled multi-tone test input for a BIT solution with envelope detector is shown in Figure 14.

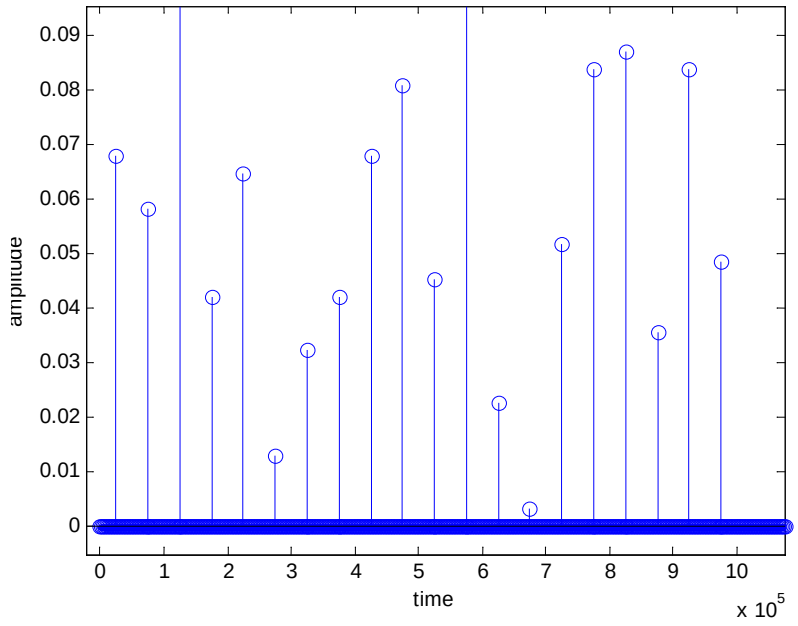

Figure 14: Optimized multi-tone test stimulus

3.1.3.2 Prediction Accuracy for the Optimized Test Input

The quality of the alternate test procedure employed is determined by the accuracy with which the specifications of the DUT could be predicted from the obtained BIT response. The RMS prediction error over a large number of evaluation instances of the DUT is used to quantify the quality of the BIT technique. This RMS error in prediction for IIP3 is shown in Table 1 for a set of optimized multi-tone inputs. It can be observed that the BIT candidate with envelope detector at the output of the PA results in the least RMS error in prediction.

Table 1: Evaluation of the test quality for three types of DfT solution for IIP3 estimation

Error Type	Envelope	Peak	RMS
RMS error	0.1475	0.2	0.21

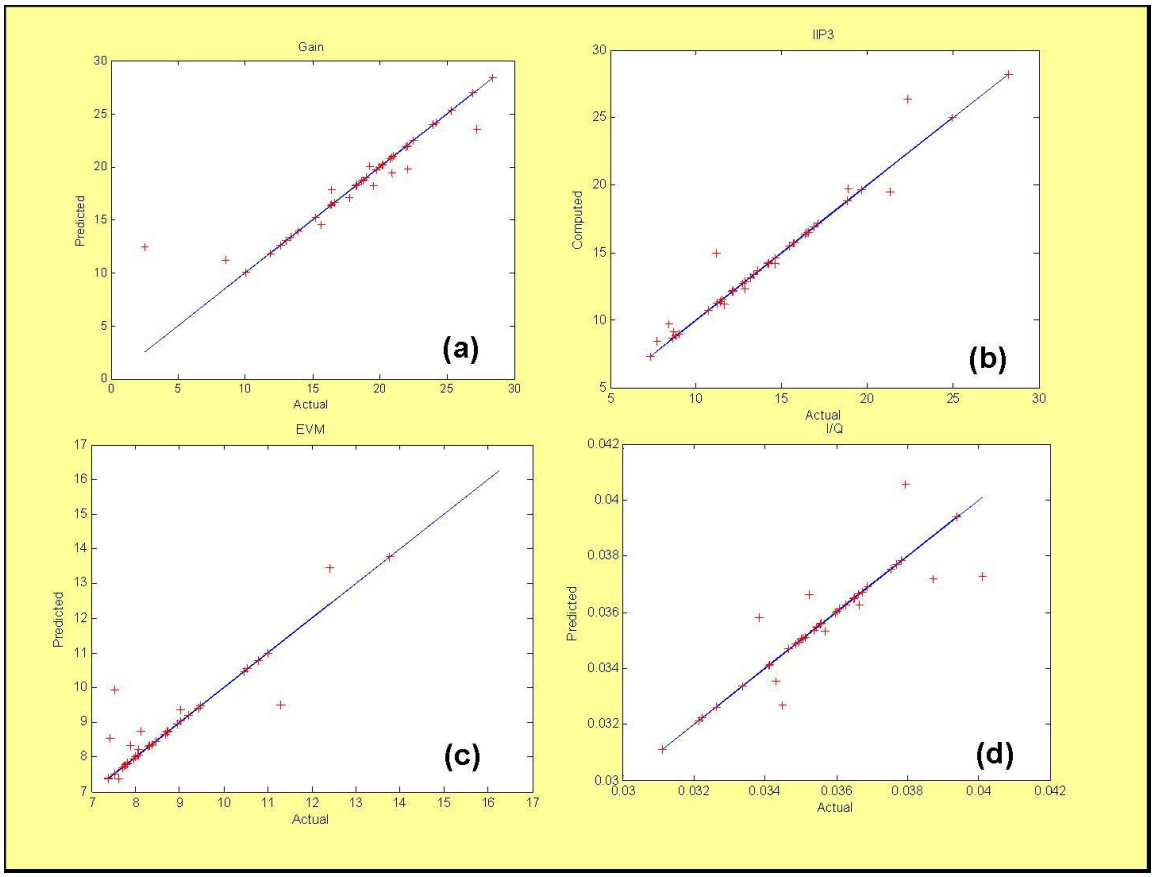

Figure 15: Estimation plots for (a) Gain (b) IIP3 (c) EVM and (d) I/Q phase mismatch

3.1.3.3 Performance Degradation

For simplicity the sensors are deployed only at the output of the power amplifier of the RF transmitter. This results in lower performance degradation of the transmitter in comparison to the case where sensors are placed at the output of the mixer as well. The performance degradation simulations are run using ADS (Agilent Advanced Design System). The performance degradation plots in terms of the operating *gain* of the transmitter are shown in Figure 16. The results are quantified numerically in Table 2 for a specified level output power level of the transmitter. It is observed that the envelope

detector provides the least performance degradation of 1dB at an output power of 15 dBm.

Table 2: Performance degradation of the Power amplifier @ 15dBm output power level

Component	Actual	Envelope	Peak	RMS
PA	15.16 dB	14.14 dB	10.58 dB	10.64 dB

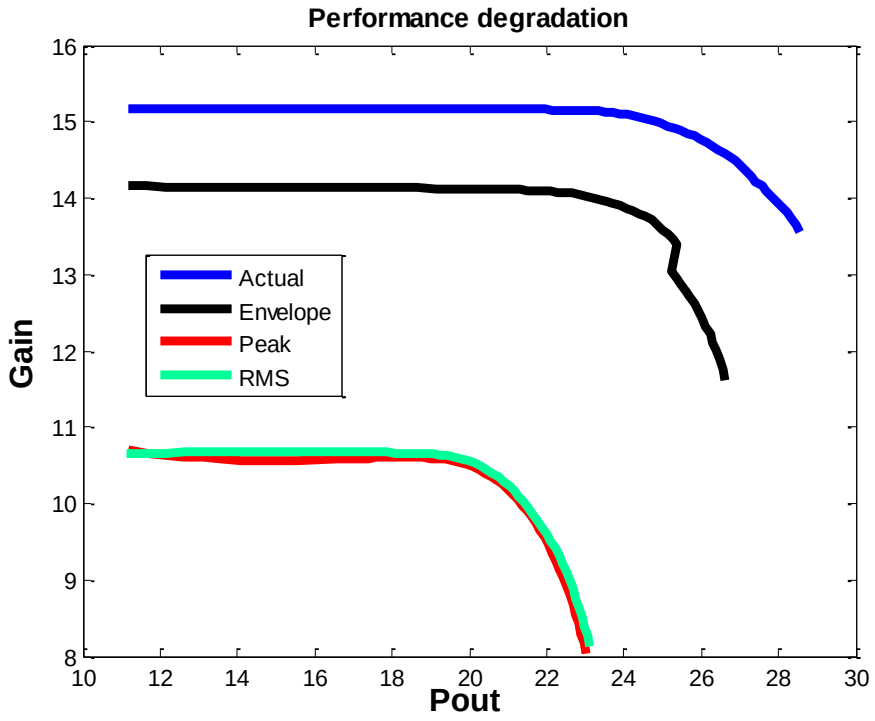

Figure 16: Performance degradation of the power amplifier for three types of sensors

3.1.3.4 Bit Candidate Selection

The BIT candidate that provides the least amount of performance degradation while providing acceptable accuracy of specification prediction from the test response is chosen as the final test solution. In this regard, the envelope detection sensor attached to

the output of the transmitter is found to have the best performance of the three sensors investigated in this work. It is important to note here that the developed tool has the capability to select the best possible embedded sensor solution given a library of sensors and their designs (e.g. there are many different ways an RMS sensor can be designed). The scatter plots obtained for the final test solution for Gain, IIP3, EVM, and I/Q phase mismatch specifications are shown in Figure 15. It can be observed that the co-optimization of the test stimulus, response capture and the sensor solutions result in a high accuracy of prediction for the proposed alternate test based BIT technique.

3.1.4 KEY ADVANTAGES

The key advantages of co-optimizing the multi-tone test input for specification test accuracy, test signal path artifacts and the embedded sensor artifacts are summarized below,

- Co-optimization of the test stimulus and the response capture (data converters) characteristics results in developing a BIT solution with high accuracy of prediction for an alternate test based BIT methodology. This is achieved by modeling the data converters by their non-idealities to quantify their impact on the test input.
- The proposed methodology is capable of selecting the best 'test DfT' solution from a library of sensors. The co-optimization technique is used to compute the test quality for a given sensor. Based on the requirements of the test engineer, the knowledge gained through the developed methodology can be used to trade-off between the test quality, performance degradation, dynamic range etc to select a viable BIT solution.
- The proposed methodology is amenable for a production floor deployment using a low-cost infrastructure to accurately estimate multiple RF specifications

3.2 CROSS-LOOPBACK BASED SPECIFICATION TESTING OF MULTI-BAND, MULTI-HARDWARE RADIOS

Commercial mobile handsets available today such as iPhone4 integrate UMTS/HSDPA/HSUPA (850, 900, 1900 and 2100 MHz), GSM/EDGE (850, 900, 1800 and 1900 MHZ), 802.11 b/g/n Wi-Fi (2.4 GHz) and Bluetooth standards (2.4 GHz) into a single device. Due to the impact of process variations on the system performance, it will be very important to perform rigorous testing and diagnosis of such transceiver systems. Due to the broadband nature of the transceiver architecture, the cost of a precision external tester for manufacturing test will be significant.

To resolve the problem of testing such integrated multi-band/multi-standard radios, a *cross-loopback* test approach is proposed. In *cross-loopback*, a transmitter corresponding to a selected frequency band and RF standard is used to *test a receiver corresponding to a completely different frequency band and RF standard* using optimized *multi-tone* alternate test stimulus. During the test procedure all the standard signal modulation and demodulation are algorithms turned "off". As an example, a GSM transmitter may be used to test a Bluetooth receiver and vice versa. The proposed methodology is validated on the '*behavioral level'* model of a multi-hardware, multi-standard radio.

3.2.1 GOALS AND OBJECTIVES

The key objectives for testing multi-hardware, multi-band radios are

- The test methodology should be modulation independent to scale across multiple transceiver chains
- The output of a source transmitter should be frequency scalable and the output power level of a source transmitter should be scalable
- The test methodology should be able to accurately track the individual transmitter and receiver specifications

3.2.2 PROPOSED METHODOLOGY

In order to meet with above mentioned requirements, the following is proposed,

- A Test generation methodology to generate optimized 'Multi-tone' alternate test stimuli
- A 'wide-band' passive mixer with a 'programmable' VCO to provide the LO input to perform frequency translation.
- A 'programmable' attenuator to scale the power levels of a source transmitter.
- Methodology to map the test response (low frequency) of the system to its subsystem specifications

The wideband mixer, along with the programmable VCO and a programmable attenuator will be collectively referred as the DfT resource for the rest of the document. The proposed methodology is a load-board solution, in which the DfT resource is implemented on the load-board. It should also be noted that the simplicity of the solution lends itself amenable for a compact BIST implementation. The following sub-sections detail the key components of the proposed methodology.

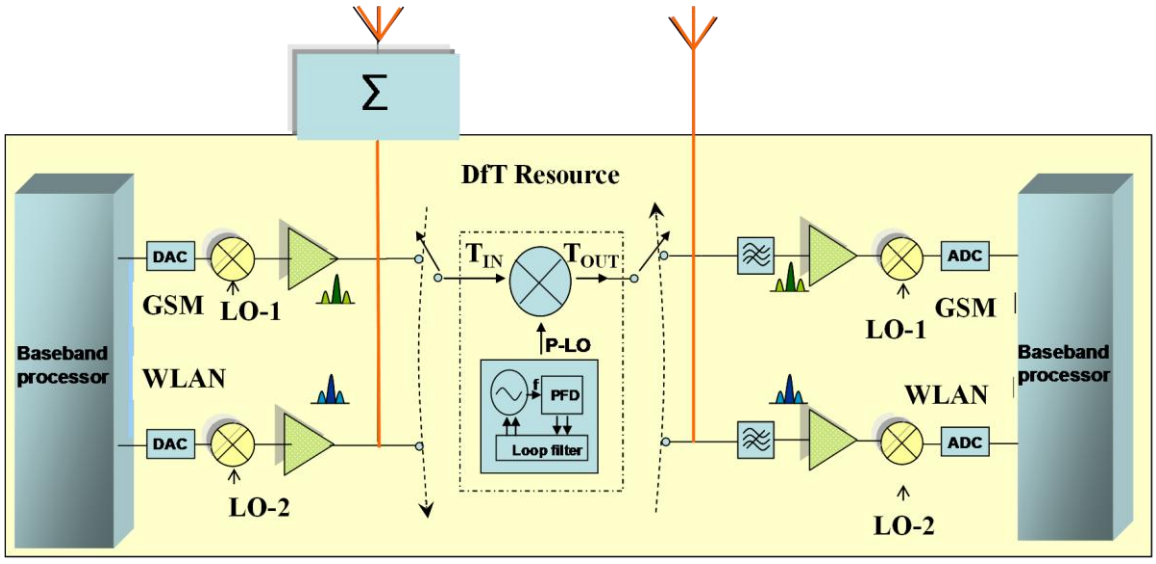

Figure 17: Cross-loopback test architecture

3.2.2.1 Test Architecture

Figure 17 shows the proposed cross-loopback architecture. The behavioral model of the multi-band radio deployed for proof of concept of the proposed methodology consists of (a) a 900 MHz GSM transceiver system and (b) a 2.4 GHz 802.11g WLAN transceiver system. These systems can be a single chip solution with a multi-hardware approach or more common tightly integrated three-chip systems on package (SoP) solution. The subsystems are cross-loop backed via the DFT resource implemented on the load-board. Cross-Loopback derives its name from the fact that it cross-loopbacks the transmitters and receivers of completely different RF standards. For the radio under consideration, the following cross-loopbacks are performed via the DFT resource

- Spectral output of the 900 MHz GSM transmitter is loop-backed (cross) with the 2.47 GHz 802.11g receiver
- Spectral output of the 2.47 GHz 802.11g WLAN transmitter is loop-backed (cross) with the 900 MHz GSM receiver

The test responses are captured at the baseband output of the receiver for the selected cross-loopback path. The advantage of doing such a multi-tone based cross-loop back is that, it alleviates the complexities [49] associated with (a) half-duplex mode of operation of the transceiver subsystems and (b) VCO modulation scheme based transceiver subsystems (Bluetooth systems typically deploy VCO modulated architectures). The cross-loopback is achieved via the DFT resource. It's necessary that the mixer has a wideband performance since it must be able to frequency translate the spectral outputs of the transmitters across multiple frequency bands. A simple wideband passive mixer can be used for such purposes. Linear Technology's LT5521, is one such mixer (passive) with an operating frequency range of 10MHz to 3.7GHz. Similarly, programmable attenuators can be implemented using typical log- amplifiers, thereby rendering the above proposed DFT resources feasible for a production test deployment.

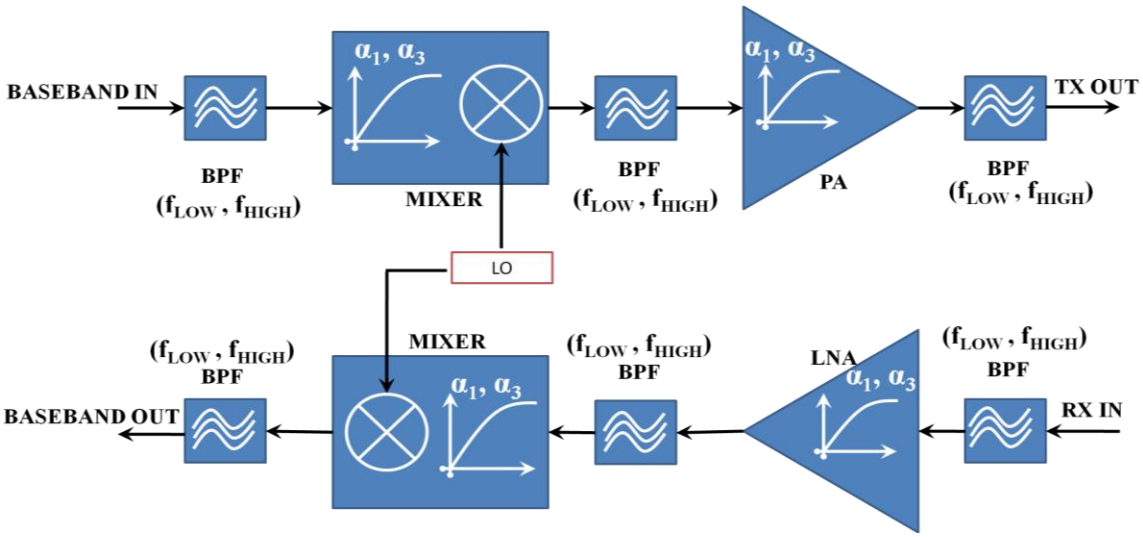

Figure 18: Behavioral Modeling of the Transceiver

Observed test responses at the receiving ends of the architecture are then used to build a non-linear regression model that can be used to accurately predict the performance parameters of the subsystems.

3.2.2.2 System Modeling, Test Generation and Specification Estimation

The mixer and the amplifier modules of the transmitters and the receivers are defined similar to the models discussed in previous section. The block diagram representations of the models are shown in Figure 18. The multi-tone test input definition and the test generation is performed similar to the algorithm proposed in Section 3.1.2.1. The test generation is performed for each cross-loopback path. For a given cross-loopback path MARS is used to build the regression map (built-offline) between the observed test responses and the specifications of the individual transmitters and receivers. During the test generation procedure, for a chosen cross-loopback path, the prediction accuracy of the MARS model evaluated over a set of instances is defined as the fitness value of the *genetic individual* that defines the test input. Once the test generation is performed, during production testing the test response captures of the selected cross-loopback path for an optimized multi-tone test input are used to estimate the

specifications of the individual transmitter and the receiver using the developed MARS models. The specifications targeted are gain and IIP3 of the individual transmitters and receivers.

3.2.3 VALIDATION RESULTS

The proposed methodology is validated on a behavioral model of a multi-band radio with GSM and WLAN modes of operation. The 900 MHz GSM transmitter is cross-looped with the 2.47 GHz WLAN receiver and vice versa via the load board DfT. The programmable 'lo' and the programmable attenuator are set to 1.57 GHz and 10 dB respectively. The genetic algorithm based test generation results for the cross-loopback paths are shown in Figure 19. The multi-tone is defined to have 20 tones within a 1 MHz bandwidth. The amplitudes of the tones are determined by the optimization algorithm.

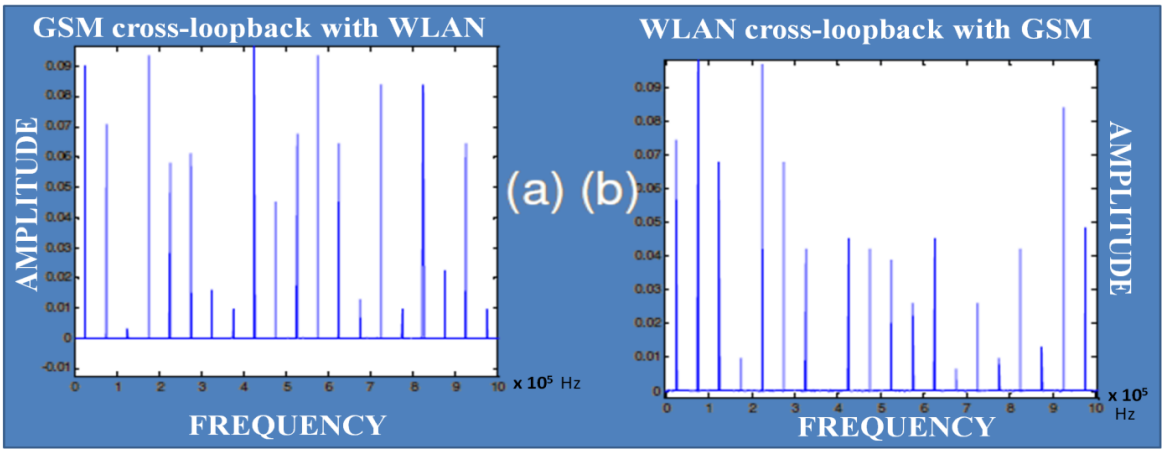

Figure 19: Frequency spectrum of the Optimized multi-tone for (a) GSM transmitter cross-loopback with WLAN receiver and (b) WLAN transmitter cross-loopback with GSM receiver

The MARS model is built for a training set of instances generated by Monte Carlo simulations on the behavioral parameters in MATLAB. A set of 80 instances and a set of 20 instances of the transmitter and the receiver were used as the training set and the evaluation set for each cross-loopback path respectively. The scatter plots presenting the

prediction results for GSM transmitter cross-loopback with WLAN receiver are shown in Figure 20 and WLAN transmitter cross-loopback with GSM receiver are shown in Figure 21.

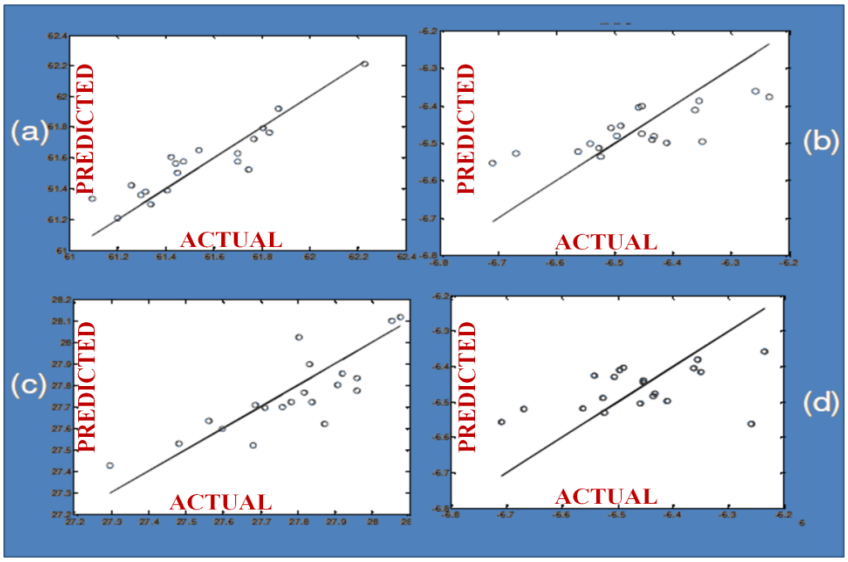

Figure 20: Prediction results for GSM transmitter (a) gain (b) IIP3 and WLAN receiver (c) gain (d) IIP3

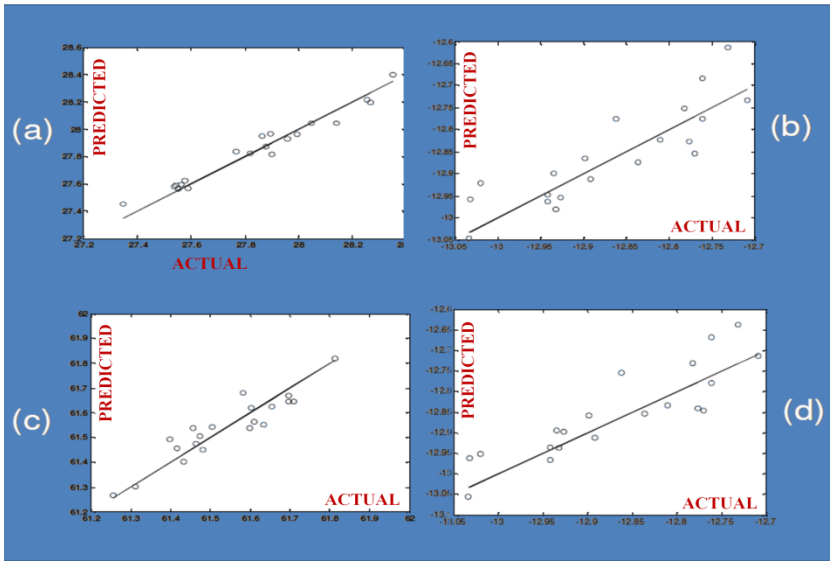

Figure 21: Prediction results for WLAN transmitter (a) gain (b) IIP3 and GSM receiver (c) gain (d) IIP3

The percentage relative error in prediction between the actual and the predicted values were observed to be less than 5% in the scatter plots shown in Figure 20 and Figure 21. The prediction results can further be improved by increasing the number of instances for which the MARS model is built. However, this increases the computation time exponentially for test generation purposes. The results discussed here are simply meant to demonstrate the capability of the proposed test at a proof-of-concept capacity.

3.2.4 KEY ADVANTAGES

The key advantages of performing cross-loopback testing of multi-band radios using a multi-tone test stimulus are

- The cross-loopback test procedure allows each transceiver in the multi-band radio to *operate in its native half-duplex mode*. The DfT resources with careful planning can be designed into the SoP solution, there by rendering the developed methodology amenable for BIST implementation.
- The proposed technique can also be extended to a multi-site testing environment where, the transmitter of DUT at one site can be cross-loopbacked with the receiver of a DUT (designed for a different standard) in another site and vice-versa. This enables parallel testing of different families of transceiver products at the same time, thereby contributing to a significant reduction in the test cost.
- *The technique uses multi*-tone stimulus as a test input, thereby making the test procedure modulation independent. Further, problems with loopback in VCO modulated architectures that result in modulation cancellation such as faced while doing loopback test of a Bluetooth device are automatically resolved.
- The test generation procedure is a one-time cost and can be performed extensively and can be performed on processors with powerful computation capability to allow accurate prediction of the various transmitter and receiver test specification values.

3.3 LOW COST EVM TESTING OF WIRELESS RF SOC FRONT-ENDS USING MULTI-TONES

Typically RF devices are tested for fundamental specifications such as gain, linearity metrics (second and third order amplitude and phase distortion metrics), quadrature mismatches (amplitude, phase), phase noise, noise figure (NF) and end-to-end system level specifications such as EVM (error vector magnitude), BER (bit-error-rate) etc. Due to the reduced visibility imposed by high levels of integration, testing for fundamental module level specifications are becoming more and more complex. Hence, design and test engineers rely heavily upon design-for-test (DfT) solutions to perform testing on individual blocks, thereby increasing the overall design complexity.

In order to reduce test time and complexity, it's desirable to migrate towards system level testing for specifications such as EVM that are sensitive to module level impairments. EVM, a critical specification, is primarily a measure of the digital modulation quality of a wireless RF system. EVM is sensitive to fundamental impairments introduced by the various building blocks (digital, mixed signal and analog blocks) of a RF system and hence has the potential to replace the testing of fundamental specifications such as gain, linearity quadrature mismatch, noise etc, to ensure the quality of a RF system [50]-[52]. Further, EVM exhibits strong correlation to the BER (an end-end quality of service metric that quantifies the errors introduced into the transmitted digital bits) of a communication system [53]. Hence production testing of EVM in lieu of individual RF and baseband specifications is of critical importance to reduce the overall test cost.

Conventionally, EVM is tested by sending and receiving digitally modulated symbols through a RF system for a communication scheme of choice. The most common communication scheme in use today is the orthogonal frequency division multiplexing (OFDM as specified in standard [54]). The IEEE WLAN 802.11 standard for EVM measurement [54] requires that "*the test shall be performed over at least 20 WLAN*

frames and the packets under each frame shall be at least 16 OFDM symbols long. Random data shall be used for generating the symbols". To perform EVM measurement in accordance to the standard specified in [54] incurs significant test time to transmit and capture 320 OFDM symbols and requires a test system with full OFDM modulation and demodulation capability. In production testing, such requirements translate to higher test cost per unit device. Further, for testing a RF transmitter, the measurement system must duplicate the entire receiver chain accurately (and vice versa). Such requirements escalate the overall test cost and contribute significantly towards the overall manufacturing cost of a RF system. Hence, there is an urgent need to develop new EVM test methods that are fast and inexpensive in terms of the complexity and cost of test instrumentation. Further, it's desirable to develop techniques that are scalable across multiple standards to benefit EVM test cost reduction in general. Prior research [10]-[14] & [55]-[57] in the area of production testing of EVM offer reduction in test cost and test time however they fail to address the key bottleneck in obtaining significant test time savings by using modulated symbols as test input. Hence it's critical to develop techniques using multi-tone test input to significantly reduce test time.

In this section, a new EVM test approach that has the potential to significantly reduce overall EVM test cost is presented. *The proposed approach involves the usage of multi-tones to perform EVM testing and consists of two components: (1) Quantification of the deterministic attributes of EVM from fundamental static impairments and (2) Quantification of the random attributes of EVM from fundamental dynamic impairments. The deterministic and the random components are the used to compute the overall EVM of the system.*

3.3.1 CONVENTIONAL TESTING OF EVM AND LIMITATIONS

EVM offers insight into the performance of a digital communication system. EVM is gaining in popularity as a mainstream production test to quantify the system-

level functionality of a radio and is already integrated into several emerging communication standards [52],[54]. Under production test conditions the EVM of a radio (ideal channel) quantifies the overall effect of digital, mixed-signal and RF impairments on the quality of digitally modulated signals [50]-[52]. EVM is typically measured by sending digitally modulated symbols (QPSK,QAM etc) through a DUT and capturing the appropriate symbols (demodulated from the DUT response). The symbols (both transmitted and received) are typically plotted on a complex I/Q plane and is referred to as a constellation diagram (shown in Figure 22a for QPSK modulation). Figure 22b shows the error vector corresponding to a single constellation point in the first quadrant. The root mean square of several such error vectors between the normalized received symbols and the transmitted symbols is calculated for a sufficiently large number of symbols.

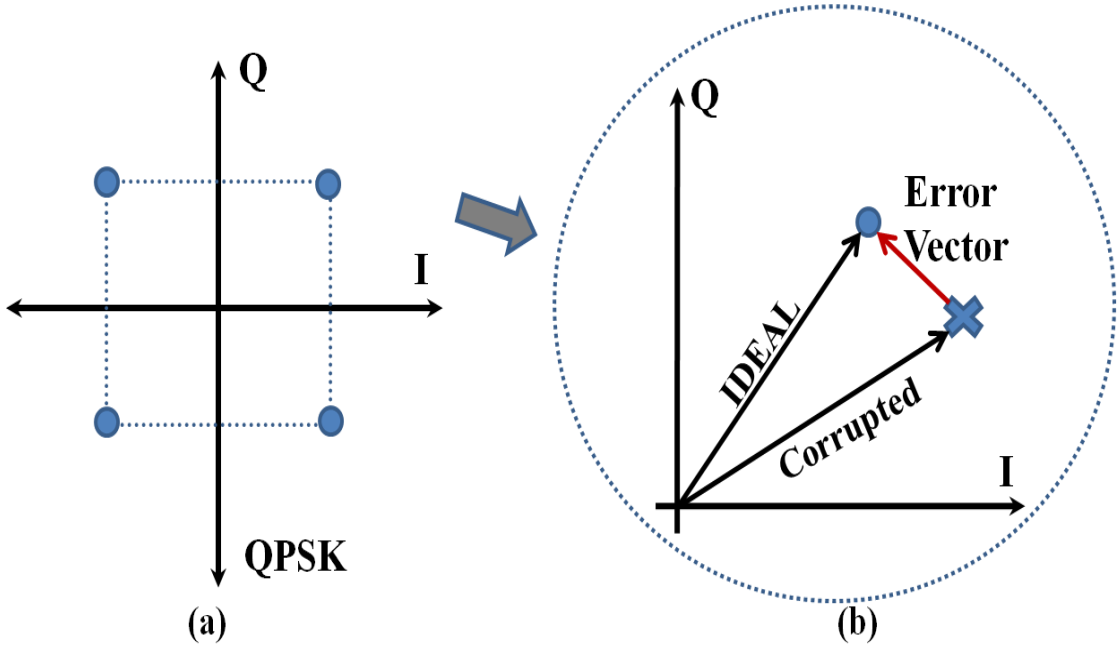

Figure 22: (a) Constellation plot for QPSK, (b) Error vector for a transmitted and received symbol in the 1st quadrant

The root mean square error is typically represented as a percentage of the average power of the transmitted symbols for a multi-carrier system and is commonly referred to as EVM_{RMS} [58]. From this point forward in this thesis, for simplicity EVM_{RMS} is denoted as EVM and is expressed as follows

$$EVM = 100 * \frac{\sqrt{\frac{1}{N}\sum_{i=1}^{N}\left|S_{IDEAL,i} - S_{MEAS,i}\right|^2}}{\sqrt{\frac{1}{N}\sum_{i=1}^{N}\left|S_{IDEAL,i}\right|^2}} \tag{12}$$

Where, $S_{IDEAL,i}$ denotes a transmitted (ideal) data symbol, $S_{MEAS,i}$ denotes a received (corrupted) data symbol and N denotes the number of data symbols for which EVM is computed. It's common to perform normalization of the received data symbols and the transmitted data symbols before computing EVM. As recommended by the WLAN standard at least 320 randomly generated OFDM symbols are required to perform the EVM test. Each OFDM symbol is constructed using 48 data symbols, there by requiring at least 15360 data symbols. The number of bits required depends on the type of digital modulation technique. For e.g. a 16 QAM technique would require 61440 bits (4-bits/symbol) to generate the required 320 OFDM symbols.

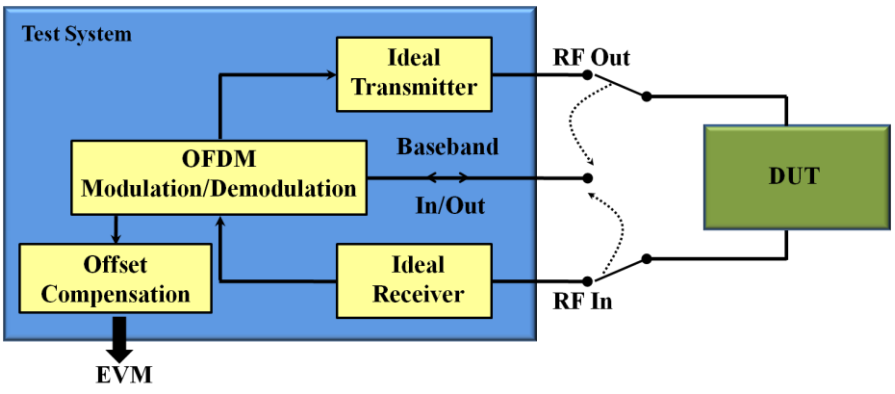

Figure 23: Production test setup for EVM

A typical production test setup for EVM testing of a generic DUT is shown in Figure 23. The requirements of an ATE to perform EVM testing vary based on the type of RF device that is being tested for and are summarized below based on the 802.11 standards

Stand-alone modules: Devices that fall under this category typically are power amplifiers (PA), low noise amplifiers (LNA) and up/down conversion mixers. To test these devices, the ATE should have high precision RF/Baseband sourcing and sinking capability. The ATE should also have sophisticated digital modulation and demodulation capability to send and receive 802.11 OFDM frames.

Transmitter/Receiver: The modulation/demodulation requirements are identical to the first case. For transmitters, the ATE should be capable of replicating an *ideal* receiver with an appropriate architecture. For receivers the ATE should be capable of replicating an *ideal* transmitter with an appropriate architecture.

Transceiver: For an integrated transceiver, the current industry practice is to test for transmitter and receiver EVM separately. Although it's desirable to perform loopback testing to relax RF requirements on the ATE, it's infeasible due to the masking of transmitter and receiver EVM values. Hence, the ATE requirements for conventional testing of EVM for transceivers are identical to the previous case.

3.3.1.1 Limitations of Conventional Testing of EVM

With growing demand for EVM testing by various standards (and customers), there is an urgent need to address some of the key limitations of the production testing of EVM. The limitations are,

- To achieve good test coverage, it's critical to compute EVM over a *sufficient* number of symbols. This results in *longer test times*, and affects the overall *test cost* directly. As the number of data symbols (N) is dropped the ability of EVM to quantify signal quality degrades significantly.

- The *requirements of ATE* coupled with long test times to perform EVM testing affects the overall *test cost* significantly. To have a generic EVM test setup, the ATE should accommodate RF/IF sourcing and sinking along with digital modulation capability to test any of the devices discussed above.

3.3.2 INTRODUCTION ON OFDM

While the proposed approach targets multi-tone testing for EVM to obviate the need for performing OFDM modulation and de-modulation, an understanding of the OFDM methodology is necessary to understand the complexities in performing OFDM modulation. Hence in this section a brief introduction on OFDM is discussed.

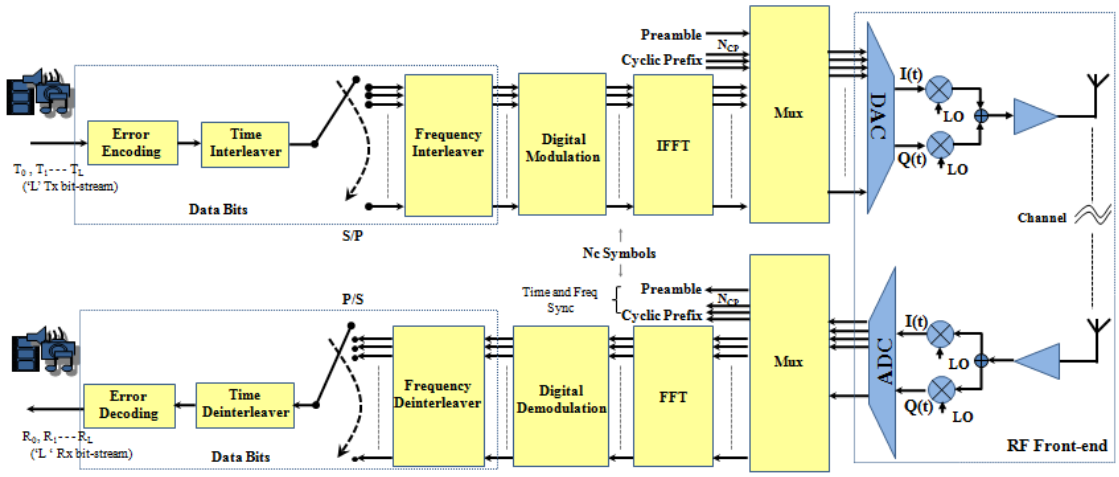

Figure 24: OFDM Transceiver

In OFDM a large number of orthogonal sub-carriers are encoded with digital data bits resulting in a high spectral efficiency as compared to single carrier systems. OFDM is preferred due to its inherent robustness to multipath fading and narrow-band channel interferences. A conceptual diagram of a typical OFDM link is shown in Figure 24. The input to the baseband transmitter is a serial digital bit stream that carries information about the data being transmitted (e.g. Voice, Video etc). The incoming serial bit stream is

converted into Nc parallel bit streams where, Nc denotes the number of orthogonal subcarriers in the modulation scheme. The parallel bit streams are then digitally modulated using any standard modulation scheme such as quadrature phase shift keying (QPSK), quadrature amplitude modulation (QAM) etc.

The modulated symbols are denoted as "data symbols", to avoid any ambiguity with the term "OFDM symbol" (explained below). OFDM as conceived by *Chang* in 1966 [59], was a continuous time modulation scheme, where the parallel bit streams are modulated onto orthogonal subcarriers using a mixer bank. In 1971, *Weinstein and Ebert* [59] proposed the usage of discrete Fourier transforms (FFT & IFFT) to replace the mixer bank approach resulting in a discrete time OFDM scheme that has been adopted into standards prevalent today such as 802.11 [54], WiMax etc. In a discrete OFDM scheme the complex representation of the modulated *data symbols* are treated as frequency domain information and are fed as input to an inverse fast Fourier transform (IFFT) block. The IFFT block converts the input symbols into discrete data samples in complex representation. Cyclic prefix (Tcp) values are then added to the discrete data samples to result in a complex *OFDM symbol* (OFDM frame). In a typical WLAN standard [54], one OFDM symbol is made up of 48 *data symbols*. The real and imaginary parts of the complex OFDM symbol are separated and passed on to the analog/RF front-end via digital to analog data converters (DAC). The analog signal is then up-converted and transmitted by the RF front-end. In a receiver, the signal is down-converted to intermediate frequency by the RF front-end and converted into complex discrete samples by analog to digital data converters (ADC). The complex samples are cleaved off the cyclic prefix values followed by FFT operation and demodulation to obtain the received data bits.

In addition to the cyclic prefix, the data bits are interleaved in both time and frequency domain along with the addition of guard bands and pilot carriers to facilitate time and frequency synchronization in the receiver (to minimize inter symbol

interference-ISI). Further, to minimize ISI, the number of subcarriers (Nc) and the frequency spacing (Δf) need to be carefully chosen. The frequencies of the subcarriers generated by the IFFT block are integer multiples of the slowest subcarrier. Hence to maintain orthogonality, its necessary to ensure that the duration 'T' of each IFFT output data block contain integer number of cycles of the slowest subcarrier (fundamental subcarrier frequency).

3.3.3 GOALS AND OBJECTIVES

To capitalize on the advantages of EVM testing, it's critical to address the key limitations of the conventional EVM testing approach. The objectives of the proposed approach are

- Goal 1: To *reduce test time* associated with EVM testing to result in a feasible production test scheme. This would necessitate the development of test solutions that can compute EVM with good accuracy (in par with conventional EVM test) in a shorter amount of time.
- Goal 2: To *reduce test cost* associated with the test setup infrastructure by *relaxing the requirements* of ATE. This would necessitate development of *load board infrastructure* to eliminate RF requirements from the tester coupled with test solutions that can *eliminate the modulation/demodulation* capability of the ATE.

3.3.4 PROPOSED METHODOLOGY

In this section, the methodology proposed to address the shortcomings of a conventional EVM test is discussed briefly. Figure 25 shows the block diagram of the proposed approach to perform low-cost production testing of wireless RF front-ends. The key idea of the approach is to exploit the high correlation between EVM and the parametric impairments (both static and dynamic) of RF systems.

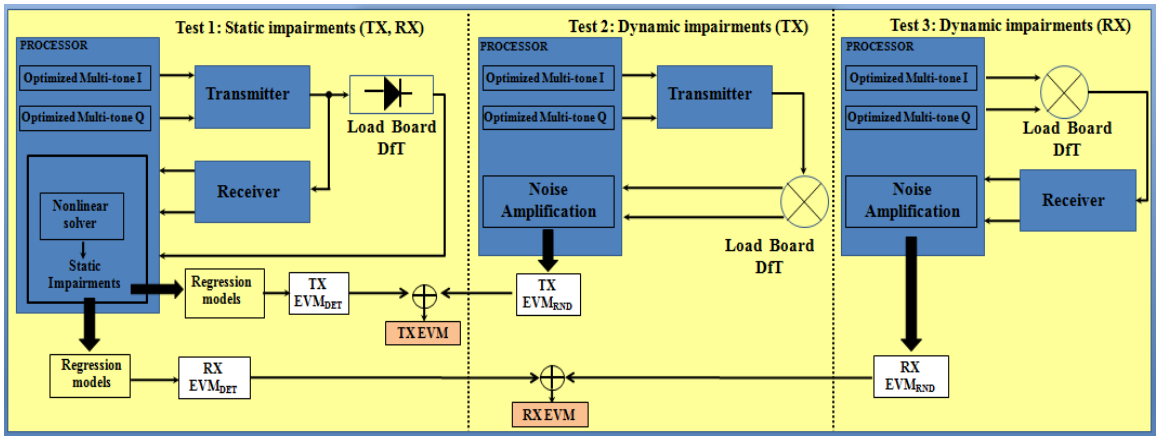

Figure 25: Proposed test architecture

- *To address goal 1, a model based approach to compute EVM from the static and dynamic impairments of a system is proposed.* The key advantage of this method is that the static and dynamic impairments can be computed at a significantly reduced time in comparison to conventional EVM.
- To address goal 2, *multi-tone test input is proposed to be used along with load board DfT circuitry such as up/down conversion mixers and an envelope detector to significantly relax the requirements of ATE*. The key advantage of multi-tone test inputs is that it eliminates the need for modulation/demodulation capability and the associated signal processing algorithms such as time/frequency inter-leavers, guard-band/cyclic prefix algorithms, synchronization algorithms etc.

The proposed approach is demonstrated on a 2.4 GHz 802.11 wireless OFDM transmitter and a receiver both in software and hardware. By definition, EVM is a measure of the variance of the received constellation points from the ideal (sent) constellation points and quantifies the combined influence of all the system impairments on the ideal constellation points. In this approach, the system impairments are classified into two categories: Static and dynamic. The effect of static impairments on the ideal constellation points are quantified by EVM_{DET} and the effect of dynamic impairments on the ideal constellation points are quantified by EVM_{RND}. The variance quantified by

EVM_{DET} and EVM_{RND} are uncorrelated and hence can be added to obtain the overall EVM of the system as shown in (13)-(15). The EVM_{DET} and EVM_{RND} values are estimated from the static and dynamic impairments respectively using the proposed multi-tone test as explained below.

$$EVM = fn(Static, Dynamic) = \sqrt{EVM_{DET}^2 + EVM_{RND}^2} \quad (13)$$

$$EVM_{DET} = fn(Static\ impairments) \quad (14)$$

$$EVM_{RND} = fn(Dynamic\ impairments) \quad (15)$$

The following steps outline the operation of the proposed approach (as shown in Figure 25).

- Test 1: Apply an optimized multi-tone test input and setup the *transmitter and the receiver* in a *loopback configuration* to capture the low frequency test responses at the output of an envelope detector (DfT) and the receiver baseband.
- The captured test responses are then used to compute the static impairments of the transceiver using a non-linear solver. The *static impairments* considered are transmitter and receiver gain, IIP2, IIP3, P1dB and quadrature mismatches (amplitude and phase)
- Test 2: Apply the same multi-tone test stimulus and capture the low frequency test response of the *transmitter* via the load board mixer to compute *dynamic impairments*. The dynamic impairments considered are (VCO phase noise and thermal noise)
- Test 3: Apply the same multi-tone test stimulus to the *receiver* via the load board mixer and capture the baseband response to compute the *dynamic impairments* of the receiver.

- Compute EVM_{DET} and EVM_{RND} from the static and dynamic impairments respectively for the transmitter and receiver.
- Compute the overall EVM for the transmitter and receiver

Each of the steps involved and the underlying concepts behind them are discussed in the following sub-sections.

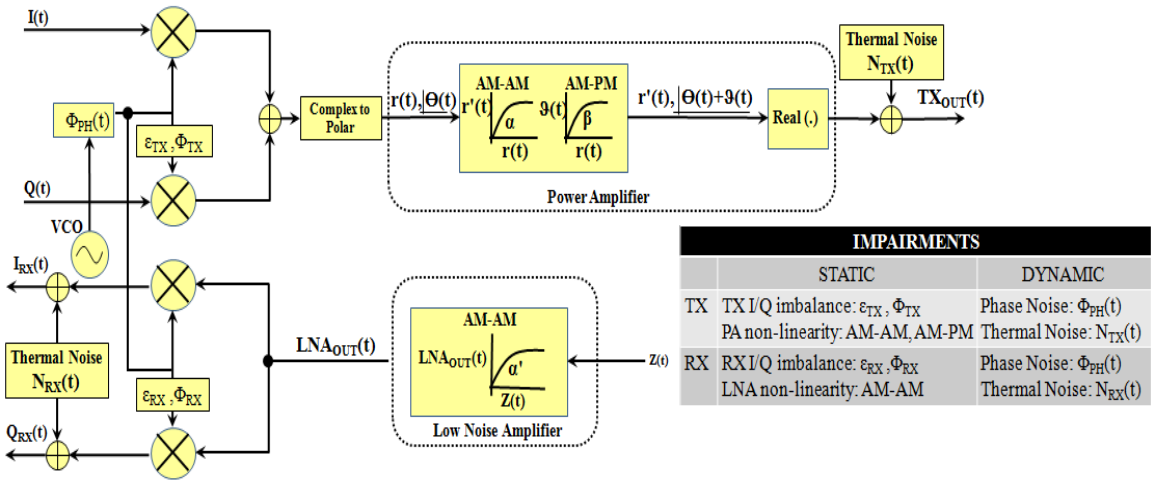

IMPAIRMENTS		
	STATIC	DYNAMIC
TX	TX I/Q imbalance: $\varepsilon_{TX}, \Phi_{TX}$ PA non-linearity: AM-AM, AM-PM	Phase Noise: $\Phi_{PH}(t)$ Thermal Noise: $N_{TX}(t)$
RX	RX I/Q imbalance: $\varepsilon_{RX}, \Phi_{RX}$ LNA non-linearity: AM-AM	Phase Noise: $\Phi_{PH}(t)$ Thermal Noise: $N_{RX}(t)$

Figure 26: Behavioral modeling of a 2.4 GHz OFDM transceiver

3.3.4.1 Behavioral Modeling of RF Front-Ends

The model is implemented in MATLAB. The behavior level model parameters for the amplifiers are extracted in MATLAB from the circuit level simulations performed in Agilent ADS (advanced design system). The transmitter chain is modeled by a quadrature up conversion mixer followed by a power amplifier. The receiver is modeled by a low noise amplifier followed by a qudrature down conversion mixer.

The *static impairments* modeled in this research are, transmitter I/Q amplitude and phase imbalance, PA AM/AM and AM/PM non-linearity, LNA AM/AM non-linearity and receiver I/Q amplitude and phase imbalance. The *dynamic impairments* modeled are VCO phase noise, transmitter thermal noise and receiver thermal noise. A

block diagram of the transceiver architecture along with the modeled impairments is show in Figure 26.

The input to a quadrature mixer is modeled as a complex signal 'X(t)' with the in-phase component as 'I(t)' and the quadrature component as 'Q(t)' as shown in (16).

$$X(t) = I(t) + j * Q(t) \tag{16}$$

During actual operation, I(t) and Q(t) represent the real and imaginary components of the complex IFFT output of an OFDM modulation scheme. During testing, I(t) and Q(t) represent the optimized multi-tone test input fed into the I and Q channels. To perform quadrature mixing, the carrier signals corresponding to I and Q channels need to be phase shifted by 90 degrees and the amplitudes of the carrier signal need to be the same as shown below,

$$S_{LO-TX} = \cos(2\pi . f_c . t) + j * \sin(2\pi . f_c . t) \tag{17}$$

Where, '$S_{LO\text{-}TX}$' is the transmitter carrier signal, 'f_c' is the carrier frequency and 't' is the time base for simulation. However in reality, the amplitudes and the phase of the carrier signals differ from their ideal values giving rise to amplitude and phase mismatches (also referred to as I/Q imbalance [21]). Asymmetric modeling (modeling the impairments into one of the channels) of the mismatch effects result in,

$$S_{LO-TX} = \cos(2\pi . f_c . t) + j . (1 \pm \varepsilon_{TX}) . \sin(2\pi . f_c . t \pm \varphi_{TX}) \tag{18}$$

Where, ε_{TX} denotes the amplitude mismatch (modeled as percentage error, for e.g. 5% mismatch results in ε_{TX} being set to 0.05) and φ_{TX} denotes the phase mismatch (2 degrees typically).

Apart from quadrature mismatch, the carrier signal also suffers from a dynamic phenomenon called as phase noise. Phase noise quantifies the noise on the phase of a carrier signal that varies with time. Phase noise is studied in the frequency domain for RF circuits. Ideally, a clean carrier signal will have a single tone in the frequency spectrum. Phase noise corrupts the frequency spectrum and results in a skirt around the carrier frequency. In this research, the phase noise values are modeled based on the amplitude in relation to the carrier amplitude (dBc/Hz characteristics, where dBc denotes dB below carrier) at certain frequency offsets from the carrier signal [21].

For e.g. the frequency spectrum of the carrier signal can be defined to have a noise power of -80 dBc at 1kHz offset from the carrier frequency and so on. The resulting skirt in the frequency can be represented as phase noise in time domain and is represented as $\varphi_{PH}(t)$. The carrier signal in the presence of I/Q imbalance and phase noise can be represented as follows,

$$S_{LO-TX} = \cos(2\pi.f_c.t + \varphi_{PH}(t)) + j.(1 \pm \varepsilon_{TX}).\sin(2\pi.f_c.t \pm \varphi_{TX} + \varphi_{PH}(t)) \quad (19)$$

Both transmitter and the receiver share the same oscillator in a typical transceiver architecture. Hence $\varphi_{PH}(t)$ also represents the phase noise component of the receiver 'LO' as shown in Figure 26. The output of the quadrature up conversion mixer 'Y(t)' can be represented as follows,

$$Y(t) = \mathrm{I(t)}.\cos(2\pi.f_c.t + \varphi_{PH}(t)) + j.Q(t).(1 \pm \varepsilon_{TX}).\sin(2\pi.f_c.t \pm \varphi_{TX} + \varphi_{PH}(t)) \quad (20)$$

Mixer non-linearity is not modeled in this approach because in most systems the mixers are operated in a linear range due to the highly non-linear operation of the power amplifiers. At this stage its common to retain only the real value of the signal 'Y(t)' as input to the power amplifier. However in this work, the complex values are retained to facilitate AM/AM and AM/PM modeling of a RF power amplifier.

Power amplifier is a non-linear device and introduces amplitude and phase distortion into the transmitted signal quantified by AM/AM and AM/PM characteristics. AM/AM and AM/PM are modeled as a polynomial function of the magnitude of the amplitude modulated input signal. The input of the power amplifier signal is represented as follows,

$$PA_{in}(t) = r(t).e^{j\theta(t)} \quad (21)$$

Where, r(t) is the magnitude and $\theta(t)$ is the angle of the complex signal Y(t). The output of the power amplifier is then modeled as follows,

$$PA_{out}(t) = \Re e[\, r'^{(t)}.e^{j(\theta(t)+\vartheta(t))}] \quad (22)$$

Where, $\Re e$ represents the real component of the complex waveform, r'(t) represents the AM/AM distortion and $\vartheta(t)$ represents the AM/PM distortion. The distortion characteristics are modeled as follows,

$$r'^{(t)} = [\alpha_0, \alpha_1, .. \alpha_5].[1, r(t), r^2(t)..r^5(t)]^T$$
$$\vartheta(t) = [\beta_0, \beta_1, .. \beta_7].[1, r(t), r^2(t)..r^7(t)]^T \quad (23)$$

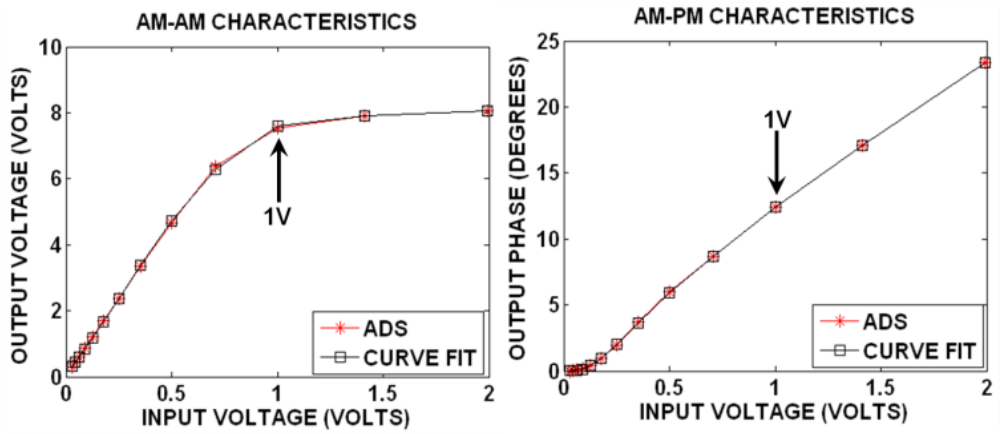

Figure 27: (a) AM-AM and (b) AM-PM curves for a 2.4 GHz power amplifier simulated in ADS

The polynomial coefficients α and β are extracted from circuit level simulations through a curve fitting process. A power amplifier design in ADS environment, implemented in CMOS 0.18u technology is used for this purpose. The AM/AM (V_{OUT} vs V_{IN}) and AM/PM (Output phase vs V_{IN}) curves are simulated using ADS templates. The AM/AM curves are characterized up to a 5th order polynomial (α) and the AM/PM curves are characterized up to a 7th order polynomial (β). The AM-AM and AM-PM curves obtained for a single instance of the PA is shown in Figure 27. The gain, IIP2 and IIP3 of the PA can be represented as follows

$$Gain = 20 * \log_{10}(\alpha_1)\ dB \quad (24)$$
$$IIP2 = |\alpha_1/\alpha_2|\ volts \quad (25)$$
$$IIP3 = \sqrt{4/3.|\alpha_1/\alpha_3|}\ volts \quad (26)$$

The signal being transmitted suffers from the thermal noise of various transistors present in the chain (determined significantly by PA) and is modeled as white Gaussian noise with zero mean. MATLAB function 'wgn' is used to model the white Gaussian as follows,

$$N_{TX}(t) = wgn(TX\_Noise_{power}) \tag{27}$$

$$TX_{OUT}(t) = PA_{OUT}(t) + N_{TX}(t) \tag{28}$$

Where, TX_Noise_{power} is set to result in a typical NF value of around 14dB for the transmitter.

$$\begin{aligned} TX_{out} = \Re e \Bigg[\Bigg\{ & \alpha_0 \\ & + \sum_{i=1}^{5} \alpha_i . \big| \boldsymbol{I}(\boldsymbol{t}) . cos\big(2\pi . f_c . t + \varphi_{PH}(t)\big) \\ & + j . \boldsymbol{Q}(\boldsymbol{t}) . (1 \pm \varepsilon_{TX}) . sin\big(2\pi . f_c . t \pm \varphi_{TX} + \varphi_{PH}(t)\big) \big|^i \Bigg\} . exp \Big\{ \theta(t) \\ & + \beta_0 \\ & + \sum_{i=1}^{7} \beta_i \big| \boldsymbol{I}(\boldsymbol{t}) . cos\big(2\pi . f_c . t + \varphi_{PH}(t)\big) \\ & + j . \boldsymbol{Q}(\boldsymbol{t}) . (1 \pm \varepsilon_{TX}) . sin\big(2\pi . f_c . t \pm \varphi_{TX} + \varphi_{PH}(t)\big) \big|^i \Bigg\} \Bigg] + N_{TX}(t) \end{aligned} \tag{29}$$

Combining (16)-(28), the output of the transmitter in terms of the input and other impairments (static and dynamic) of the system can be expressed as shown in (29).

The input to the LNA is the received signal captured by the receiver antenna. To represent a generic model, the input to LNA is defined as Z(t). The Z(t) value is set

depending on the type of test. LNA is a non-linear device that injects AM-AM non-linearity into the signal received. The output of LNA is modeled as follows,

$$LNA_{out}(t) = [\alpha'_0, \alpha'_1, .. \alpha'_3].[1, \mathrm{Z}(t).., \mathrm{Z}^3(t)]^T \tag{30}$$

Where, α' denotes the polynomial coefficients of LNA AM/AM non-linearity. A LNA design in ADS (Agilent advance design system) environment, implemented in CMOS 0.18u technology is used for this purpose. The AM/AM (V_{OUT} vs V_{IN}) curves are simulated using ADS templates. The AM/AM curves are characterized up to a 3rd order polynomial (α'). The receiver gain, IIP2 and IIP3 values are calculated similar to (24)-(26).

The receiver I/Q imbalance (both amplitude and phase) is modeled similar to the transmitter. The phase noise ($\varphi_{PH}(t)$) of the receiver is the same as transmitter due to the fact that the transmitter and receiver share the same RF oscillator. The receiver carrier signal in the presence of I/Q imbalance (amplitude and phase) and phase noise is modeled as follows,

$$\begin{gathered} S_{LO-RX} = \cos(2\pi.f_c.t + \varphi_{PH}(t)) + \\ j.(1 \pm \varepsilon_{RX}).\sin(2\pi.f_c.t \pm \varphi_{RX} + \varphi_{PH}(t)) \end{gathered} \tag{31}$$

Where, ε_{RX} and φ_{RX} denotes the receiver I/Q amplitude and phase mismatch values. The received baseband signal ('RX_{BB}') is modeled as follows,

$$RX_{BB}(t) = LNA_{OUT}(t).S_{LO-RX} \tag{32}$$

The NF of the receiver is modeled as white Gaussian noise similar to the transmitter NF. The noise added baseband signal is represented as follows,

$$N_{RX}(t) = wgn(RX\_Noise_{power}) \tag{33}$$

$$\begin{aligned} I_{RX}(t) &= \Re e[RX_{BB}(t)] + N_{RX}(t) \\ Q_{RX}(t) &= \Im m[RX_{BB}(t)] + N_{RX}(t) \end{aligned} \tag{34}$$

Where, RX_Noise_{power} is set to result in a typical NF value of around 10dB for the Receiver. Combining (30)-(34), the output of the receiver ($I_{RX}(t)$ and $Q_{RX}(t)$) in terms of the input (Z(t)), and other impairments can be expressed as follows,

$$I_{RX} = \Re e\left[\left\{\alpha_0' + \sum_{i=1}^{3} \alpha_i'.[\boldsymbol{Z(t)}]^i\right\}.\begin{Bmatrix}\cos\left(2\pi.f_c.t + \varphi_{PH}(t)\right) + \\ j.(1 \pm \varepsilon_{RX}).\sin\left(2\pi.f_c.t \pm \varphi_{RX} + \varphi_{PH}(t)\right)\end{Bmatrix}\right] + N_{RX}(t) \tag{35}$$

$$\begin{aligned} Q_{RX} = \Im m\Bigg[\left\{\alpha_0' + \sum_{i=1}^{3} \alpha_i'.[\boldsymbol{Z(t)}]^i\right\}.\Big\{&\cos\left(2\pi.f_c.t + \varphi_{PH}(t)\right) \\ &+ j.(1 \pm \varepsilon_{RX}).\sin\left(2\pi.f_c.t \pm \varphi_{RX} + \varphi_{PH}(t)\right)\Big\}\Bigg] + N_{RX}(t) \end{aligned} \tag{36}$$

3.3.4.2 Decomposition of EVM into Deterministic and Random EVM

In order to decompose EVM into EVM_{DET} and EVM_{RND} it's critical to understand the relationship between the system impairments and EVM. In this analysis, for a single transmitter instance, the overall EVM, EVM_{DET} and EVM_{RND} values are computed to demonstrate the decomposition of EVM. The analysis of the receiver yields similar results and hence are omitted for reasons of brevity. The analysis is performed based on standard 16 QAM Modulated OFDM data frames.

The modeling parameters that define the OFDM transmitter chain are shown in Table 3. Phase noise ($\varphi_{PH}(t)$) is defined by the carrier signal frequency spectrum characteristics. The AM-AM and AM-PM coefficients are extracted from the curves shown in Figure 27.

Table 3: Modeling parameters for EVM computation

IQ Imbalance		AM-AM	AM-PM	Phase Noise	NF
Amp	Phase				
$\varepsilon_{TX} = 0.019$	$\varphi_{TX} = -0.91°$	Figure 27a	Figure 27b	-112dBc@100KHz -134dBc@500KHz -140dBc@1MHz	14 dB

The input to the transmitter model I(t) and Q(t) are defined by the real and the imaginary components of the OFDM symbols obtained at the output of the IFFT block. I(t) and Q(t) computed for a single OFDM symbol are expressed as follows,

$$I(t) = \Re e\left[\sum_{n=0}^{N_c-1} S_{IDEAL}(n).\, e^{j2\pi n\frac{t}{T}}\right] \tag{37}$$

$$Q(t) = \Im m\left[\sum_{n=0}^{N_c-1} S_{IDEAL}(n).\, e^{j2\pi n\frac{t}{T}}\right] \tag{38}$$

Where, 'T' is the time duration of a single OFDM symbol, S_{IDEAL} denotes the 16QAM modulated data symbols. The output of the transmitter is calculated as shown in (29). The output of the transmitter is down-converted using an ideal receiver. The measured symbols (S_{MEAS}) are obtained by computing the FFT at the output of the ideal receiver. The EVM values are calculated as shown in (12). Figure 28 shows the constellation plot obtained under the influence of all the system impairments modeled in this work.

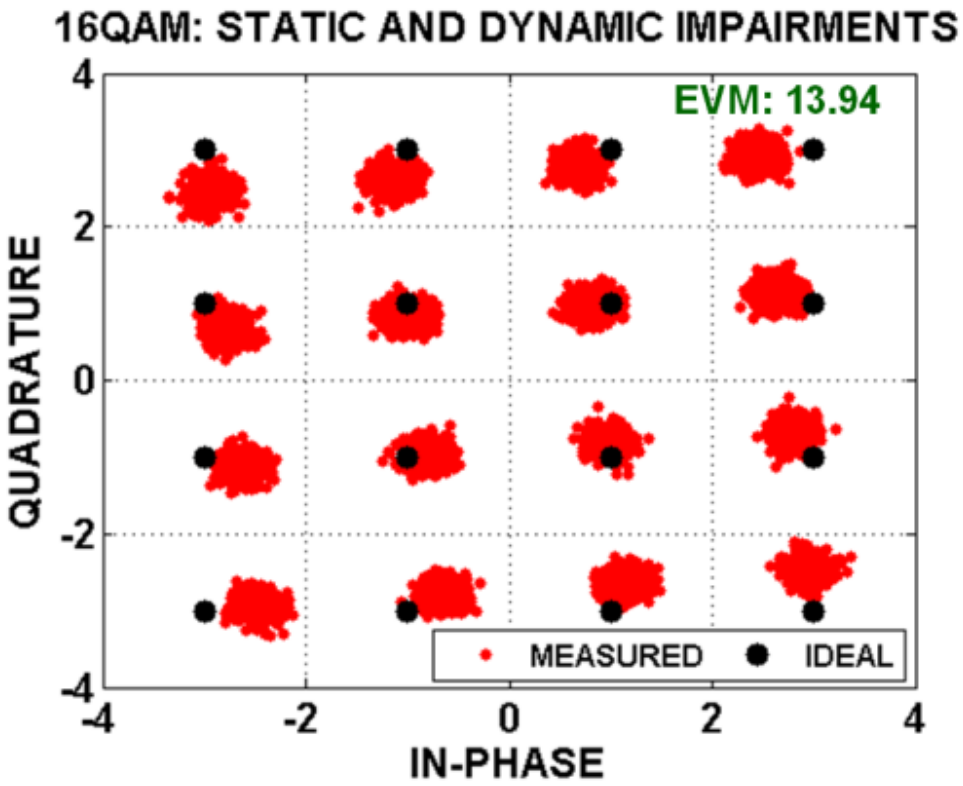

Figure 28: Combined effect of all system impairments

The static impairments of the system are set as shown in Table 3. The dynamic impairments are set to be ideal (i.e. $\varphi_{PH}(t) = 0$ and $N_{TX}(t) = 0$). For the same data symbols shown in (37)-(38), the effects of static impairments on the received constellations (computed similar to previous case) are shown in Figure 29a.

The key difference between the multi-carrier and the single carrier schemes is that the static impairments result in amplitude dependant effects along with symbol dispersion (i.e. noise is introduced into the constellation plot along with the amplitude dependant constellation shifts) as shown in Figure 29a.

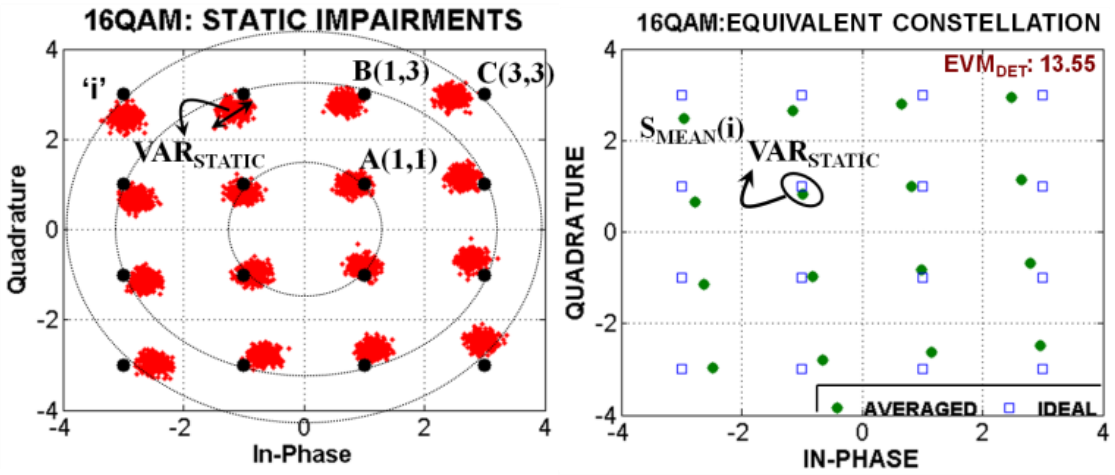

Figure 29: (a) Effects of Static impairments (I/Q imbalance, AM-AM and AM-PM) (b) Equivalent representation by Mean shifted constellation and variance

The symbol dispersion is due to the fact that the static impairments in a multi-carrier scheme introduce inter-carrier-interference (ICI) [60]-[61] into the orthogonal sub-carriers. Due to the randomness in the data between the sub-carriers, the ICI effects result in symbol dispersion. The received constellation plot (Figure 29a) can be modeled by an averaged constellation point (S_{MEAN}) for each constellation cloud and a variance value (VAR_{STATIC}) for each constellation cloud as shown in Figure 29b. S_{MEAN} quantifies the amplitude dependant static impairment effects on the received symbols and VAR_{STATIC} quantifies the symbol dispersion effects of the static impairments and is observed to be the same across all the constellation clouds. The S_{MEAN} and VAR_{STATIC} values are calculated as follows,

$$S_{MEAN}(i) = \frac{\sum_{j=1}^{M} S_{MEAS}(i,j)}{M} \tag{39}$$

$$VAR_{STATIC} = \frac{\sum_{j=1}^{M} |S_{MEAS}(i,j) - S_{MEAN}(i)|^2}{M} \tag{40}$$

Where, '(i,j)' denotes the j^{th} symbol in the i^{th} constellation cloud and 'M' denotes the number of symbols in the i^{th} constellation cloud. The EVM_{DET} component can then be further decomposed into EVM_{STATIC_MEAN} (computed from S_{MEAN}) and EVM_{STATIC_VAR} (computed from VAR_{STATIC}). The EVM_{STATIC_MEAN}, EVM_{STATIC_VAR} and EVM_{DET} values are calculated as shown in (41)-(43).

$$EVM_{STATIC-MEAN} = 100.\frac{\sqrt{\frac{1}{M}\cdot\sum_{i=1}^{M}\left|S_{IDEAL,i} - S_{MEAN,i}\right|^2}}{\sqrt{\frac{1}{M}\cdot\sum_{i=1}^{M}\left|S_{IDEAL,i}\right|^2}} \tag{41}$$

$$EVM_{STATIC-VAR} = 100.\frac{\sqrt{var_{STATIC}}}{\sqrt{\frac{1}{M}\cdot\sum_{i=1}^{M}\left|S_{IDEAL,i}\right|^2}} \tag{42}$$

$$EVM_{DET} = \sqrt{EVM_{STATIC-MEAN}^2 + EVM_{STATIC-VAR}^2} \tag{43}$$

While (29), (37) and (38) show how the impairments are analytically related to the received constellation points, the symbol dispersion introduced by ICI along with the randomness of the data are not direct (analytically) under the combined influence of all the static impairments. However, *a key observation is that the S_{MEAN} and VAR_{STATIC} values exhibit high correlation to the static impairments of the system when computed for sufficiently large number of symbols. This property is exploited in this work to compute/predict the S_{MEAN} and VAR_{STATIC} values from the static impairments, thereby obviating the need for sending data bits to compute the same.*

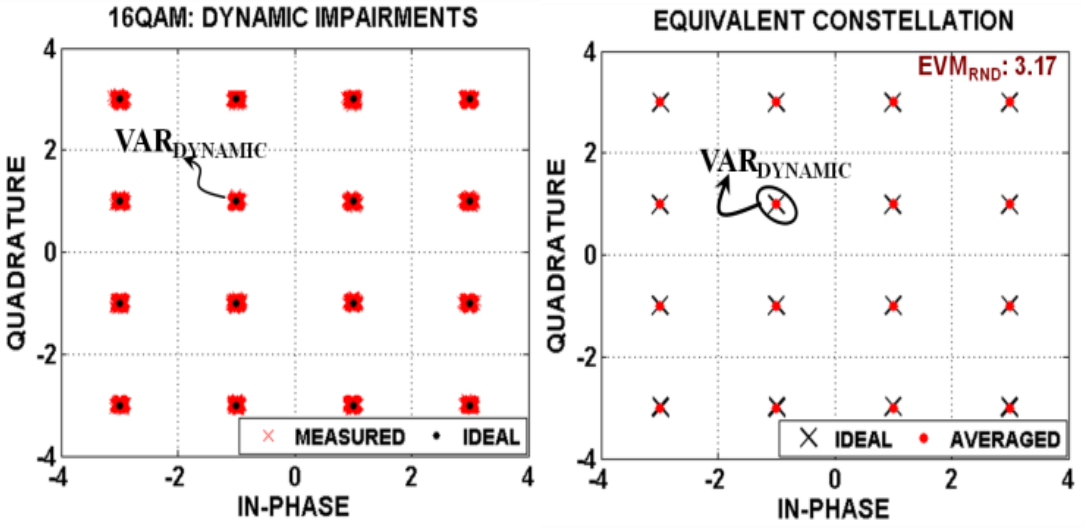

Figure 30: (a) Effects of dynamic impairments (b) Equivalent representation by variance

In this case study, the static impairments are set to be ideal (i.e. $\varepsilon_{TX} = 0, \varphi_{TX} = 0, \alpha = [0,1,0,0,0,0],\ \beta = [0]$) and the dynamic impairments are set according to values shown in Table 3. In multi-carrier systems, deterministic component in the phase noise results in a common phase rotation (CPR) across all the sub-carriers and the random component introduces symbol spreading across the constellation clouds. The CPR effects are compensated in the receiver by making use of the pilot tones [62] in the OFDM frame prior to EVM computation.

For the same data symbols modeled in (37)-(38), the effects of dynamic impairments on the received constellations (after compensating for CPR) is shown in Figure 30a. The received constellation plot can be modeled with a variance ($VAR_{DYNAMIC}$) associated with the ideal constellation points (noise results in a distribution with zero mean) as shown in Figure 30b. Similar to VAR_{STATIC}, $VAR_{DYNAMIC}$ is also observed to be the same across all constellation clouds. EVMRND can then be computed as follows,

$$EVM_{RND} = 100.\frac{\sqrt{var_{DYNAMIC}}}{\sqrt{\frac{1}{M}\cdot\sum_{i=1}^{M}\left|S_{IDEAL,i}\right|^2}} \quad (44)$$

Table 4: EVM decomposition analysis

EVM (combined)	EVM_{DET}	EVM_{RND}	$\sqrt{EVM_{DET}^2 + EVM_{RND}^2}$
13.94	13.55	3.17	13.9159

Table 4 shows the results of the decomposition analysis where, EVM is calculated as shown in (12), EVM_{DET} is calculated as shown in (43) and EVM_{RND} is calculated as shown in (44). It can be observed from Table 4 that the EVM of the system can be accurately decomposed into its deterministic and random components. Based on the formulation described above, the key observations are,

- To compute the overall EVM accurately using the decomposition model, the S_{MEAN}, VAR_{STATIC} and $VAR_{DYNAMIC}$ values need to be computed.
- S_{MEAN} and VAR_{STATIC} relationship with the static impairments are not direct analytically; however, they exhibit high correlation to the static impairments of the system (suggesting a deterministic but highly non-linear relationship).
- If techniques are developed to compute S_{MEAN}, VAR_{STATIC} and $VAR_{DYNAMIC}$ using multi-tones, then the need to send modulated data to compute EVM can be eliminated.

3.3.4.3 Estimation of Static Mean and Variance Using Multi-Tones

In (39) and (40), the values for S_{MEAN} and VAR_{STATIC} are computed using a 16QAM modulated 802.11 OFDM frame. However, the goal of this work is to develop an approach to perform EVM testing with multi-tones. In order to accomplish the goal,

the strong correlation between S_{MEAN} and VAR_{STATIC} and the static impairments of the system is exploited. First a methodology to determine the transmitter and receiver static impairments of the system using a multi-tone stimulus is developed. Second a regression tool called MARS is used to build a regression function quantifying the highly non-linear relationship between S_{MEAN} and VAR_{STATIC} and the computed static impairments.

In this work, a n*on-linear solver* based approach proposed in [63] to solve for the static impairments of a transceiver in a loopback configuration (shown in Figure 25) is adopted. For an optimized multi-tone, the low frequency test responses are captured at the output of a load-board envelope detector (deployed at the output of the transmitter) and at the baseband of the receiver.

A model parameter solving based testing approach has been used in this work to compute static non-idealities of the RF transceiver system. At first comprehensive models of the different blocks of the transceiver chain are built that includes the significant non-ideal effects such as: transmitter I/Q imbalance, AM-AM and AM-PM effects of the power amplifier, nonlinearity of the LNA and receiver I/Q mismatch. The transmitter and receiver are connected in loopback mode and an envelope detector is placed at the output of the transmitter. The optimized test stimuli are applied to the I and Q input and output of the envelope detector and the I and Q output of the receiver are captured and digitized for analysis. A MATLAB based nonlinear equation solver is used for solving the model of the transmitter and the receiver. The nonlinear solver computes the non-idealities by solving the model parameters in such a way that the simulated output of the modeled transceiver matches with the actual hardware (DUT) output. The whole process is performed in two steps. In first step, using the output of the envelope detector, the non-idealities of the transmitter are calculated. Then in the second step the non-idealities of the transmitter computed in first step are used as known parameters and receiver non-idealities are calculated.

To accelerate the convergence time of the non-linear solver and to increase the accuracy of the estimation a genetic algorithm based test generation technique is used in this research.

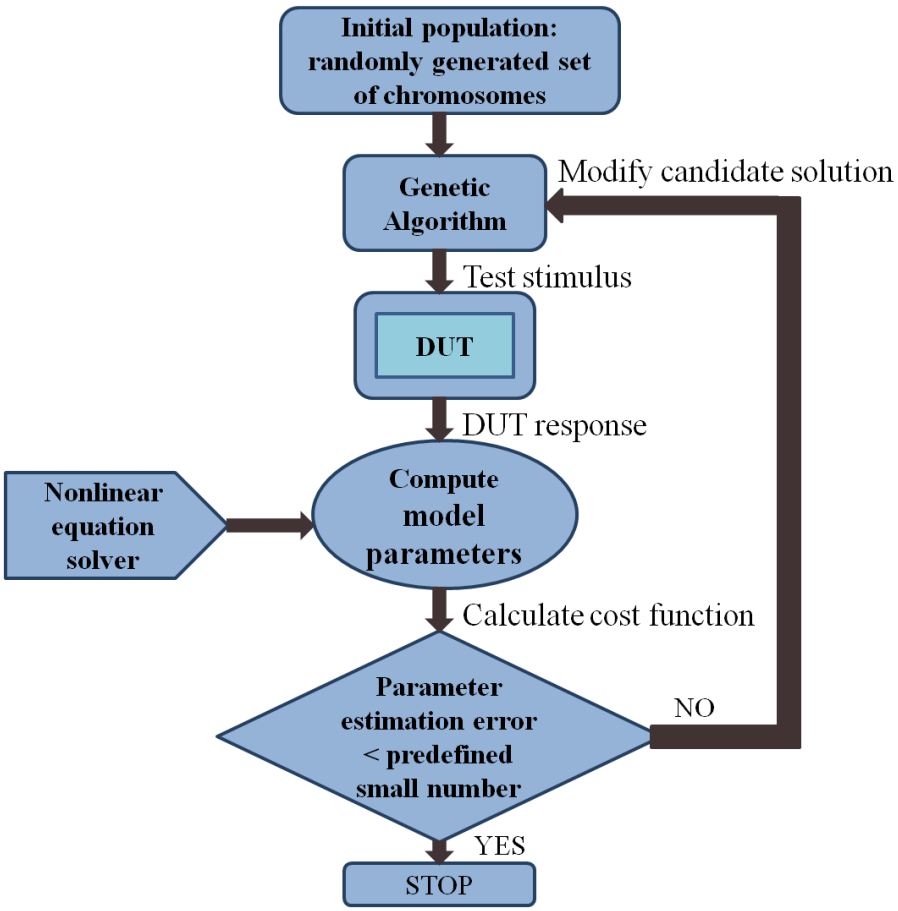

Figure 31: Test generation

The multi-tone test stimuli that are applied to the I and Q input of the transmitter are optimized using genetic algorithm in such a way that the accuracy of the parameter estimation improves. In simulation, several instances of the RF transceiver are created from ADS circuit simulation data and a set of randomly generated multi-tone test signal are applied to them and for each input, the static parameters are computed using the nonlinear solver.

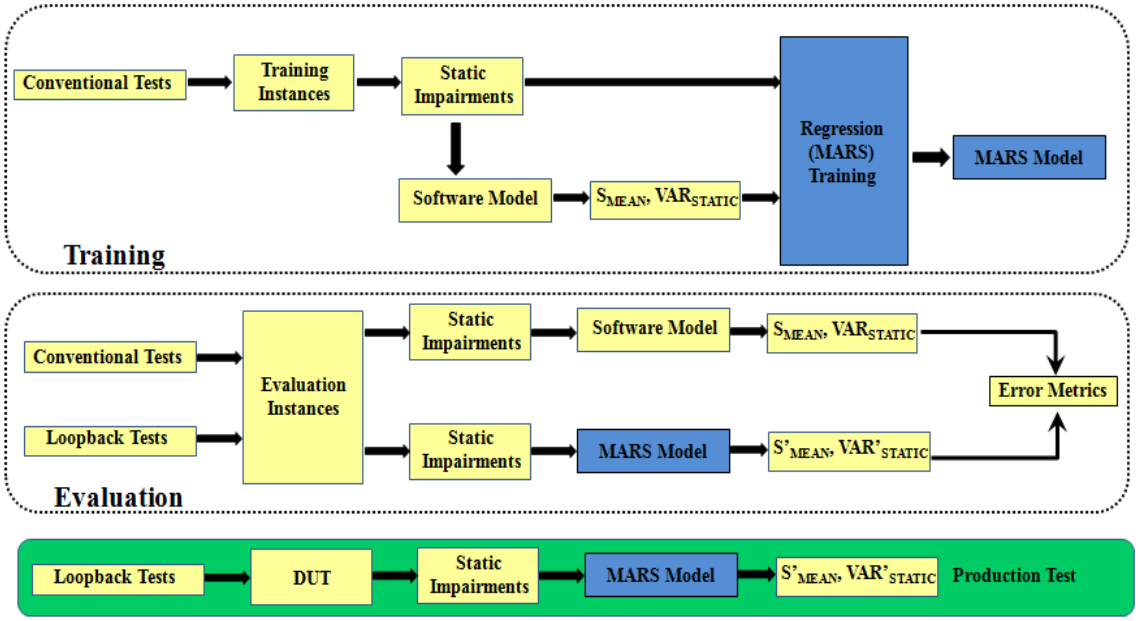

Figure 32: MARS model building: Training and Evaluation

Then the squared errors between the computed values of the parameters and the actual values are calculated to define the cost function of the genetic algorithm. GA uses crossover and mutation operators to modify the initial population of candidate solutions (test stimuli) and generates new set of solutions. The cost function value decreases with iterations of genetic algorithm and when GA converges, the optimum test stimulus is obtained for which parameter estimation error is minimized. By performing test generation as discussed above and by using the optimized multi-tone as test input it is possible to perform loopback testing accurately, in a short period of time.

As mentioned earlier, S_{MEAN} and VAR_{STATIC} exhibit high correlation to the static impairments of the system when simulated for a sufficient number of symbols. Hence in order to quantify this relationship a regression tool called MARS is used.

The steps involved in developing the MARS model as shown in Figure 32 are as follows,

- For a training set of devices, using a software model of the system under the influence of only static impairments, compute the S_{MEAN} and VAR_{STATIC} values for the transmitter and receiver with standard 802.11 OFDM (16QAM modulated) frames. For the same training set of devices compute the static impairments for the transmitter and receiver using the proposed multi-tone loopback test.
- Using MARS build a regression function between the static impairments (input to MARS) and the S_{MEAN} and VAR_{STATIC} (output of MARS) values.
- For an evaluation set of instances, validate the goodness of the built MARS model by comparing the predicted S_{MEAN} and VAR_{STATIC} values against the actual S_{MEAN} and VAR_{STATIC} values.

The goodness of a model in estimating a parameter over a set of instances is quantified by error metrics such as mean squared error (mse) and percentage relative error (pre). The 'mse' and 'pre' values can be calculated as follows,

$$mse = \frac{\sum_{i=1}^{P}(Actual_i - Predicted_i)^2}{P} \tag{45}$$

$$pre = 100.\frac{\|Actual - Predicted\|}{\|Actual\|} \tag{46}$$

Where, P denotes the instances used for evaluation, 'Actual' and 'Predicted' denotes the parameters being evaluated for model accuracy. It's desirable to have the *mse* and *pre* values as close as possible to zero. During production testing the static impairments are computed based on the test responses to a multi-tone input and are fed as input to the MARS models to predict S_{MEAN} and VAR_{STATIC} values, which are then used to compute EVM_{DET} as shown in (41) - (43).

3.3.4.4 Noise Amplification Analysis to Estimate Dynamic Variance

A noise amplification technique developed in [64] is adopted in this work to compute $VAR_{DYNAMIC}$. EVM_{RND} estimation generally requires longer test time (or more test frames being transmitted and received) than EVM_{DET} estimation since the EVM_{RND} estimation process is a type of noise analysis, which requires a set of observations to determine with confidence the statistical characteristics of noise of the signal being tested. To reduce test time required for the EVM_{RND} estimation, a noise amplification technique that exploits a sliding window demodulation is discussed in this section. In the standard EVM measurement of OFDM transceivers as shown in Figure 24, transmitted symbols are decoded in the receiver by performing N-point FFT of digitized I/Q signals to detect symbols (or constellation points on the I/Q plane). The spatial dispersion of detected symbols represents how much noise resides on the communication systems and channels. However, the standard EVM test cannot fully respond to the noise whose frequency is higher than the baseband frame rate since the N-point FFT is performed frame by frame.

The proposed noise amplification performs inter-frame noise analysis in comparison with the frame-by-frame noise analysis of the standard EVM test. Figure 33 summarizes the sliding window demodulation technique, which is designed to enhance the EVM estimation sensitivity to high-frequency noise. For the demodulation of received baseband I/Q signals, the sliding discrete Fourier transform (SDFT), which calculates an N-point DFT within a sliding window, is used as a band division filter. The SDFT module for a frequency bin of ω_k computes the inter-frame spectral components of $I_{RX}(t)+jQ_{RX}(t)$ for ω_k as shown in Figure 33.

In this SDFT based demodulation, the received baseband signal is required to be periodic within any selected time window since using the DFT implies that the finite segment being analyzed is one period of an infinitely extended periodic signal unless a special time window function is used to reduce the non-periodicity induced artifacts in

the spectrum. In the transceiver, such a periodic test signal can be generated by repeatedly transmitting the same multi-tone stimulus generated by the optimized test generation introduced in Section 3.3.4.3 so that any windowed data of the test signal can be analyzed using the sliding DFT without additional artifacts.

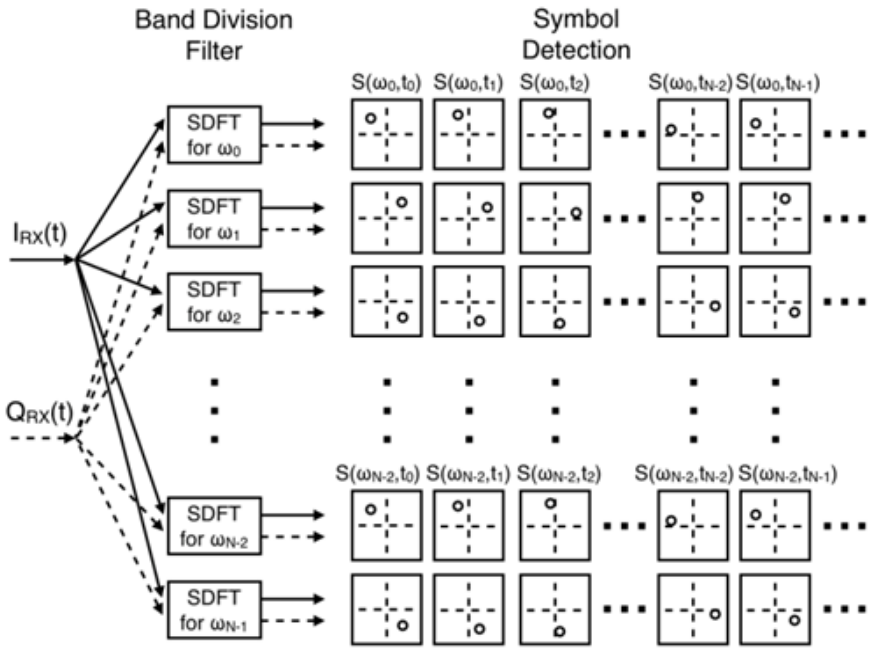

Figure 33: Noise amplification methodology

As shown in Figure 33, the filtered I/Q signal using the SDFTs for a frequency band of ω_k results in a series of the received symbols $S(\omega_k, t_0)$, $S(\omega_k, t_1)$, …, $S(\omega_k, t_{N-1})$, … Notice that these symbols are related with one another in terms of a deterministic phase shift due to the sliding window operation of the SDFT. When static distortions of the transmitter/receiver are considered, the symbols are affected by such distortions on top of the phase shift. However, the phase shift and static distortions affect every frame in the same way since the received baseband signal is periodic with a period of a single frame. By this reason, all the symbols detected during one frame are considered unique.

Symbol locations are compared frame by frame to measure the signal noise in terms of variance. The variance value is calculated from

$$var_{DYNAMIC} = \frac{\sum_{i=0}^{L-1}\sum_{k=0}^{N-1}[S(\omega_k, t_{N+i}) - S(\omega_k, t_i)]^2}{N \cdot L} \quad (47)$$

where L denotes the number of time instances used for the $var_{DYNAMIC}$ computation.

Thus by performing loopback testing and noise amplification, the VAR_{STATIC}, S_{MEAN} and $VAR_{DYNAMIC}$ values are computed using a multi-tone test input. The computed values can then be used to determine EVM, thereby eliminating the need to use OFDM modulated data bits to do the same.

3.3.5 SIMULATION RESULTS

In this section the simulation results are shown for a behavioral model of a 2.4 GHz transceiver using MATLAB. First the decomposition of EVM under process variations is demonstrated using modulated data-bits. Then proposed loopback test methodology results are presented. The performance of MARS regression models to compute S_{MEAN} and VAR_{STATIC} are presented. Noise amplification results are then presented to validate the estimation of $VAR_{DYNAMIC}$. Finally EVM is computed from the S_{MEAN}, VAR_{STATIC} and $VAR_{DYNAMIC}$ values as shown in (41) - (44), and are validated against the conventionally computed EVM. The simulation is performed for a set of 200 instances of the transmitter and receiver. The modeling parameters in MATLAB (Imbalance, phase noise, NF) are picked from a random distribution with a 10% variation from their nominal values. For the amplifiers, monte-carlo simulations are performed in ADS to generate multiple AM-AM and AM-PM curves for PA and AM-AM curves for LNA.

3.3.5.1 Proof of EVM Decomposition

The key idea of decomposing EVM into EVM_{DET} and EVM_{RND} values under process variation as a case study for the transmitter is validated in this section. The decomposition is performed on a set of 200 instances by using 16QAM modulated 802.11 OFDM frames as an input to the transmitter. 320 OFDM symbols are used to perform the analysis. The frames are scaled to be at 1Volt at the input of the PA. First the EVM values are computed conventionally ($EVM_{CONVENTIONAL}$) using (12). For the same set of frames, using simulations on a software model of the transmitter for only static impairments, the EVM_{DET} values are computed using (41) - (43). For the same set of frames transmitter is simulated for only dynamic impairments and compute EVM_{RND} using (44). The overall EVM is computed ($EVM_{DECOMPOSED}$) using (13). Figure 34 shows the scatter plot of $EVM_{CONVENTIONAL}$ vs $EVM_{DECOMPOSED}$ and the *mse* (using (45)) value between the $EVM_{CONVENTIONAL}$ and the $EVM_{DECOMPOSED}$ values.

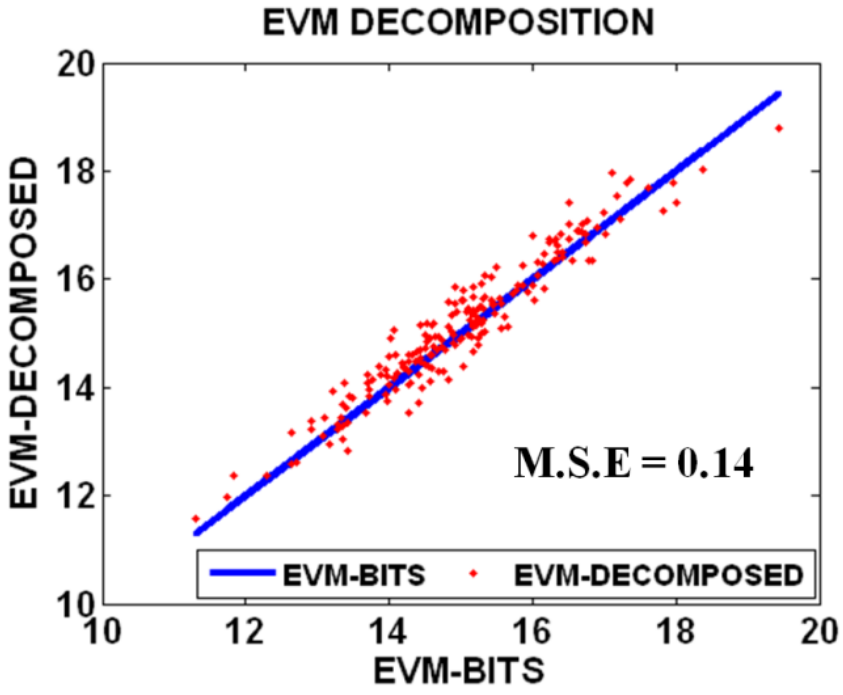

Figure 34: $EVM_{CONVENTIONAL}$ vs. $EVM_{DECOMPOSED}$

It can be observed from the Figure 34 that the conventionally computed EVM can be accurately decomposed into EVM_{DET} and EVM_{RND} values.

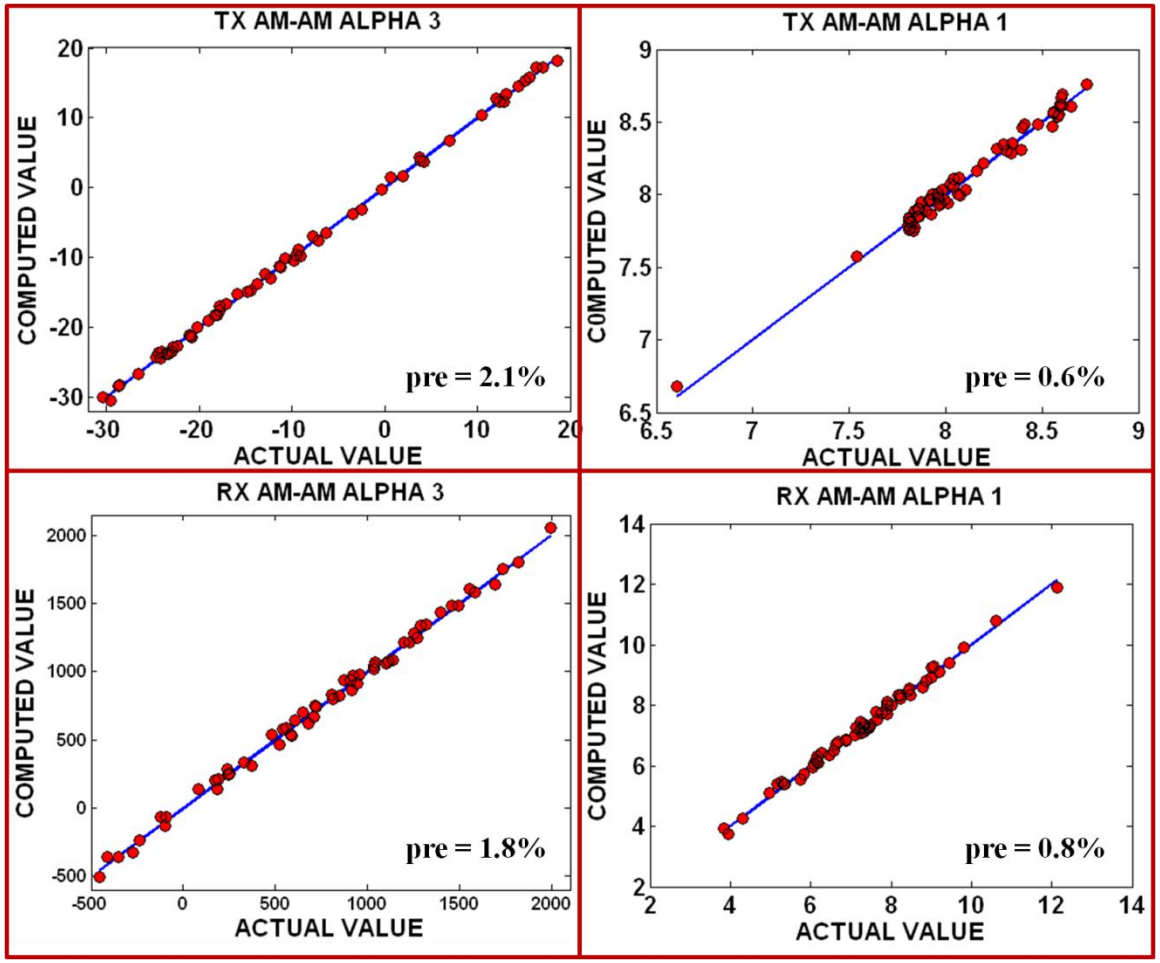

Figure 35: Computed vs Actual static parameters for Transmitter and Receiver

3.3.5.2 Loopback Testing of Static Impairments

In this section the loopback results obtained using the non-linear solver approach is presented. The loopback test is performed as shown in Figure 25. The optimized multi-tone is fed into channels I and Q. The envelope detector response is captured at the transmitter output to compute the gain mismatch (ε_{TX}), phase mismatch (φ_{TX}), AM-AM polynomial coefficients ($\alpha_0, \dots \alpha_5$) and AM-PM polynomial coefficients ($\beta_0, \dots, \beta_7$). The

loopback response at the baseband of the receiver is captured to compute receiver AM-AM coefficients ($\alpha'_0,..,\alpha'_3$), gain mismatch (ε_{RX}) and phase mismatch (φ_{RX}). A total of 22 model parameters that characterizes the static impairments of the transceiver (as shown in Figure 26) are computed from the loopback test methodology. Due to brevity the scatter plots that compare the computed model parameters from the non-linear solver approach with the actual model parameters are shown only for 4 such model parameters (transmitter AM-AM coefficients α_3, α_1 and receiver AM-AM coefficients α'_3, α'_1) in Figure 35 for 100 instances of the transceiver. The pre values computed using (46) for all the static parameters are observed to be less than 2.5%.

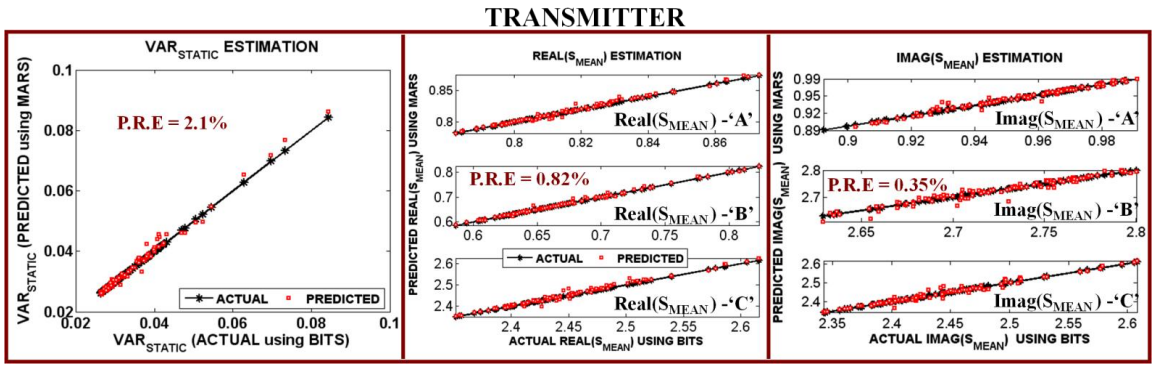

Figure 36: Predicted vs Actual S_{MEAN} and VAR_{STATIC} for transmitter

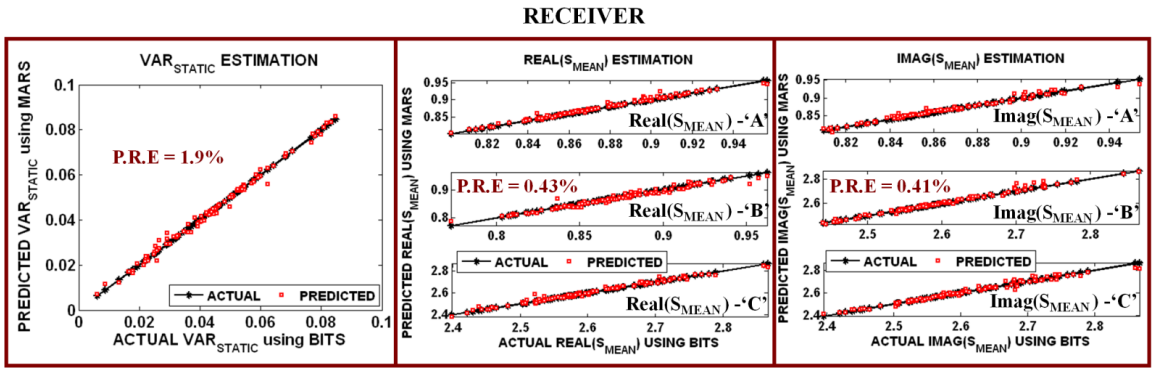

Figure 37: Predicted vs Actual S_{MEAN} and VAR_{STATIC} for Receiver

3.3.5.3 EVM Computation

In this case study, 100 devices are used as the training set to develop the MARS regression models and 100 devices are used as the evaluation set. For the evaluation set of instances, the static impairments are computed using the multi-tone, loopback test methodology. The computed static impairments are then fed as input to the MARS model to predict the S_{MEAN} and VAR_{STATIC} values. Figure 36 and Figure 37 shows the comparison of the predicted values against the actual S_{MEAN} and VAR_{STATIC} values computed using OFDM data frames at symbol locations 'A', 'B' and 'C' (see Figure 29a) for the transmitter and receiver respectively. The *mse* and *pre* values calculated using (45)-(46) are also shown in Figure 36 and Figure 37.

For the evaluation set of instances, the predicted SMEAN and VARSTATIC values are used to compute EVMDET as shown in (41) - (43) for the transmitter and the receiver.

For the evaluation set of instances the $VAR_{DYNAMIC}$ values are estimated using the proposed noise amplification methodology for the transmitter and the receiver. The computed $VAR_{DYNAMIC}$ values are used to compute EVM_{RND} as shown in (44). Five cycles of the multi-tone test input is used to perform the noise analysis.

Table 5: Comparison with Conventional EVM tests

	Best case Prediction			Worst case Prediction		
	BITS	**Multi-tone**	**error**	**BITS**	**Multi-tone**	**error**
TX	13.4832	13.4754	0.0078	15.158	16.3431	1.1852
RX	12.2374	12.2390	0.0016	5.5945	6.7957	1.2012

The overall EVM denoted as $EVM_{MULTI-TONE}$ is then computed from the EVM_{DET} and EVM_{RND} values as shown in (13) for the transmitter and the receiver. For the set of evaluation instances the EVM values denoted as EVM_{BITS} are computed conventionally

using 320, 16QAM OFDM symbols for the transmitter and the receiver. The scatter plot comparisons between the $EVM_{MULTI\text{-}TONE}$ and EVM_{BITS} and the *mse* computed using (45) - (46) are shown in Figure 38 and Figure 39 for the transmitter and the receiver. From the *mse* values shown in Figure 38 and Figure 39, it can be observed that the EVM values computed using multi-tone closely tracks the EVM values computed conventionally. Table 5 shows the best and worst case error in estimation for the transmitter and receiver.

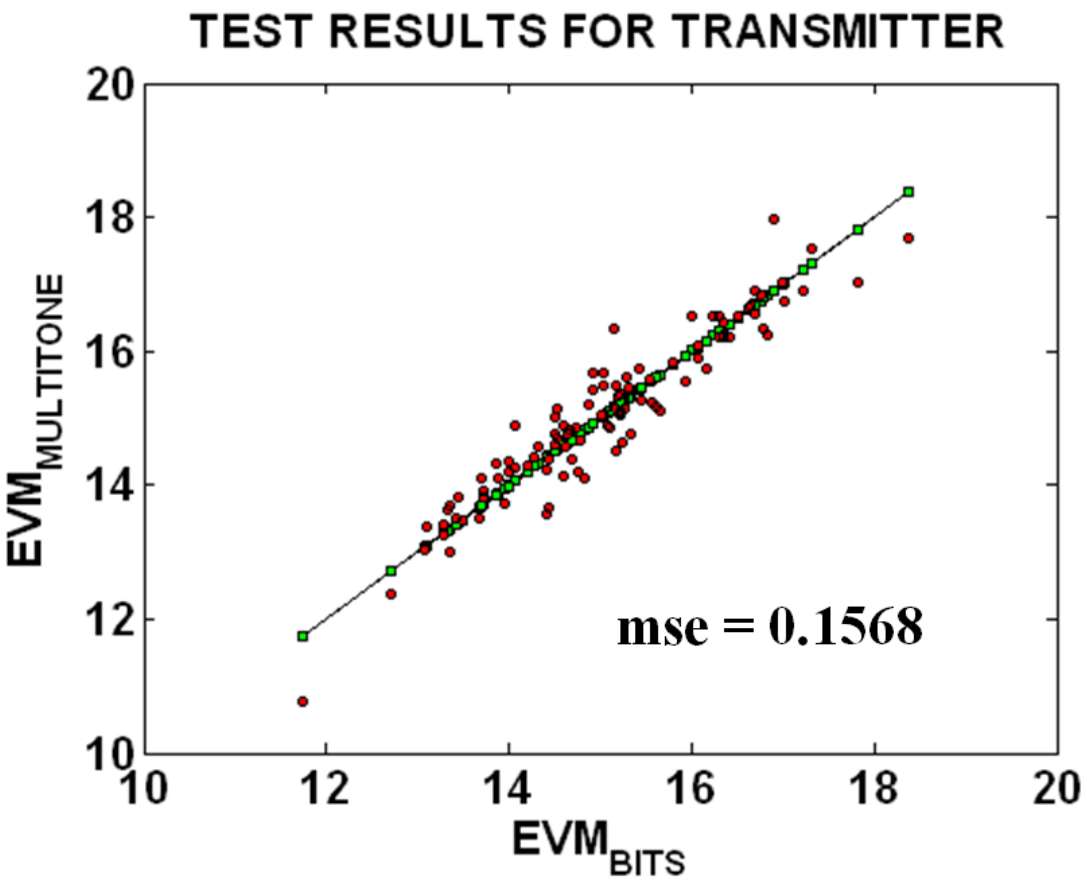

Figure 38: $EVM_{MULTI\text{-}TONE}$ vs. EVM_{BITS} for Transmitter

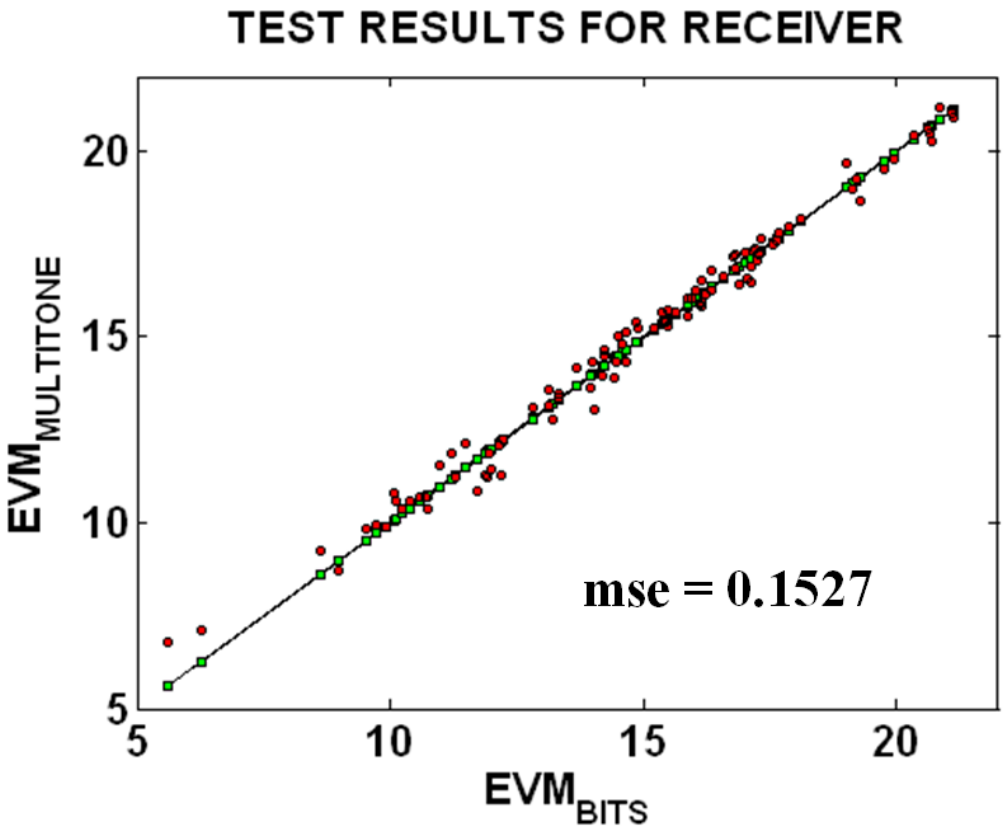

Figure 39: $EVM_{MULTI\text{-}TONE}$ vs. EVM_{BITS} for Receiver

3.3.6 HARDWARE RESULTS

In order to demonstrate the feasibility of the proposed approach at proof of concept capacity, experiments are conducted on a hardware prototype. An industrial 802.11 a/b/g industrial RF front-end (PA/LNA) from Texas Instruments, is used to validate the approach. The transmitter and receiver chains are constructed in an ad hoc manner. The following steps detail the outline of the hardware experiments.

- Conventional testing of EVM to compare against the proposed approach.
- Proposed loopback testing of RF front-ends to compute static impairments.
- Conventional testing of distortion characteristics of the RF front-end to compare against loopback testing.
- EVM computation from the decomposition model.

3.3.6.1 Instrumentation and RF Modules

The RF, baseband instrumentation and the RF modules used to conduct experiments, are listed below,

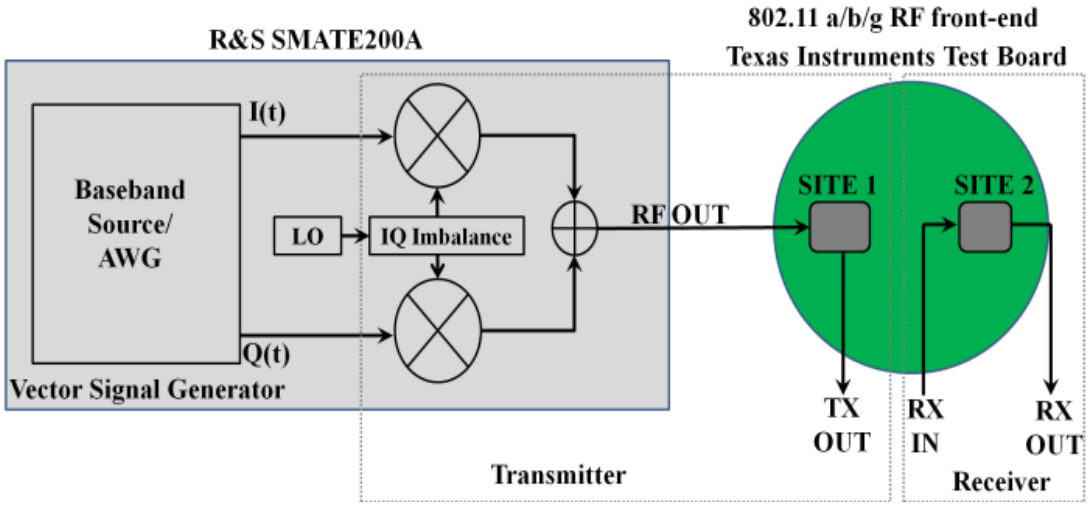

Figure 40: Ad hoc setup of the transceiver

- A production test capable '*R&S SMATE200A*' vector signal generator is used to source RF signals. The vector signal generator is capable of simulating multiple I/Q imbalance characteristics using an in-built quadrature modulator. The baseband sources in the instrumentation support both standard OFDM signal generation as well as arbitrary waveform generation of up to 128 Msamples.
- The WLAN signals are captured and analyzed by *R&S FSQ* vector signal analyzer. The vector signal analyzer is used to demodulate the WLAN signals to compute EVM conventionally.
- *HP E3631* DC supplies are used to power up the RF front-ends.
- The RF front-ends are housed on a multi-site test board via RF sockets. The 802.11 a/b/g chip is capable of operating as both PA and LNA. However, only one amplifier can be enabled at any given time. Hence site 1 of the multi-site board is assigned to

house chips designated as PA's and site 2 is assigned to house chips designated as LNA's.

- The transmitter chain is represented by the inbuilt quadrature modulator of R&S SMATE200A along with the PA at site 1 as shown in Figure 40.
- The receiver is represented by the LNA at site 2 as shown in Figure 40.
- A prototype envelope detector and a commercial off the shelf Analog devices I/Q demodulator, AD5382 are used to mimic the load-board DfT to perform loopback experiments
- The low frequency responses for the loopback experiments are captured by a VLCT tester (very low cost tester) from Texas instruments.
- Conventional measurements of the distortion characteristics of the RF front-ends (PA/LNA) are measured using an Agilent E8363b PNA series network analyzer.

In the hardware demonstrations, the effects of dynamic impairments are not included. This is due to the lack of facilities to inject phase noise in a controlled manner (because the chips measured are primarily amplifiers and the R&S SMATE200A used for mimicking an up-conversion mixer does not allow for phase noise control). The inherent phase noise of the instrumentation is designed to be extremely small to cater for production testing. Further the thermal noise effects of the front-ends on the EVM value are minimal due to the high gain operation of the PA (SNR is low) and due to the low NF design of the LNA. Hence, only S_{MEAN} and VAR_{STATIC} values determine the overall EVM in this setup. However this is acceptable because the key motivation behind the hardware experiments is to demonstrate the feasibility of the proposed approach at a proof-of-concept capacity.

3.3.6.2 Conventional Testing of EVM

The experiments are conducted for 8 instances of the transceiver. The setup for this experiment is shown in Figure 41.

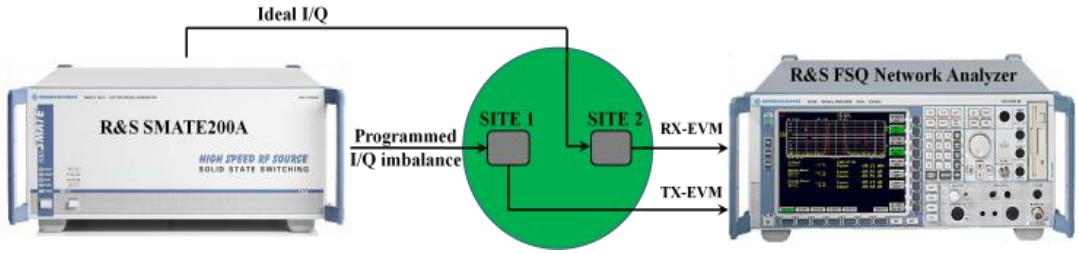

Figure 41: Conventional EVM measurement setup

The vector signal generator R&S SMATE200A is programmed to generate 802.11 16 QAM modulated WLAN OFDM frames. The I/Q imbalance characteristics of the instrumentation are set appropriately and the output of site 1 of the multi-site board is captured by R&S FSQ analyzer to compute transmitter EVM. Table 6 shows the conventionally computed EVM values and the programmed quadrature offset values for 8 instances of the transmitter.

Table 6: Conventional measurements of TX EVM

Instance	Quadrature offset		Burst Power (dBm)	Crest factor	EVM (%)
	Gain (dB)	Phase (deg)			
1	-0.17	-0.05	8.22	7.37	8.9125
2	-0.05	-1.34	5.81	8.44	5.2060
3	0.15	1.98	6.47	6.45	14.672
4	-0.08	-0.7	8.35	7.94	7.3030
5	0.09	0.04	7.7	6.91	11.981
6	-0.03	0.85	7.9	7.95	7.5683
7	-0.02	-0.04	7.98	7.17	9.8855
8	-0.02	0.09	8.08	7.2	7.9799

The vector signal generator R&S SMATE200A is programmed to generate 802.11 16 QAM modulated WLAN OFDM frames. The I/Q imbalance characteristics are set to be ideal for this experiment. The RF output of the generator is fed as input to the LNA at site 2 of the test board. The WLAN frames at the output of the LNA are captured by R&S FSQ analyzer to compute receiver EVM. Table 7 shows the conventionally measured EVM values for 8 instances of the receiver.

Table 7: Conventional measurements of Receiver EVM

Instance	Burst Power (dBm)	Crest factor	EVM (%)
1	-20.22	6.7	12.2039
2	-23.91	8.39	7.9250
3	-21.14	6.92	11.3763
4	-20.93	6.86	11.5080
5	-22.8	7.8	9.89
6	-22.68	8	9.772
7	-22.86	8	9.311
8	-21.61	7.4	10.9018

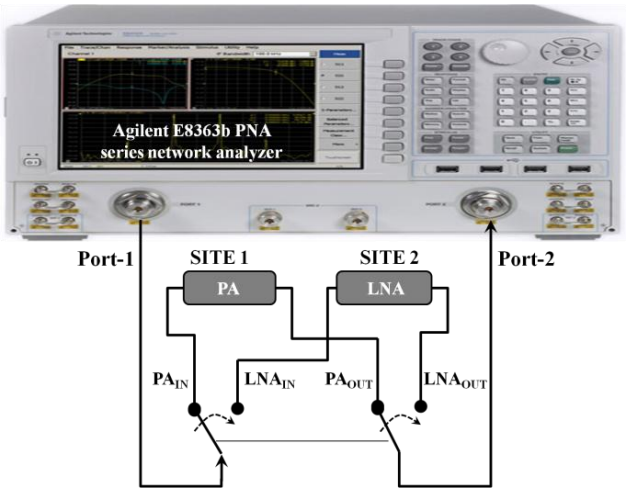

Figure 42: Conventional Distortion measurement setup

3.3.6.3 Conventional Measurements of Distortion Characteristics

The setup for this experiment is shown in Figure 42. The Agilent E8363b PNA series network analyzer is set to make continuous wave (CW) power sweep measurements at 2.4 GHz to measure the AM-AM and AM-PM characteristics of PA at site 1 and the AM-AM characteristics of LNA at site 2. The input power to the RF front-ends is swept from their linear range to their input P1dB values. Figure 43 and Figure 44 show the measured curves for a single instance of the transmitter PA and the receiver LNA.

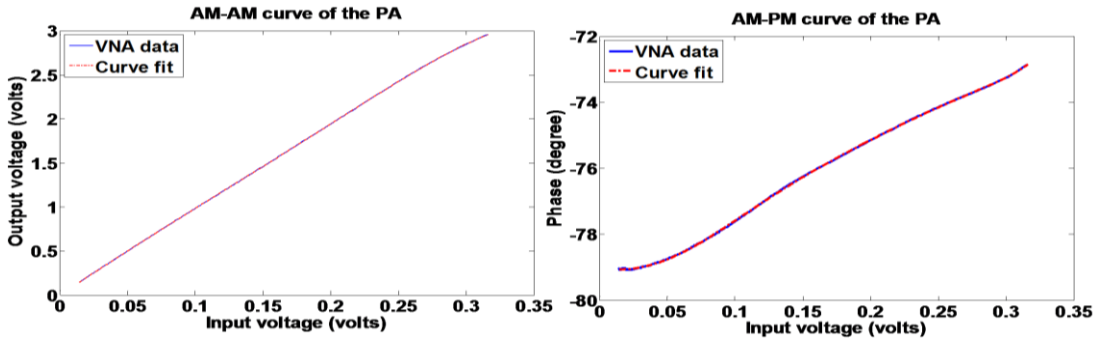

Figure 43: Conventionally measured AM-AM and AM-PM curves for the PA

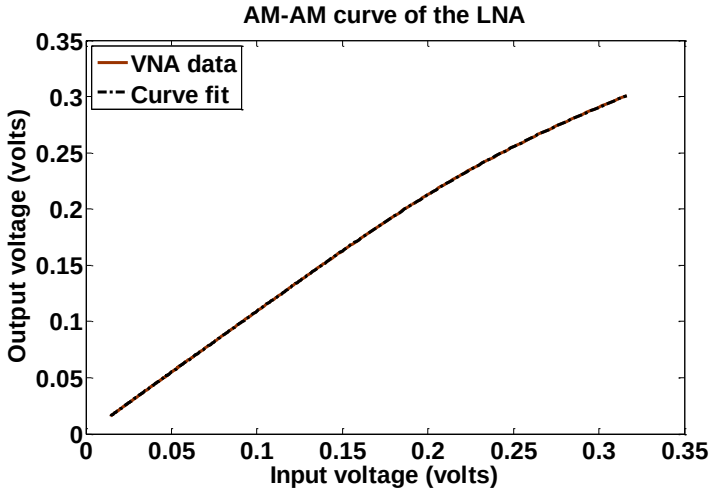

Figure 44: Conventionally measured AM-AM curves for the LNA

3.3.6.4 EVM Computation Using Proposed Methodology

The baseband source of the vector signal generator R&S SMATE200A is programmed to generate an optimized multi-tone stimulus for the I and Q channels. The I/Q imbalance characteristics are set appropriately for the transmitter. The transmitter and the receiver are setup in a loopback configuration. The output of an envelope detector is captured by the VLCT to compute transmitter impairments. The output of LNA is captured by VLCT via a load board down-conversion mixer (AD5382) to compute the receiver impairments. The setup for this experiment is shown in Figure 45.

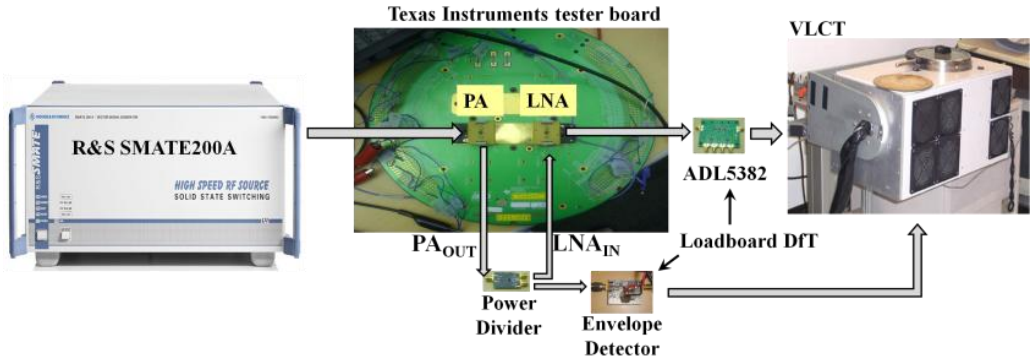

Figure 45: Loopback test setup

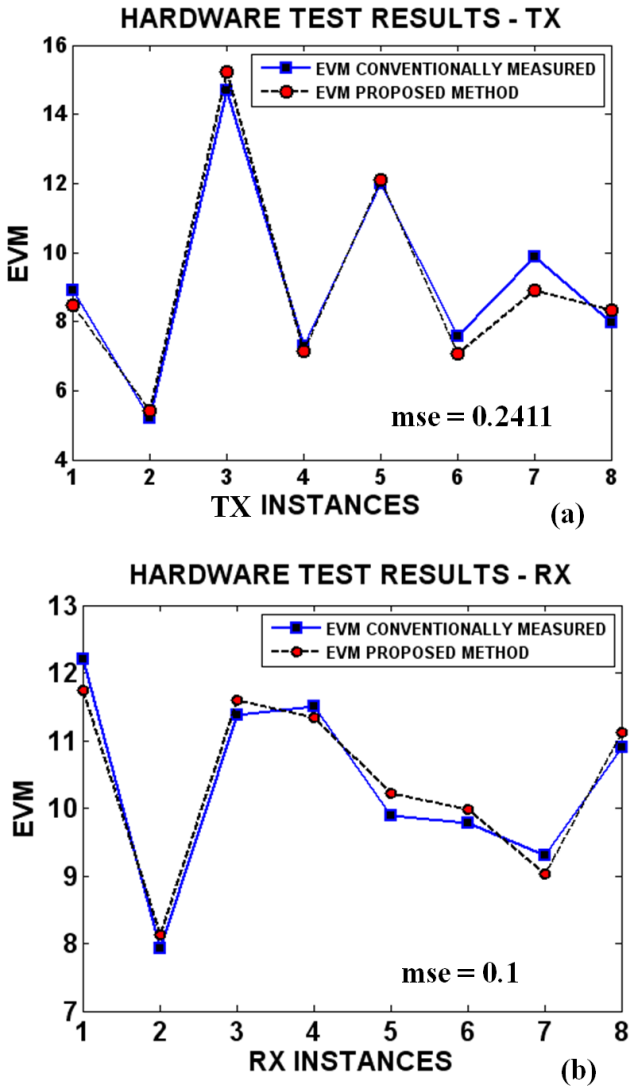

Figure 46: Comparison of multi-tone EVM tests vs. conventional EVM tests for (a) Tx and (b) Rx

The transmitter and receiver impairments are computed from the low-frequency responses captured using the proposed loopback methodology. The loopback test results are skipped for brevity. The computed impairments using the loopback test technique are fed as input to the MARS model (built offline) to predict the S_{MEAN} and VAR_{STATIC} values. Due to the minimal impact of dynamic impairments in this set-up the overall EVM is approximately equal to the EVM_{DET}. The EVM_{DET} is calculated from the

predicted S_{MEAN} and VAR_{STATIC} values as shown in (41) - (43). The error between conventional EVM and proposed EVM is quantified by the *'mse'* values as shown in (45). Figure 46 shows the comparison between the conventionally measured EVM and the proposed multi-tone test based EVM, for the transmitter and the receiver. The low values of '*mse'* demonstrate the feasibility of the proposed low-cost multi-tone testing of EVM

3.3.7 KEY ADVANTAGES

The following sub-sections summarize the key advantages of this research.

3.3.7.1 Test Time Reduction

The decomposition of EVM into deterministic and random components significantly reduces the test time required to compute EVM accurately. The comparison in test and computation times is shown below for the transmitter (receiver operations are similar). From the comparison it can be observed that the proposed methodology offers significant improvements over conventional testing techniques.

- Conventional EVM testing requires at least 20 frames of 802.11 WLAN data. Each frame requires the presence of at least 16 OFDM symbols. Thus a minimum of 320 OFDM symbols is required to perform EVM testing (320 OFDM symbols with 48 data symbols per an OFDM symbol = 15360 data symbols).
- The proposed approach requires a maximum of 5 symbols of the multi-tone signal (1 multi-tone symbol (20 MHz) ≅ 1 OFDM symbol) to perform EVM testing.
- Conventional EVM testing requires 320 IFFT/FFT operations to modulate and demodulate data symbols across 320 OFDM symbols. Further additional time is required to perform synchronization, guard band removal etc.
- The proposed technique, requires 160 FFT operations (32 operations per 1 multi-tone symbol) to perform noise analysis.

3.3.7.2 Test Cost Reduction

In this approach, EVM testing is demonstrated with a multi-tone test input. The key advantages of the proposed approach are,

- Multi-tone input can be generated by a low-cost arbitrary waveform generator.
- Eliminating the need for OFDM modulation and demodulation capability.
- Eliminating the need for performing time and frequency synchronization, time and frequency interleaving and guard banding, thereby *significantly relaxing the requirements of ATE*.
- Computation of multiple system impairments (I/Q imbalance, AM-AM and AM-PM characteristics and Noise power) along with EVM.

To summarize, in this section, a low-cost multi-tone EVM testing methodology is presented. The proposed methodology computes EVM by decomposing it into its deterministic and random components. The deterministic EVM component exhibit strong correlation to the static impairments present in the system. A simple loopback test approach is developed to compute the static impairments to estimate the deterministic component of EVM. The random component of EVM is computed using a noise amplification technique. The EVM of the DUT is then computed from the deterministic and random components. Simulation results and experiments on a hardware prototype demonstrate the accuracy of the proposed approach. The developed solution is low-cost primarily due to the use of multi-tones generated by a low-cost ATE as test input. The proposed methodology offers significant reduction in test time in comparison to conventional testing techniques and is amenable for deployment in the production floor using a low-cost infrastructure. With minor modifications the proposed methodology can be extended for a self-healing framework as well.

3.4 RESPONSE FITTING DRIVEN DEVICE MODEL EXTRACTION FOR LOW COST SPECIFICATION TESTING OF RF SYSTEMS

Alternate testing offers a low-cost alternative to conventional production testing schemes by estimating multiple RF specifications form a single data acquisition resulting in significant test time reduction. Alternate test coupled with DfT solutions such as embedded sensors make production testing using a low-cost infrastructure feasible. However, considerable effort is expended in developing the regression based mapping. Specifically, the training set of devices for developing the mapping using supervised learning techniques must include devices across as many process corners as possible. In practice, a *defect filter* [65]-[66] is used to first determine if the DUT specifications can be predicted accurately from its response (the specifications of devices that are significantly outside the performance domain of devices in the training set are not predicted accurately by the alternate test procedure). If not, then standard specification tests are applied to these "outlier" devices for pass/fail classification and the resulting data is used to "update" the supervised learner. In the presence of unanticipated process shifts, it is expected that the resulting outlier devices are "kicked-back" to standard testing procedures and the resulting information fed to the supervised learning algorithm. In such a scenario, the system "learns" about process shifts and adjusts appropriately over time. *However, the learning process can be lengthy and does not eliminate the use of standard test mechanisms*.

Hence it's desirable to develop testing techniques that can obviate the need to perform training and compute multiple performance metrics using a low-cost infrastructure in a shorter period of time compared to conventional testing techniques. In this section, a response fitting based device model extraction (also referred to as parameter estimation/identification) technique is discussed to compute multiple performance metrics from a single data acquisition. In a parameter identification technique, the DUT is defined by a black box model. The model parameters are extracted

by observing the output response of the DUT to a carefully chosen test input. The extracted models are then used to compute the specifications of the DUT. [67]-[70] illustrate prior literature concerning various parameter identifications techniques.

3.4.1 GOALS AND OBJECTIVES

The key objectives for low-cost testing of multiple specifications of RF devices are

- The test methodology should allow for RF devices to be tested with the *least test time possible* using a single data acquisition.
- The test methodology should allow for *multiple RF specifications* to be determined concurrently from a *single data acquisition* using *low cost test equipment.*
- The test methodology *should eliminate the need for training* of supervised learners for accurate test specification computation**.**

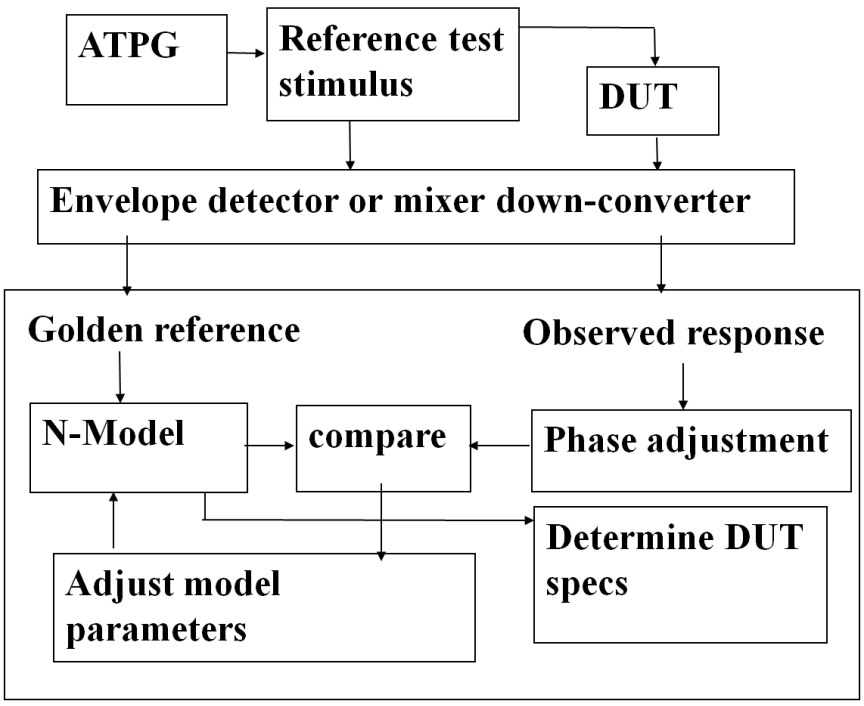

Figure 47: Device model extraction approach

3.4.2 PROPOSED METHODOLOGY

An ADS design of the RF PA is used as a test vehicle. Behavioral models of the PA are extracted from the AM-AM and AM-PM curves obtained using ADS templates. Figure 47 shows the flow-graph of the proposed response fitting based device model extraction approach. The behavioral model of the PA in MATLAB is referred to as the DUT in Figure 47. The black box model extracted by the response fitting approach is denoted as the 'N-model'. N-model determines the specifications that can be computed from the same. In this work, the AM-AM characteristics are targeted. Note that the behavioral model used to simulate the device is different from the N-model extracted from the response fitting approach. In production testing, the DUT block in Figure 47 represents an actual device. The complexity of the N-model is determined based on the specifications of interest.

3.4.2.1 Approach

A single or multi-tone amplitude-modulated RF test stimulus (optimized via a genetic test generation algorithm) is computed in such a way that the *response of the RF DUT* to the stimulus *exhibits strong statistical correlation with its test specification values* under multi-parameter DUT perturbations (this is similar to the manner in which the test stimulus is constructed for the alternate test approach). The resulting stimulus is called the *reference test stimulus* (RTS). The DUT is excited by the RTS and its response is down-converted to baseband using either a mixer or envelope detector. The down-converted signal is digitized for analysis and is referred to as the *observed response* of the DUT. Note that the observed response is distorted by the DUT gain and phase transfer non-idealities. Hence, this response is also called the *distorted response signal* (DRS). The DUT is removed and the input signal (RTS) is directly down-converted by the same mixer or envelope detector and digitized by a data converter. This is the ideal or *golden reference signal* (GRS).

For comparison of the golden signal and the observed test responses, the phases of the same are adjusted digitally. Given a finite order non-ideality model (N-Model in Figure 47) for the RF DUT including AM-AM distortion effects, the input to the model is assumed to be the golden reference signal and its output is assumed to be the observed response of the DUT to the RTS. The model parameters are then computed in such a way that the input and output of the model are consistent with each other using a combination of algebraic methods and optimization algorithms. The process of mapping the golden reference signal to the observed DUT response via the DUT model is called *response fitting*. The relevant specifications of the DUT are computed from the model parameters so extracted.

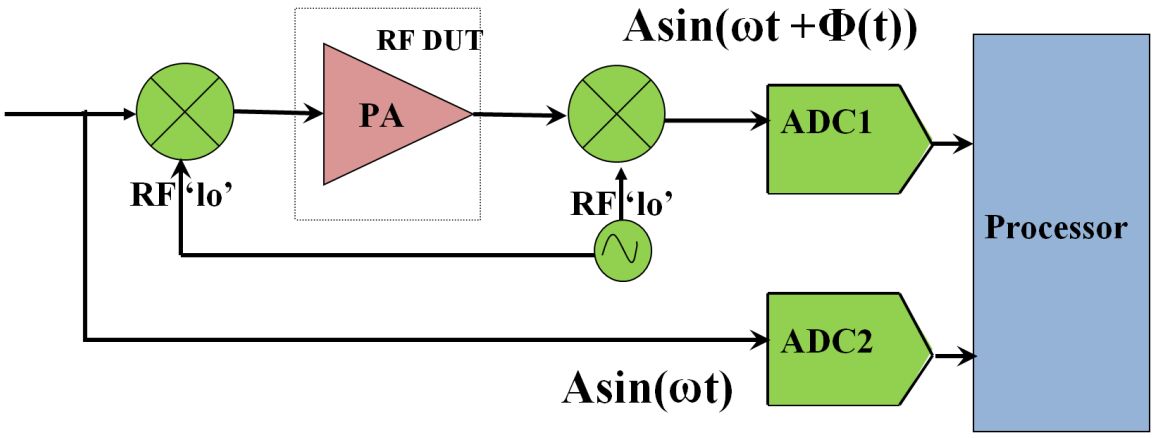

Figure 48: Response fitting based model extraction test setup

3.4.2.2 Test Setup

Figure 48 shows the test setup on which the proposed theory is validated. The test input is sourced from a low frequency multi-tone signal generator. The low frequency RTS is up-converted by a pre-characterized load board mixer. The test setup is evaluated for two different sensors: 1) Envelope sensor and 2) Mixer. The low frequency outputs at the sensor is digitized and transported to a low-cost tester/processor for further analysis.

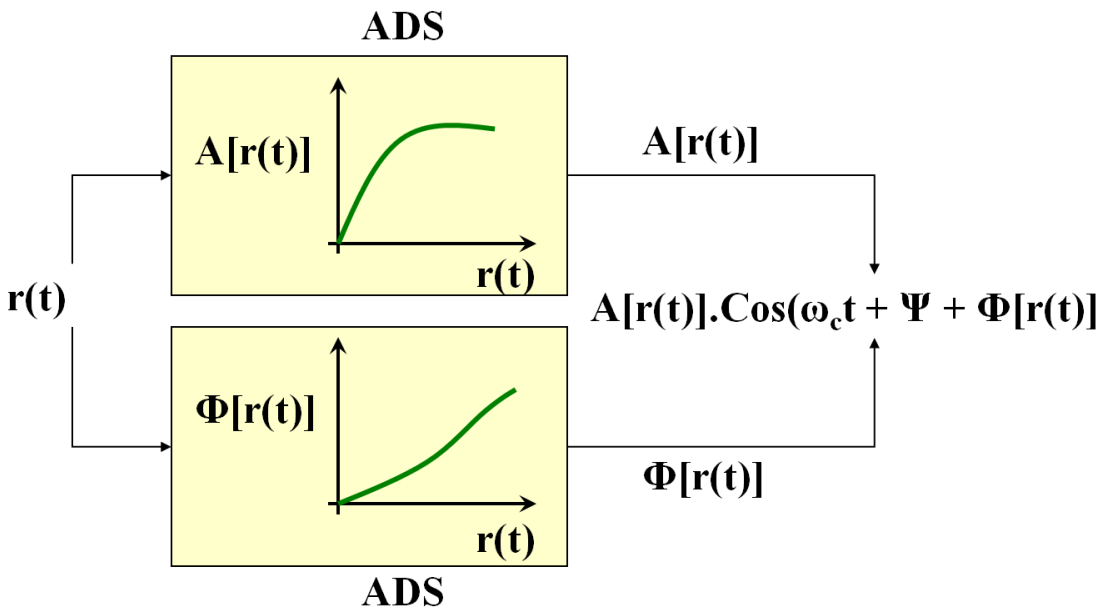

Figure 49: AM-AM and AM-PM modeling of the PA

3.4.2.3 Modeling of AM-AM and AM-PM Characteristics of the PA

A two stage RF PA was designed at the transistor level using CMOS 0.18um technology and simulated in Agilent Advance Design Systems (ADS). HP-ADS design templates were used to simulate for AM-AM and AM-PM characteristics. The extracted characteristics were then imported to MATLAB. The developed models are then used to simulate transient DUT response waveforms. The reference test stimulus (RTS) is generated in the baseband using low frequency multi-sines. The test waveform is then up-converted using a mixer on the tester load board. Let ω_c be the carrier frequency of the RF signal shown in the test setup. The input to the PA is of the form 'r(t).Cos(ω_ct + Ψ)', where r(t) is the modulated envelope at the input of the PA and Ψ is the phase of the carrier. The output of the PA is then given by,

$$Y(t) = A[r(t)].Cos(\omega_c t + \Psi + \Phi[r(t)] \quad (48)$$

Where, A[r(t)] is defined by the AM-AM distortion characteristics and Φ[r(t)] is defined by the AM-PM characteristics (measured using HP-ADS). The modeling approach is shown in Figure 49. The sensor responses for the PA output are then computed and digitized for analysis.

3.4.2.4 Nonlinearity Model (N-Model) For Use in Response Fitting

In this research, the focus is on measuring AM-AM distortion effects in the presence of AM-AM distortion as well as AM-PM distortion in the RF power amplifier (PA). The N-model is assumed to be of polynomial form defined by α 's with a predefined degree. The third order polynomial is defined to be of the form $y = \alpha1*x + \alpha2*x^2 + \alpha3*x^3$. For an ideal device, α1 = gain, α2 = 0 and α3 = 0. For a specific DUT, the objective is to find the values of α1, α2 and α3 such that when *x* is the *golden reference signal*, *y* is the *distorted signal response*.

The golden response for a given test is mapped to the distorted response obtained from ADS characterization data to compute the polynomials that define the AM-AM characteristics of the device. It is observed that the degree of the polynomial model affect the accuracy of the characterization. In this work a polynomial of up to '6th' degree is computed from the captured responses to result in accurate characterization of the RF DUT. Once the polynomial y = f(x) for a specific RF DUT is known, the specifications that define the AM-AM distortion characteristics such as Gain, IIP2, IIP3 and P1dB (input) can be computed from the computed N- model parameters. Coefficients α1, α2 and α3 (from a 6th degree fit) are used to calculate specifications based on the equations shown below

$$Gain = 20.\log(\alpha_1) \qquad (dB) \qquad (49)$$

$$IIP2 = \left|\frac{\alpha_1}{\alpha_2}\right| \qquad (volts) \qquad (50)$$

$$IIP3 = \sqrt{\frac{4}{3}\left|\frac{\alpha_1}{\alpha_3}\right|} \quad (volts) \quad (51)$$

$$P1dB\ (input) = \sqrt{0.145.\frac{\alpha_1}{\alpha_3}} \quad (volts) \quad (52)$$

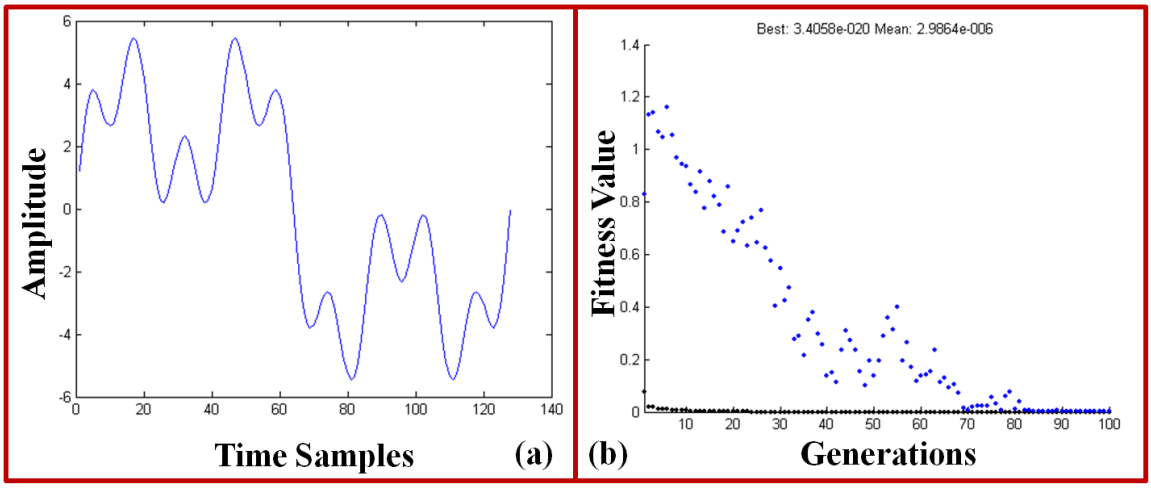

Figure 50: (a) Optimized test waveform (b) fitness metric across generations

3.4.2.5 Test Stimulus Generation

Genetic algorithm is used to obtain an optimized multi-tone test stimulus. For test generation, a sample set of devices under statistically significant process variations is created. For each device, the values of the polynomial coefficients are computed using data from HP-ADS simulation runs. During test generation, for each candidate test stimulus (corresponding to a chromosome), the "best-fit" N-model polynomial coefficients (α's) corresponding to each device in the sample set, is computed by mapping the golden response signal *x* to the corresponding distorted signal *y*.

The error between the calculated α's and actual values of α's (known) for all of the devices in the sample set are weighted appropriately to obtain the fitness function that the genetic algorithm minimizes. For accurate computation, the input stimulus has to

capture all the non-ideal effects of each DUT. The optimization is done over both frequency and amplitude of the baseband signal within the 20 MHz baseband bandwidth (typical for an OFDM system) to finally determine a multi-tone for which the best accuracy in computing the N-model parameters is achieved. Figure 50 shows the progression of the fitness metric vs. the no. of iterations on the left and the optimized multi-sine test stimulus on the right.

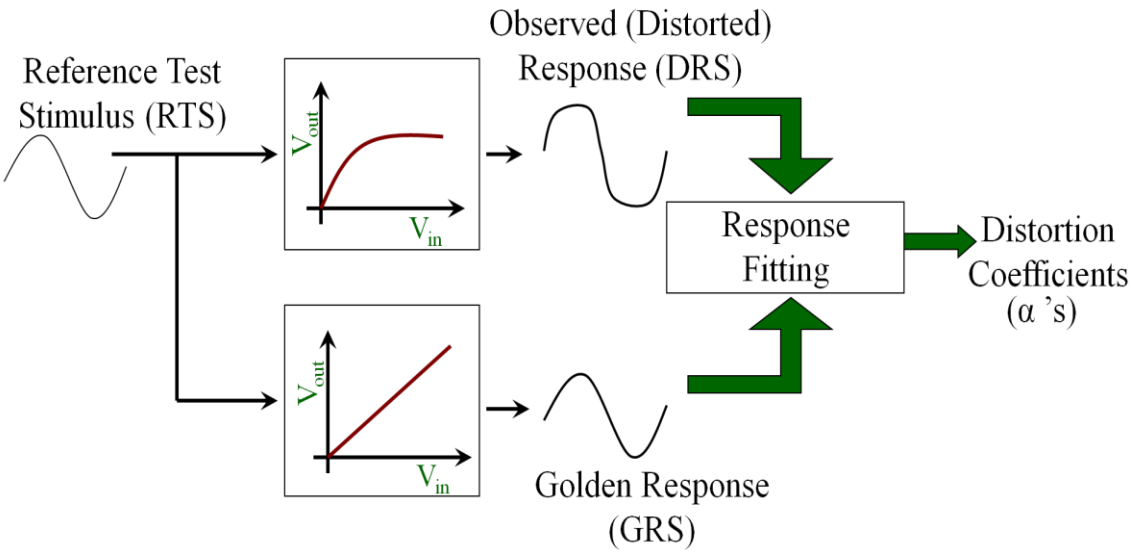

Figure 51: Conceptual block diagram for response fitting

3.4.2.6 Response Fitting

In this sub-section the basic theory behind signal transformation based testing of multiple specifications of the RF DUT is discussed. The conceptual block diagram for N-model identification is given in Figure 51. In this procedure, for a given reference test stimulus (RTS) the golden response signal (GRS) and the distorted response signal (DRS) are captured. For simplicity, the RTS is shown to be a single tone sine wave. The key idea is that the polynomial that maps the golden response signal (GRS) to the distorted

response signal (DRS) captures the distortion characteristics of the nonlinear transfer function of the RF device under test (DUT).

For a given test setup, the GRS and the DRS of a DUT are known. The polynomial that characterizes the distortion can then be computed by constructing the "*Vandermonde" matrix 'V'*. The GRS is assigned as *x* and DRS is assigned as *y*. The objective is to determine the polynomials 'p' that map *x* to *y*. Let the degree of the polynomial be defined to be '*n*'. For a given '*x*' and a degree '*n*' the Vandermonde matrix can be constructed as follows,

$$v_{i,j} = x_i^{n-j} \tag{53}$$

Where $v_{i,j}$ is an element of the Vandermonde matrix **V** with row index 'i' and column index 'j'. Once the Vandermonde matrix is computed, the polynomials are obtained by solving the following equation in the 'least squares' sense as follows,

$$\mathbb{V}.p \approx y \tag{54}$$

(54) is solved by using standard QR factorization techniques (inv(V)* y) to calculate p in a computationally efficient manner. In practical test setups the DRS undergoes transformations from the measurement setup artifacts in addition to the distortion characteristics of the RF device. However since the GRS is captured into the digital signal processor via the same measurement setup/path, the artifacts introduced by the measurement setup can be ignored. Further, any mismatch between the measurement setup paths can be de-embedded based on prior characterization.

3.4.3 VALIDATION RESULTS

In this section the simulation results obtained for the two-stage PA designed in ADS is presented. The nominal AM-AM and AM-PM characteristics obtained from ADS simulations are shown in Figure 52. Monte Carlo simulations are then performed in ADS to generate process variations to obtain multiple AM-AM and AM-PM curves for 100 instances of the PA.

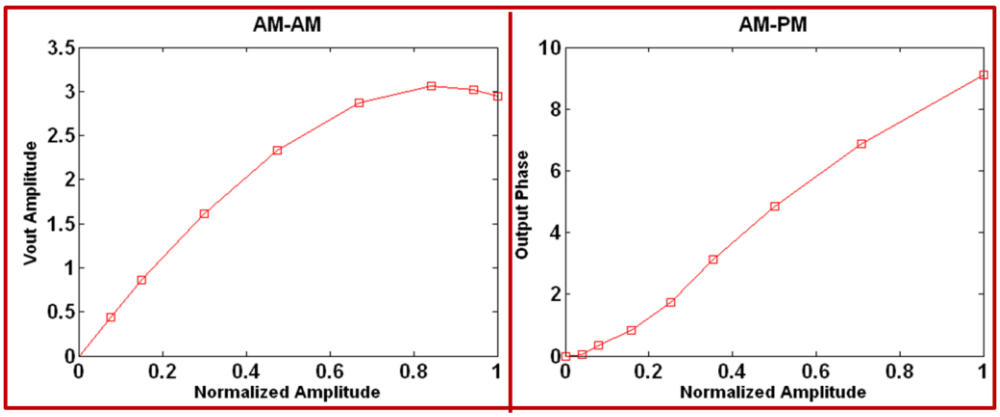

Figure 52: AM-AM and AM-PM curves from the ADS design of PA

3.4.3.1 Case 1: Test Results with No AM-PM Effects

AM-PM effects of the DUT model are turned off in this case study. The optimized test shown in Figure 50a is used to compute the black box models for all the instances. Equations 7 to 10 are then used to compute the specifications such as Gain, IIP2, IIP3 and P1dB. The accuracy of the proposed test is evaluated by comparing the computed specifications against specifications obtained from ADS simulations as shown in Figure 53 for an envelope detector. Figure 54 shows the test results for a mixer as sensor. The ‘x’ axis for the plots refers to specs from ADS and the ‘y’ axis refers to specs obtained from the proposed signal transformation technique. For a PA with AM-AM artifacts only, it can be observed from the figures that the test results are accurate for both envelope and mixer sensors at the output of the DUT

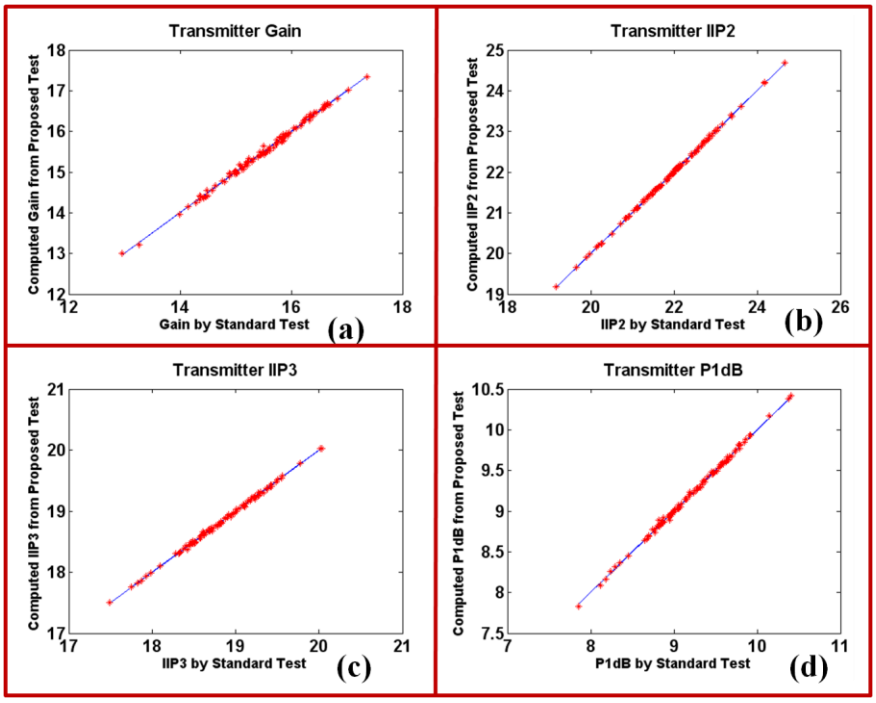

Figure 53: Calculated Specifications vs. Actual Specifications for Envelope detector (a) Gain (dB) (b) IIP2 (dBm) (c) IIP3 (dBm) and (d) input P1dB (dBm)

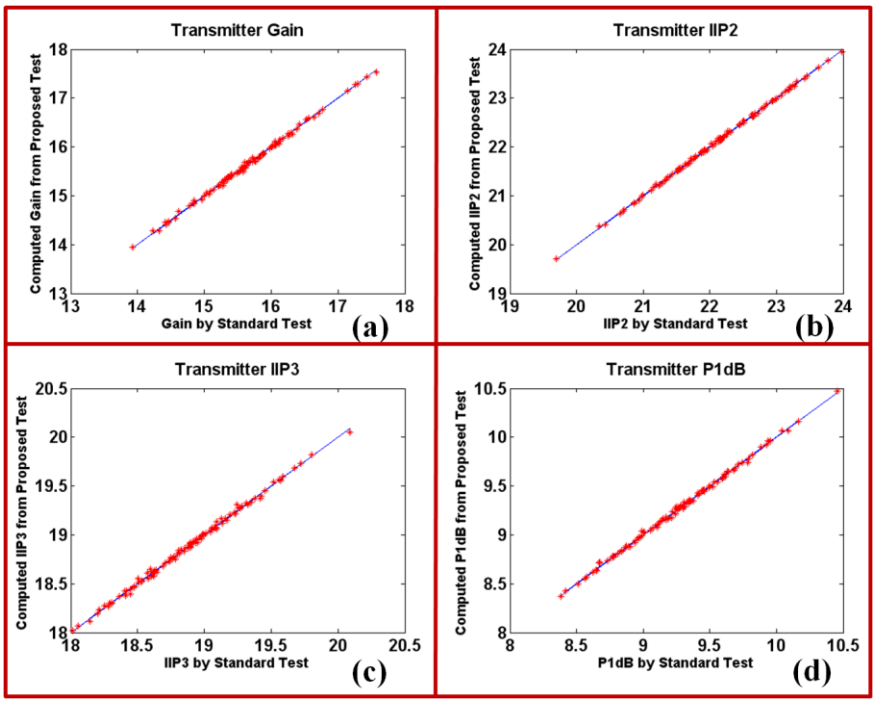

Figure 54: Calculated Specifications vs. Actual Specifications for Mixer (a) Gain (dB) (b) IIP2 (dBm) (c) IIP3 (dBm) and (d) input P1dB (dBm)

3.4.3.2 Case 2: Test Results with AM-PM Effects

The test results shown in Figure 53 and Figure 54 ignore the AM-PM effect of the amplifier on the output. However, a cause for concern is the fact that the effects of AM-PM phase additions on the RF carrier, corrupt the amplitudes of the envelope and mixer sensor's outputs. This results in inaccurate specification computations. The impact of AM-PM effects on the accuracy of the test results are studied for two scenarios, nominal AM-PM (10 degrees max) and exaggerated AM-PM (up to 80 degrees) for both the envelope and mixer sensors. Figure 55 and Figure 56 shows the test results for IIP3 for realistic AM-PM effects and exaggerated AM-PM effects respectively.

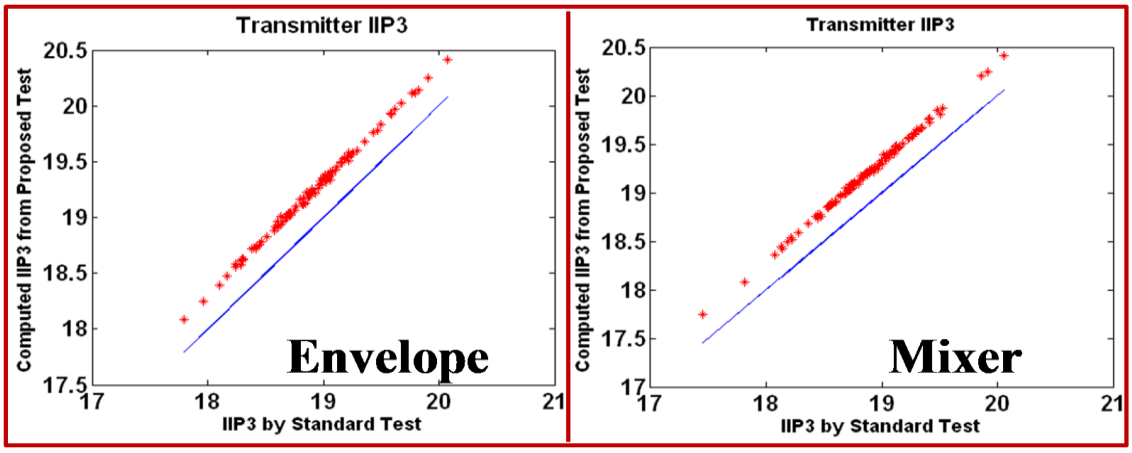

Figure 55: Impact of Realistic AM-PM on IIP3 estimation

It can be observed Figure 55 that the presence of realistic AM-PM results in a slight DC shift in the computed specifications from the actual specifications for both the sensors. It can be observed from Figure 56 that even for high values of phase distortion (exaggerated AM-PM) the envelope detector shows only a DC shift in the computed specifications. This is due to the fact that the envelope is dominated by the AM-AM effects.

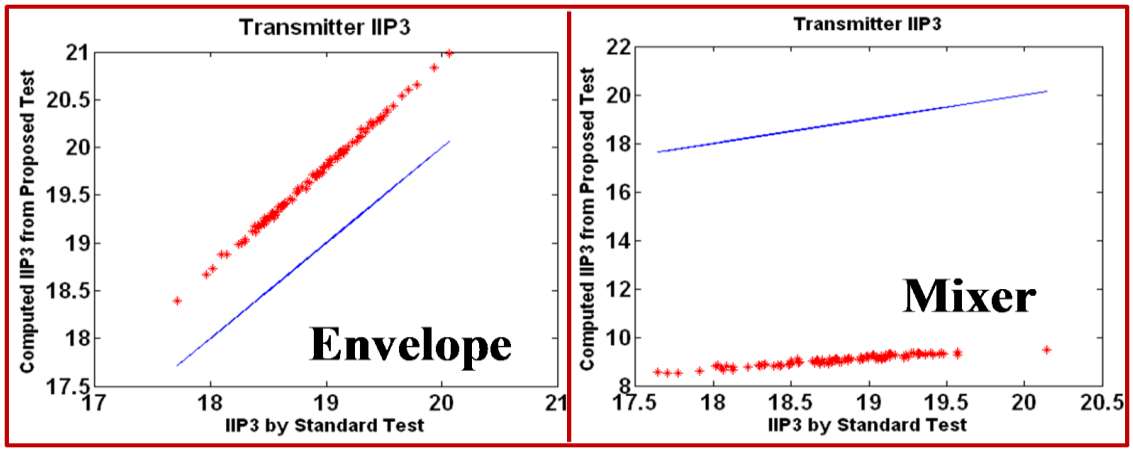

Figure 56: Impact of Exaggerated AM-PM on IIP3 estimation

This DC shift in estimation for envelope detectors can be compensated by comparing the developed test results with standard test results for a nominal device to determine the amount of DC shift in computation. However from Figure 56 it can be seen that in the case of mixer the results get corrupted significantly. Hence it's desirable to use an envelope detector to accurately estimate the AM-AM specifications under the influence of AM-PM distortion.

3.4.4 KEY ADVANTAGES

The key advantages of the proposed response fitting based device model extraction technique are,

- The proposed technique is a *low-cost test solution.* The signals are sourced and measured at low frequencies.
- The response fitting algorithms are simple and hence offer accurate testing in a significantly reduced amount of time using low-cost infrastructure.
- Results show that accurate computation of AM-AM distortion effects such as Gain, IIP2, IIP3 and P1dB is possible using a black box model approach
- The proposed test is accurate for multiple specifications using a single data capture without the need for training of a supervised learner

In conclusion, this chapter presented several low-cost test solutions that are amenable to production floor deployment. Three methodologies based on the alternate testing principle and a response fitting test methodology is developed to test for multiple RF specifications using a single data capture. The proposed methodologies reduce overall test time and are capable of estimating multiple RF specifications of the system. The methodologies are implemented using a low-cost infrastructure with minimal RF requirements.

The test cost of an RF system contributes significantly to the manufacturing cost of a wireless product. With the high levels of integration and the advent of deep-submicron technologies, the impact of process variations on the RF system performance is increasingly severe resulting in a significant increase in the overall test cost. The low-cost production test methodologies discussed in the chapter address the issue of test cost and test time, to significantly reduce the overall test cost of highly integrated advanced RF SoCs. This has direct impact on the *reduction of overall manufacturing cost* of advanced RF SoCs and consequently the *reduction of time to market* of these advanced systems, to guarantee a success in the marketplace.

CHAPTER 4

ANALOG TUNING METHODOLOGIES FOR COMPENSATING WIRELESS RF FRONT-ENDS

RF ICs suffer from severe process variations for technologies approaching 45 nanometer (nm) regimes. *Reduction in the production yield of RF ICs significantly affects the overall manufacturing cost of the final product*. In order to address process variability, design engineers perform design centering [71] to guarantee the design across a set of process corners. In addition during the early stages of production, engineers spend considerable amount of time in developing meticulous characterization routines across each process corner to guarantee the performance of the system. In most cases, the devices that are deemed bad during production test exhibit parametric variations as opposed to a catastrophic fault in the system. Such deviations *can be tuned* for by *designing a set of control knobs* into the system during the design phase. Once the tuning knobs are in place, a tuning strategy (using optimization routines) can be developed to run low cost tuning routines (to compute the cost function) during the production testing phase (referred to as *post manufacture tuning* in this thesis). The ***key challenges*** of analog tuning are as follows:

- Developing a fast and accurate low cost test to compute multiple performance parameters using a single data capture.
- Developing a rapid low cost tuning to improve the product yield.

In this chapter, several post manufacture analog tuning strategies to combat process variability are discussed. The key objective of these techniques is to perform post manufacture tuning of advanced RF SoCs in a low-cost environment with emphasis on reducing the time taken to perform tuning. Once a desirable yield is achieved the tuning knob values are fixed to their optimal values.

4.1 ANALOG SIGNATURE DRIVEN MULTI DIMENSIONAL POST MANUFACTURE TUNING OF RF SYSTEMS

Researchers have proposed various tuning strategies to combat process variability. The key drawback of prior research is that the existing techniques target specific system-level RF performance metrics without regard to the impact that tuning might have on other system-level RF specs. In the past, alternate test has been used to obtain multiple specifications of a RF system using a single test. However, this involves extensive training to develop accurate regression models to estimate the specifications from a single data capture. Although training can be performed offline (before production floor deployment), it is desirable to have solutions *without the need for training* to **"***implicitly tune*" multiple specifications in cases where training can be hard to perform.

In this section, a low-cost analog signature drive post manufacture tuning approach is discussed. The emphasis is on performing rapid tuning using simple measurements to improve the overall yield of a system.

4.1.1 GOALS AND OBJECTIVES

The key requirements for developing an analog signature driven post manufacture tuning approach are,

- Development of a test methodology to assess multiple performance metrics of the system for a chosen combination of the analog tuning knobs, without the need to perform extensive training.
- Development of an optimal control law (cost function) to improve the overall production yield of RF systems
- Development of optimization techniques to determine the best way to perform multi-dimensional tuning of analog knobs built into the system.

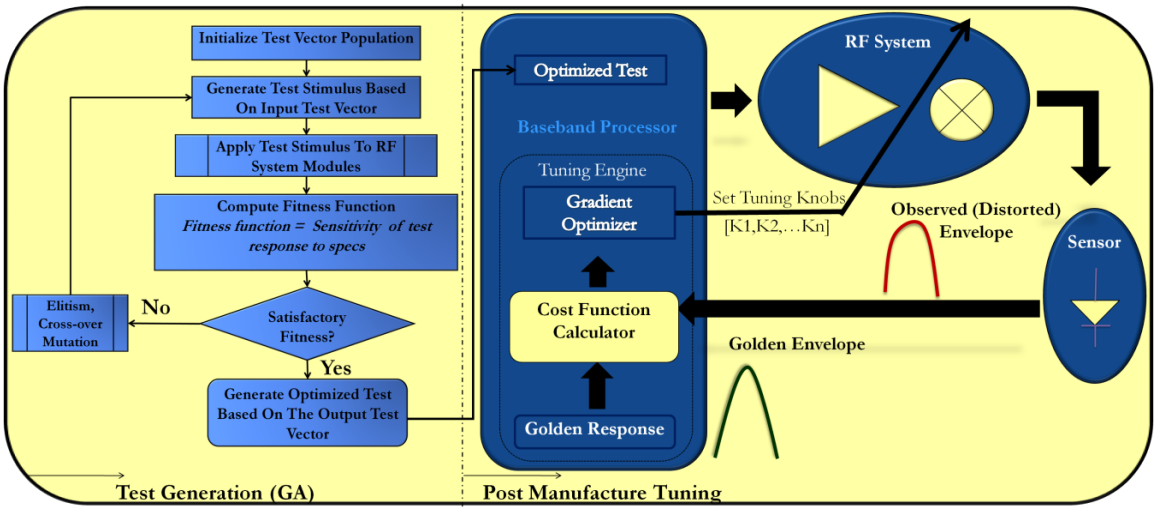

Figure 57: Conceptual diagram of the proposed analog signature driven tuning methodology

4.1.2 PROPOSED METHODOLOGY

The conceptual diagram of the proposed approach is shown in Figure 57. The proposed methodology is demonstrated on a 2.4 GHz wireless OFDM transmitter. An envelope detector is used at the output of the transmitter to a capture low-frequency response. The key idea is to perform tuning by comparing the performance of a DUT to the performance of a golden device that is identified during the characterization phase of the product cycle. The performance of the RF system is quantified by the envelope response captured for an optimized test input. The objective of tuning is then to minimize the difference between a process perturbed test response and a golden response (implicit tuning of specifications) by controlling the analog tuning knobs to implicitly guarantee an improvement in the overall yield of the system. The specifications targeted in this work are transmitter gain and IIP3.

Process variations perturb the non-idealities in the system and hence the observed response. By sampling responses (golden response) from known good devices that exhibit nominal behavior and comparing them against the responses obtained from a process perturbed device one can develop a metric (cost function) that relates to the deviation in the performance parameters of the process perturbed system from its nominal

performance (indicating the amount of tuning required). An important observation is that the tunability of a process perturbed instance can be maximized by maximizing the sensitivity of the captured test response to the multiple specifications of the system.

4.1.2.1 Test Generation

In order to maximize the sensitivity of the observed waveform to the perturbed process, a 'Genetic algorithm' based test generation is performed. The genetic algorithm is similar the ones discussed in Chapter 3. Alternate test is used as a test vehicle to perform test generation. The success of alternate test depends on the *statistical correlation* between the *observed test response* and the *process perturbations* in the system. The goal of this test generation is to identify a test stimulus with a high degree of alternate test accuracy. The quality of the alternate test is determined by the prediction accuracy of the developed regression functions, meaning that an alternate test response with high statistical correlation (for an optimized test stimulus) to the process perturbations result in good prediction accuracy. By optimizing for the prediction accuracy the sensitivity between the test response and the multiple specifications of the system is maximized implicitly.

Note: Alternate test is only used as a vehicle to perform test generation to guarantee a test response (envelop capture) that is highly sensitive to process perturbations. *During the tuning phase alternate test is not used* to perform tuning. Once an optimized test stimulus is obtained the test response is used to '*deterministically'* compute the cost function.

4.1.2.2 Cost Function Derivation

A simplistic approach to determine the cost function to perform optimization is to compute the least squared error (LSE) between the observed envelope response and the golden envelope response for an optimized test input. However a key drawback of the approach is the aliasing of the effect of one specification over the other, especially in the

case of opposing specifications. Intuitively it's easy to identify that the LSE computed between the golden and observed envelope response is dominated by the difference in gain between the two instances (difference in IIP3 values have a minimal impact on the LSE). However, a simple signal processing trick can be performed on the captured test responses to obtain metrics that have strong correlation to both gain and the distortion characteristics (IIP3) of the system. The idea is to develop two independent metrics with each having a high degree of correlation to the specifications of interest (gain and IIP3). The cost function of the analog optimization strategy is then derived as a weighted sum of the independent metrics

The LSE between the observed and golden envelopes is calculated to obtain a metric with high gain correlation (denoted as gain error). The LSE between normalized observed and golden envelopes is calculated to obtain a metric with high IIP3 correlation (denoted as IIP3 error). The two metrics are combined together to compute the cost function as follows,

$$(Cost\ Function)\ f = W_1.\|(Observed) - (Golden)\| + W_2.\left\|\left(\frac{Observed}{Observed_{max}}\right) - \left(\frac{Golden}{Golden_{\max}}\right)\right\| \quad (55)$$

Where, W1 and W2 refer to the weight assignments for the individual metrics. By appropriately allocating W1 and W2 the technique can exercise the flexibility of tuning one metric over the other depending on the requirements of the system.

4.1.2.3 Tuning Strategy

The objective of this research is to develop algorithms that can determine the best way to tune the control knobs. Designing the knobs by itself is a separate area of study and hence is out of the scope of this research. For a given RF system, it is assumed that

multiple "tuning knobs" are available for modulating device performance (e.g. capacitances, resistances *or* voltages and currents of a circuit module). In this research the focus is on some common analog control knobs that influence the performance of the system: mixer supply, mixer bias, power amplifier supply and power amplifier bias. Figure 58 shows the flow graph of the proposed steepest descent based analog tuning strategy.

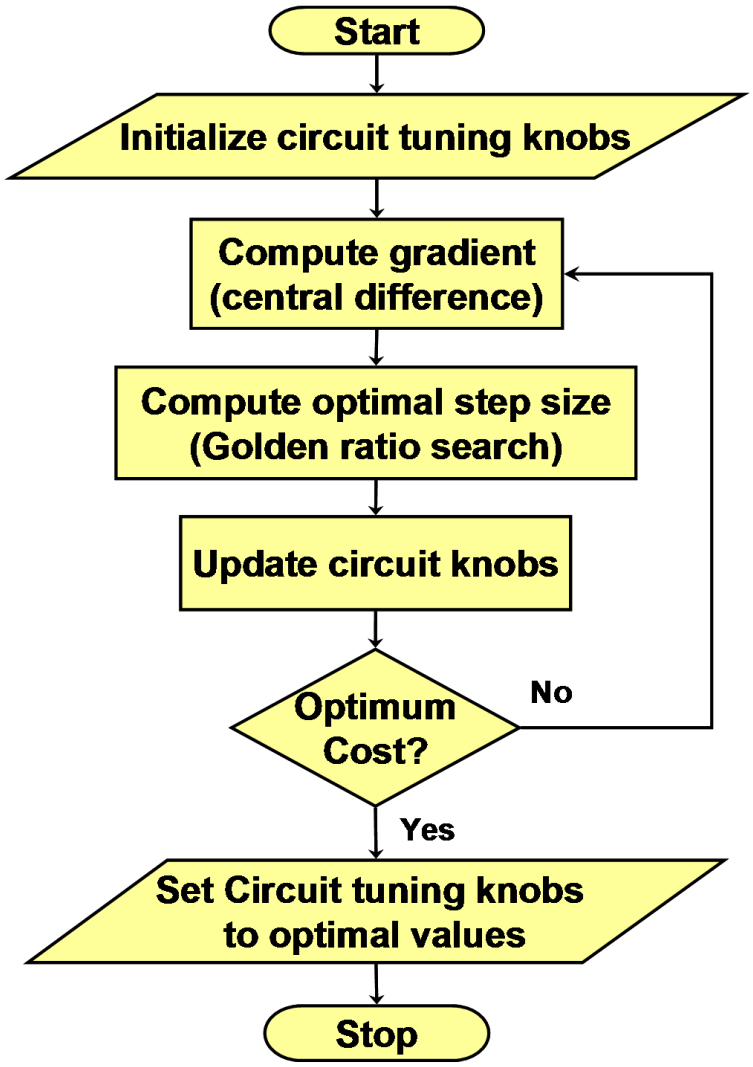

Figure 58: Steepest Descent based Gradient Search Technique

In general the tuning knobs should be chosen such that they can accommodate tradeoffs between specifications. Let K = [K1,K2,..KN] be a vector that defines 'N' such tuning knobs. For a process perturbed device the tuning algorithm starts from a nominal value of the K vector. A steepest descent based gradient search algorithm is the used to minimize a cost function 'f(K)'(computed from (55)). The tuning is performed in an iterative manner. The following steps outline the proposed analog signature driven tuning strategy,

- For each iteration the test response (a low frequency capture of the envelope detector's output) of the RF system to a carefully crafted test stimulus for a unique vector 'K' is captured. The obtained low frequency response is used to compute the cost function 'f(K)' for a given iteration
- A central derivative approximation of the cost function is used to identify the gradient vector for each tuning knob as shown in (56). The gradient vector indicates the direction of maximum benefit (performance improvement in this case). The central derivative is obtained by perturbing each tuning knob by a small value 'δ' and running the proposed test to ascertain the effect of the change in tuning knob values on the specifications of the RF system (hence, the term *hardware-iterated*).
- The gradient vector obtained through this procedure is used to compute the search direction as shown in (58).
- Once the search direction is found an optimal step size (critical to reduce the number of iterations) for each iteration is obtained using a golden ratio line search technique [72]. To obtain h_{opt}, a line search is performed on the step size 'h' as a variable to minimize function 'Z(h)'as shown in (59).
- The control vector K is then updated as shown in (60).

The mathematical framework of the hardware iterated gradient search is shown below:

$$\frac{\Delta f}{\Delta K_i} = \frac{f(K_i + \delta) - f(K_i - \delta)}{2\delta} \tag{56}$$

$$\frac{\Delta f}{\Delta K} = \left[\left(\frac{\Delta f}{\Delta K_1}\right), \left(\frac{\Delta f}{\Delta K_2}\right) \ldots \left(\frac{\Delta f}{\Delta K_N}\right)\right] \tag{57}$$

$$S_K = -\frac{\Delta f}{\Delta K} \Big/ \left\| \frac{\Delta f}{\Delta K} \right\| \tag{58}$$

$$h_{OPT} = \min\left[Z(h) = f(K + h * S_K)\right] \tag{59}$$

$$K_{new} = K + h_{OPT}.S_K \tag{60}$$

4.1.3 VALIDATION RESULTS FROM SIMULATION

In this section the validation results obtained from the simulations performed in MATLAB on a behavioral model of a 2.4 GHz wireless OFDM transmitter are discussed. An ADS design of a RF mixer and a power amplifier is used to construct the OFDM transmitter chain. A two stage RF PA design (similar to the ones in Chapter 3) in CMOS 0.18um technology is used in this study. For the mixer, a double-balanced Gilbert cell architecture is chosen. The operating range of the mixer is from 2-7GHz, and the power consumption is 6.6mW at a nominal supply voltage of 1.8V and bias of 0.8V.

4.1.3.1 Tuning Knob Definitions

The chosen analog tuning knobs for the mixer and PA designs are mixer bias, mixer supply, PA bias1 (stage1) and PA bias2 (stage2). The mixer bias values are set to operate from 1.7 to 2.2V. The mixer supply is set to operate from 0.5 to 0.9V. The PA bias1 is set to operate from 2.6 to 3.4 V. The PA bias2 values are set to operate from 2.6 to 3.4V. The voltage resolution for all the tuning knobs is set to 0.1V. The voltage resolution defines the minimum voltage value by which the tuning knob can be controlled. All possible combinations of the tuning knobs within the prescribed ranges result in a ‘search space’ of 2430 unique tuning knob combinations (‘K’).

4.1.3.2 Modeling RF Transmitter

Monte-Carlo simulations are performed in ADS to generate multiple instances of the PA and mixer. The design templates in ADS are used to generate multiple AM-AM curves for each process perturbed instance across the entire range of the tuning knobs. The tuning data obtained for all the instances of the transmitter is exported to MATLAB to extract the behavioral parameters. The amplifiers and the mixers are modeled in MATLAB as non-linear polynomial transfer functions as discussed in Section 3.1.2.1. For a selected tuning knob combination, the coefficients extracted from appropriate ADS curves define the performance of the transmitter.

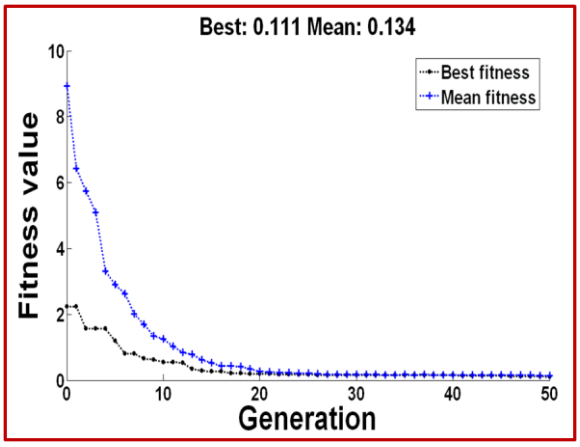

Figure 59: Test generation, Fitness function vs. number of iterations

4.1.3.3 Test Generation Results

The test input is defined to by a two-tone multi-tone. The genetic optimization is performed by evaluating the accuracy of alternate test. The core algorithm is similar to the technique discussed in Section 3.1.2.1. The MARS models are built using a training set of 100 instances of the transmitter. The model accuracy is evaluated for a set of 50 evaluation instances of the transmitter. The accuracy of the regression models across the evaluation set is set as the fitness function for the chosen genetic individual. The

amplitude and the frequency of the two input tones are optimized. Figure 59 shows the fitness function values across the generations. Figure 60a shows the final optimized test waveform and Figure 60b shows the envelope response for a process perturbed instance.

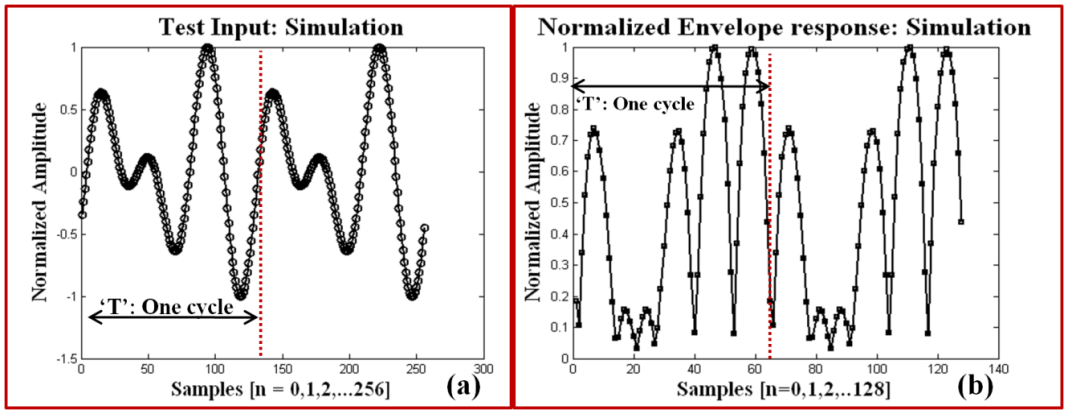

Figure 60: (a) Optimized test waveform, (b) Envelope response for a process perturbed instance

4.1.3.4 Cost Function Analysis

The goal of this exercise is to determine whether the cost metric (shown in (55)) can closely track the perturbations in performance parameters (multiple) of the system due to process variation across all the tuning knob values. For an optimized test stimulus shown in Figure 60, the following steps are performed,

- Capture and store the golden envelope response at the output of the envelope detector for a golden device (identified during the characterization phase)
- For a process perturbed instance, capture the envelope response (designated as observed in (55)) and compute the cost function (f) for a chosen weight selection, across all the tuning knob values.
- For the same instance, calculate the specification values across all the tuning knob values.
- Compare the cost function values with the specification values across the search space of the instance.

The minimum value of the cost function 'f' is expected to correspond to specification values closest to the nominal specification values. As shown in (55), the cost function can be modified by assigning weights W1 and W2 appropriately. The experiments are performed for three case studies (equal weights, gain preference and IIP3 preference). The nominal performance of the system is determined to be 43 dB for gain and -13 dBm for IIP3.

Case1 (Equal weights): In this case study the weights *W1 and W2 are set to unity* values to tune for *both gain and IIP3 simultaneously*. It can be seen Figure 61 that the gain and IIP3 values converge towards the nominal gain and IIP3.

Case2 (Gain preference): In this study W1 is set to 1 and W2 is set to 0. It can be seen from Figure 62a that the gain values converge towards the nominal gain value.

Case3 (IIP3 preference): In this study W1 is set to 0 and W2 is set to 1. It can be seen from Figure 62b that the IIP3 values converge towards the nominal IIP3 value.

It should be noted that it's impossible to improve gain alone without impacting IIP3 and vice-versa. Cases 2 and 3 are used only when the other specification (not being tuned) can tolerate some degradation (enough design margin) without being classified as bad. *For the rest of the analysis, the tuning results are shown for the most common scenario (Case1) to implicitly tune both gain and IIP3.* Case study 1 allows for implicit tuning and trade-offs between Gain and IIP3. It should be noted that the cost function 'f' with equal weights have contributions from both gain and IIP3 there by resulting in some aliasing of the specifications (i.e a single cost function value can correspond to multiple combinations of gain and IIP3). Hence it's critical to perform careful test generation (one-time and is done offline) to minimize the aliasing effects to achieve yield improvement in a statistical sense. Alternatively one can perform sophisticated signal processing to do the same, however such techniques are time consuming and are not feasible for a low-cost post manufacturing approach.

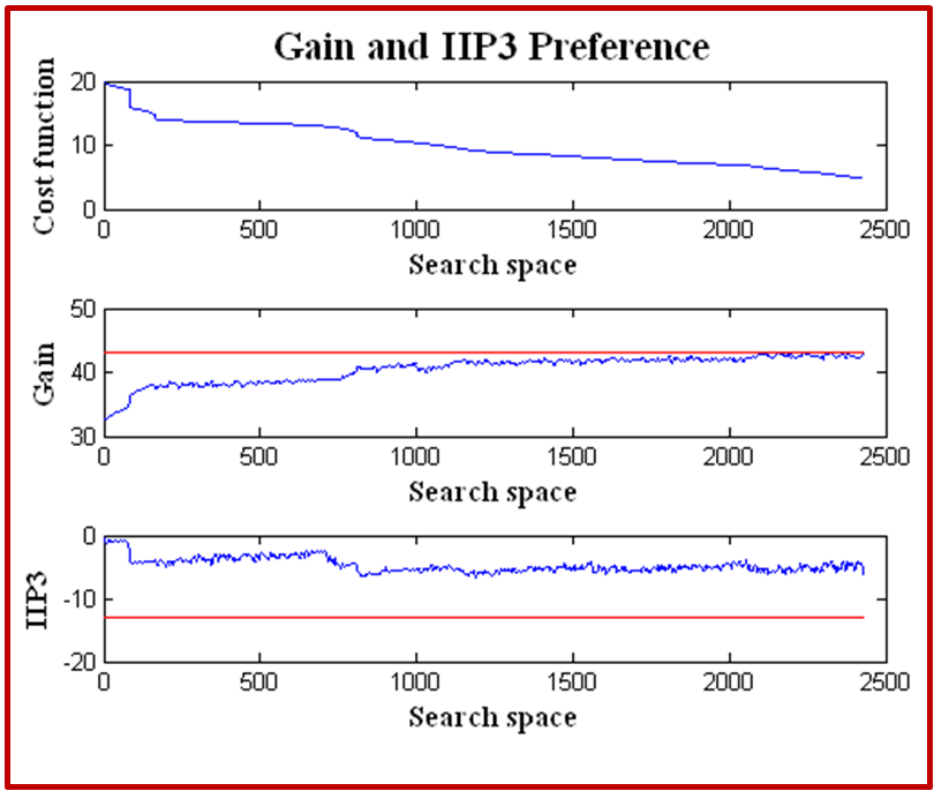

Figure 61: Cost function across search space for equal weights (Gain and IIP3 preference)

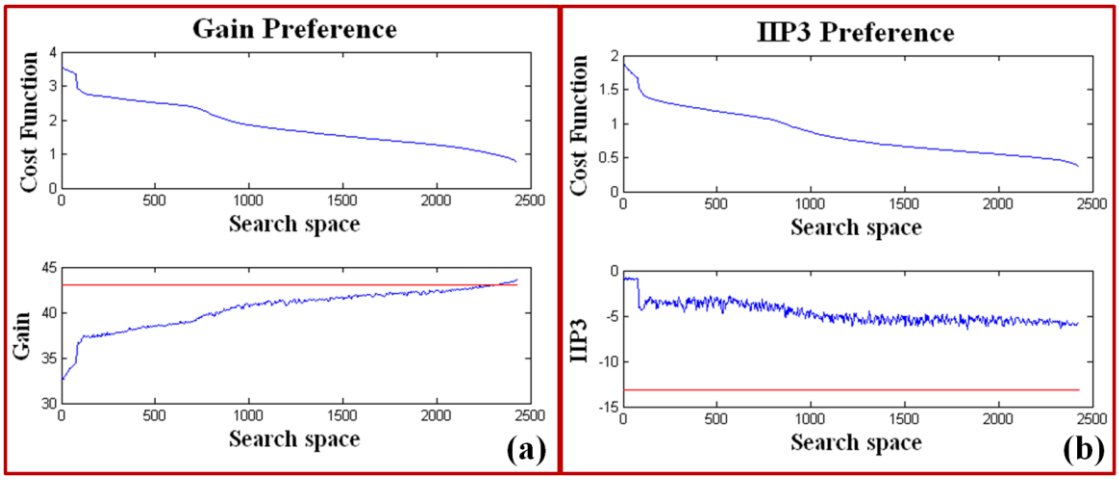

Figure 62: Cost function across search apace for (a) Gain preference (W_1=1, W_2=0) and (b) IIP3 preference (W_1=0, W_2=1)

4.1.3.5 A Note on Power Penalty

It should be noted here that the improvement in specification values incurs a power penalty in most of the cases. The power consumption however should be increased only as much as required to classify the device as good. In this methodology this is achieved by computing the golden response for a nominal device, thereby, guaranteeing performance improvement only up to the nominal performance. The tuning results show an acceptable power consumption penalty for the proposed approach.

Table 8: Nominal Specifications and test bounds for yield analysis

Type of Spec	*Spec Nominal*	*Spec Bound*
Gain	**43.06 dB**	**3 dB (double sided)**
IIP3	**-13.05 dBM**	**1 dB (single sided)**
Power	**268.8 mW**	**-**

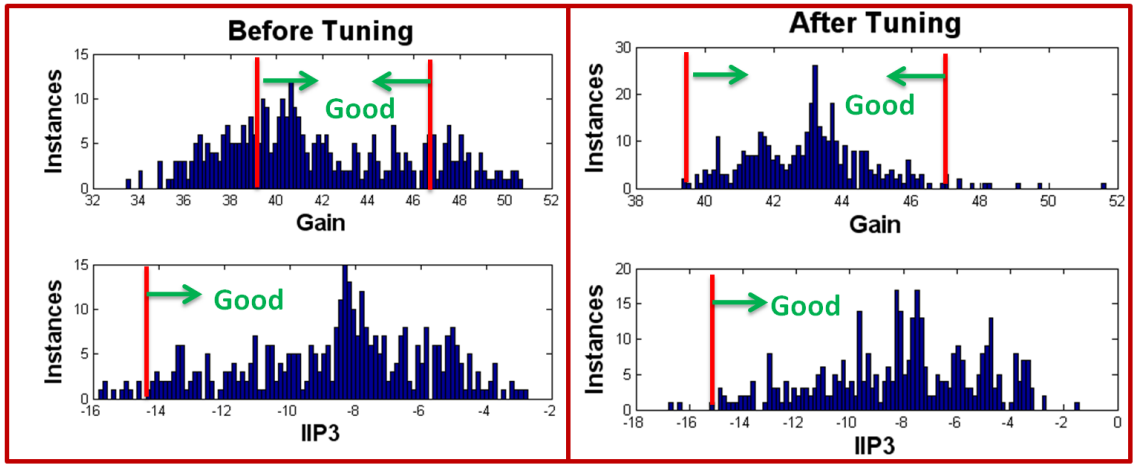

Figure 63: Production Yield for Transmitter before and after tuning

4.1.3.6 Yield Improvement in Simulation

In this case study a set of '368' instances (obtained using ADS Monte Carlo simulations) are considered for the tuning study. Out of the '368' transmitters '289' were determined to be good and '79' were determined to be bad. The yield bounds are set to the values shown in Table 8. For testing purposes a device is considered to be good when both its Gain and the IIP3 values satisfy the yield bounds. For each instance the tuning is performed as described above. The optimized test input shown in Figure 60a is used to perform tuning. The cost function is computed by setting equal weights. Based on the given bounds the yield is observed to be '78.53' before tuning and '94.57' after tuning thereby resulting in an overall yield improvement of '16%'. Figure 63 shows the yield plots before and after the tuning process for the RF prototype transmitter.

4.1.4 VALIDATION RESULTS FROM HARDWARE EXPERIMENTS

In order to demonstrate the feasibility of the proposed approach, experiments are conducted on a hardware prototype (setup shown in Figure 64). An industrial 802.11 a\b\g RF front-end (PA/LNA) in production at Texas Instruments is used to obtain realistic process variations. The details of the transmitter chain are described below

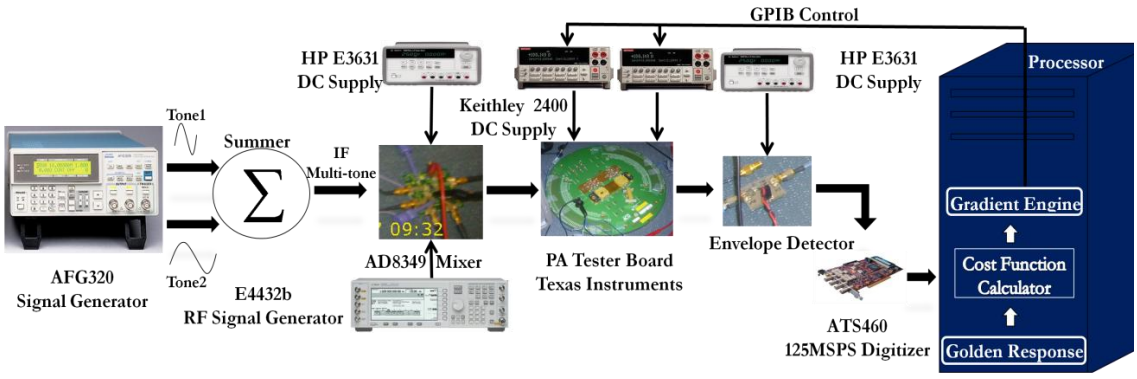

Figure 64: Experimental Block Diagram of the Transmitter Setup

4.1.4.1 Experimental Setup

A multi-tone from an arbitrary function generator AFG320 is used as the test input (two-tones with the amplitude and frequency set according to the test generation results) in this study. A quadrature modulator AD8349 from analog devices is used to up-convert the baseband signal generated by the AFG320. A RF source (Agilent E4432B) is used to generate a 2.4 GHz 'lo' for the up-converter evaluation board. The up-converted output from AD8349 is fed into the tester board provided by TI. The board deployed is a multi-site testing board with an RF socket capability to facilitate process analysis. Digital control pins (Set by Vctrl) of the RF front-end facilitate the selection of the front-end (PA/LNA), the frequency of operation and the linearity mode of the PA. A set of 10 instances of the 802.11 a/b/g front-end is used to obtain process variation. The PA is set to operate on a 2.4 GHz 802.11b band by setting the appropriate digital pins. Based on preliminary experiments it is determined that the PA's supply (Vcc: 2.3 to 3.9V) and PA's digital control (Vctrl: 2.5 to 3.9V) voltages can be used to control the performance parameters (Gain and IIP3) and hence are designated as tuning knobs. While this is acceptable as a proof-of-concept solution, ideally it's desirable to have tuning knobs custom built during the design phase to perform tuning. The frequency spectrum at the output of the transmitter is captured by an Agilent ESA 4407B spectrum analyzer for verification purposes. The output of the board level envelope detector is sampled into the PC via an Alazar ATS460 digitizer. The power supplies used in this work are Keithley 2400s that are capable of remote control by a PC via a NI 488.2 GPIB controller.

4.1.4.2 Tuning Procedure

During the tuning operation, the envelope sampled at the output of the transmitter is compared against a golden response stored in the PC for an optimized test input generated by AFG320. The cost function (55) computed using equal weights is then used to iterate the hardware knobs (PA VCC and PA Vcontrol) via the keithley 2400s

4.1.4.3 Results

A total of 10 instances are considered for the tuning purposes. The nominal gain of the transmitter is determined to be 7 dB and the IIP3 is determined to be +2 dBm. Figure 65 shows the surface plots of the specifications under consideration across the entire search space for a process perturbed instance. For the same instance, the sampled low frequency envelope responses across the search space for the optimized multi-tone (shown in Figure 60a) input are shown in Figure 66.

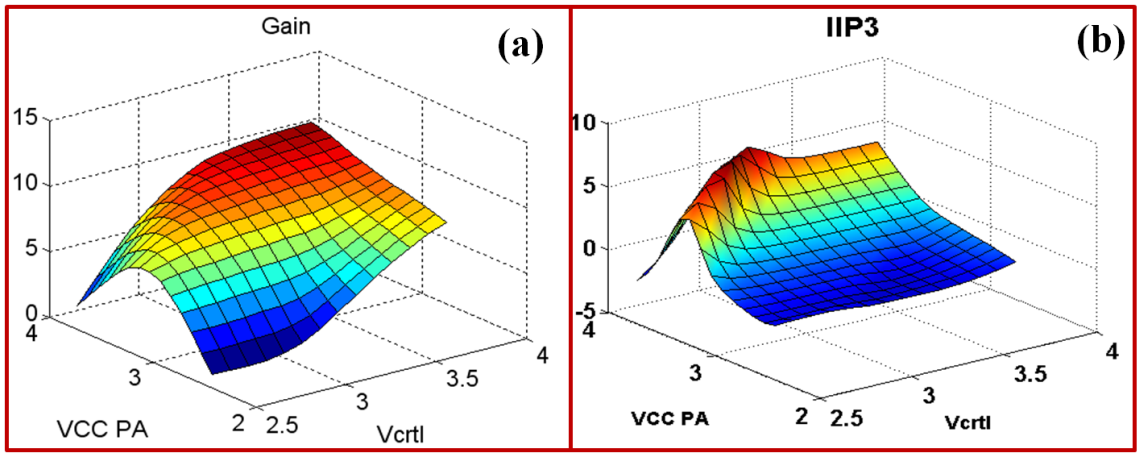

Figure 65: Specification across the search space for a single instance

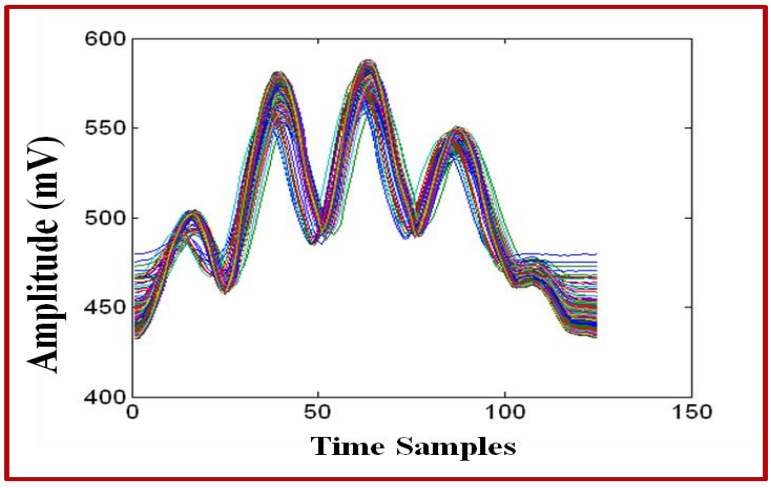

Figure 66: Envelope Test Response across the search space for a single instance

Similar to the simulation analysis, the cost function is computed for all combination of the tuning knob values for the hardware prototype with equal weight assignments. The results obtained for the experiment are shown in Figure 67. It can be observed that the minimum value of the cost function corresponds to the performance measures of a process perturbed instance close enough to the nominal performance.

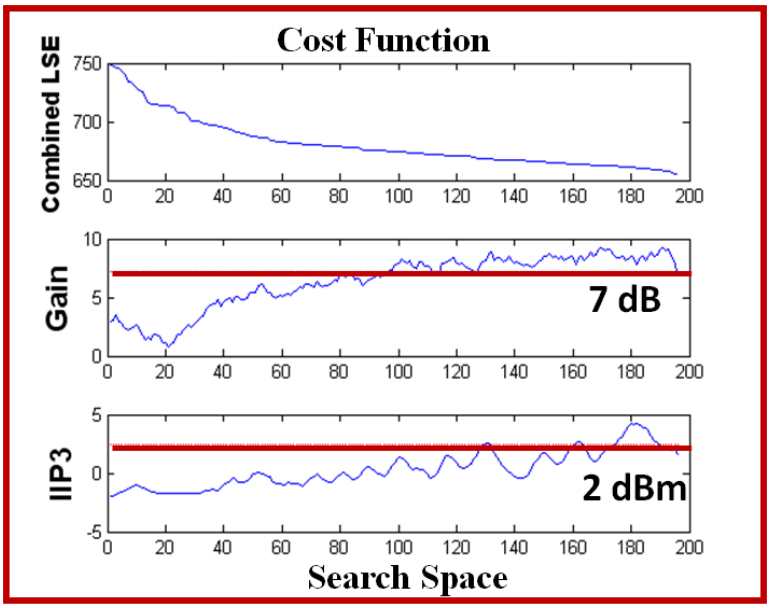

Figure 67: Cost function values across the search space for a single instance

Figure 68a shows the test input captured by the digitizer at the output of the AFG320. Figure 68b shows the golden (black), after tuning (red) and before tuning (blue) envelope responses for a single process perturbed instance. Figure 68c and Figure 68d shows the frequency spectrum of the transmitter before and after tuning. It can be observed from the spectrum that the difference in amplitudes between the signal tones and the inter-modulation tones increase after performing tuning thereby resulting in improved gain and IIP3 performance. Table 2 summarizes the results of the tuning experiment described above for 10 such instances using the proposed gradient search algorithm.

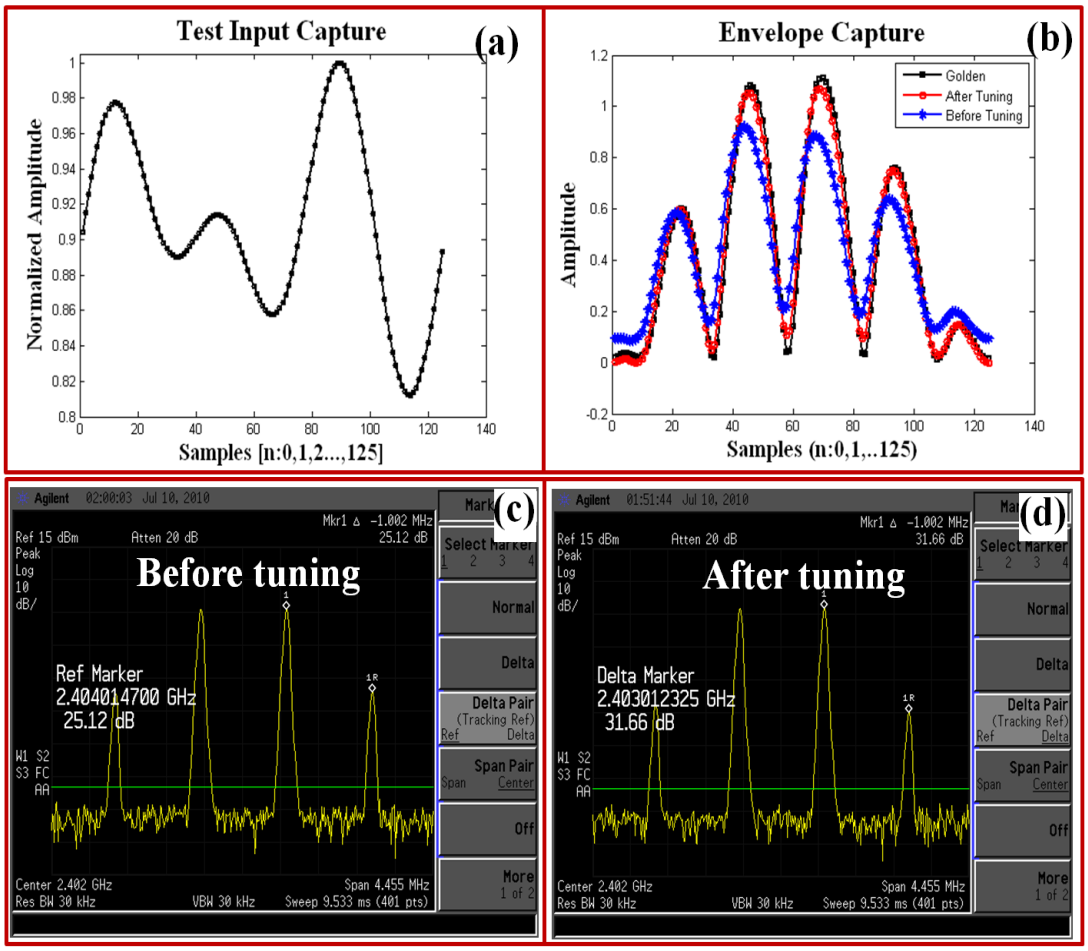

Figure 68: Hardware Tuning results for a single instance

Table 9: Hardware Tuning results for multiple instances

Instance	Gain (dB) Before	IIP3 (dBm) Before	Power (mW) Before	Gain (dB) After	IIP3 (dBm) After	Power (mW) after	Iterations Required
1	6.485	-0.835	265.7	8.32	1.782	309.8	4
2	6.99	-0.606	274	6.35	2.32	296.5	3
3	10.6	6.12	278.5	7.721	4.32	264.2	3
4	7.1	0.08	260.7	6.83	3.62	272.3	3
5	8.64	-0.061	253.1	7.85	4.88	268.9	4
6	9.9	3.917	257.6	6.3	2.86	249.4	5
7	10.1	2.55	281.1	8.42	2.873	278.7	2
8	9.1	3.07	255.9	6.85	3.86	251.2	3
9	11.2	5.07	280.4	8.21	4.49	269.8	3
10	10.7	5.04	268.9	7.73	2.85	252.3	5

4.1.5 KEY ADVANTAGES

The key advantages of the proposed analog signature driven post manufacture tuning approach are,

- Significant improvement in the production yield of advanced RF SoCs for multiple RF specifications by performing multi-dimensional tuning of analog tuning parameters to determine the best combination of the tuning knob values
- The proposed test technique is a *low-cost test solution.* The signals are sourced and measured at low frequencies. Information about multiple RF specifications are obtained, without the need to perform training and hence is amenable for a production floor deployment using a low-cost infrastructure.
- The time taken to perform the iterative testing and tuning is significantly small and is comparable to conventional production test times for a DUT. A single envelope capture (for an approximate bandwidth of 10 MHz) takes about 10us. 25 cycles are captured for noise averaging to result in overall a time of 250 us for a single capture. It was observed that the iterative algorithm converged in 3 to 5 iterations on an average. Each iteration involves the computation of the envelope 4 times (to determine the optimal step size) taking the overall test-tune time to a maximum of 5 ms per chip. The use of golden search algorithm to determine optimal step size during each iteration of the gradient search results in a significant speed up and reduces the number of iterations required for convergence.

In conclusion, in this section, hardware iterated gradient search technique is discussed to tune out the process variability of a 2.4 GHz transmitter system. Simulation and experimental studies are shown to demonstrate the proposed technique. A maximum of up to 4 knobs (simulation) were tuned with minimal complexity in less than 5 iterations. The key advantage of the proposed solution is the ability to tune and trade-off multiple performance metrics with a low-cost infrastructure, amenable for production floor deployment.

4.2 ALTERNATE TEST DRIVEN POWER CONSCIOUS POST MANUFACTURE TUNING OF WIRELESS TRANSCEIVERS USING HARDWARE-ITERATED GRADIENT SEARCH

The objective on the tuning methodology discussed in Section 4.1 is to perform a rapid low-cost post manufacture tuning without the need for training. The emphasis is on an improvement in the overall yield in a statistical sense rather than computing the best possible tuning knob combination for each device. In this section, an accurate alternate test based post-manufacture tuning methodology for yield improvement of RF transceiver systems is presented with the emphasis on achieving the best possible tuning knob combination for each device. The core algorithms optimize *multiple transceiver performance metrics concurrently* using a *hardware-iterated gradient search algorithm* similar to the gradient search performed in the previous case. However, the key difference between the two methodologies is the manner in which the cost function is computed to achieve accurate tuning.

4.2.1 GOALS AND OBJECTIVES

The key objectives of the alternate test driven power conscious post manufacture tuning approach are,

- Multi-dimensional optimization of multiple analog tuning knobs for a *complete RF transceiver system (transmitter and receiver).*
- Testing of *multiple specifications* (e.g. Gain, IIP2, IIP3) of an RF system under a unified BIST framework for tuning purposes.
- Co-optimization of power along with multiple performance metrics *across all the modules of the RF system.*
- Development of a RF BIST-driven hardware-iterated gradient descent tuning approach that is supported by a learning algorithm which intelligently guesses the starting point of the gradient descent search.

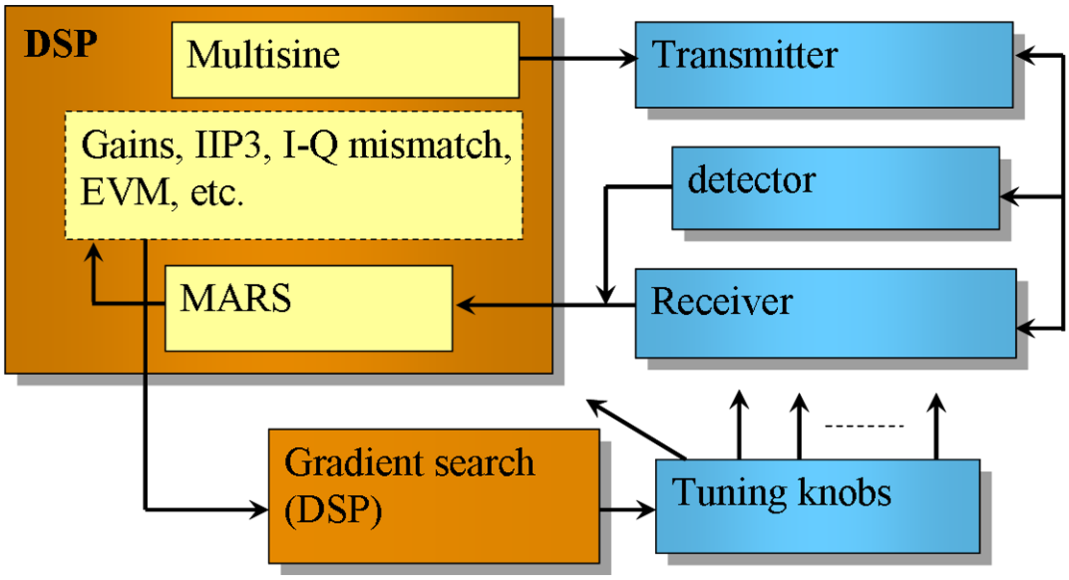

Figure 69: Proposed alternate test driven post manufacture tuning methodology

4.2.2 PROPOSED METHODOLOGY

The conceptual diagram of the proposed methodology is shown in Figure 69. The methodology is demonstrated on a 2.4 GHz wireless OFDM transceiver. The analog tuning knobs are carefully chosen during the design cycle to optimally control the performance of the DUT. For an optimized test stimulus, the envelope response at the output of the transmitter and the baseband response of the receiver are computed for a given combination of the tuning knob values. The hardware-iterated gradient search shown in Section 4.1 is used to perform tuning based on the cost function (alternate test based BIST data) derived from the computed from the captured test responses.

4.2.2.1 Alternative Expanded Based BIST (AE-BIST)

An optimized multi-tone signal is applied to the RF front end from the baseband DSP (see Figure 69). This stimulus is up-converted by the transmitter data-path, passed through the mixer and power amplifier and down-converted by the envelope detector, digitized and passed back to the baseband processor. The signal is de-noised using wavelet de-noising methods (not shown in Figure 69) and converted to the frequency

domain. A nonlinear regression function is then used to predict the specifications of the transmitter from the observed response to the applied stimulus. This regression mapping is obtained via careful calibration experiments and is based on the MARS algorithm. Subsequently, using data from both the envelope detector of Figure 69 as well as the output of the receiver obtained from operating the transceiver in loopback mode as shown in Figure 69 (this may require the use of a frequency offset mixer in the loopback path), the relevant specifications of the receiver are predicted using a MARS based specification prediction methodology as before.

There is one key difference, however, between AE-BIST and the "regular" alternate test based BIST. The difference is that the MARS regression map must be accurate not only across the space of process variations across which the transceiver specifications must be predicted, but also simultaneously across all tuning knob values allowable for self-tuning. Hence, the "training set" of devices used to "train" the regression functions of MARS must *sample the process space and the tuning knob value space appropriately.* In this approach, the sensitivities of the specs to the tuning knob values are used to determine how finely the same are sampled for generating the MARS "training set" of devices.

Once the MARS model is developed, during the tuning procedure the developed AE-BIST routine is run to identify the RF specifications of the DUT to compute the cost function for a chosen combination of the tuning knob values. The cost function is then used to determine the best way to update the tuning knob values for yield improvement.

4.2.2.2 Cost Function Computation

The cost function used in the gradient search routine is implemented as a weighted sum of the RF specifications along with their guard bands (Gb). The RF specifications are obtained from the AE-BIST routines. The cost function is a function of the tuning knob vector (K). In (61), $S_i(K)$ denotes the estimated value (AE-BIST) of the

'i^{th}' specification; $Snom_i$ denotes the nominal value for the i^{th} specification; P denotes the number of specifications considered for tuning; and W denotes the weight assignments for specifications. By assigning appropriate weights, the proposed cost can be manipulated to achieve different trade-offs between multiple specifications for overall yield improvement.

$$f(K) = \sum_{i=1}^{P} W_i * \left(1 - \frac{S_i(K)}{Snom_i - GB_i}\right) * \left(1 - \frac{S_i(K)}{Snom_i + Gb_i}\right) \quad (61)$$

This manner in which the cost function is computed (as shown in (61) is the key difference between the tuning technique proposed in this section as opposed to the strategy in Section 4.1.2.3. Performing AE-BIST and computing the cost function as shown in (61), allows for an accurate post manufacture tuning of RF SoCs.

4.2.2.3 Tuning Strategy

The core gradient search algorithm that determines the best way to update the tuning knob vector is similar to the engine used in Section 4.1.2.3. However, for the sake of completeness the methodology is briefly discussed here. Let $K = [K_1, K_2 \ldots K_N]$ be a vector describing the values of N such control knobs. For a process-perturbed device, the tuning algorithm first makes a *power-aware intelligent initial guess of the values K* (discussed below). Then, starting from this initial guess, a *steepest descent gradient search algorithm* is used to minimize a cost function (f(K)) that represents the difference between the desired and the observed performance specifications of the RF system. This cost function evaluation requires the use of the AE-BIST procedure discussed above. A central difference based first derivative approximation of the cost function is used to obtain the *gradient value along the steepest direction for each tuning knob*. The optimum step size by which the control knob vector K needs to be updated is then computed using

'golden ratio' based line-search for faster convergence. The set of equations describing the mathematical formulation of the optimization technique is shown in (56)-(60).

4.2.2.4 Power Conscious Initial Guess

As mentioned above, making an intelligent initial guess of the control knob value (K) significantly accelerates the developed gradient search algorithm. The key idea is to make an intelligent guess that is close enough to a power optimal solution of the optimization problem. Power is often compromised as a penalty while performing post manufacture tuning. However, the power penalty should be proportionate to the amount of tuning required. Due to the size of search space defined by the tuning knobs, there exists multiple solutions with similar performance improvements but different power penalty values. Hence it's critical to choose a near optimal solution to obtain yield improvement with minimal penalty in terms of power consumption. From this perspective, it's desired to make an initial guess of the control knob vector K that is close enough to a power optimal solution. Once the initial values are guessed the gradients search routine converges to a near optimal solution with minimal power penalty.

The intelligent power conscious initial guess algorithm works as follows. First a large sample set of multi-parameter process variations is created using statistical sampling techniques. These include the effects of large process shifts, inter and intra-die process variability effects. Starting from *random* initial guess values of the tuning knob vector K, the gradient descent algorithm is applied (using software, off-line, not hardware-iterated), to find tuning knob values for acceptable performance of the RF transmitter and receiver. Since the initial guess for the gradient search is random, different solutions are obtained for different initial guess values. The solution vector K that corresponds to the *lowest power consumption* value is selected as the vector corresponding to which all the tuning knob values must be set for the simulated process perturbation. Note that for each process perturbation, there exists a corresponding set of

test specification values of the transmitter and receiver. Let the set of specifications S_m correspond to the power optimal tuning knob vector K_m. Over the total set of process perturbations, a set of specifications S_m and corresponding vectors K_m are similarly created via repeated application of gradient search as discussed above.

For a specific transceiver, during the first application of AE-BIST, the vector of specifications S for that transmitter or receiver is obtained from the BIST application. This vector S is compared against all the vectors S_m and the vector S_n for which $\|S - S_n\|$ is minimized is determined. The corresponding tuning knob values K_n are selected to the initial guess values for that transmitter or receiver for subsequent application of hardware-iterated gradient search. The flow graph of the optimization strategy is shown in Figure 70.

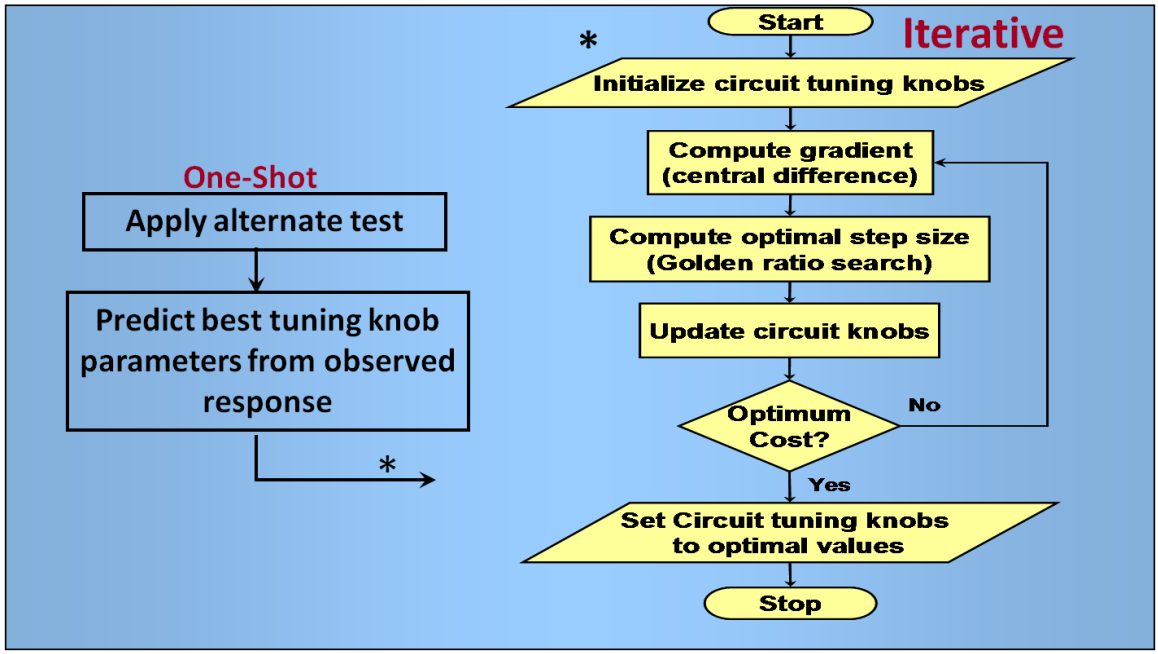

Figure 70: Steepest descent gradient search with a power optimal initial guess

AE-BIST offers significant test time reduction (at least 10X) and the golden ratio search along with intelligent initial guess accelerates the convergence of the gradient search routine. The time taken to perform tuning is less than or equal to the time taken for

conventional production testing of all the RF specifications thereby resulting in a feasible production-floor ready post manufacture tuning approach to improve the overall yield of a RF system. It should be noted that the solution is accurate in terms of performance improvement for each device; however, the key idea is to not obtain the exact solution to the optimization problem in terms of the power penalty but to rather obtain an approximate solution. The developed methodology allows for accurate yield improvement with an acceptable solution in terms of power penalty and hence the term '*power conscious post manufacture tuning'*.

4.2.3 VALIDATION RESULTS FROM SIMULATION

The proposed self healing technique is demonstrated in simulation on a behavioral model of a 2.4 GHz OFDM RF transceiver. The impairments are modeled at the behavioral level. ADS designs of the amplifiers (PA and LNA) and the mixers are used to generate appropriate circuit level data. The curves obtained are then exported into MATLAB to determine the gain and linearity characteristics of the devices.

4.2.3.1 Modeling the RF Transceiver

The transmitter chain is consists of an up-conversion mixer followed by a power amplifier. An envelope detector is placed at the output of the transmitter to capture the low-frequency response. The output of the transmitter is looped back to the receiver after appropriate attenuation. The receiver chain consists of a low noise amplifier followed by a down conversion mixer. The baseband data at the output of the receiver and the low frequency capture of the envelope detector is input to the AE-BIST routine to estimate the RF specifications.

The amplifiers of the RF sub-system (PA and LNA) are realized by implementing a non-linear transfer function of the type $y(t) = \alpha_0 + \alpha_1 x(t) + \alpha_2 x^2(t) + \alpha_3 x^3(t)$, where, α_0 = amplifier offset, α_1 = small signal gain, α_2, α_3 = non-linearity coefficients are used to realize the linear (gain) and non-linear (harmonics and inter-modulation terms) effects

of the amplifier. For test generation purposes, the mixer of the RF subsystem is modeled as a non-linear transfer function followed by an ideal multiplier. The frequency mixing operation is realized by the multiplication operation $y(t) = C \,.\, x_1(t) \,.\, x_2(t)$.

The Vin vs. Vout curves for circuit level designs of mixers, PA and LNA are obtained using *Agilent-ADS simulations across the selected range of process perturbations (generated by Monte-Carlo simulations for active and passive devices) and tuning knob values (bias currents and supply voltages)*. The behavioral models for the amplifiers and mixers are then fitted to the observed ADS simulation data for accurate behavioral level simulation (without such simulation repeated BIST application for tuning is difficult to simulate). The static non-idealities are then extracted from the models obtained using standard formulae where applicable or extracted via simulation. The transmitter gain variation with tuning knobs (PA ad mixer supply) for two such process instances, obtained from circuit level ADS simulations are shown in Figure 71.

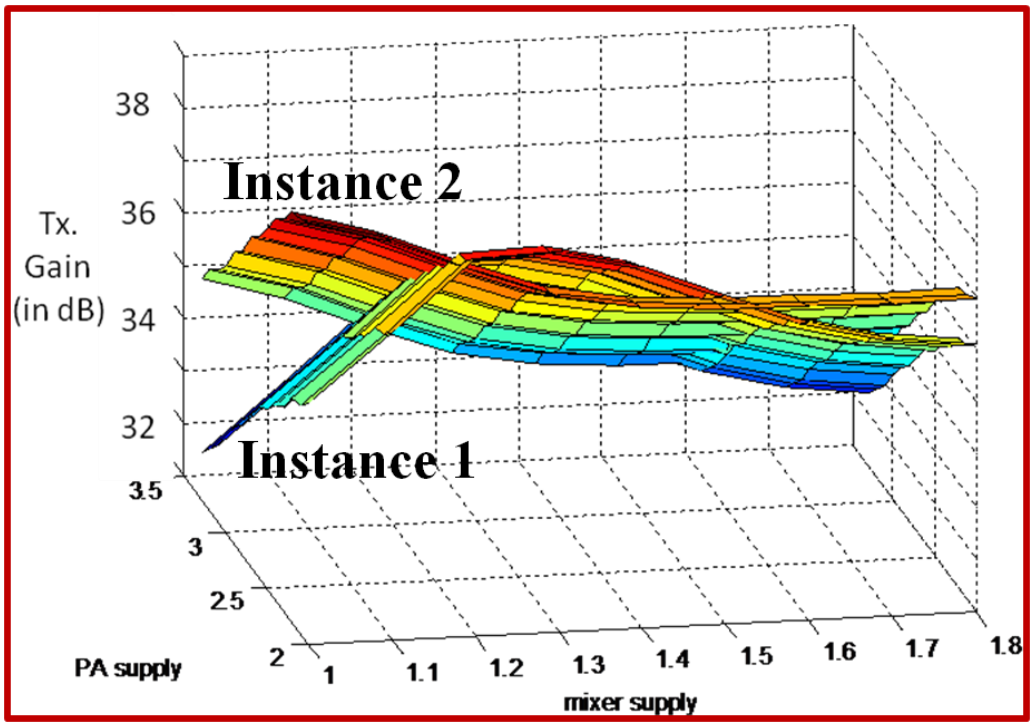

Figure 71: Gain variation with tuning knobs (search space) for two prcess perturbed instances

4.2.3.2 Test Input

A multi-tone waveform is used as a test input. Genetic algorithm based test generation routines are used to determine an optimized test stimulus to guarantee the AE-BIST test accuracy across process as well as tuning knobs. The optimized test stimulus used in this approach is shown in Figure 72.

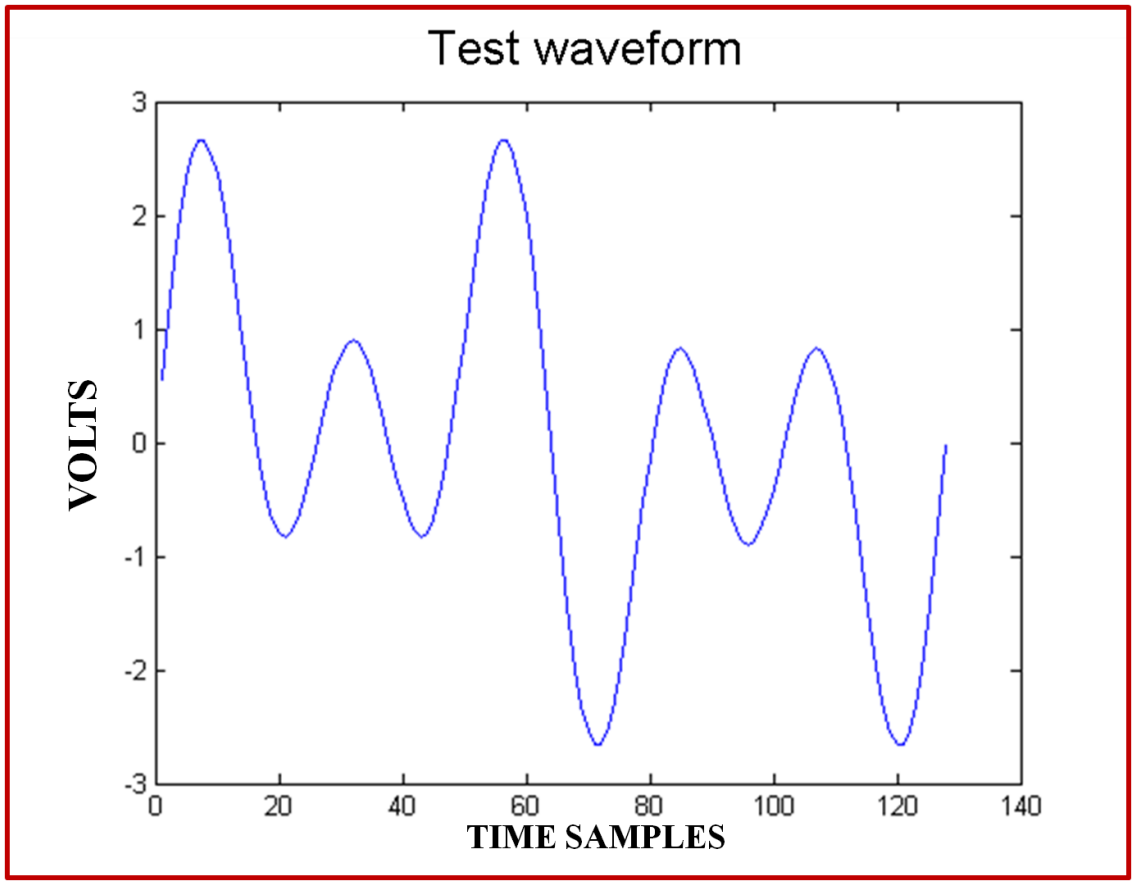

Figure 72: Optimized test waveform for AE-BIST

4.2.3.3 AE-BIST Evaluation for Transmitter and Receiver

The specifications targeted for AE-BIST and tuning are gain, IIP2 and IIP3. The MARS model is built for a training set of 100 transceivers across the entire search space of the tuning knob values. The developed model is evaluated on a set of 10 transceivers

across the entire search space of the tuning knob values. The envelope detector response is used as in input to the MARS model to estimate the specifications of the RF transmitter. Figure 73 shows the prediction results of the AE-BIST routine for the transmitter. It can be observed that the RF specifications of the transmitter are estimated accurately across process perturbations and across the tuning knob values.

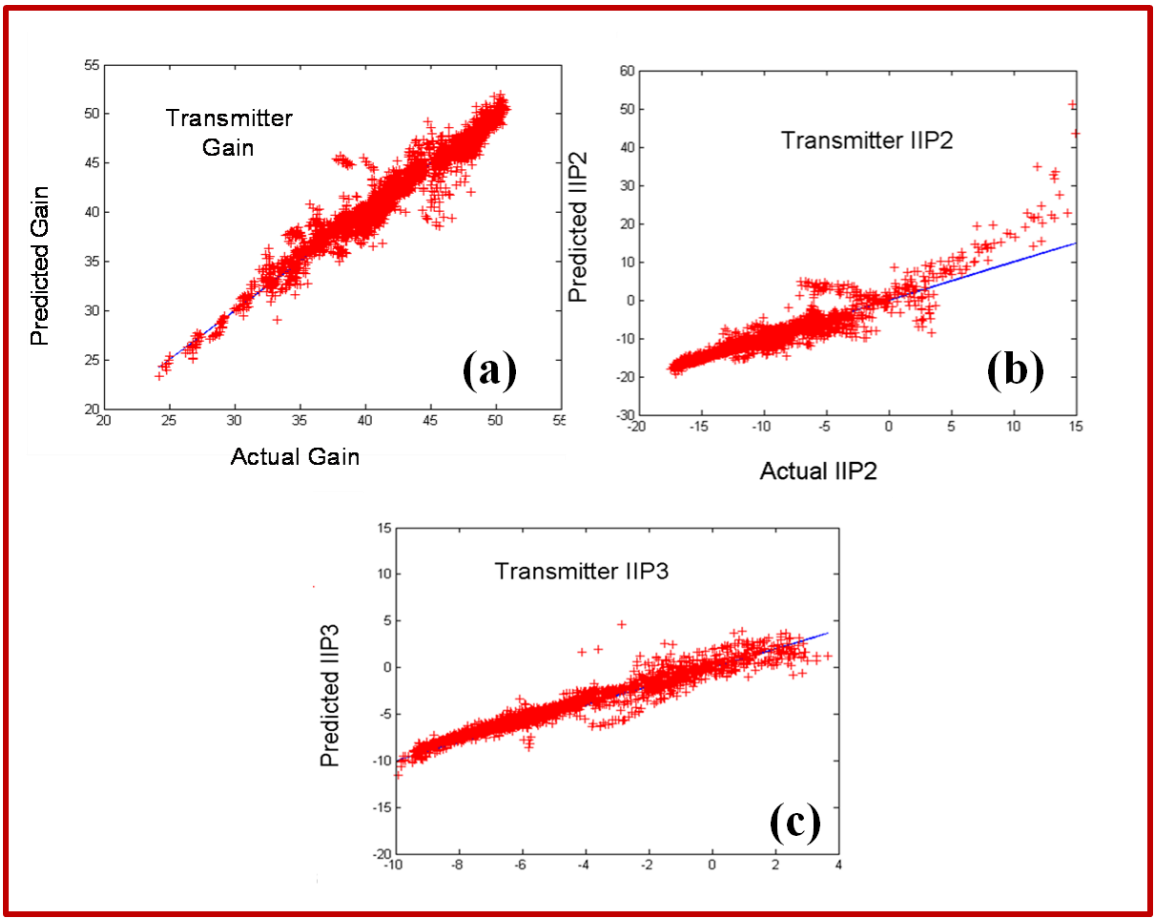

Figure 73: AE-BIST results for transmitter (a) gain (b) IIP2 (c) IIP3

The output of transmitter is looped back into the receiver. The baseband response of the receiver is used as an input to the MARS model to estimate receiver specifications. Figure 74 shows the prediction results of the AE-BIST routine for the receiver. It can be

observed that the receiver specifications are estimated accurately across process perturbations and across the tuning knob values.

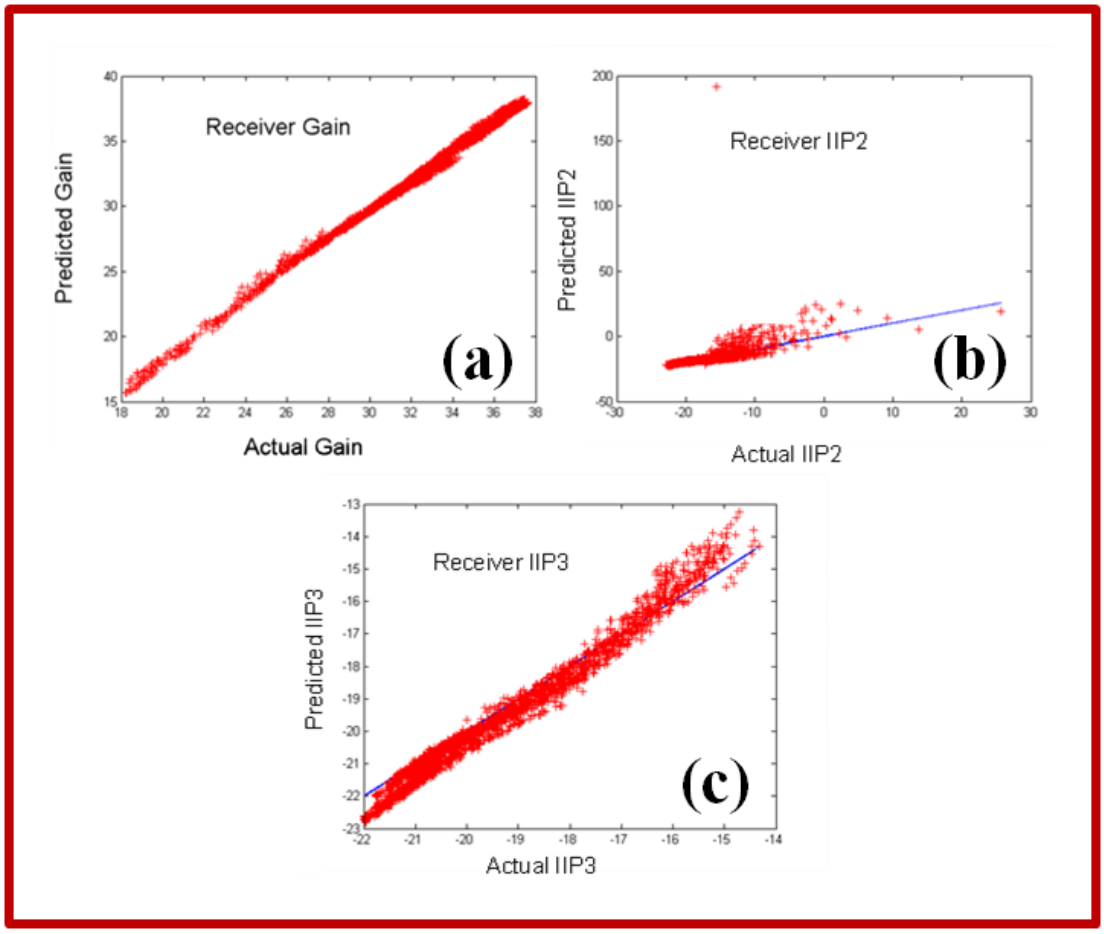

Figure 74: AE-BIST results for receiver (a) gain (b) IIP2 (c) IIP3

4.2.3.4 Tuning Results for Transmitter and Receiver

It is possible to tune the transmitter and receiver concurrently or first tune the transmitter and then tune the receiver. The latter strategy results in fewer tuning iterations and is used in the current research. The tuning ranges of the circuit knobs are selected to allow only acceptable degradation of the NF through the tuning process. The estimated static non-linearities from the static BIST routines explained above, is fit into the cost function formulation shown in (61). Starting from the power optimal initial guess, the

gradient search based optimization engine determines the optimal knob settings for yield improvement. Table 10 shows the *nominal specifications* and the acceptable values for a nominal 2.4GHz RF transceiver

Table 10: Nominal specifications for the transceiver

Nominal	Gain (dB)			IIP2 (dBm)			IIP3 (dBm)		
	Min	Typ	Max	Min	Typ	Max	Min	Typ	Max
Transmitter	34	36	38	-6	-4	-2	-7	-5	-3
Receiver	27	29	31	-14	-12	-10	-18	-16	-14

Table 11: Specification values for the transceiver before and after tuning for a process perturbed instance 'P1'

Tuning Data Power Comparison		Gain (dB)		IIP2 (dBm)		IIP3 (dBm)		Power (mW)
		Before	After	Before	After	Before	After	
Transmitter	Power consciousness	40.9	37.7	-7	-4	-9.5	-6.5	105.28
	W/o power consciousness	40.9	37.6	-7	-3.9	-9.5	-6.2	171.5
Receiver	Power consciousness	36.45	27.86	-18	-12.2	-20.8	-15.85	16.95
	W/o power consciousness	36.45	27.06	-18	-13.6	-20.8	-17.09	47.65

For a process perturbed instance 'P1' the specification values before and after performing the tuning technique is summarized in Table 11. It can be observed that the instance P1 was deemed as bad before tuning and is considered as good after tuning. To highlight the need for a power conscious tuning approach, the tuning methodology is again applied to the instance P1. However, this time the initial value for the control knob is chosen to be random. Table 11 shows the comparison results between the self-healing

methodologies with and without power consciousness. It can be observed that the power initialized gradient search technique converges to a significantly lower power consumption value without compromising the accuracy of tuning.

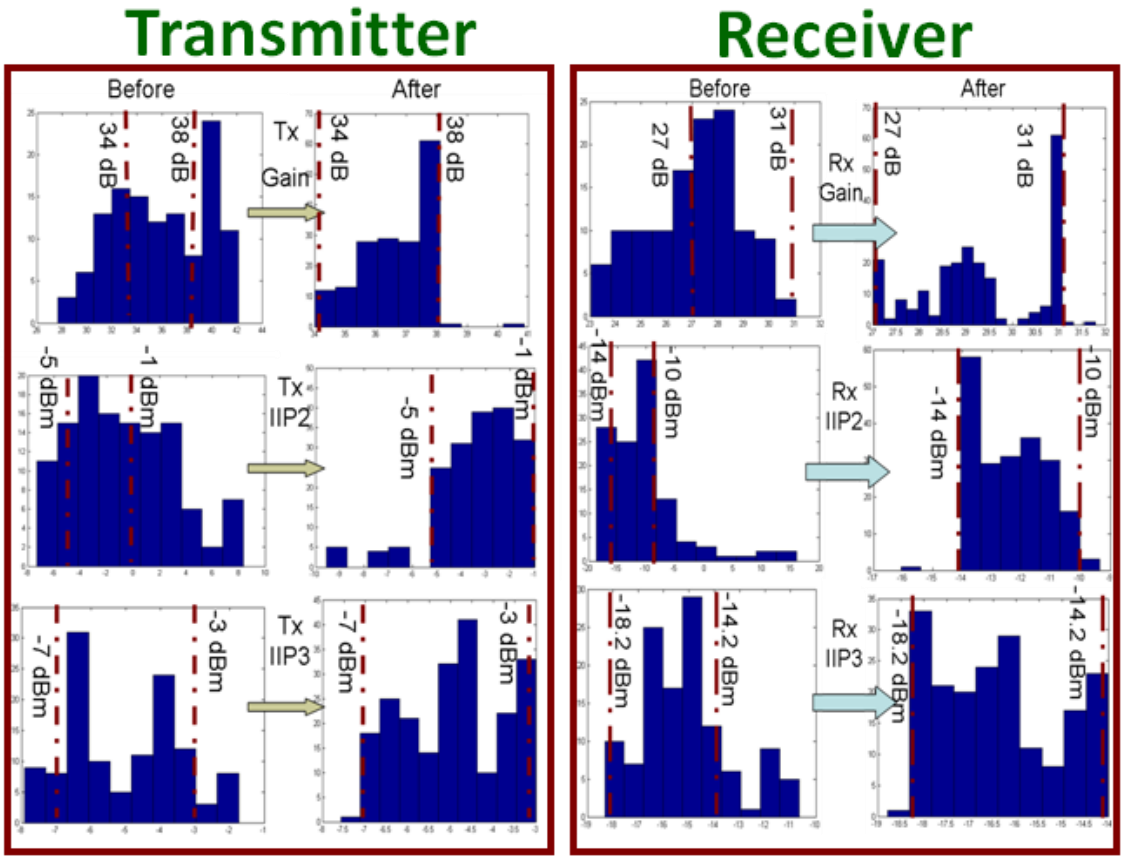

Figure 75: Yield histograms for the transmitter and the receiver

The developed tuning methodology is then validated for a set of 200 instances of the transceiver in simulation to study the amount of yield improvement possible. On an average it is observed that the optimization engine converges in 3 to 4 iterations for each process instance. Such accelerated convergence is the direct result of an intelligent initial guess along with the optimal step size identified during each iteration using the golden ratio search. In order to compute the yield of the product the bound for specifications for the transmitter and the receiver are determined as shown in Table 10. Figure 75 shows the yield plots before and after tuning for the transmitter and the receiver. Based on the given

bounds the yield is determined to be 63.46% before tuning and 96.69% after tuning for the transmitter instances thereby resulting in a yield improvement of 33.23%. Based on the given bounds the yield is determined to be 61.2% before tuning and 95.04% after tuning for the receiver instances thereby resulting in a yield improvement of 33.84% with the application of the self healing technique.

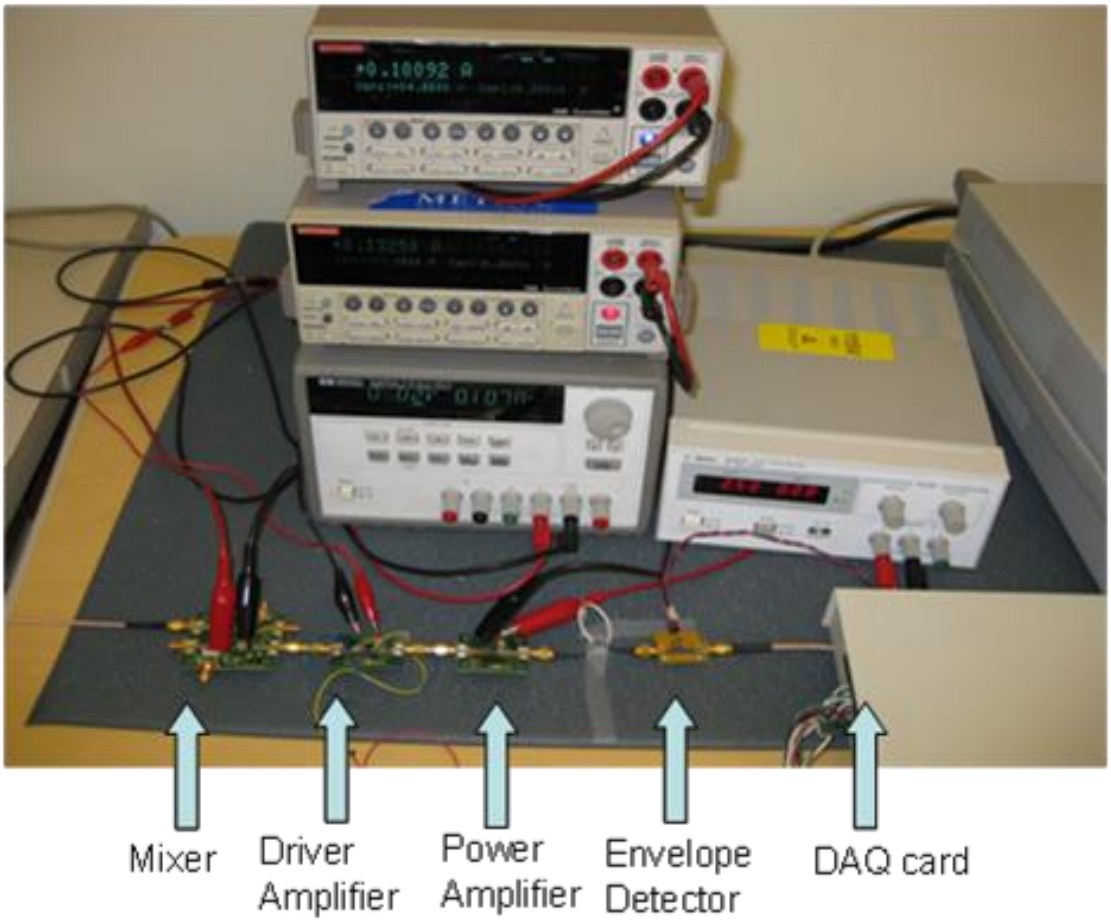

Figure 76: Hardware setup of the transmitter

4.2.4 VALIDATION RESULTS FROM HARDWARE EXPERIMENTS

In this section the results pertaining to hardware experiments are discussed. An off-the shelf transmitter chain is constructed to perform the hardware experiments. The

chain is built using an ADL8349 I/Q modulator followed by an ADL5320 Driver Amplifier feeding off to another ADL5320 Driver Amplifier. The supply voltages of the circuits were controlled using 2 precision Keithley 2400 DC power supply sources and a HP Agilent E3631A with GPIB control from the PC. The frequency of operation of the hardware setup is determined to be 1.9 GHz. Process variation is induced by replacing a capacitor in the input matching circuit of the driver amplifier with a varactor. Different instances were generated by varying the supply voltage values across the varactor.

The experimental setup is as shown in Figure 76. During each step of the iteration alternate tests are invoked and the corresponding response is captured using envelope detector. The gradient algorithm for tuning the transmitter is run in the software and the interface to the hardware and the software is facilitated by a PCI 6115 data acquisition card.

Table 12: Nominal specifications of the hardware transmitter prototype

Nominal	Gain (dB)			IIP3 (dBm)		
	Min	Typ	Max	Min	Typ	Max
Transmitter	2.5	3.5	4.5	9.5	10.5	11.5

Table 13: Specification values before and after tuning for a process perturbed hardware transmitter prototype

Tuning Data Power Comparison		Gain (dB)		IIP3 (dBm)		Power (W)
		Before	After	Before	After	
Transmitter	Power consciousness	6	3.965	8	10.23	1.402
	W/o power consciousness	6	4.45	8	10.04	1.652

Only gain and IIP3 were considered for hardware verification. Table 12 shows the nominal specification values of the transmitter chain. Table 13 shows the specification

values of a process instance before tuning and after tuning. Table 13 also shows the results of tuning the transmitter without power consciousness. It can be observed that the tuning of the transmitter without power consciousness converges to a significantly high power consumption value. In conclusion, in this section, a power initialized gradient technique is discussed to combat process variability for a 2.4 GHz transceiver system. Software and hardware experimental studies are shown to demonstrate the proposed technique. The developed technique is observed to be reliable and rapid converging mostly within 5 iterations. A maximum of upto 9 knobs are tuned with minimal complexity. The key advantage of the proposed solution is the ability to tune and trade-off multiple performance metrics with minimal impact on the power consumption of the system.

4.2.5 KEY ADVANTAGES

The key advantages of the alternate BIST driven post manufacture tuning technique are

- AE-BIST technique to accurately estimate multiple RF specifications of the transmitter across process perturbations and across the entire range of the tuning knob values using a low-cost infrastructure in a significantly reduced amount of time (10X) in comparison to conventional production test routines.
- Significant production yield improvement for RF SoCs with a minimal impact on the power penalty
- Rapid power conscious tuning technique to tune for multiple performance parameters of interest that allows for explicit as well implicit trade-offs possible using low-cost techniques
- Rapid convergence and reduced test time lends the post manufacture tuning technique feasible for a low-cost production floor deployment. The time taken to perform tuning is less than or equal to the time taken to perform conventional production testing.

4.3 A HOLISTIC APPROACH TO AN AUGMENTED LAGRANGE BASED ACCURATE TUNING OF RF SYSTEMS FOR LARGE AND SMALL PARAMETER PERTURBATIONS

In this section, a holistic yield recovery approach based on post manufacture tuning of RF circuits and systems under large as well as small multi-parameter process variations is developed. Marginally failing devices (small parameter deviations) are tuned using a nonlinear "Augmented Lagrange" algorithm driven optimization engine that includes test specification values and power consumption in its optimization framework. A built-in alternate tuning test is used to explicitly evaluate all the DUT specifications at each optimization iteration. For large parameter deviations well beyond the test specification limits of the DUT, determination of the different specification values is difficult. Such devices are tuned using a golden response tuning approach which optimizes the DUT specifications implicitly until the DUT is "good enough" to be tuned by the prior Augmented Lagrange algorithm. The proposed methodology enables yield recovery of devices not possible with earlier methods, avoids local minima and can be implemented at low cost.

4.3.1 GOALS AND OBJECTIVES

The key requirements for performing augmented Lagrange based tuning of RF systems for large and small parameter deviations are,

- Accurate tuning of large and small parametric deviations for significant improvement in the overall yield of RF SoCs, amenable for implementation using a low-cost infrastructure.
- Explicit consideration of power consumption requirements by integrating the power consumption values in the optimization framework.

- Accelerated convergence in a reasonable time to facilitate the production floor deployment of the tuning methodology.

4.3.2 PROPOSED METHODOLOGY

The key focus of this research is on a holistic tuning approach for *small as well as large* parameter variations in RF systems while *enhancing yield recovery* using an advanced Augmented Lagrange nonlinear optimization approach [73] that avoids local minima while tuning. Small parameter deviations are defined as those that result only in marginally failing devices. Large parameter deviations are loosely those that cause specification values to be significantly degraded beyond the specification acceptance limits. A modified superset of the alternate tests called *alternate tuning tests*, are used to predict the DUT specifications, for *small* parameter deviations, from the DUT response to the applied test.

The predicted DUT specifications are used to determine the cost function for the nonlinear Augmented Lagrange optimization algorithm. This prediction is performed by a nonlinear regression model that maps the DUT response to its test specification values. However, due to the lack of significant statistical data for *large* parameter variations, an accurate regression model for predicting the corresponding DUT specification values is difficult to construct. Hence, an implicit tuning methodology called *golden response tuning* is used to drive the DUT into a region of operation where the prior alternate tuning tests in association with the specification prediction models and nonlinear optimizer can be used to tune the DUT to comply with specification limits. This optimization is performed carefully to minimize the power consumption of the final "tuned" DUT.

4.3.2.1 Testing and Tuning Infrastructure

The proposed test and tuning infrastructure is described in Figure 77. The transmitter and receiver modules (mixers, LNA, PA are designed with built-in tuning knobs that tradeoff power consumption with performance. The transmitter and receiver

subsystems are also equipped with built-in sensors for monitoring the quality of signals at intermediate nodes of the RF signal path. While multiple sensors may be used, in this research, a single envelope detector at the output of the transmitter is used to monitor the health of the transmitter and produces a low frequency signal that is analyzed by the DSP after digitization (the input to the A/D converter of Figure 77 is multiplexed for test purposes).

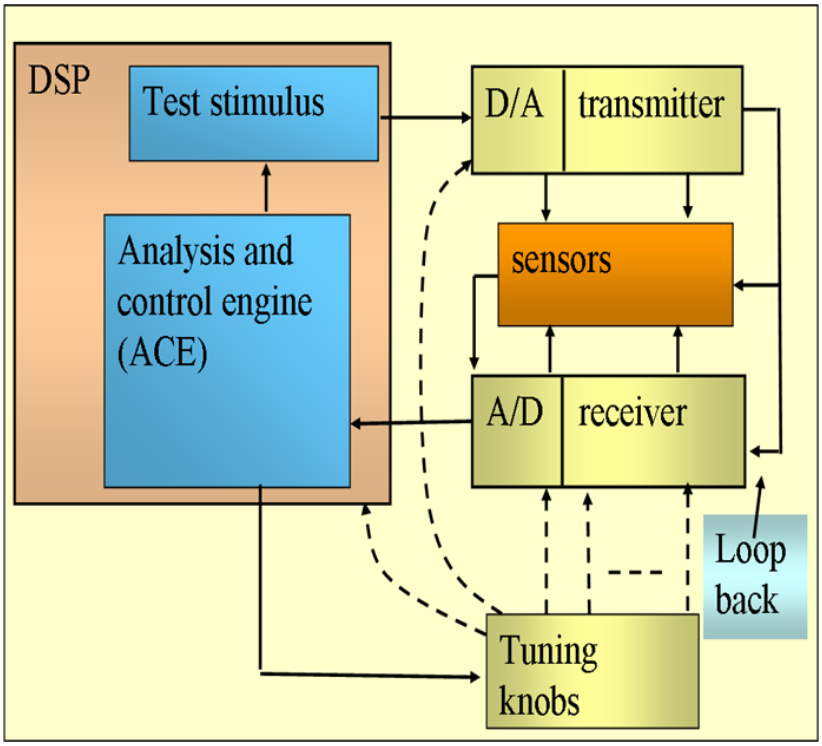

Figure 77: Testing and tuning infrastructure for a holistic tuning approach

The test-and-tuning procedures work as follows: The DSP sends a multisine stimulus through the D/A converter to the transmitter which is then "looped back" to the receiver via an external feedback path (through the package or on the DUT load board). The data obtained from the sensor at the output of the transmitter is used to determine the performance of the same. The data obtained from the receiver is used to determine the health of the receiver. In this context, the data obtained from the sensor allows accurate

determination of receiver quality in the presence of *simultaneous* transmitter imperfections. From the test results (obtained in a few ms) software residing in the DSP that implements the analysis and control engine (ACE) determines how to "turn" the hardware and software tuning knobs of the design to improve transceiver performance. This is an iterative test-tune-test procedure which terminates when acceptable transceiver performance is achieved.

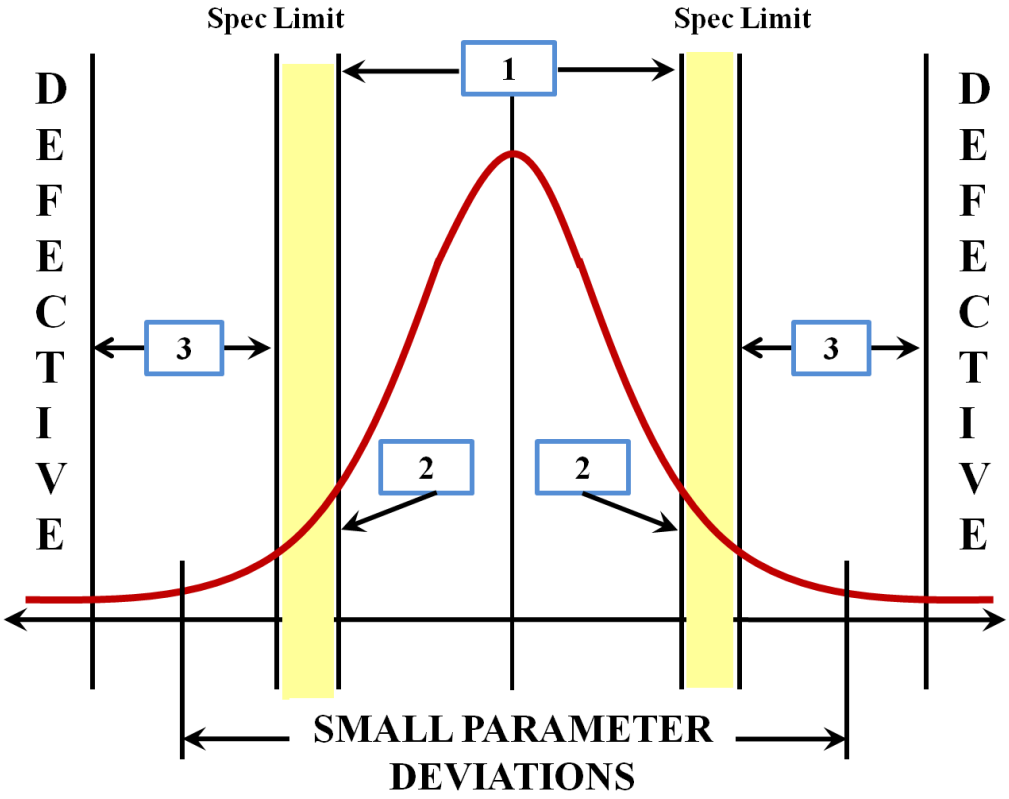

Figure 78: Tunability Regions

4.3.2.2 Alternate Tuning Test

Figure 78 shows the distribution of a two-sided RF specification (not necessarily Gaussian). The region of *small* parameter deviations consists of regions 1, 2 and part of region 3 while the extreme ends of region 3 on both sides of the mean correspond to

large parameter deviations. Region 2 consists of a set of devices which cannot be classified as good with 100% confidence because of measurement uncertainties. Beyond region 3 are *defective* devices which cannot be tuned to within the given specification limits of the DUT.

An *alternate tuning test* (stimulus applied from DSP of Figure 77) is one which is computed in such a way that the DUT response to the test shows *strong statistical correlation* with the test specifications of the DUT in the *presence of random process variations as well as random simultaneous variations in all the tuning knob values*. An alternate tuning test (ATT) as defined above is computed by modifying the test optimization algorithms to include the tuning knob values as input parameters to the algorithms and is a superset of the conventional alternate tests of which are designed to exhibit such correlation for only the nominal values of the tuning knobs. By virtue of this correlation, it is possible to build a regression mapping ***R*** using the MARS regression tool that maps the DUT's ATT response to its test specification values with high accuracy, *independent* of the values of the circuit tuning knobs. Note that such a model ***R*** will predict the test specifications of the DUT from its test response *more accurately* in regions 1 and 2 of Figure 78 as compared to region 3 containing large parameter variations.

This is because for any finite sample set of "training" devices on which ATT measurements as well as specifications measurements are made to build the regression model ***R***, there are many more devices in regions 1 and 2 as compared to region 3 due to the nature of the mean-centric specification distribution of Figure 78. Note that the *accuracy of* ***R*** *is important as it determines the quality of tuning* when it is used to predict all the DUT specs through the different iterations of the test-tune-test procedure as outlined for the transceiver in Figure 77. This *accuracy of prediction for marginal devices* is factored into measurement inaccuracy while determining the extent of the region 2 of Figure 78 corresponding to each DUT test specification.

Small parameter deviations are defined to be the range of parameter deviations for which the mapping ***R*** is determined to have a specification prediction error from the alternate tuning tests results to be less than X% , (where X is an input to the tuning procedure (impacts yield recovery). X can be selected to be a small number (say, less than 10%) depending on the application.

To determine if the mapping ***R*** can be used to predict the specifications of arbitrary DUTs, a *small parameter deviation filter* is first used to analyze the response of the DUT to the applied ATT. This is similar to the defect filters except that the alternate tuning test response is used to design the filter which determines if the DUT has the same response features as devices corresponding to the small parameter deviations of Figure 78. If the latter is affirmative, then the DUT specs are predicted from its response using the mapping ***R*** and the Augmented LaGrange test-tune-test procedure is applied iteratively until convergence is achieved.

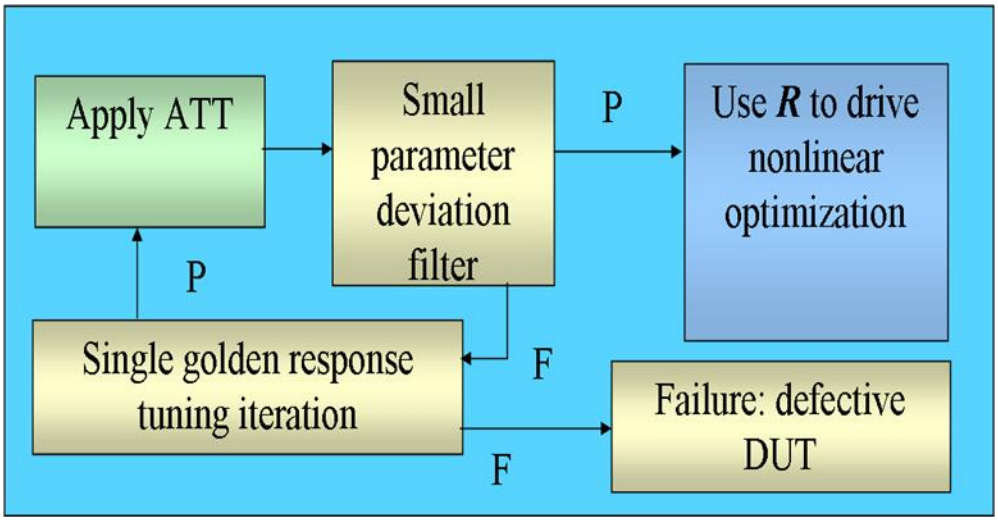

Figure 79: Alternative tuning test flow

If the small parameter deviation filter analysis for the DUT is negative, then it is not possible to use ***R*** to predict the DUT specifications. In this case, the test response to the alternate tuning test for a nominal DUT with nominal tuning parameter values is selected as the "golden response" and the mean square error between the observed

response and the golden response is minimized. This procedure is referred to as "golden response" tuning and does not require the use of a regression mapping or prior regression "training" procedure. Golden response is based on the heuristic that as the above *mean square error is minimized, the DUT specifications converge towards their nominal values* (although along unknown specification trajectories). This heuristic has been validated through tuning experiments across a large number of DUTs. The overall alternative tuning test flow is shown in Figure 79.

In summary, first the ATT is applied and it is determined whether the mapping ***R*** can be used to drive the Augmented Lagrange algorithm driven tuning procedure using the small parameter deviation filter. If not then golden response tuning is performed one iteration at a time until the small parameter deviation filter "passes" the DUT. At this point, the mapping R can be used to carefully optimize a specification-based cost function for each DUT until convergence is achieved. In case, no cost improvement for golden response tuning is possible for 3 consecutive iterations, the DUT is deemed to have failed and it is classified as a defective device that cannot be tuned.

4.3.2.3 Augmented Lagrange Based Small Parameter Tuning

In this section an "Augmented Lagrange" based nonlinear optimization approach is used to search for the best possible way to turn a knob with the least impact on power for devices that exhibit small parameter deviations. A typical constrained optimization problem is formulated as follows,

$$\begin{gathered} Minimize\ f(x) \\ Subject\ to\ g_i(x) \leq 0,\ \ for\ i = 1,2..n\ \ Inequality\ constraints \end{gathered} \tag{62}$$

Where f(x) is the main objective function that needs to be minimized and the function set $[g_1(x), g_2(x)...g_n(x)]$ are the set of constraints that need to be satisfied while

minimizing f(x). The key objective of this work is to improve the overall yield of the system with minimal impact on the power consumption. Hence, the DC power consumption of the RF transmitter system across the supply and bias tuning knobs is formulated as the main objective function that needs to be minimized. The accompanying specs are formulated as multiple constraints.

For a given process the nominal specification is defined as ***'Snom'*** and the DUT's specification is defined as ***'S'***. It's common to guard band the nominal specifications in order to trade-off multiple specs. Let ***'gb'*** be defined as the guard bands (yield bounds) associated with the nominal specs. It is desirable to enforce ***abs(Snom-S)*** ≤ ***gb*** to improve the overall yield of the system**.** The previous equation can be slightly modified as shown (63) to represent a typical inequality constraint similar.

$$g_i(x) = -gb_i + |Snom_i - S_i| \tag{63}$$

The constraints considered are ***Gain,*** and distortion measures such as ***IIP2*** and ***IIP3***. A method frequently used to find solutions for optimization problems like (62) is the 'Augmented LaGrangian method' that combines both the 'penalty methods' and the 'laGrangian' methods for solving a constrained optimization problem. The augmented Lagrange function can be formulated in many different ways. In this research the formulation given by [73] is used to convert a constrained problem to an unconstrained function as shown in (64).

$$L(x, \lambda, \gamma) = f(x) + \sum_{i=1}^{n} \left[max \left\{ \left(\frac{1}{2} . \lambda_i + \gamma . g_i(x) \right), 0 \right\} \right]^2 \tag{64}$$

Where λi are the LaGrangian multipliers and the γ is the penalty parameter. A detailed discussion of this technique is beyond the scope of this research. For the interested reader further insights into the search technique can be found in [73]. In (64) 'x' refers to a unique combination of the tuning knob values. The update conditions for the λi variables can then be derived to the expression shown below. Throughout the optimization process the penalty values (γ) are increased only if λ variables fail to update in a particular iteration. A simple pseudo code of the algorithm is as follows:

- Start with an initial x_0, $\lambda = 0$ and $\gamma = 1$.
- Use gradient descent approaches to solve for the optimal solution (x_k^*) of the function L(x, λ, γ) shown in (64).
- Update $\lambda_{i,k+1} = max\{(\lambda_{i,k} + 2.\gamma_k.g_i(x_k^*)), 0\}$
- Update $\gamma_{k+1} = 2.\gamma_k$ if λ has not changed from previous iteration
- Iteratively optimize till $\|x_k^* - x_{k+1}^*\| < \xi$ or if a preset number of iterations are run

The conceptual diagram of the ATT driven augmented LaGrange tuning technique and a flow graph of the optimization approach is shown in Figure 80.

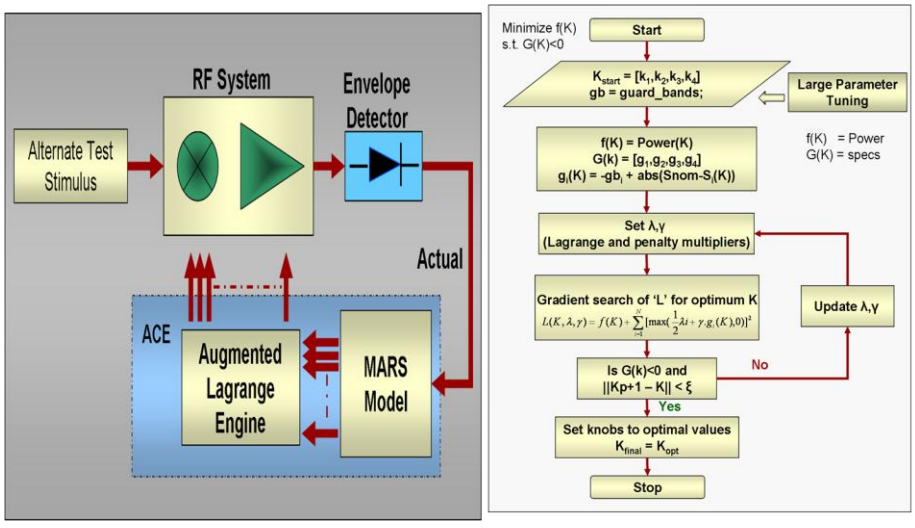

Figure 80: Conceptual diagram and a flow graph of the ATT driven Augmented LaGrange approach

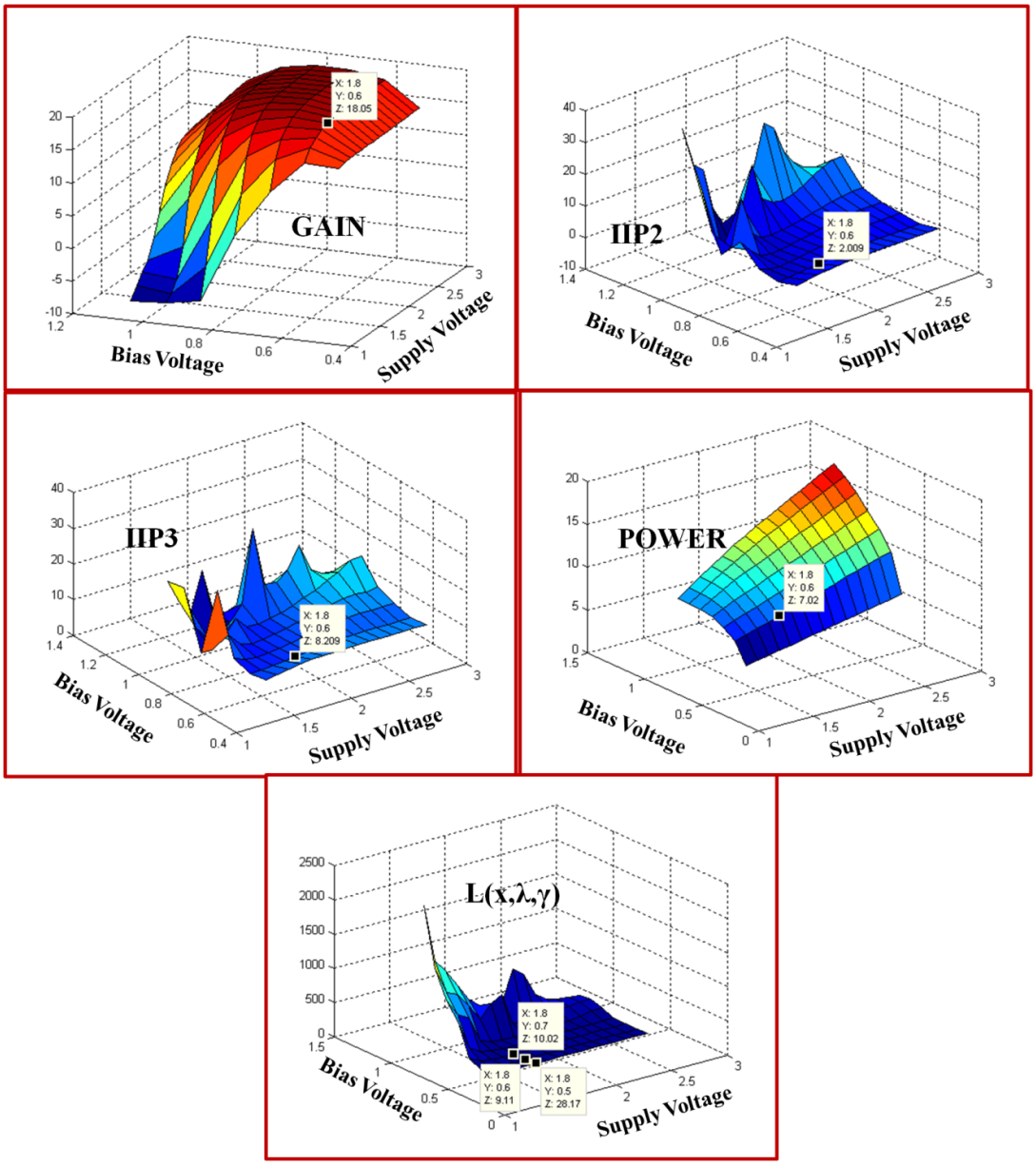

Figure 81: RF specifications (gain, IIP2, IIP3), Power consumption and Augmented LaGrange cost (L(x, λ, γ) across the search space defined by 'x'

The Augmented LaGrange techniques and LaGrange techniques in general do not rely on starting points because they evolve continuously until the constraints are satisfied [74]. While gradient search techniques do tend to get caught up in the local minima, the penalty and the lambda functions ensure that the overall search approach recovers quickly from a local minimum. While some advanced techniques can be performed to ensure

effective immunity against local minima [74], for the purposes of this problem and the test vehicle on which it's demonstrated, the basic nature of the search technique by itself would suffice.

As an example, surface plots are computed for the mixer design used in prior solutions in this thesis to demonstrate the Augmented LaGrange approach. The tuning knobs considered here are mixer supply and mixer bias. The values of the tuning ranges are restricted to 1.4 to 2.8V for the supply and 0.5 to 0.9V for the bias knobs. Figure 81 shows the exhaustive specification surfaces for Gain, IIP2 and IIP3 across the entire search space for a device that exhibits small parameter deviation. Figure 81 also shows the cost function surface (which is nothing but (64) evaluated across all the knobs values 'x') for the final iteration across the tuning knob values for a particular value of λ and γ parameters. It can be seen from the figures that minimum of the cost function surface located at a supply voltage of 1.8 and bias of 0.6 satisfies all the constraints with the least impact on the power consumption.

4.3.3 VALIDATION RESULTS FROM SIMULATION

The methodology described in Section 4.3.2 is developed for a transceiver. However to demonstrate the feasibility of the approach, experiments are run only for a transmitter. A total of 160 process instances were created using Agilent ADS Monte-Carlo simulations.

4.3.3.1 RF Transmitter Modeling

ADS designs of the mixer and power amplifier are used to extract the circuit characteristics such as gain, IIP2 and IIP3 etc. The behavioral modeling procedure is similar to the techniques described in prior solutions in this work. The behavioral transistor model consists of a mixer model followed by a PA model. The output of the PA block is connected to the behavioral model of the envelope detector to capture the test response.

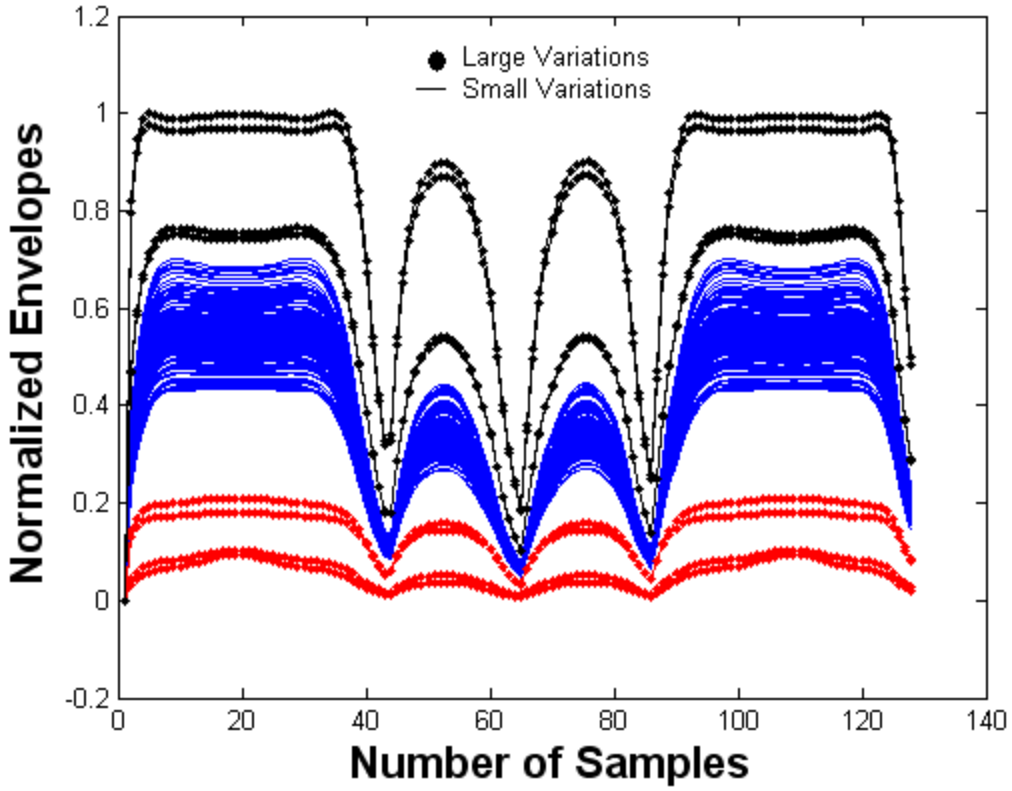

Figure 82: Envelope responses for large and small parameter instances

4.3.3.2 Large Parameter Identification and Golden Response Tuning

In order to detect a large parameter deviation from a small parametric variation use a simple golden signature based filter approach is used. A golden response obtained from a set of sampled nominal processes at the nominal knob setting is compared against the test response of a DUT for a given test input to differentiate small and large parameter variations. Figure 82 shows the envelope responses obtained for a two tone test input for all the 160 process instances for the nominal knob settings.

The envelopes marked as ‘dots’ in black and red exhibit large parameter variations and envelopes marked in blue with smooth lines represent instances that exhibit small parameter variations. Figure 83 shows the developed parametric filter metric for a rough identification between large and small parameter variations. In Figure

83 the blue dots represent the error between small parameter instances and the golden instance and the black/red dots above the green dotted line

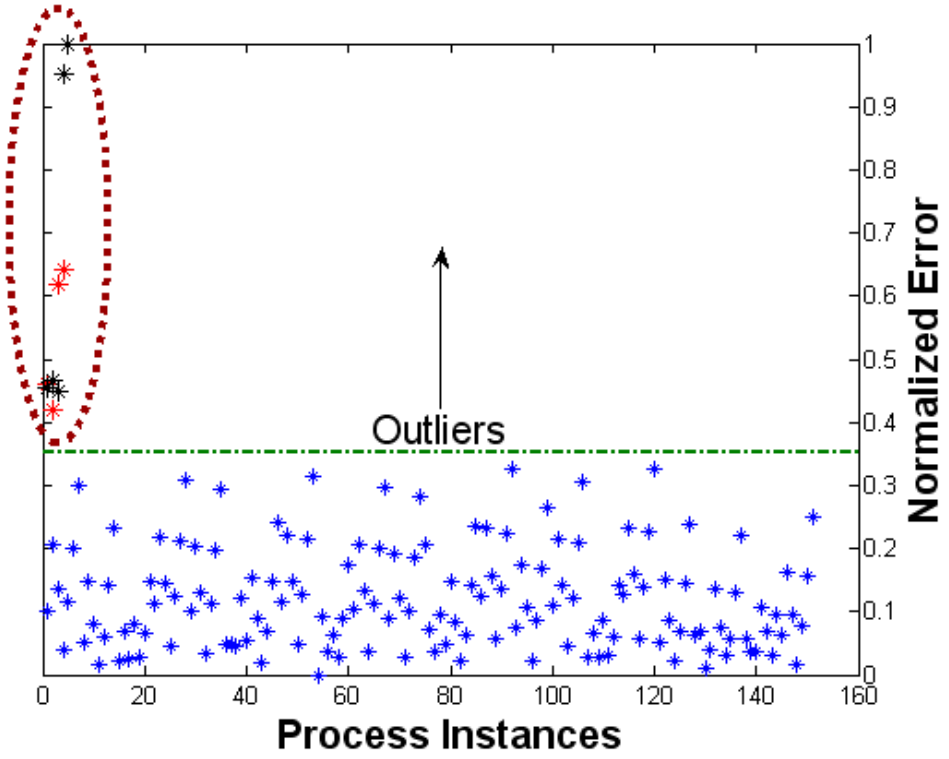

Figure 83: Large parameter filter metric (normalized error between golden response and process perturbed responses for the nominal knob setting)

The filter metric threshold is determined to be '0.3' to differentiate between small and large parametric deviations. Instances that have normalized error more than '0.3' are tuned by a golden signature based tuning approach. A gradient descent based approach is used to perform the golden response based optimization. The cost function is formulated as the normalized error between the golden envelope and the actual response of the DUT for a given test input. The objective of the optimization is to minimize the normalized error to go below '0.3'. Out of the 160 instances 9 were identified to exhibit large parameter deviations by the parametric filter. The gradient descent based tuning results for an instance with large parametric deviation is shown in Figure 84. Table 14 summarizes the tuning results for all the instances. Its observed that the instances O(8)

and O(9) were non-tunable since none of the analog tuning knobs could reduce the normalized error to a value below '0.3'.

Table 14: Golden response tuning instances for all instances with large parameter deviations

Instances	O(1)	O(2)	O(3)	O(4)	O(5)	O(6)	O(7)	O(8)	O(9)
Iterations	3	5	6	4	3	2	4	2	2
Filter Metric	0.28	0.29	0.29	0.26	0.30	0.31	0.29	0.56	0.59

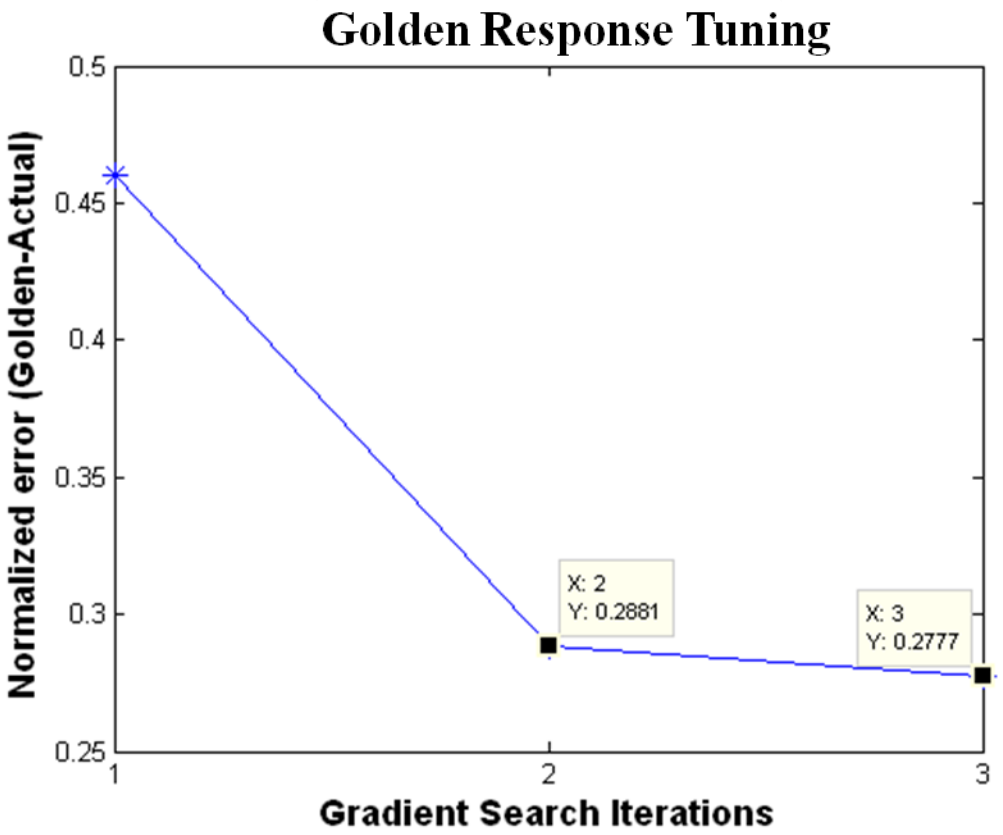

Figure 84: Golden response tuning results for an instance with large parameter deviation

At the onset of error going below 0.3 the tuning technique switches from Golden signature based approach to an augmented Lagrange approach. In this research the value was determined based on the simulations for a large set of instances. In general the

threshold for parametric filter is defined based on heuristic data obtained during the characterization phase.

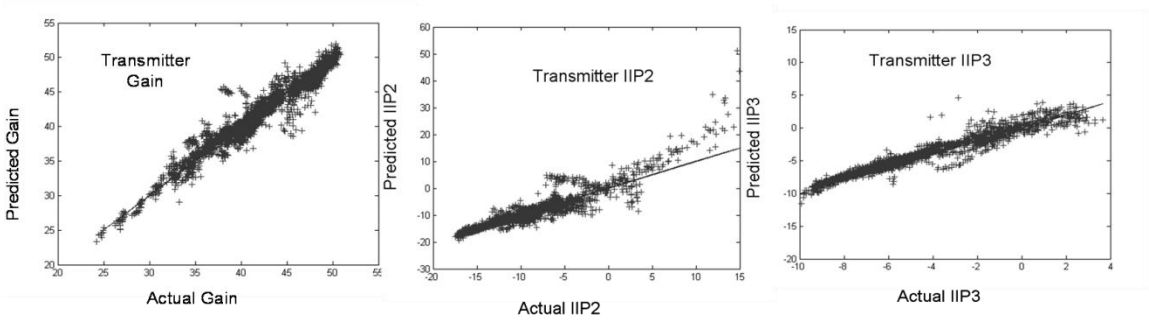

Figure 85: ATT prediction results for transmitter

4.3.3.3 Alternate Tuning Test Results

151 instances were identified to exhibit small parameter deviations out of a set of 160 process instances considered for the tuning approach. The regression models were then trained for a subset (training set) of the remaining 151 small parameter instances across the process and knobs using sophisticated test generation algorithms. The developed models are then evaluated across process and tuning knobs for a set of 10 instances. The scatter plots shown in Figure 85 show the ATT prediction plots for three specs: Gain, IIP2 and IIP3.

4.3.3.4 Augmented Lagrange Tuning Results

Table 15 summarizes the nominal specifications of the RF transmitter system and the yield bounds for each specification. The augmented LaGrange based tuning of an instance P1 that exhibits small parameter deviation is discussed here. Table 16 summarizes the specification values before and after the tuning procedure. The algorithm took 3 iterations to converge (external loop involving λ and γ) where each iteration involves performing a gradient search. The gradient search took 3 iterations to converge there by resulting in a minimum of 9 iterations. It can be observed from Table 16 that the

device P1 that was deemed bad before tuning can be considered as good after tuning for all the specifications under consideration. The power consumption value after the optimization was calculated to be ***0.5724 W.***

Table 15: Nominal specification of the RF transmitter design

	Gain	IIP2	IIP3
Nominal	42.5 dB	-11.5 dBm	-7 dBm
Lower bound	41.5 dB	-12.5 dBm	-8 dBm
Upper bound	43.5 dB	-10.5 dBm	-6 dBm

Table 16: Augmented LaGrange tuning results for 'P1' with small parameter deviation before and after tuning

	Gain	IIP2	IIP3
Before	40.1 dB	-10 dBm	-5.3 dBm
After	41.57 dB	-11 dBm	-7.25 dBm

For the transmitter instance P1, there are 7650 possible tuning knob combinations that define the optimization search space. Out of the 7650 tuning knobs 207 tuning knobs were identified (under exhaustive search) as satisfying all the constraints (i.e. acceptable for yield improvement) with different power consumption values. The lowest power value among all the 207 possible tuning knob values turned out to be the same as the final converged solution at ***0.5724W.*** Hence, it can be concluded that the augmented LaGrange approach can optimize for production yield improvement with a minimal impact on the power penalty values.

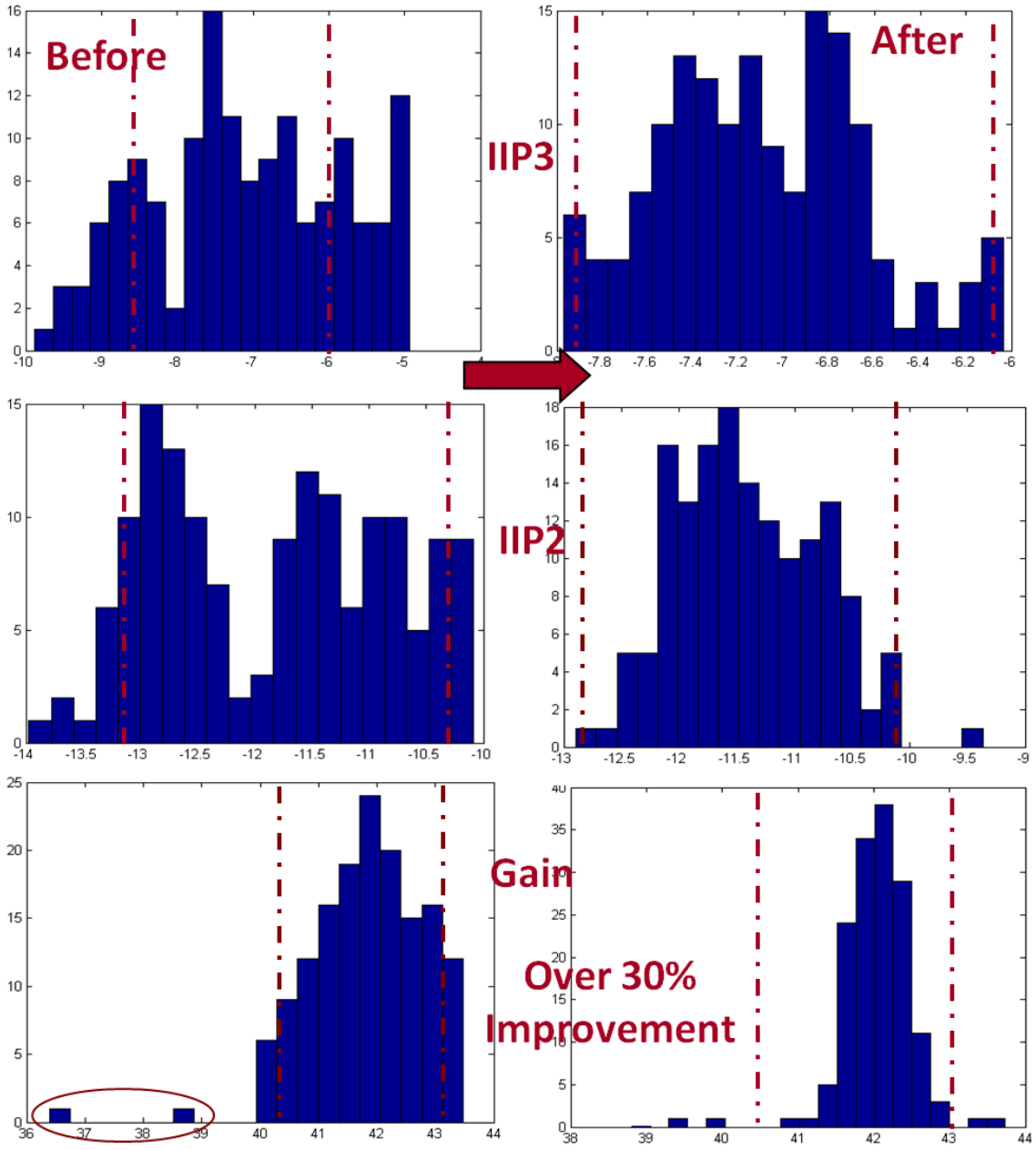

Figure 86: Yield analysis for the transmitter before and after performing the holistic tuning approach

4.3.3.5 Yield Analysis

The holistic tuning approach described above is performed for all the 160 instances under consideration. Gain, IIP2 and IIP3 specifications were used for the yield calculation. The bounds for gain, IIP2 and IIP3 were fixed according to Table 15. Figure 86 shows the yield plots before and after tuning for the transmitter and the receiver.

Based on the test bounds the yield was observed to be 61.59% before tuning and 96.02% after tuning for the transmitter process lot thereby resulting in a yield improvement of 34.43%

4.3.4 KEY ADVANTAGES

The key advantages of the augmented LaGrange based tuning approach are,

- Explicit consideration of power consumption as a performance metric using sophisticated algorithm in a time efficient manner to significantly improve the overall production yield of the system with a minimal impact on the power penalty.
- Capability to identify and accurately tune for RF devices with large and small parameter deviations in a low-cost environment.

In conclusion, in this chapter, several post manufacture tuning techniques are discussed. First, a simplified rapid analog signature driven tuning approach is discussed to achieve yield improvements in a statistical sense. Next a power initialized gradient search approach is discussed to perform accurate tuning of RF ICs in a coarsely power efficient manner. Finally, a holistic tuning approach to accurately tune for large and small parameter deviations in a power efficient manner is discussed. The techniques discussed are production floor ready, and hence can be adopted depending on the type of requirement. The techniques offer significant improvement in production yield and have the capability to *significantly reduce the overall manufacturing cost* of advanced deep sub-micron regime wireless products.

CHAPTER 5

APPLICATION EXAMPLES OF ALTERNATE TEST

Alternate testing methodology is a powerful philosophy and has the potential to significantly reduce the production testing cost of a DUT. In the past, several alternate test based production test, BIT and BOT techniques have been developed to address the growing concerns of test cost and test time for advanced deep-submicron products primarily concerning RF applications. Alternate test has also been applied to great success in the domains of analog operational amplifier testing to reduce the production test cost.

In this chapter, the applications of alternate test methodology in the field of "online testing of RF front-ends" and "MEMS accelerometer testing" are discussed to further highlight the broad implications of alternate test methodology.

5.1 ON-LINE ERROR DETECTION IN WIRELESS TRANSMITTERS USING REAL-TIME DATA

The transmitters employed in present generation high speed broadband communications like WLAN and Wi-MAX are designed to deliver signals at a power level of ~1-2 Watts in end-user applications and ~50 Watts in base station applications. During normal operation, losses arising from the antenna switches and mismatch errors cause nearly 20-30%(this number is constantly on the rise) of this power to be dissipated as heat. These high rates of heat dissipation and thermal cycling affect the overall system reliability in an adverse manner. In addition to the thermal problems, one also needs to consider the effects due to the deep sub-micron processes used to manufacture these systems. Communication protocols require the signal transmitted by the RF system to comply with a preset mask to maintain spectral purity of the transmitted signal. Any unwanted distortion arising from the above mentioned effects could disrupt the Quality of

Service (QoS) or may cause spectral content to spill over into adjacent communication channels. Traditional off-line BIST procedures need to be run at regular intervals that may impede normal system operation. Hence, the need arises to develop online error detection schemes that address permanent drifts (due to the thermal effects) or transient drifts (due to soft and transient errors). Further, the on-line error detection schemes must be triggered on the basis of the *impact of transient errors on system-level performance metrics.* That is, if a desired system-level performance or quality-of-service (QoS) metric is not violated by transient error phenomena, then it is not desired to take any corrective action. Going by the literature survey in the test domain, no previous work has been done in the area of online test for RF circuits/systems.

In this section, a novel on-line error detection technique for wireless RF transmitters is discussed. The baseband DSP of the RF transmitter is used monitor spectral features of the real time streaming baseband data. The FFT of data is computed in the DSP and the power spectral density (PSD) of this spectrum in specific FFT bins is computed and compared to a preset PSD mask. Based on the result of the comparison, a decision on the triggering of the online test is made. In the case of a trigger, the envelope detectors are used to capture the corresponding RF spectrum at the RF node under test (i.e. transmitter output). The envelope detector generates a spectrum of the signal at baseband frequencies that corresponds to the spectrum in the RF frequency band (upon FFT computation of the time domain signal). This response is sampled by existing ADC resource in the transceiver system and is fed back to the DSP. Based on the PSD values of the streaming data and the sampled spectral response of system, the DSP computes the linear and non-linear measures of the system, viz. Gain, IIP3. The linear and non-linear measures of the system help to monitor the health of the system and the QoS. The key contribution of this work is that the performance of the transmitter is *analyzed in real time without the need of off-line tests.* Applications of the on-line testing technique include real time monitoring of the health of a system to obtain diagnostic data and

knowledge about the operational reliability of a RF system to aid other fault tolerance mechanisms such as reconfiguration etc.

The feasibility of the approach has been demonstrated on a RF transmitter system that is designed to operate in the GSM band. Behavioral models of the modules in the RF transmitter were used for this purpose. Although, the transistor-level simulations for all the modules can yield high accuracy of simulation, the long simulation time makes system simulation using transistor-level description of the circuit impractical for the proof of concept. Moreover, the primary objective of this experiment is to show the feasibility and performance of the approach rather than to verify the functionality of the design.

5.1.1 GOALS AND OBJECTIVES

The key goals for online test of RF systems are,

- The methodology must be robust to the randomness present in the real time input data.
- The methodology must be able to dynamically track system performance for randomly varying input

5.1.2 PROPOSED METHODOLOGY

In this section, the online test methodology proposed to monitor the performance of a RF transmitter while streaming real time data is presented. Figure 87 shows the block diagram of a typical direct conversion RF transceiver system that is used to validate the proposed approach.

In order to achieve the above mentioned goals the following are proposed:

- The methodology used to estimate the ‘test mask’ on the random streaming data is presented.
- The methodology used to capture the spectral response at the output of the RF transmitter.

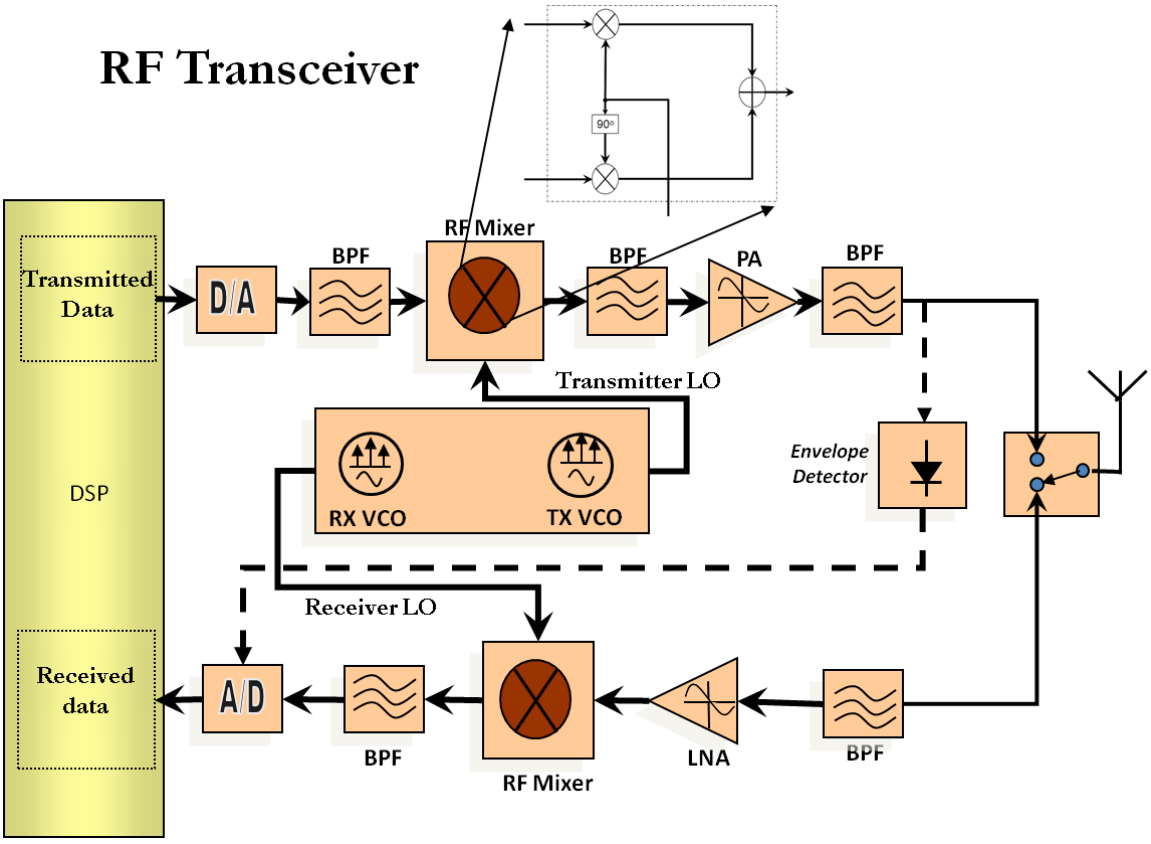

Figure 87: Block diagram of direct conversion transceiver

- The methodology used to map the spectral response of the system to its performance parameters in the presence of randomly streaming data.

5.1.2.1 Test Mask Estimation

The data for wireless communication is processed by the DSP of the transmitter system before it is up-converted in frequency and transmitted. The PSD of each data packet in specific bins is computed and this information is used to create a *'test mask'* on the random streaming data. The DSP of the system is used to compute the FFT and the PSD. The PSD of a bit stream, (represented in (65)) is a measure of the power (or variance) of a time series distributed across a frequency index. Mathematically, it is defined as the Fourier transform of the autocorrelation sequence of the time series. An

equivalent definition of PSD is the squared modulus of the Fourier transform ($F_T(\omega)$) of the time series, scaled by a constant term.

$$S_F(\omega) = \lim_{T\to\infty} \frac{|F_T(\omega)|^2}{T} \tag{65}$$

The scaling constant *'T'* is the bandwidth over which the PSD is estimated. The PSD of an input bit-stream is a feature describing the inherent nature of the bit-stream that is used to characterize the input data. The computed PSD values are used to estimate the *'test mask'* of the system. In order to generate the 'test mask', a large set of N data packets corresponding to the transmitted data are generated (i.e. voice samples in the case of telephony applications). The spectrum of each of the packets is computed and their PSD values for a set of M pre-defined frequency bins are determined. Statistical analysis performed on this large set is used to estimate the mean and variance of the PSD values at each of the specified bins. The upper and lower bound values at each bin is set to be the standard deviation of the distribution of PSD values at each particular bin. The 'test mask' is thus formed for a training set of N data packets that closely resemble the real time streaming data. In order to demonstrate this, a set of 2000 random data sequences were generated and their PSD values were calculated from their 512-point FFT plot.

Figure 88 shows the FFT plot of a single data packet which contains a set of 100 random data bits. The entire frequency range was divided into 10 equal bins and the PSD in each of the bins was computed. Based on their standard deviation values the mask was generated. Figure 89 shows the plots of the PSD values in the 10 frequency bins for the set of 2000 random data packets. Also, the mask (upper and lower bounds) obtained from this training set is shown in the same figure using a dotted legend. Any data packet that falls within this *'test mask'* is used to trigger the online test. This *'test mask'* estimation addresses ***Goal 1*** of this work

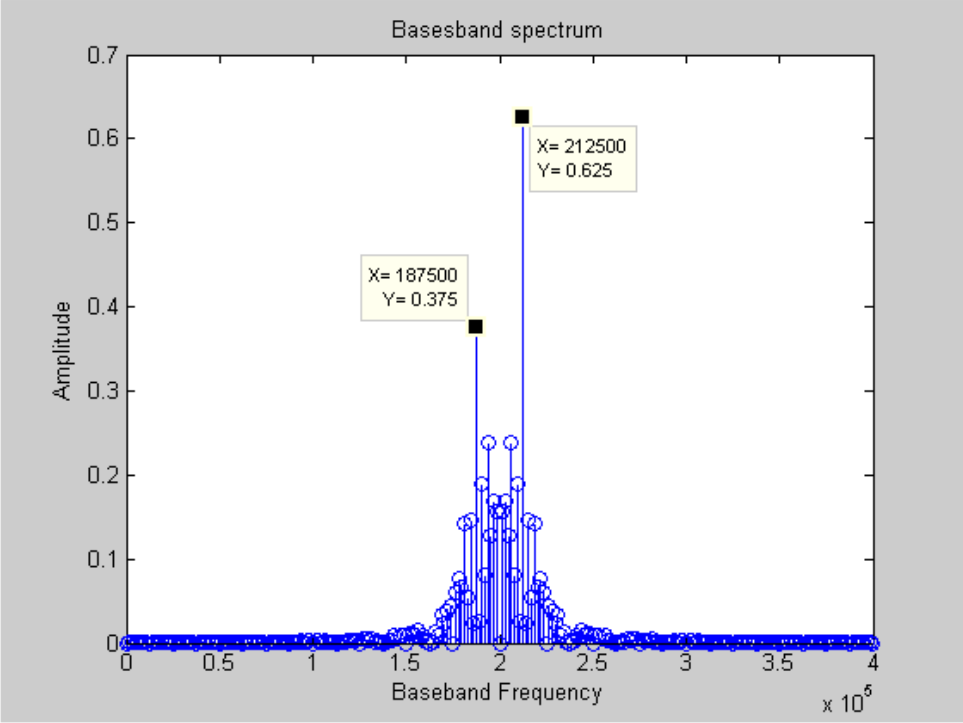

Figure 88: 512 point FFT of a single data packet

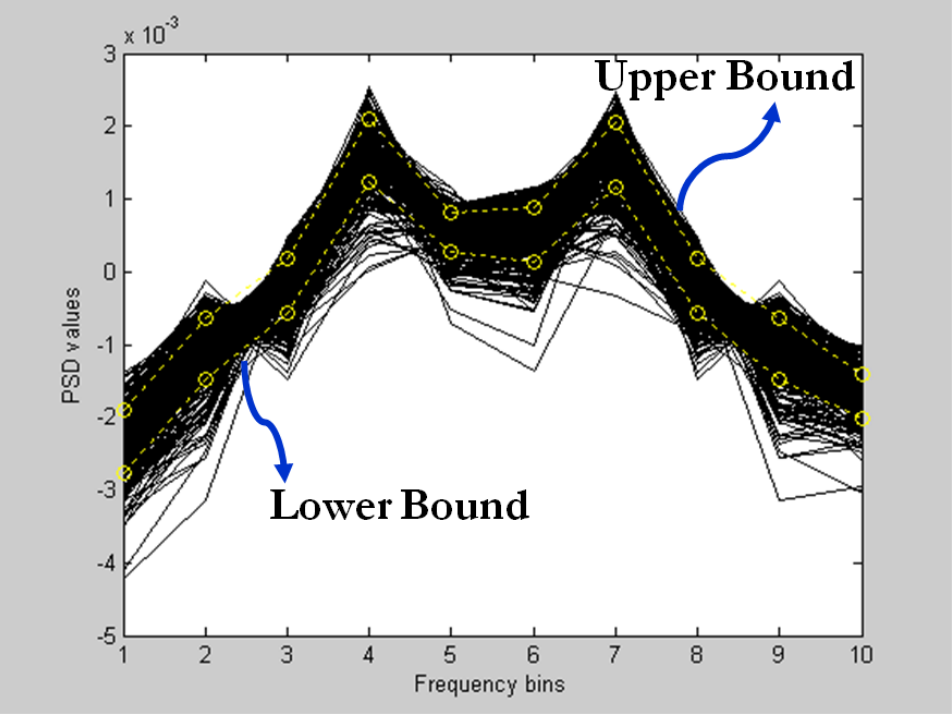

Figure 89: Plot of PSD values with lower and upper bounds for 2000 random bit-streams

5.1.2.2 Spectral Capture by Embedded Sensors

As shown in Figure 87 an embedded spectral sensor is used to capture the spectral response of the transmitter system. The spectral sensors generate a baseband spectrum corresponding to the spectrum in the RF frequency band at the output of the system. These low frequency signals (baseband) can be sampled by the ADC and the corresponding digital codes are input back to the DSP. The DSP uses this information along with specific information extracted from the baseband of the transmitted signal to monitor the performance of the system. These transceivers are typically designed for TDMA half duplex applications. Hence the ADC in the receiver chain is practically unused during the transmit operation.

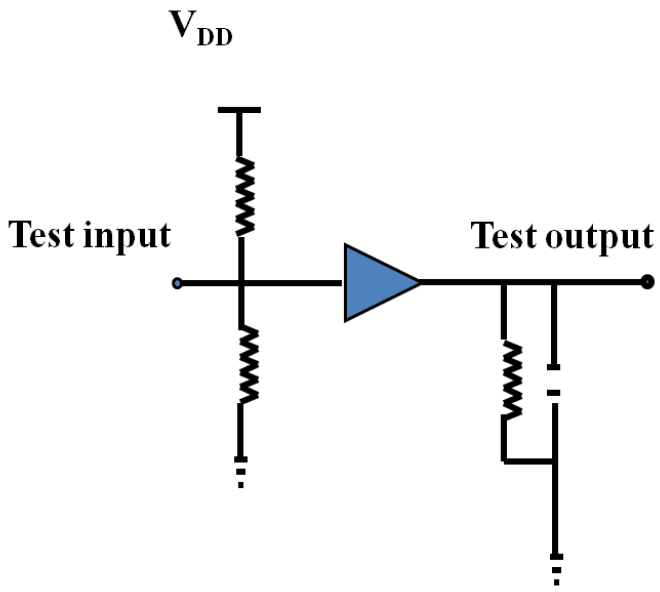

Figure 90: Envelope Detector

In this work, an envelope detector as depicted in Figure 90 is used as the spectral sensor. This envelope detector is a simple one diode structure consisting of a diode, a resistor and a capacitor. The resistor pair at the input of the detector is used for biasing the device. The RC values are chosen appropriately to perform the requisite

envelope detection. The key advantage of an envelope detector is that, it down converts a high frequency signal into a low frequency signal while conveying the essential data contained in the original signal. Also, the envelope requires very little overhead in terms of space, power and power attenuation.

5.1.2.3 Multi-Variate Statistical Estimation of System Health

The spectral content observed at the output of a transmitter has a high degree of dependency on the parameters of the system. But additional complexity is added to this problem by the random nature of the real time streaming data. A slight difference in spectral content causes a large difference in system performance. This is because of the different non-linearities exerted by different random bit-stream. This overall effect largely affects the spectrum captured by the sensor. Due to the more than one order of randomness involved multi-variate statistical estimation is used to determine the system performance. The PSD vales of the real time data that is within the 'test mask' along with the corresponding sampled response of the detector are used to jointly estimate the performance of the system. This kind of performance estimation would require the use of advanced statistical tools like Multi-variate Adaptive Regression Splines (MARS)

The MARS models are developed according to the theory described in Chapter 2. Thus, once a regression equation has been computed over a set of training data, the subsequent spectral response of the system, and the PSD values of the real time data that trigger the online test are used to determine the system performance. The DSP fits the real time captured data into the regression equation to determine the performance parameters of the system.

5.1.3 VALIDATION RESULTS

The proposed methodology has been validated on a behavioral model of a GSM band wireless RF transmitter. The RF transmitter is modeled similar to the previous descriptions of the transmitter model in Chapters 3 and 4. The random nature of the voice

or data packets in wireless communications was replicated in the set up by a pseudo-random bit-stream generator. In this experiment 2-level Frequency Shift Keying (FSK) modulation was employed at the baseband. Also frequency domain simulations were used to their inherent speed. The resulting 512-point FFT data for a particular data packet at the baseband of the RF transmitter after performing folding, phase reversal etc is shown in Figure 88. This spectrum is then up-converted by the mixer and is amplified to the desired power level by the power amplifier. The BPFs' are used to attenuate the undesired signals. The spectral content observed at the output of the RF transmitter is shown in Figure 91. The additional tones present at the output spectrum are due to the non-linear effects of the mixer and power amplifier that are modeled by the coefficients 'α'_1 and 'α'_2.

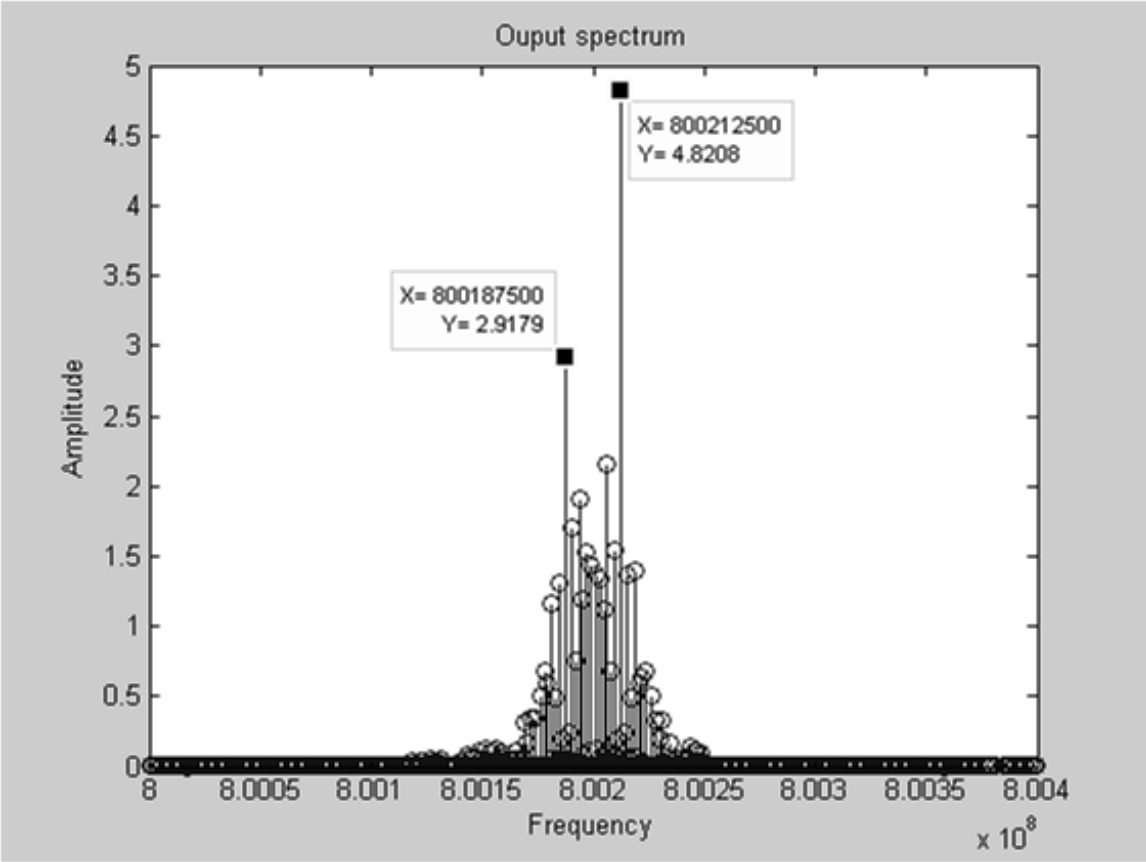

Figure 91: FFT spectrum at the RF transmitter output

The bit-streams that pass the test mask were used to trigger the online test. The proposed methodology requires a training set of devices to build the statistical regression functions using MARS.

5.1.3.1 Generating Multiple Training and Evaluation Instances

Parametric variation in the system parameters such as PA gain, mixer gain etc is used to create multiple instances of the system to generate the training set based on Monte Carlo simulations. Each behavioral model can be viewed as a discrete event of the RF transmitter. Table 17 shows the nominal system parameters along with their percentage perturbation limits used to create multiple instances of the system. A normal distribution is used to generate the training set of the required perturbation.

Table 17: Nominal parameters and percentage process variation for generating training instances

Process	Nominal-Patterns				% Variation
	Mixer Distortion	Mixer Gain	PA Distortion	PA Gain	
P[1]	3	5	1	30	10
P[2]	3	5	1	30	30
P[3]	3	5	1	30	60
P[4]	3	5	1	30	100

The training set consists of instances spread over four different process indices as mentioned above. The model is trained over a dataset that included parametric variations (<10%) as well as some catastrophic effects modeled by big shifts in the performance parameter values such as the instances belonging to process index P[2,3,4]. It can be observed from Table 17 that the generated training dataset consist of instances operating at different regions. This is necessary to ensure that the model is trained to operate over diverse regions of operation to enable good tracking during online tests.

5.1.3.2 Model Building

A training set size of 500 instances is used to build the regression equations. Each instance can be viewed as a discrete event of the transmission cycle. A set of 500 random data packets that have passed the computed 'test mask' are fed as input to 500 different training instances. The spectral response for each of the instance to the corresponding data packet is sampled and stored. The PSD values of these random data packets and the spectral content of the response of the system were used to train the model. Also, the performance parameter viz. gain and IIP3 is calculated for each instance of the training set. These values were computed using standard formulas that relate behavioral parameters of the modules in the system to the system-level performance parameters. MARS is used to compute the regression equations from the vector containing the spectral response of the device and the PSD values of random data packet to map to the system performance parameters over the training set.

5.1.3.3 Model Evaluation

The developed model is then evaluated with the evaluation data set to analyze the accuracy of the proposed approach. The evaluation set consists of 250 instances with parametric variations as well as catastrophic effects across the four process indices mentioned in Table 17. A new set of 250 random data packets were generated and their PSD values were computed. The spectral response of these devices and the PSD values of the random streaming data are fit into the regression equation to determine the performance parameters of the system. This data is compared to the performance parameters of the same instances, calculated using standard formulae. For an accurate performance prediction, the predicted parameters would track the actual parameters. The scatter plots of the performance parameters: Gain and IIP3 are shown in Figure 92 & Figure 93 respectively. The closer the predicted specification values are to the strait line having a slope of +1 (representing error free prediction), the higher the effectiveness.

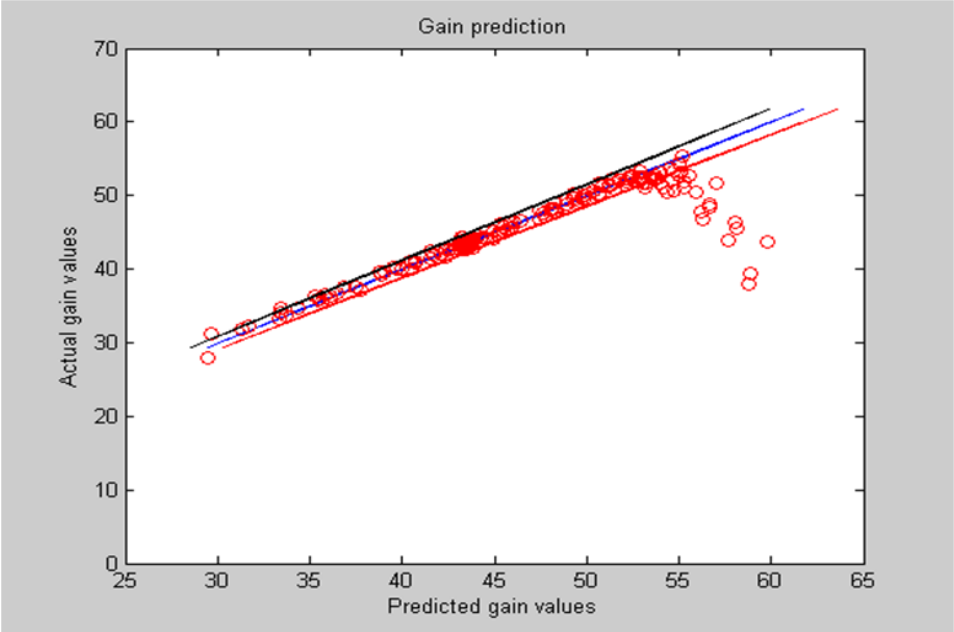

Figure 92: Prediction results for gain of the transmitter

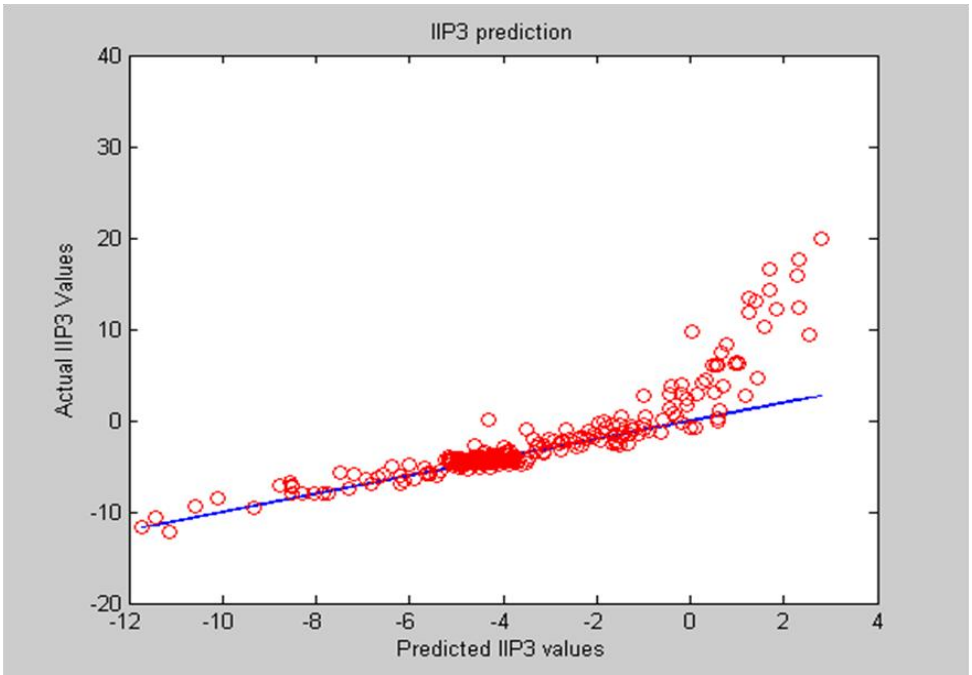

Figure 93: Prediction results for the IIP3 of the transmitter

5.1.3.4 Performance Classification Based on Transmitter Gain

In this case study, the system gain parameter predicted by MARS for the random input data is used to analyze the performance of the system. The evaluation set consists of 129 ‘good’ instances with a nominal process shift (10%) and 121 ‘bad’ devices with catastrophic fault effects (250 in total). An acceptance region with lower and upper bounds (42dB and 45dB respectively) is defined based upon the observed nominal variation of the system gain. The devices with predicted gain values lying within the bounds are classified as ‘good’ and those found lying outside these bounds are classified as ‘bad’. The results of this case study are summarized in Table 18. The developed model is able to provide a classification of upto 98% with just 2% (overall) error in classification.

Table 18: Performance classification based on gain

Evaluation set		GOOD classified as GOOD	**GOOD classified as BAD**	BAD Classified As BAD	**BAD Classified As GOOD**
Good	Bad				
129	121	127	**2**	118	**3**

It can be observed from the table that two good devices are misclassified as bad and three instances of the bad dataset are misclassified as good resulting in a 2.45% misclassification rate for good devices and 1.55% misclassification rate for bad devices. In overall, 5 devices are misclassified out of 250 evaluation devices which results in a 2% overall error. Whenever the parameters of the bad instance were way beyond its nominal value, the regression model predicts a value significantly different from the original value. However the predicted values are also way out of the prescribed bounds thereby making sure that a ‘bad device’ is classified as ‘bad’. For example the instance with a system gain value of 60 dB is mapped back to 13.5 dB which is way beyond the specified bound. This abnormality in the prediction for such a data, though not a cause of concern,

can be easily overcome by improving the training set to MARS by the addition of instances that lie in the same process index.

5.1.3.5 Performance Classification Based on Transmitter IIP3

IIP3 is a measure of non-linearity of the system. Tracking IIP3 requires highly robust theory and models since its value can vary by a large amount for a small variation in the behavioral parameters of individual modules. The classification result for an evaluation set 136 good and 114 bad devices (based on a lower bound of -5 and an upper bound of -3) is shown in Table 19. It can be observed from the table that two good devices are misclassified as bad and five bad devices are misclassified as good resulting in a 1.47% error for good devices and a 4.3% error for bad devices. Overall, 7 devices are misclassified resulting in a 2.8 % error in classification.

Table 19: Performance classification based on system IIP3

Evaluation set		GOOD classified as GOOD	**GOOD classified as BAD**	BAD Classified As BAD	**BAD Classified As GOOD**
Good	Bad				
136	114	134	**2**	109	**5**

To summarize, in this section, a novel on-line error detection technique for wireless RF transmitters using real time streaming data is discussed. Specific spectral features of the real time streaming data are monitored at the baseband input of the system, to trigger the online-tests at regular intervals based on a preset mask. The spectral features at the baseband input and the corresponding spectral signature at the RF node are jointly processed by the DSP in the system to determine the performance the transmitter *without impeding normal service*. Behavioral models of the RF system are used to provide validation results. The result show that the performance parameters of the RF transmitter can be accurately tracked using the proposed approach.

5.2 ALTERNATE ELECTRICAL TESTS FOR EXTRACTING MECHANICAL PARAMETERS OF MEMS ACCELEROMETER SENSORS

In this section the application of alternate test in the field of MEMS testing is discussed. Micro electro-mechanical systems (MEMS) integrate mechanical structures such as beams, actuators and associated signal conditioning electronics on a common silicon substrate through use of high precision "micromachining" techniques. The large signal to noise performance of MEMS devices makes them ideal for several sensing applications. Some of the applications of MEMS sensors include deployment of airbags in automotives, development of precision guided ammunition, development of nano-bio technologies for DNA amplification and identification and development of bio sensors for detecting pathogens in the environment. MEMS devices are also used to build tunable RF MEMS passives for use in wireless data transceivers. These small, high quality factor devices offer a powerful alternative to integrated passives. Over the last decade, significant advances have been made in the development of design tools for MEMs systems. However, the area of testing and characterization of micro electro mechanical sensors is still evolving. MEMS devices are complex electromechanical devices with energy interactions across multiple energy domains. The diversity of MEMS structures and various defect sources makes testing a challenging issue.

A MEMS device is an electro-mechanical transducer, where a mechanical vibration to the cantilever beam of the device is transformed to an electrical response at the output of the device. Conventionally MEMS accelerometers are tested by measuring the electrical response of a DUT to a controlled mechanical input. This poses limitations on the test infrastructure and test quality due to the difficulties in producing precise mechanical movements and consumes significant amount of time to identify the mechanical parameters of the cantilever beam.

5.2.1 GOALS AND OBJECTIVES

The key objective is to perform testing of MEMS devices in a cost efficient manner using an electrical test input. The goal is to obtain critical diagnostic data about the mechanical parameters of the cantilever beam, a fundamental component of the MEMS device, in a significantly reduced test time.

5.2.2 PROPOSED METHODOLOGY

In this section, the methodology of determining the mechanical properties of a MEMS accelerometer using purely electrical stimulus is discussed. The key idea is to exploit the fact that, in MEMS accelerometers, the proof mass (cantilever beam) and a static electrode form an air-dielectric capacitor. The alternate electrical test methodology is performed as follows,

- A large signal optimized AC stimulus with a carefully chosen frequency is applied across the capacitor, causing an oscillating motion due to electrical forces resulting from accumulated charge on the capacitor plates.
- A high frequency small-signal AC stimulus superposed on the large-signal stimulus is used to monitor the change in capacitance vs. time caused by the beam motion.
- The large signal electrical stimulus is designed in such a way that the transient capacitance vs. time waveforms are *sensitive to changes in the mechanical properties of the cantilever beam* and are then mapped back to the mechanical properties of the accelerometer structure using regression based techniques (MARS).

5.2.2.1 Overview of MEMS Accelerometer Systems

The cantilever beam (as shown in Figure 94) is a micro-machined structure built on top of a silicon wafer. Poly-silicon springs suspend the beam over the surface of the wafer and provide resistance against acceleration forces. External acceleration deflects the beam and “unbalances” a differential capacitor that consists of independent and fixed plates. This change in the capacitance value is sensed by signal conditioning circuitry

resulting in an electrical output that is proportional to the input mechanical acceleration. The signal conditioning circuitry as shown in Figure 95 typically consists of a capacitance sensing circuit, a demodulating circuit followed by a filter output stage. The filter in the output stage determines the bandwidth of operation of the system.

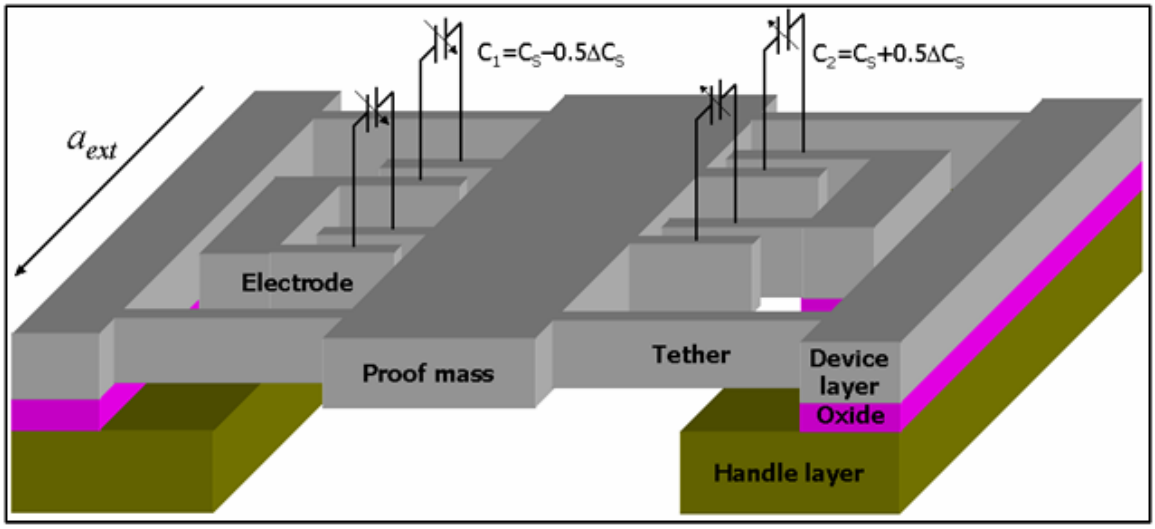

Figure 94: Mechanical structure of the MEMS accelerometer **Error! Reference source not found.**

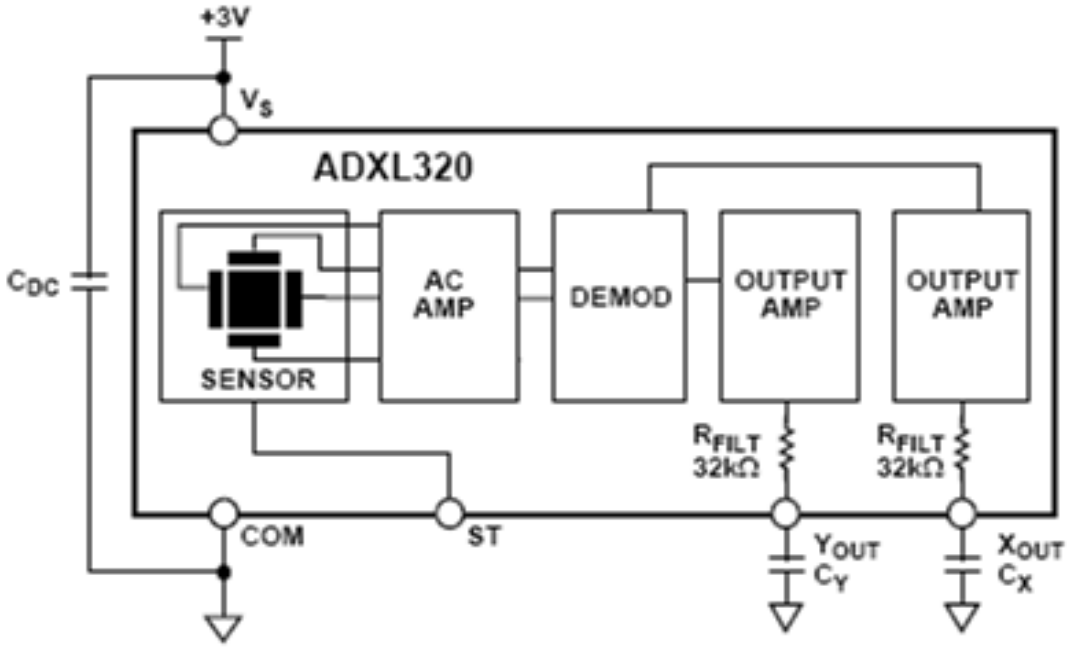

Figure 95: Functional block diagram of an accelerometer (ADXL 320 [76])

5.2.2.2 Mechanical Modeling of the MEMS Accelerometer

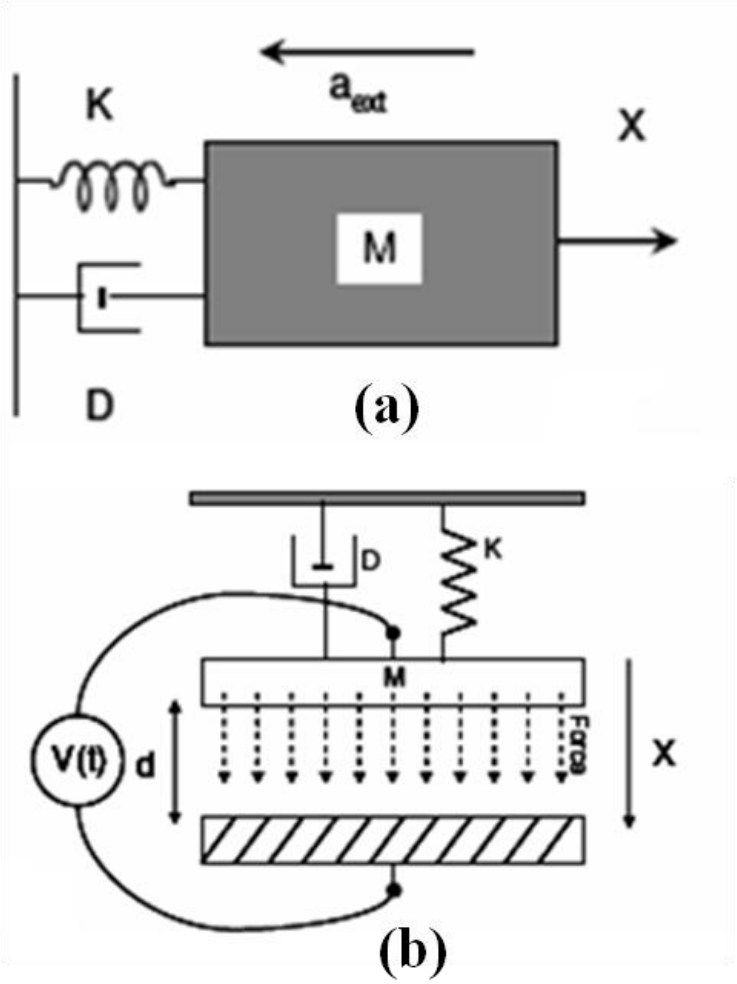

Figure 96: (a) Mechanical model of MEMS accelerometer (b) Parallel plate capacitance representation

The mechanical model of a typical accelerometer (as shown in Figure 96a) consists of a proof mass 'M' that is displaced by the external inertial forces acting on the accelerometer. The proof mass is suspended by means of poly-silicon springs with a spring constant 'K' and damping coefficient 'D'. It is assumed that the bottom plate of the transducer is fixed and the top plate is free to move under the application of an external force. Further, it is assumed that the movement of the beam is in a direction

normal to the plates of the accelerometer, denoted by *x* in the following analysis. For purposes of simplicity, it is also assumed that there is no bending of the beam under the influence of the applied external force due to acceleration. Under these assumptions, the MEMS accelerometer can be considered as a parallel plate capacitor. The distance between the plates vary under the influence of external inertial forces. The initial distance between the plates is denoted by d. The 'rest capacitance' of the transducer is then given by

$$C = \frac{\varepsilon_O . A}{d - x} \tag{66}$$

Where ε_0 = 8.854e-12, is the permittivity of free space, A is the area of cross section of the beam. The dynamic behavior of the system under the application of an external mechanical acceleration can then be explained by the Newton's second law of motion as follows,

$$M.\frac{d^2x}{dt^2} + D.\frac{dx}{dt} + K.x = F_{EXT} \tag{67}$$

Where F_{EXT} is the external force developed. In case of a mechanical input (acceleration, A_{EXT}) it can be expressed as M*A_{EXT}. Alternatively, the beam can also be stimulated by means of an electrical input. The force developed in this case is given by

$$F_{EXT} = -\frac{d}{dx}.\left(\frac{1}{2}.C.V^2\right)_{x=0} = \frac{1}{2}.C.\frac{V^2}{d} \tag{68}$$

Where ‘C’ is the rest capacitance of the system and ‘V’ is the input voltage applied to the system. The input voltage ‘V’ is a sinusoidal signal riding on a DC voltage. The frequency of motion of the beam during test is carefully chosen such that the beam is in steady state oscillation with low vibration amplitude during the testing mode of operation. Equation (67) can then be solved for displacement x(t) and hence for the capacitance of the system for an appropriate value of input voltage. The number of tones and their corresponding values can then be adjusted to result in an accurate measurement of the mechanical parameters of the accelerometer beam.

5.2.2.3 Test Generation

The input voltage considered for our analysis is defined as $V_{DC} + V_{AC}.\sin(\omega.t)$. This is a single tone input with a frequency near 50 Hz using which, (67) can be solved to obtain the value of displacement and hence the value of the capacitance of the beam system. The dimensions of the ‘proof-mass’ beam used for analysis is given in Table 20.

Table 20: Mechanical dimensions of the cantilever beam

Parameter	Value (Meters)
Width (W)	50e-6
Length (L)	100e-6
Thickness (h)	3e-6
Initial Distance (d0)	1e-6

The resonant frequency determined by the mechanical parameters of the structure, is 11.25 Hz. A small value of input voltage is enough to actuate the beam if the input frequency is this value. This is illustrated by the plot shown in Figure 97 where the beam is actuated with a 1V AC signal running at the natural frequency of the beam and riding on a DC voltage of 15V.

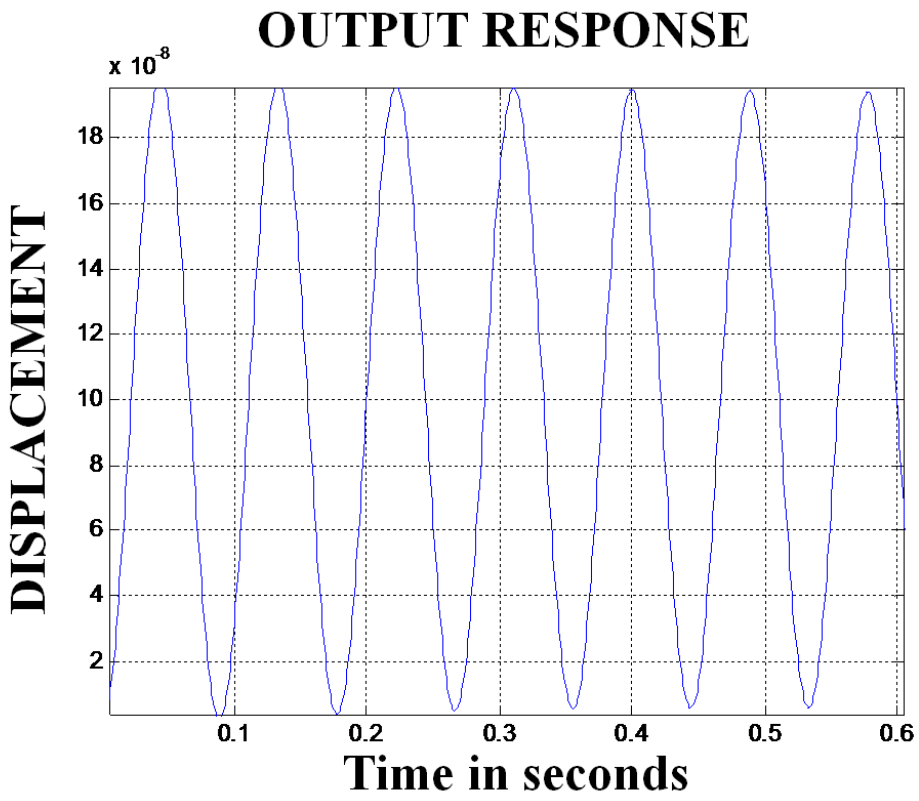

Figure 97: Displacement at natural frequency

The maximum displacement between the capacitor plates is observed at the natural frequency (11.25Hz) of the beam. Even though this phenomenon is ideally the best for prediction of the beam mechanical parameters, mechanical limitations such as fatigue of the beam, fracture strength of the beam, etc., pose a major cause of concern. If the input frequency is high (>50 Hz), the beam displacements die out and reach a steady state value quickly. Hence the stimulus frequency should be selected in such a way that the device is in steady state oscillation with minimum vibration amplitude as depicted in Figure 98

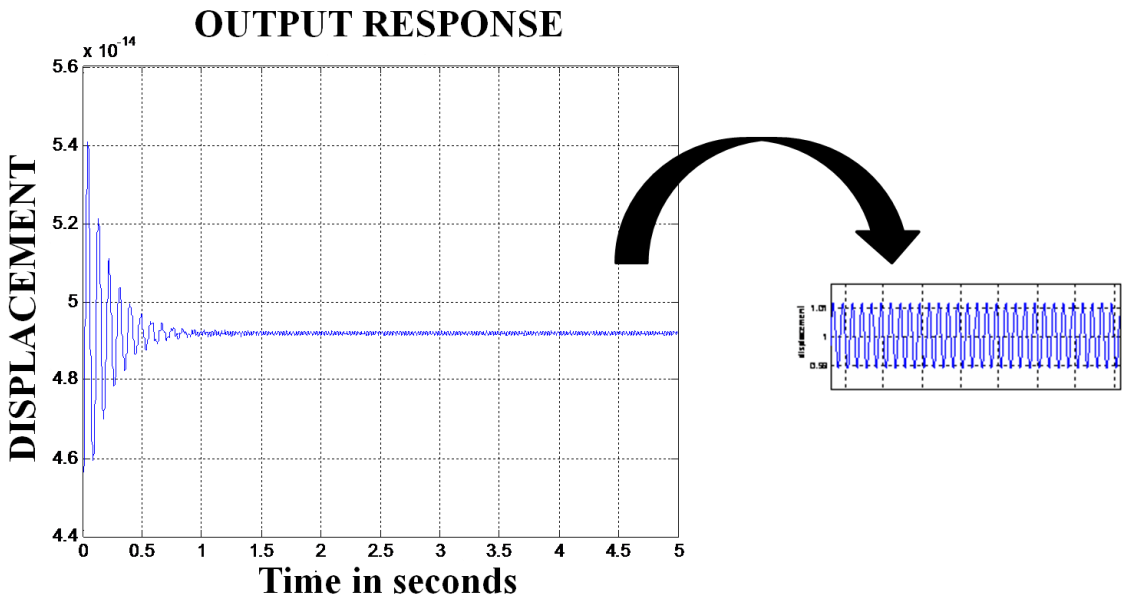

Figure 98: Displacement at 40 Hz

This study is performed to determine the range of frequencies that the input can take to ensure that the device operates in a "safe" region of operation, while providing a reasonable amount of information for measuring the mechanical parameters of the beam. The primary goal of the test generation module is to come up with an input stimulus, which can be applied to the DUT such that the corresponding test response has *high statistical correlation* with the mechanical parameters of interest. The test generation algorithm implemented in this research is a 'gradient-search' based optimization algorithm. The prediction error (error between the actual value and the predicted value of a parameter) of the developed MARS model is used as a cost function to optimize the input stimulus. The optimization is done for (a) a single tone input, (b) three tone input with each tone optimized for a specific parameter of the system. The pseudo code of the implemented gradient search algorithm to perform test generation is shown in Figure 99. The test generation engine is the same for generating single tone and the multi-tone alternate electrical test stimulus

Psuedo-code of the implemented gradient-search algorithm

Step1: Create a training set of devices (by varying mechanical parameters M, D and K) of size M

Step2: Create a search space of input frequency (f) (15 To 50 Hz)

Step3: Pick a frequency(f) from the search space

Step4: delF = 0

Step5: while (err>desired_err ||f>50||f<15)

(a) for i = 1:M
Simulate the DUT
Meas_space{} = Store the response
End

(b) Develop a mars model between Meas_space and the parameters (M, D and K)

(c) Compute the error in prediction between actual Values P_a and predicted values P_p

Rms error $\varepsilon_{rms} = \frac{\|P_a - P_p\|}{\sqrt{M}}$

Rel error $\varepsilon_{rel} = \frac{\varepsilon_{rms}}{range(Pa)}$

(d) Compute mean error of the parameters

$$Mean\_err = \frac{\sum_{i=1}^{3} \varepsilon_{rel}(i)}{3}$$

(e) f1 = f + delF, f2 =f-delF
goto 5(a), compute Mean_err1, Mean_err2
Select f
End while

Step6: loc = Compute the stimulus with least mean error

Step7: f = f+coarse_sweep, goto step5

Step8: EXIT when iteration exceeds a Defined count (or) error<desire_ err

Step9: Test output =input stimulus with global_ min(local(errors))

Figure 99: Pseudo-code of the test generation algorithm

5.2.2.4 Single Tone Test Generation

The input voltage considered for our analysis is defined as $V_{DC} + V_{AC}.\sin(\omega.t)$. The optimization range of frequencies is fixed from 15Hz to 50Hz based on preliminary analysis on the system. Below 15 Hz, it is observed that the initial overshoot of the beam is more than two-third of the initial distance between the plates, thereby violating the safety margins of the design. The optimization algorithm is observed to determine a frequency of 45 Hz for the input alternate electrical signal as the optimum frequency for a single tone input.

5.2.2.5 Multi-Tone Test Generation

The input considered here is a multi-sine waveform and is defined as $V_{DC} + V_{AC}.[\sin(\omega_1.t) + \sin(\omega_2.t) + \sin(\omega_3.t)]$. The optimization is run with each tone being optimized for one of the parameters of interest. The optimization algorithm optimized the values of three tones to 44 HZ, 45 Hz and 48 Hz based on the minimum relative error values of damping, stiffness and mass of the system respectively.

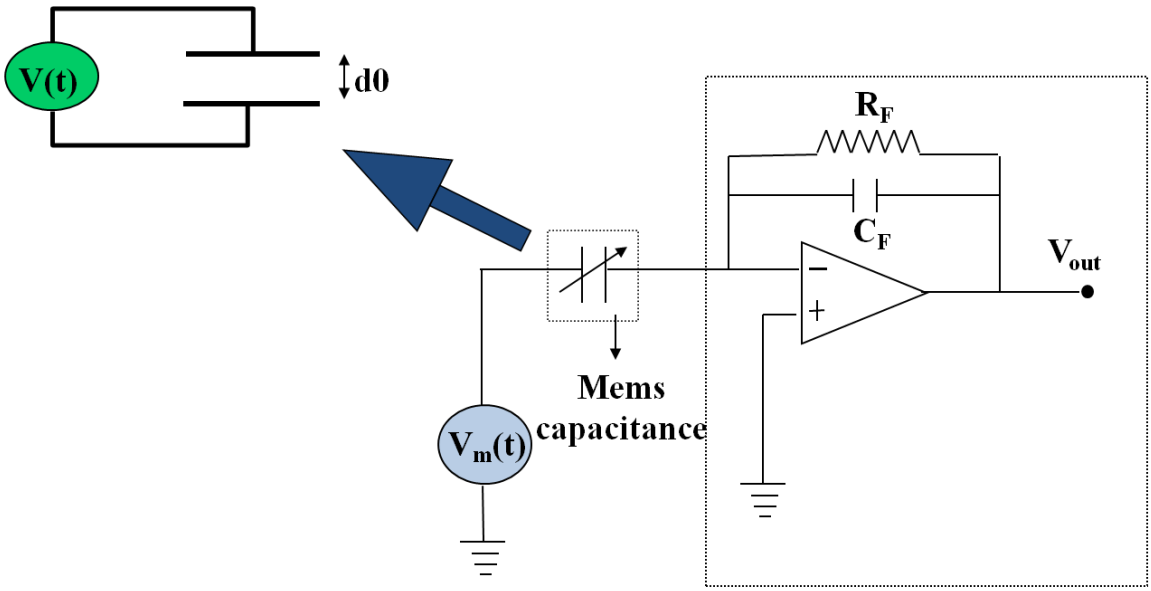

Figure 100: MEMS capacitance sensing circuit

5.2.3 VALIDATION RESULTS

The effective capacitance of the MEMS accelerometer beam is measured by means of a simple op-amp capacitance sensing circuitry [77] as shown in Figure 100. The behavior model of the op-amp circuitry is simulated with the help of MATLAB. The measurement input is a simple sinusoid of frequency that is significantly higher than the input frequency to the MEMS capacitor. The measurement frequency is fixed at 1 MHz, with amplitude of 1volt in the simulation environment. The gain measurements from the

capacitance sensing circuit are used to predict the parameters of the system. Only the steady state oscillation data is used for measurement purposes. The targeted parameters are mass, damping coefficient and spring constant of the accelerometer of Figure 96. Monte Carlo simulations are performed to build a non linear mapping between the measurement space and the parameter space (using MARS), on a set of 100 instances (generated by randomly varying the accelerometer beam mechanical parameters) out of which 70 is used for building the model and the remaining 30 is used for evaluation purpose. The relative error and the RMS error form the basic figure of merit for the developed model.

5.2.3.1 Arbitrary Single Tone Input Test Results

The MEMS system is actuated with a single tone frequency at 20 Hz. This tone is arbitrarily picked from the recommended range of frequencies (15 Hz to 50 Hz). The gain measurements are captured for the selected test input to build the MARS models. The prediction plots of the mechanical parameters obtained for the evaluation set of instances are shown in Figure 101 and the results are summarized in Table 21.

Table 21: Prediction accuracy for an arbitrary single tone input

Parameters	**Nominal value**	**% Variation**	**ε_{rms}**	**ε_{rel}**
Mass	**10 mg**	**5 %**	**4.979e-5**	**3%**
Damping	**0.1**	**10 %**	**0.0010**	**3.2%**
Spring Constant	**50**	**10 %**	**1.0526**	**5.14%**

5.2.3.2 Optimized Single Tone Test Results

The system is actuated with a single tone input at the optimized frequency of 45 Hz and the MARS model is developed. The gain measurements of the evaluation set of devices (30 instances) are mapped back to the mechanical parameter values and the resulting plots and error values (between the predicted and actual) are summarized in Figure 102 and Table 22.

Table 22: Prediction accuracy for an optimized single tone input

Parameters	Nominal value	% Variation	ε_{rms}	ε_{rel}
Mass	10 mg	5 %	5.5390e-5	2.75%
Damping	0.1	10 %	0.0013	2.62%
Spring Constant	50	10 %	1.3747	6.72%

5.2.3.3 Optimized Multi-Tone Test Results

The system is simulated with optimized three tone frequency with each frequency optimized towards the reduction of error of a particular parameter. The tones are placed at 44, 45 and 48 Hz. The resulting plots and error values are summarized in Figure 103 and Table 23

Table 23: Prediction accuracy for an optimized multi-tone input

Parameters	Nominal value	% Variation	ε_{rms}	ε_{rel}
Mass	10 mg	5 %	3.374-5	1.72%
Damping	0.1	10 %	0.0012	4.19%
Spring Constant	50	10 %	0.2079	1.119%

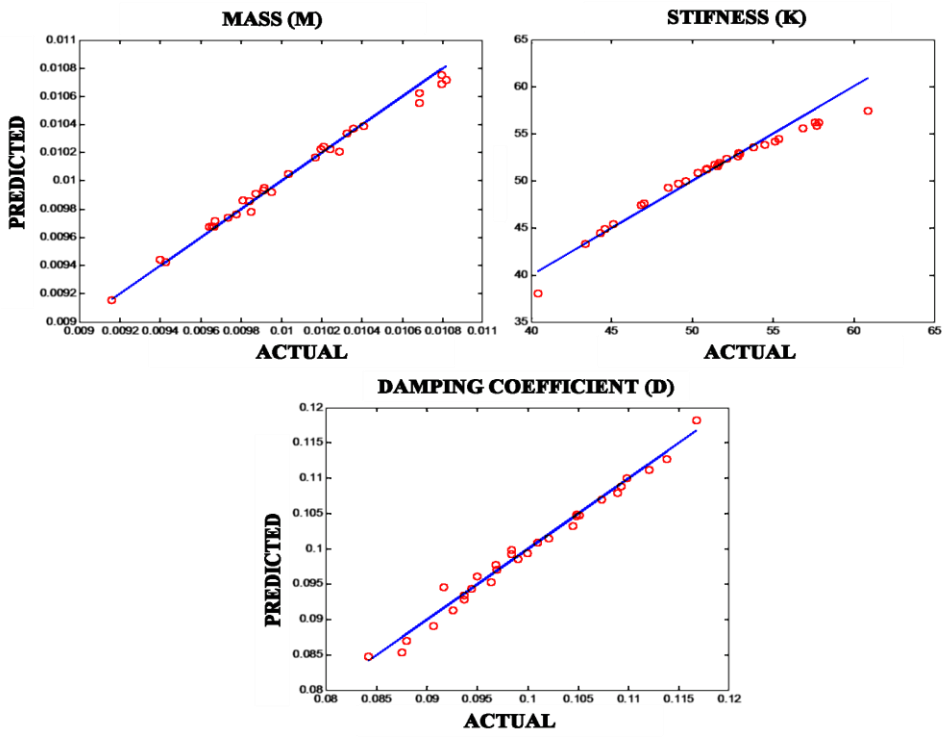

Figure 101: Prediction accuracy for an arbitrary single tone

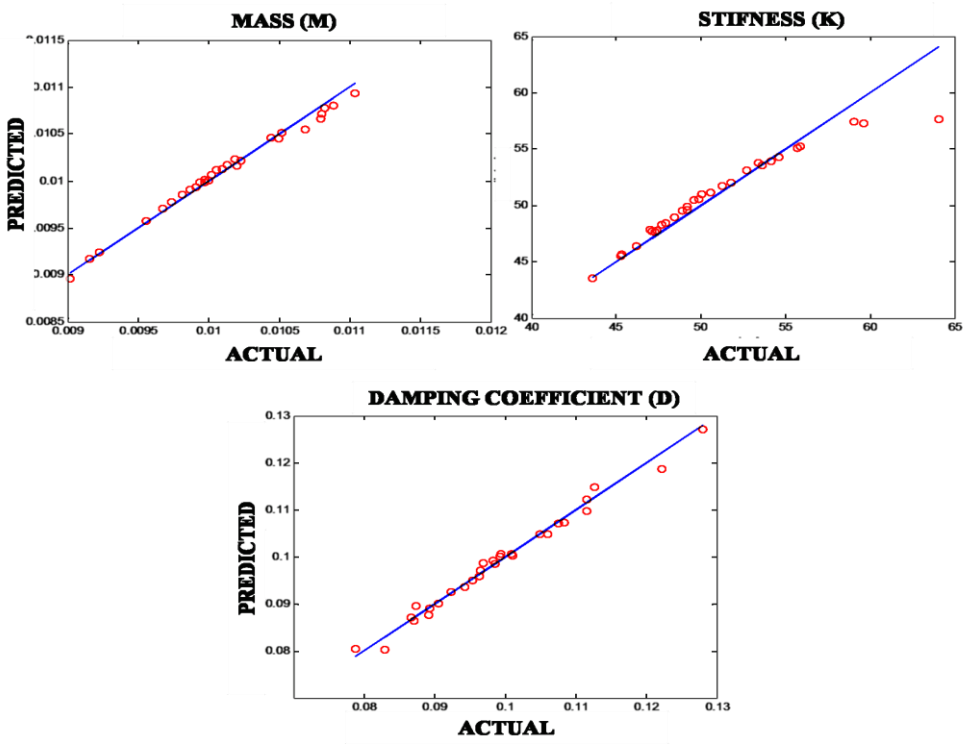

Figure 102: Prediction accuracy for an optimized single tone

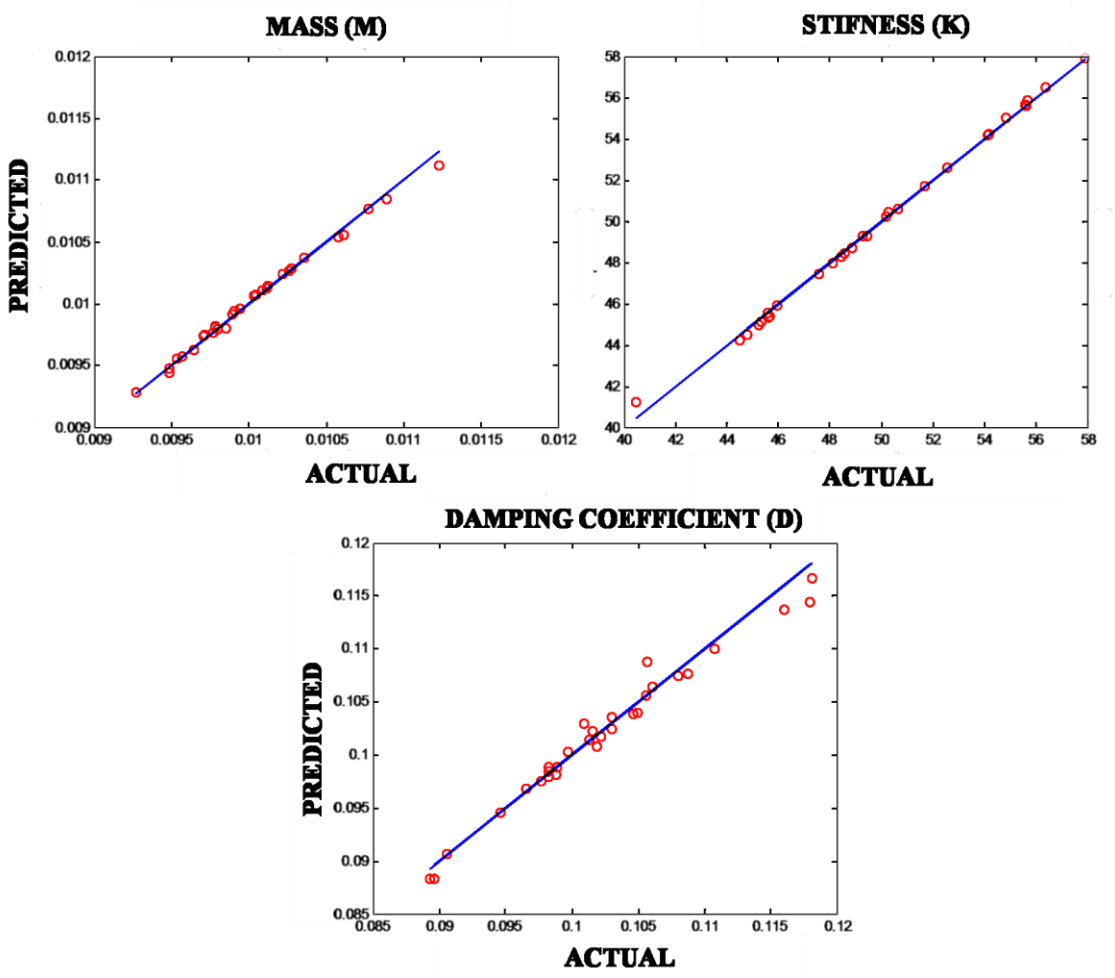

Figure 103: Prediction accuracy for an optimized multi- tone

It can be observed from the results that the relative error for 'each' parameter is less than 5% for the multi-tone test input which is an improvement over the single tone case studies. To summarize in this section, a novel alternate electrical testing strategy to estimate the mechanical parameters of a MEMS cantilever beam is discussed. The dynamics of the cantilever beam is exploited by the application of electrical stimulus to result in a steady state vibration of the cantilever beam. The steady state vibration in turn affects the MEMS capacitance value over time and is captured to estimate the mechanical parameters of the beam using regression analysis. The accuracy in prediction demonstrates the feasibility of the proposed approach.

In this chapter, the applications of alternate test methodology are discussed. Application of alternate test principles in the field of on-line testing of RF systems demonstrate the capability of the developed regression models to accurately track the performance of the system 'on-the-field'. This capability is critical to develop self adapting systems that can reconfigure according to environmental conditions and other factors such as aging, transient faults etc. Alternate test is capable of estimating multiple specifications in a short amount of time and hence are ideal to perform on-line testing (where it's important to not impede the normal operation of a RF system).

Application of alternate tests in the field of MEMS testing demonstrates significant improvement over conventional testing procedures and relaxes the requirements of testing a complex system such as MEMS. The discussed methodology in this chapter, demonstrate that it is possible to accurately compute the mechanical parameters of the cantilever beam using electrical test inputs which are much easier to generate in a controlled manner as opposed to conventional testing procedures. Further the developed methodology also demonstrates a significant reduction in test time in comparison to the conventional test procedures.

CHAPTER 6

CONCLUSIONS AND FUTURE WORK

The manufacturing cost of a wireless product is significantly affected by the impact of process variations on the performance of the system. The impact of process variations result in (a) an increased test cost arising primarily due to the complexity of the highly integrated DUT architecture that exhibits a wide variation in the performance parameters and (b) product yield loss arising primarily due to the significant amount of devices being classified as bad based on the test findings.

In this thesis, several low-cost test procedures are developed to reduce the overall test cost of deep sub-micron RF systems. In Chapter 3 four examples are discussed to address the issue of test cost and test time. First example, demonstrates the advantages of performing test generation for an alternate test technique by considering the artifacts of the signal path and the embedded sensors along with the DUT to develop a low-cost production test technique. Second example, demonstrates the reduction in test times possible by performing alternate test to estimate the RF specifications of a multi-band radio. Third example proposes a low-cost technique to estimate EVM an end-to-end system level specification of critical value and demonstrates the significant reduction in test times and test cost possible. The methodologies are mainly based on the alternate test philosophy where multiple module level and end-to-end system level specifications are estimated from a single data capture using MARS regression models.

However, a key limitation of the alternate test approach is the one-time cost associated with the development of the regression models during the training phase. In order for the regression models to accurately estimate multiple RF specifications it's necessary that the models are trained over a sufficient set of training instances. However, the training process can be lengthy and does not eliminate the use of standard test

mechanisms. Hence it's desirable to develop low-cost test techniques that obviate the need for performing training. The fourth example in Chapter 3, discusses a response fitting based model parameter extraction technique to explore the possibilities of testing multiple specifications using a single data capture without the need for regression models to do the same. However, the technique is just a preliminary proof of concept. Model parameter identification techniques promise a powerful methodology for testing multiple specifications of RF systems. At present, research in the parameter identification area is still premature and a significant amount of work is required in the area of identifying the type of model to be used and in the area of test generation algorithms to ensure accurate estimation of the model parameters. In future, *model extraction based techniques can be used in conjunction with alternate tests to develop powerful low-cost test methodologies* to significantly reduce the test cost (and the manufacturing cost) of wireless products.

Product yield loss is another significant contributor to the overall manufacturing cost of advanced wireless products. In deep submicron technologies, process variations introduce a significant deviation in the performance of a device from its nominal behavior to result in some devices to be deemed as bad. However, most of these devices exhibit parametric deviations (not catastrophic) and hence can be recovered. *In this thesis, several post-manufacture tuning approaches are proposed to significantly improve the overall product yield of a wireless product.* In Chapter 4, three examples are discussed to perform post-manufacture in a realistic time frame. First example, demonstrates the yield improvements possible by performing a simple signature based analog tuning to recover bad devices that exhibit parametric deviations. Second example, demonstrates the yield improvements possible by using an alternate test driven analog tuning approach. The penalty in power consumption in this example is kept minimal by following a heuristic approach. In the third example, a comprehensive tuning approach is discussed to tune for devices that exhibit large as well as small parametric deviations. In this example, the penalty in power consumption because of tuning is modeled explicitly

in the tuning framework to obtain an accurate power optimal tuning solution in a realistic time frame. Due to aggressive scaling and constant demand for integration, such techniques will be imperative in the near future to reduce the product yield loss and hence the manufacturing cost of wireless products.

In this thesis, the techniques developed for post manufacture tuning primarily deal with the paradigm of "how to tune" a set of control knobs to achieve optimum performance in a short amount of time. The tuning knobs chosen to demonstrate the techniques are preliminary and include knobs such as supply voltage bias voltage/current etc. *However in future, it's critical to develop carefully designed control knobs that can be built in the design to optimally control the performance of the system*. In particular it is desirable to identify control knobs that can offer orthogonal control of multiple performance parameters. The *orthogonal knobs can then be used in conjunction with the post manufacture methodologies* developed in this thesis to significantly reduce the product yield loss with minimal impact on power consumption. *Such techniques are critical* and have the potential to *significantly reduce the manufacturing cost of advanced deep submicron wireless products.*

6.1 PAPERS PUBLISHED

The following lists the journal, conference and workshop publications that have resulted from this research

6.1.1 JOURNAL PUBLICATIONS

1. Natarajan, V.; Sen, S.; Chatterjee, A., "Built-In Test Enabled Diagnosis and Tuning of RF Transmitter Systems," Journal Of VLSI Design, Vol. 2008, Article ID 418165, 10 Pages, 2008.
2. Natarajan, V., Sen, S., Banerjee, A., Chatterjee, A., Srinivasan, G., Taenzler, F., "Analog Signature Driven Post Manufacture Multi-Dimensional Tuning of RF Systems", accepted, to appear in IEEE Design and Test Magazine.

3. Natarajan, V., Choi, H., Banerjee, A., Sen, S., Chatterjee, A., Srinivasan, G., Taenzler, F., Bhattacharya, S., "Low Cost EVM Testing of Wireless RF SoC Front-ends Using Multi-Tones", submitted for review in IEEE Transactions on Computer Aided Design.

6.1.2 CONFERENCE AND WORKSHOP PUBLICATIONS

1. Chatterjee, A.:, Han, D.:, Natarajan, V.:, Devarakond, S.:, Sen, S.:, Choi, H.:, Senguttuvan, R.:, Bhattacharya, S.:, Goyal, A.:, Lee, D.:, Swaminathan, M., "Iterative Built-in Testing and Tuning of Mixed-Signal/RF Systems", **Invited Paper,** *International Conference on Computer Design, pp. 319-326, Lake Tahoe, California, October 4-7, 2009*
2. Natarajan, V.; Sen, S.; Devarakond, S.K.; Chatterjee, A., "A Holistic Approach to Accurate Tuning of RF Systems for Large and Small Multi-Parameter Perturbations" *to appear in the Proceedings of VLSI Test Symposium, April 18-21, 2010*
3. Natarajan, V.; Devarakond, S.K.; Sen, S.; Chatterjee, A., "BIST Driven Power Conscious Post-Manufacture Tuning of Wireless Transceiver Systems Using Hardware-Iterated Gradient Search," *Asian Test Symposium,* pp. 243-248, *Taichung, Taiwan, November 23-26, 2009.*
4. Natarajan, V.; Choi, H.; Lee, D.; Senguttuvan, R.; Chatterjee, A., "EVM Testing of Wireless OFDM Transceivers Using Intelligent Back-End Digital Signal Processing Algorithms," *International Test Conference*, pp.1-10, *Santa Clara, California, October 28-30, 2008*.
5. Natarajan, V.; Bhattacharya, S.; Chatterjee, A., "Alternate electrical tests for extracting mechanical parameters of MEMS accelerometer sensors," *VLSI Test Symposium*, pp.192-197, *Berkeley, California, April 30 –May 4, 2006*.

6. Natarajan, V.; Srinivasan, G.; Chatterjee, A.; Force, C., "Novel Cross-Loopback Based Test Approach for Specification Test of Multi-Band, Multi-Hardware Radios," *VLSI Test Symposium,* pp.297-302*, Berkeley, California, May 6-10, 2007.*
7. Natarajan, V.; Senguttuvan, R.; Sen, S.; Chatterjee, A., "ACT: Adaptive Calibration Test for Performance Enhancement and Increased Testability of Wireless RF Front-Ends," *VLSI Test Symposium*, pp.215-220*, San Diego, California, April 27 – May1, 2008.*
8. Natarajan, V.; Srinivasan, G.; Chatterjee, A., "On-line error detection in wireless RF transmitters using real-time streaming data," *International On-Line Testing Symposium, pp.159-164, Lake of Como, Italy, July 10-12, 2006.*
9. Natarajan, V.; Choi, H.; Lee, D.; Senguttuvan, R.; Chatterjee, A.; "EVM Testing of Wireless OFDM Transceivers Using Intelligent Back-End Digital Signal Processing Algorithms," *Proceedings of TechCon, Austin, Texas, November 3-4, 2008.*
10. Natarajan, V.; Devarakond, S.K.; Sen, S.; Chatterjee, A., "Power-Aware Self Healing of RF transceiver Systems: Low-cost Test Driven Simultaneous Tuning of Multiple Performance Metrics," *Accepted, to appear in the Proceedings of TechCon, Austin, Texas, September 14-15, 2009.*
11. Sen, S.; Natarajan, V.; Senguttuvan, R.; Chatterjee, A., "Pro-VIZOR: Process tunable virtually zero margin low power adaptive RF for wireless systems," *Design Automation Conference*, pp.492-497*, Anaheim, California, June 9-12, 2008.*
12. Lee, D.; Natarajan, V.; Senguttuvan, R.; Chatterjee, A., "Efficient Low-Cost Testing of Wireless OFDM Polar Transceiver Systems," *Asian Test Symposium*, pp.55-60*, Sapporo, Japan, November 24-27, 2008.*
13. Kook, S.; Natarajan, V.; Chatterjee, A.; Goyal, S.; Jin, L., "Testing of High Resolution ADCs Using Lower Resolution DACs via Iterative Transfer Function Estimation," *European Test Symposium*, pp.3-8*, Sevilla, Spain, May 25-29, 2009.*

14. Devarakond, S.K.; Natarajan, V.; Sen, S.; Chatterjee, A., "BIST-assisted power aware self healing RF circuits," *Mixed-Signals, Sensors, and Systems Test Workshop*, pp.1-4, Scottsdale, Arizona, June 10-12, *2009*.
15. Senguttuvan, R.; Natarajan, V.; Sen, S.; Chatterjee, A.; "Built-in Test Enabled Diagnosis and Tuning for RF Transmitter Systems," *Proceedings of International Mixed Signals Testing Workshop*, Pova De Varzim, Portugal, June 18-20, 2007.
16. Devarakond, S.K.; Natarajan, V.; Sen, S.; Chatterjee, A., "Built-In Test Driven Power Aware Self Tuning of Wideband RF Devices," *Electronic Symposium Digest of papers, European Test Symposium, Sevilla, Spain, May 25-29, 2009.*
17. Bhattacharya, S.; Natarajan, V.; Chatterjee, A.; Nair, S., "Efficient DNA sensing with fabricated silicon nanopores: diagnosis methodology and algorithms," *VLSI Design*, pp.729-733, *Hyderabad, India, Jan 3-6, 2006.*
18. Kook, S.; Choi, H.; Natarajan, V.; Chatterjee, A.; Gomes, A.; Goyal, S.; Jin, L., "Low Cost Dynamic Test Methodology for High Precision ΣΔ ADCs," *Asian Test Symposium*, pp. 69-74, *Taichung, Taiwan, November 23-26, 2009.*
19. Srinivasan, G.; Chatterjee, A.; Natarajan, V., "Fourier Spectrum-Based Signature Test: A Genetic CAD Toolbox for Reliable RF Testing Using Low-Performance Test Resources," *Asian Test Symposium*, pp.139-142, *Beijing, China, October 9-11, 2007*.
20. Senguttuvan, R.; Nisar, M.M.; Sen, S.; Natarajan, V.; Chatterjee, A., "End-to-End Test-Enabled Wireless Transceivers with Low-Power and Process Variation Adaptation," *Proceedings of Silicon Errors in Logic-System Effects, University of Texas at Austin, March 27-28, 2008.*

6.2 AWARDS

Margarida Jacome Award for the "Best Project Work and Student Poster" for "Adaptive Low-Power RF Systems", at Gigascale Research Center Annual Symposium

(NSF Funded center), San Jose, CA September 2007, awarded to Rajarajan Senguttuvan, Shreyas Sen, *Vishwanath Natarajan*, Hyun Choi, Abhijit Chatterjee.

6.3 INVENTION DISCLOSURES

1. **Published patent application disclosure,** Shankar Nair, Soumendu Bhattacharya, *Vishwanath Natarajan*, A. Chatterjee, "Methods and Systems for Evaluating the Length of Elongated Elements", *US Patent Application #20070099191*.
2. **Patent applied for**, *Vishwanath Natarajan***,** Shyam kumar Devarakond, Shreyas Sen, Abhijit Chatterjee, "Power Conscious Self-Healing Methodologies for Mixed-Signal and RF Systems", Georgia Tech Research Center Ref. No.:4954.
3. **Patent applied for**, Sehun Kook**,** *Vishwanath Natarajan*, Hyun Choi, Alfred Gomes, Le Jin, Shalabh Goyal, "Low Cost Dynamic Test Methodology for High Precision ΣΔ ADCs", Georgia Tech Research Center Ref. No.:4935.

REFERENCES

[1] LUIZ FRANCA-NETO, M., ELINE, R. and BALVINDER, B., "Fully Integrated CMOS Radios from RF to Millimeter Wave Frequencies, " Intel Technology Journal, Vol. 8, Issue 3, pp. 241-258, ISSN 1535-864X, August 2004.

[2] SERY, G., BORKAR, S. and DE, V., "Life is CMOS: Why chase the life after?," Proc. of DAC, pp. 78-83, 2002.

[3] BORKAR, S., KARNIK, T., NARENDRA, S., TSCHANZ, J., KESHAVARZI, A. and DE, V., "Parameter Variations and Impact on Circuits and Micro-architecture," Proc. of DAC, pp. 338-342, 2003.

[4] BROCKMAN, J. B. and DIRECTOR, S. W., "Predictive subset testing: optimization IC parametric performance testing for quality, cost, and yield," IEEE Trans. Semi. Manufacturing, vol. 2, no. 3, pp. 104-113, Aug. 1989.

[5] MILOR, L. and VINCENTELLI, A. L. S., "Minimizing production test time to defect faults in analog circuits," IEEE Trans. on Computer-Aided Design of Integrated Circuits and Systems, vol. 13, pp. 796-813, June 1994.

[6] Schaub, K.B. and Kelly, J., "Production Testing of RF and System-on-a-Chip Devices for Wireless Communications," Artech House, Boston, Chapters 1 and 3, 2004.

[7] OZEV, S., ORAILOGLU, A. and HAGGAG, H., "Automated test development and test time reduction for RF subsystems," IEEE Intl. Symposium on Circuits and Systems, pp. 581-584, 2002.

[8] OZEV, S., OLGAARD, C. and ORAIOGLU, A., "Testability implications in low-cost integrated radio transceivers: A Bluetooth case study," Proc. of Int'l Test Conf., pp. 965-974, 2001.

[9] PINEDA DE GYVEZ, GRONTHOUD, J. and AMINE, G., "Vdd ramp testing for RF circuits", Proc. of Int'l Test Conf., pp. 651 – 658, Sept. 30-Oct. 2, 2003.

[10] HELFENSTEIN, M., BAYKAL, E., MULLER, K. and LAMPE, A., "Error vector magnitude (EVM) measurements for GSM/EDGE applications revised under production conditions," IEEE International Symposium on Circuits and Systems, vol. 5, pp. 5003-5006, Kobe, Japan, 2005

[11] TRAN, L. H., MAI, T. and MOLNAR, J. A., "Matlab and COTS instrumentations to reduce time and risk factors in design to the stand-alone QAM test system," IEEE Systems Readiness Technology Conference, pp. 490-495, Anaheim, CA, USA, 2003.

[12] DABROWSKI, J. and BAYON, J.G., "Mixed loopback BIST for RF digital transceivers," Proc. of 19th IEEE International Symposium on Defect and Fault Tolerance in VLSI Systems, pp. 220-228, Cannes, France, 2004.

[13] ACAR, E., OZEV, S. and REDMOND, K. B., "Enhanced Error Vector Magnitude (EVM) Measurements for Testing WLAN Transceivers," Proc. of ICCAD, pp. 210-216, 2006.

[14] ACAR, E. and OZEV, S., "Low-cost characterization of RF transceivers through IQ data analysis", Proc. of Int'l Test Conf., pp 1-10, Santa Clara, USA, Oct 21-26, 2007.

[15] RYU, J., KIM, B.C. and SYLLA, I., "A new low-cost RF built-in self-test measurement for system-on-chip transceivers," IEEE Trans. Instrumentation and Measurement, vol. 55, no. 2, pp. 381-388, 2006.

[16] HALDER, A., BHATTACHARYA, S., SRINIVASAN, G. and CHATTERJEE, A., "A system-level alternate test approach for specification test of RF transceivers in loopback mode", 18th International Conference on VLSI design, pp. 289-294, Jan 2005.

[17] HALDER, A. and CHATTERJEE, A., "Low-cost production testing of wireless transmitters," Proceedings of 19th International Conference on VLSI Design, pp. 6-8, Hyderabad, India, 2006.

[18] VARIYAM, P.N., CHERUBAL, S. and CHATTERJEE, A., "Prediction of analog performance parameters using fast transient testing", IEEE Transactions on

Computer-aided Design of Integrated Circuits and Systems, vol. 21, No. 3, March 2002.

[19] FRIEDMAN, J.H., "Multivariate adaptive regression splines," The Annals of Statistics, vol. 19, no.1, pp.1-141, 1991.

[20] GOPALAN, A., DAS, T., WASHBURN, C. and MUKUND, P. R., "An ultra-fast, on-chip BIST for RF low noise amplifiers," Proc. of Int'l Conf. on VLSI Design, pp. 485-490, Jan 2005.

[21] BEHZAD RAZAVI., "RF Microelectronics," Prentice Hall, ISBN 0-13-887571-5, 1997.

[22] TURUMI, H. and SUZUKI, Y., "Broadband RF Stage Architecture for Software Defined Radio in Handheld Terminal Applications," IEEE Communications Magazine, pp. 90-95, February 1999.

[23] BAGHERI, R., MIRZAEI, A., HEIDARI, M., CHEHRAZI, S., MIKHEMAR, M. and ABIDI, A., "Software Defined Radio Receiver: Dream to Reality," IEEE Communications Magazine, pp. 111-118, August 2006.

[24] CAVERS, J.K. and LIAO, M.W., "Adaptive Compensation for Imbalance and Offset Losses in Direct Conversion Transceivers", IEEE Trans. on Vehicular Technology, Volume 42, Issue 4, pp. 581-588, November, 1993.

[25] PARK, C.H., PAIK, J.H., YOU, Y.H., JU, M.C. and CHO, J.W., " Techniques for Channel Estimation , DC-offset Compensation, and Link Quality Control in Bluetooth System", IEEE Trans. on Consumer Electronics, Volume 46, Issue 3, pp. 682-689, August 2000.

[26] ELAHI, I., MUHAMMAD, K. and BALSARA, P.T ., "I/Q Mismatch compensation using Adaptive De-correlation I a Low-IF Receiver in 90-nm CMOS Process", IEEE Journal of Solid-State Circuits, Vol. 41, Issue 2, pp. 395-404, February, 2006.

[27] VALKAMA, M., SALMINEN, K. and RENFORS, M., "Digital I/Q Imbalance Compensation in Low-IF Receivers: Principles and Practice", 14th Int'l Conference on Digital Signal Processing, Volume 2, pp. 1179-1182, July 2002.

[28] CAPOZIO, P., PAI, P., VIZZI, E. and DACOSTA, G., "A Novel adaptive technique for digital I/Q imbalance compensation in OFDM receivers", Proc. of IEEE Int'l Conference on Acoustics, Speech and Signal Processing, Volume 3, pp. 817-820, March 2005.

[29] RYKACZEWKI, P., PIENKOWSKI, D., CADU, R. and STEINKE, B., "Signal Path Optimization in Software-Defined Radio Systems", IEEE Trans. on Microwave Theory and Techniques, Volume 53, Issue 3, pp. 1056-1064, March 2005.

[30] VAN ROOYEN, G.J. and LOURENS, J.G., "Non-Iterative Compensation for Software-Defined Radio Quadrature Front-end Inaccuracies", Proc. of Wireless Communications, Networking and Mobile Computing, Volume 1, pp. 598-601, September 2005.

[31] HAN, D., AKBAY, S.S., BHATTACHARYA, S., CHATTERJEE, A. and EISENSTADT, W.R., "On-chip self-calibration of RF circuits using specification-driven built-in self test (S-BIST)" Proc. of 11th International On-line Testing Symposium, pp. 106-111, July 2005.

[32] JEON, O., FOX, R.M. and MYERS, B.A., "Analog AGC Circuitry for a CMOS WLAN Receiver", IEEE Journal of Solid-State Circuits, Vol. 41, Issue 10, pp. 2291-2300, Oct 2006.

[33] NEUHAUSER, M., MOLLER, M., REIN, M. and WERNZ, H., " Low-noise, high-trans-impedance Si-bipolar AGC amplifier for 10Gb/s optical-fiber links", IEEE Photonics Technology Letters, Volume 7, Issue 5, pp. 549-551, May 1995.

[34] SONG, B.S. and GRAY, P.R., "A Precision curvature-compensated CMOS bandgap reference", IEEE Jour nal of Solid-State Circuits, Volume 18, Issue 6, pp. 634-643, Dec 1983.

[35] VITTOZ, E.A. and NEYROUD, O., “A low-voltage CMOS bandgap reference”, IEEE Journal of Solid-State Circuits, Volume 14, Issue 3, pp. 573-579, Jun 1979.

[36] MOSTAFA, A., ELMALA, I. and SHERIF, H. K., “A Self-Calibration Technique for Mismatches in Image-Reject Receivers”, Proc. of IEEE CICC, Orlando, Florida, May 2002.

[37] GOYAL, A., SWAMINATHAN, M. and CHATTERJEE, A., " A novel self-healing methodology for RF Amplifier circuits based on oscillation principles" IEEE Design, Automation & Test in Europe Conference & Exhibition, pp. 1656 – 1661, 2009.

[38] BHATTACHARYA, S., HALDER, A., SRINIVASAN, G. and CHATTERJEE, A., “Alternate Testing of RF Transceivers Using Optimized Test Stimulus for Accurate Prediction of Systems Specifications,” Journal of Electronic Testing: Theory and Applications, Vol. 21, No. 3, pp. 323-339, 2005.

[39] VOORAKARANAM, R., CHERUBAL, S. and CHATTERJEE, A., “A signature test framework for rapid production testing of RF circuits,” Design Automation and Test in Europe, pp. 4-8, 2002.

[40] Burns, M. and Roberts, G. W., “An Introduction to Mixed-Signal IC Test and Measurement” New York: Oxford Univ. Press, 2001.

[41] D. H. HAN., BHATTACHARYA, S. and CHATTERJEE, A., “Built-In RF Transceiver Test and Diagnosis Using Transient Envelope Detection and Sampling,” Proc. of Int’l Mixed-Signal Testing Workshop, Edinburgh, Scotland, pp. 250-257, June 2006.

[42] YIN, Q., EISENSTADT, W., FOX, W. and ZHANG, T.,“A trans-linear RMS detector for embedded test of RF ICs,” IEEE Transactions on Instrumentation and Measurement, Volume 54, Issue 5, pp. 1708 – 1714, Oct. 2005.

[43] VALDES-GARCIA, A., SILVA MARTINEZ, A.J. and SANCHEZSINENCIO, E., “ On-Chip Testing Techniques for RF Wireless Transceivers, IEEE Design and Test of Computers, Vol. 23, No. 4, pp. 268-277, April 2006.

[44] BHATTACHARYA, S., SRINIVASAN, G., CHERUBAL, S., HALDER, A. and CHATTERJEE, A., "System-level Testing of RF Transmitter Specifications using Optimized periodic Bit-streams," Proc. VLSI Test Symposium, pp. 229-234, 2004.

[45] HALDER, A., BHATTACHARYA, S. and CHATTERJEE, A., "Automatic Multitone Alternate Test Generation For RF Circuits Using Behavioral Models", Proc. Intl. Test Conference, pp. 665-573, 2003.

[46] HAN, D.H., BHATTACHARYA, S. and CHATTERJEE, A., "Built-In RF Transceiver Test and Diagnosis Using Transient Envelope Detection and Sampling," Proc. of Int'l Mixed-Signal Testing Workshop, Edinburgh, Scotland, pp. 250-257, June 2006.

[47] BHATTACHARYA, S. and CHATTERJEE, A., "A DFT Approach for Testing Embedded Systems Using DC Sensors," IEEE Design & Test of Computers, Volume 23, Issue 6, pp: 464 – 475, June 2006.

[48] Goldberg, D., "Genetic Algorithms in Search Optimization and Machine Learning", Addison Wesley,1989.

[49] OZEV, S., OLGAARD, C. and ORAILOGLU, A., "Testability implications in Low-Cost Integrated Radio Transceivers: A Bluetooth Case Study", IEEE Int'l Test Conference, pp. 965-974, Baltimore, USA, November 2001.

[50] VOELKER, K., "Apply error vector measurements in communications design," Microwaves Amp & RF, vol. 34, 1995.

[51] WILLIAMS, R. and GETCHELL, J., "High-speed measurement of digital wireless system SNR by means of error vector magnitude analysis," in Proc. of wireless Comm. Conf., Boulder, CO, pp. 68–70, 1996.

[52] Agilent Technologies, Santa Clara, CA, "Using error vector magnitude measurements to analyze and troubleshoot vector-modulated signals," Agilent PN 89400-14 Product note, 2000.

[53] YOSHIZAWA, S. and MIYANAGA, Y., “Tunable word length Architecture for a Low Power Wireless OFDM demodulator”, IEICE Trans. Fundamentals, Vol.E89-A, No.10, October 2006.

[54] IEEE Standard for Information technology, Part 11: Wireless LAN Medium Access Control (MAC) and Physical Layer (PHY) Specifications, url:http://standards.ieee.org/getieee802/802.11.html.

[55] HALDER, A. and CHATTERJEE, A., "Low-cost production testing of wireless transmitters," 19th International Conference on VLSI Design, pp. 3-7, Jan 2006.

[56] ACAR, E., OZEV, S., SRINIVASAN, G. and TAENZLER, F., "Optimized EVM Testing for IEEE 802.11a/n RF ICs," IEEE Int’l Test Conference, pp.1-10, 28-30 Oct, 2008.

[57] SRINIVASAN, G., HUI CHUAN CHAO, and TAENZLER, F., "Octal-Site EVM Tests for WLAN Transceivers on "Very" Low-Cost ATE Platforms," IEEE Int’l Test Conference, pp.1-9, 28-30 Oct, 2008.

[58] FORESTIER, S., BOUYSSE, P., QUERE, R., MALLET, A., NEBUS, J.M. and LAPIERRE, L., "Joint optimization of the power-added efficiency and the error-vector measurement of 20-GHz pHEMT amplifier through a new dynamic bias-control method," IEEE Trans. on Microwave Theory and Techniques, Vol.52, No.4, pp. 1132- 1141, April 2004

[59] Engels, M., “Wireless OFDM Systems” Boston, MA, Kluwer, 2003.

[60] CHIA LING LIU., "Impacts of I/Q imbalance on QPSK-OFDM-QAM detection," IEEE Trans. on Consumer Electronics, Vol.44, No.3, pp.984-989, Aug 1998

[61] VAN DEN BOS, C., KSUWENHOVEN, M.H.L. and SERDIJN, W.A., "Effect of smooth nonlinear distortion on OFDM symbol error rate," IEEE Trans. on Communications, Vol.49, No.9, pp. 1510-1514, Sep 2001

[62] COSTA, E. and PUPOLIN, S., "M-QAM-OFDM system performance in the presence of a nonlinear amplifier and phase noise," IEEE Trans. on Communications, Vol.50, No.3, pp.462-472, Mar 2002

[63] ERDOGAN, E.S. and OZEV, S., "Detailed Characterization of Transceiver Parameters Through Loop-Back-Based BIST", IEEE Trans. on VLSI Systems, Vol. 18, Issue 6, pp. 901 – 911, 2010.

[64] NATARAJAN, V., CHOI, H., LEE, D., SENGUTTUVAN, R. and CHATTERJEE, A., "EVM Testing of Wireless OFDM Transceivers Using Intelligent Back-End Digital Signal Processing Algorithms," Proc. of Int'l Test Conference, pp.1-10, 28-30 Oct. 2008

[65] AKBAY, S.S. and CHATTERJEE, A., "Fault-Based Alternate Test of RF Components", Proc. of ICCD, Oct 2007.

[66] STRATIGOPOULOS. H., MIR, S., ACAR, E. and OZEV, S., "Defect Filter for Alternate RF Test," IEEE European Test Symposium, pp. 101-106, May 2009.

[67] MATTES, H., SATTLER, S. and DWORSKI, C., "Controlled Sine Wave Fitting for ADC Test," Proc. of Int'l Test Conference, pp. 963-971, 2004.

[68] HUNG, S.F., HONG, H.C. and LIANG, S.C., "A Low Cost Output Response Analyzer for BIST of Sigma-Delta Modulator Using the Controlled Sine Wave Fitting Method," Proc. of Asian Test Symposium, pp. 385-391, Nov 2009.

[69] PARK, J., CHUNG, J. and ABRAHAM, J.A., "LFSR Based Performance Characterization of Nonlinear Analog and Mixed-Signal Circuits," Proc. of Asian Test Symposium, pp. 373-379, Nov 2009.

[70] BARRAGAN, M., FIORELLI, R., VAZQUEZ, D., RUEDA, A. and HUERTAS, J.L., "A BIST Solution for the Functional Characterization of RF Systems, Based on Envelope Response Analysis," Proc. of Asian Test Symposium, pp. 255-261, Nov 2009.

[71] PRATAP, R. J., SEN, P., DAVIS, C.E., MUKHOPHDHYAY, R., MAY, G.S. and LASKAR, J., "Neurogenetic design centering," IEEE Trans. on Semiconductor Manufacturing, Vol. 19, pp. 173-182, 2006.

[72] Chapra, S.C. and Canale, R.P., "Numerical methods for Engineers", Fourth Edition, McGraw Hill, pp.: 342-349.

[73] Snyman, J.A., "Practical Mathematical Optimization", Springer Science, Business Media, Inc. New York, 2005.

[74] SHANG, Y. and WAH, B.W., "A discrete lagrangian based global search problem for solving satisfactory problems", Journal of Global Optimization, pp 66-98, 1998.

[75] AMINI, B.V. and AYAZI, F., "A 2.5-V 14-bit /spl Sigma//spl Delta/ CMOS SOI capacitive accelerometer", IEEE Journal of Solid-State Circuits, Vol. 39, Issue 12 pp. 2467 - 2476, Dec 2004.

[76] Datasheet of ADXL 320, Analog devices, 2004.

[77] Senturia, S.D., "Microsystems Design", Boston, MA, Kluwer Academic, 2000.